Volume 3
October, 2026
ISSN 2818-0313
DOI Prefix：10.62252

Naturalis Scientias



www.naturalisscientias.com

TABLE OF CONTENTS

Original Articles

1. Type and Origin of the Gallium Deposits in Mainland China 662

2. A Theoretical Analysis of Dollar-Cost Averaging Under Different Index Price Trajectories 676

3. Geology and Geochemistry of the Germanium Deposits in Mainland China 686

4. Mathematical, Physical, and Chemical Interpretations of Structural Control and Contributions to Mineralization-Taking Global Gold Deposits as an Example 710

5. Genetic Types and Geology of Cesium Deposits in Mainland China 739

6. "Historical Records" Born of Earth and Fire 763

7. Types and Metallogenic Mechanism of Rubidium Deposits in Mainland China 777

Original Article

Type and Origin of the Gallium Deposits in Mainland China

Jian Zhao Yin[1] Ⓛ

Abstract

With the continuous development of science and technology and the progress of human society, the important roles of more and more rare metals are being discovered. Gallium, the subject of this paper, is one of many rare metals. It is not only listed as one of the critical/strategic metals by an increasing number of countries, but also receives increasing attention and importance. China is one of the most important producers of many rare metals and rare earth elements. However, due to geopolitical factors and other influences, the world's understanding of China's rare metals is limited or incomplete. Based on a summary of previous work by many other geologists, this paper classifies the known genetic and industrial types of gallium in China, lists representative deposits of each type and their geological characteristics, and preliminarily discusses their mineralization mechanisms. Gallium deposits can be divided into two main industrial categories: independent and associated/symbiotic. Currently, all human exploitation and utilization is of the latter; no independent gallium deposit has been discovered globally. Known associated and/or symbiotic gallium deposits cover two main genetic types: primary and secondary, endogenous and exogenous. Endogenous gallium deposits are closely related to igneous activity and metamorphism, while exogenous gallium deposits are related to sedimentation and volcanic activity. Whether endogenous or exogenous, primary or secondary gallium deposits, they are not clearly distinct; rather, they exist as mixed and/or combined, or transitional, co- and/or associated gallium deposits. That is, both endogenous and exogenous processes jointly contribute to the formation of the same gallium deposit. For example, after sedimentary compaction of secondary gallium deposits, and/or after preliminary enrichment in gallium-bearing coal seams, further enrichment occurs through endogenous metamorphism, forming mineable co- and/or associated gallium deposits. Clearly, the cumulative and/or combined effects of multiple mineralization processes more easily lead to the formation of economically valuable gallium deposits.

Keywords: Co- and/or associated gallium deposit, genetic type, primary/secondary, endogenous/exogenous process, emerging critical/strategic mineral resource, mainland China

---

Affiliation Info: 1 College of Earth Sciences, Jilin University, Changchun 130061, China

Corresponding AurhorⓁ: Yin, J. Z., PhD, Professor, geosciences, mineral exploration and mining; Email address: jzyin7@jlu.edu.cn

Citation: Yin, J. Z. 2026. Type and origin of the gallium deposits in Mainland China. *Naturalis Scientias*, 3: 662-675. DOI: https://doi.org/10.62252/NSS.2026.1037. www.naturalisscientias.com.

Copyright © 2026 by the author. Published by *Naturalis Scientias*. This is an open access article under the Creative Commons Attribution-NonCommercial 4.0 International (CC BY-NC 4.0) License. (https://creativecommons.org/licenses/by-nc/4.0/).

---

1. Introduction

Gallium, hailed as the "backbone of the electronics industry," is an emerging critical mineral resource and a key metal on the lists of many countries. Its unique physical and chemical properties give it broad application potential in a variety of fields. With the rapid development of information technology and the continued growth in global demand for high-performance materials, gallium's strategic importance has become increasingly prominent, making it one of the most sought-after mineral resources by various countries. The rise of new-generation communications, the Internet of Things, big data, and cloud computing has led to explosive growth in the electronics and information industry. As one of the core materials of this industry, the demand for gallium has also increased dramatically (Che et al., 2022; YiruShufang, 2024; Li and Song, 2025).

With the widest liquid temperature range of any metal, Gallium melts at just 29.78 °C but boils at 2,204.8 °C. Liquid gallium can penetrate other metals, corroding them and forming alloys. It has nearly zero vapor pressure at room temperature and is low in toxicity with antibacterial properties, making it environmentally friendly (Tu et al., 2004; Gunn, 2014; Feng and Meng, 2024). Gallium easily supercools. Solid gallium is bluish-white and soft with a density of 5.937 g/cm^3.

Gallium has a wide range of applications, including semiconductor materials, optoelectronic materials, solar cells, alloy materials, medical devices, and magnetic materials. The largest application area is the emerging semiconductor industry, accounting for over 80% of total gallium consumption; followed by solar cells, medical materials, LEDs, and optical equipment (Li and Wang, 2020; YiruShufang, 2024; Li and Song, 2025).

Gallium nitride, gallium arsenide, and gallium phosphide are all gallium-containing semiconductor materials, and germanium semiconductors also contain gallium. As a second-generation semiconductor material, gallium arsenide is known as the "aristocrat of semiconductors" due to its high price. Gallium arsenide possesses better electronic properties than silicon: lower noise and higher electron mobility, and is widely used in remote control devices, mobile phones, DVD computer peripherals, lighting, and solar cells, among many other optoelectronic fields (Tu et al., 2004; Li and Wang, 2020; Che et al., 2022; YiruShufang, 2024; Li and Song, 2025).

Gallium, along with various other metals such as indium, thallium, tin, bismuth, and zinc, can form a series of low-melting-point alloys. These alloys are used in the production of temperature control equipment, mercury substitutes in instruments, special coatings for metallic materials, and cooling circuit materials in the electronics and nuclear industries (Tu et al., 2004; Zhao et al., 2017; Li and Wang, 2020; Che et al., 2022; Feng and Meng, 2024; YiruShufang, 2024; Li and Song, 2025; Xinlang Finance, 2025). Indium-gallium alloys containing 25% indium melt into a liquid state at 16 °C and can be used to manufacture sensing devices for automatic fire extinguishing systems. Gallium, along with copper, nickel, tin, and gold, can form cold welding fluxes for welding irregularly shaped, thin-walled materials that are difficult to weld with common materials, especially in cold

welding environments between metals and between metals and ceramics. Gallium arsenide (GaAs) solar cells possess characteristics such as high heat resistance, radiation resistance, and high photoelectric conversion efficiency, making them commonly used in aerospace and military fields. Copper-indium-gallium-selenium (CIGS) alloys are used to fabricate thin-film solar cells, offering advantages such as low production and usage costs and high photoelectric conversion efficiency, making them a popular choice among various solar cell products.

Gallium metal and its compounds are also widely used in biomedical fields such as antibacterial and bacteriostatic applications, biomedical imaging, medical filling materials, medical diagnostics, and disease treatment (Tu et al., 2004; Zhao et al., 2017; Li and Wang, 2020; Che et al., 2022; Feng and Meng, 2024; YiruShufang, 2024; Li and Song, 2025; Xinlang Finance, 2025). As a novel imaging agent, gallium can provide patients with entirely new information about their conditions. Gallium has a strong reflective effect on light; liquid gallium exhibits high reflectivity for light within a certain wavelength range while also adhering well to glass surfaces. This property makes gallium a suitable material for manufacturing specialized optical lenses. Gallium alloys can be used in medical devices and materials; for example, leveraging their physicochemical properties and non-toxic, non-irritating nature, gallium alloys are used as fillings and restorative materials for teeth. Indium-gallium alloy thermometers can be used in medical diagnostics; for instance, gallium citrate can be used for positive tumour imaging and the diagnosis of tumours in the lung, liver, spleen, and lymphatic system.

Based on previous research on gallium deposits in mainland China by other geologists, this paper comprehensively classifies their genetic types, summarizes the geological and geochemical characteristics of each type, and briefly discusses their formation mechanisms. It is intended as a reference for researchers interested in studying the genesis of global gallium deposits and finding more similar deposits, thus contributing to the sustainable development of human society.

2. Existence form and current resource status

Gallium, primarily existing as an associated and/or symbiotic mineral, is extremely unevenly distributed globally, making extraction difficult. Known gallium deposits worldwide are concentrated in a few countries and regions. Given gallium's increasingly important strategic value, major global powers are intensifying their competition for and strategic positioning in gallium resources, striving to enhance their competitiveness and influence in the gallium industry chain through policy support, technological research and development, and international cooperation (Yiru Shufang, 2024; Li and Song, 2025).

Although gallium is the most abundant rare metal in the Earth's crust (15 μg/g), independent gallium minerals are rare. Gallium exists in nature mostly as isomorphous and/or adsorbed forms, with very few concentrated as independent minerals. Currently, only 10 independent gallium minerals have been discovered globally, the vast majority of which are found in Africa, with the majority of these found in the Tsumeb deposit in Namibia (Wen et al., 2020; Feng and Meng, 2024; Li and Song, 2025. Table 1).

Table 1. Limited independent Ga minerals and major Ga-rich minerals (After Zhao et al., 2017; Feng and Meng, 2024; Sina Finance, 2025)

Mineral	Chemical formular	Ga %	Origin
Tsumgallite	GaO(OH)	67.9	Tsumeb, Namibia
Sohngeite	$Ga(OH)_3$	57.8	Tsumeb, Namibia
Gallite	$CuGaS_2$	35.3	Tsumeb, Namibia and Lubumbashi, DR Congo
Camevallite	Cu_3GaS_4	18.0	Tsumeb, Namibia
Gallobeudantite	$PbGa_3[(AsO_4),SO_4)]_2(OH)_6$	19.3	Tsumeb, Namibia
Richardsite	Zn_2CuGaS_4	17.8	Gem Mines near Merelani, Tanzania
Unnamed gallium sulfide	$(Cu,Fe,Zn)GaS_4$	-	Africa
Ishiharaite	(Cu,Ga,Fe,In,Zn)S	-	Capillitas, Argentina
Zincobriartite	$(Cu_2(Zn,Fe)(Ge,Ga)S_4$	-	Kipushi, DR Congo
Galloplumbogummite	$Pb(Ga,Al,Ge)_3(PO_4)_2(OH)_6$	-	Tsumeb, Namibia

Like most other rare metals on the Earth, gallium is currently known to exist in the form of associated and/or symbiotic minerals. According to incomplete statistics, over 50% of global gallium comes from bauxite, less than 40% from zinc deposits, and the remaining less than 10% from other various deposits. Global gallium resources amount to approximately 230,000 tons, with China accounting for about 80% of this (Ren, 2006; Wen et al., 2020; Che et al., 2022; Zhang et al., 2022; Feng and Meng, 2024; Li and Song, 2025). The global prospective gallium reserves exceed 1 million tons, the vast majority of which are associated with bauxite deposits, mainly distributed in Africa, Oceania, South America, and Asia. Some gallium is also associated with lead-zinc deposits, mainly distributed in Austria, Canada, China, Italy, Poland, and the United States, such as the Tri State and Upper Mississippi deposits in the United States, and lead-zinc deposits in Sichuan, Yunnan, and Guizhou provinces of China (Table 2).

Table 2. Gallium resources in mainland China (modified from Feng and Meng, 2024 and Sina Finance, 2025)

Province (Autonomous region)	Gallium resources (tons)
Guangxi	11,974.80
Jiangxi	6,808.71
Guizhou	5,074.00
Shanxi	3,050.07
Xinjiang	1,045.55
Other provinces and autonomous regions combined	912.44
National total	28,865.57

Currently, global gallium reserves are about 279,300 tons, of which China has 190,000 tons, Africa 53,900 tons, Europe 19,500 tons, South America 11,400 tons, and the United States 4,500 tons (Table 2).

China has abundant gallium reserves and resources, ranking first in the world (Ning et al., 2023; Feng and Meng, 2024; Li and Song, 2025). Ga-rich bauxite is largely found in Guangxi, Henan, Guizhou, and Shanxi (91.46% of total), while Ga-rich coal occurs mainly in Shanxi, Inner Mongolia, Xinjiang, Shaanxi, and Guizhou (80.4%) provinces and/or

autonomous regions. China's super-large coal-associated gallium deposit was discovered in 2006 in Inner Mongolia. Ga-bearing zinc deposits are mainly distributed in southern provinces such as Guizhou, Yunnan, Sichuan, Hunan, Guangdong, and Jiangxi provinces and/or autonomous regions (Table 2).

3. Deposit type

3.1 Industrial type

Like most other rare metal deposits, gallium deposits in mainland China can be divided into two industrial types: independent and associated/symbiotic (Table 3). However, to date, no independent gallium deposit has been discovered worldwide, but numerous associated/symbiotic gallium deposits of different origin have been found. Over time, independent gallium deposits may be discovered, similar to those found for the rare elements tellurium and selenium (Yin and Shi, 2020; Yin, 2025), to meet the increasing demand for rare metals in human society.

3.2 Genetic type

3.2.1 Primary exogenous

Primary exogenous gallium deposits, also known as sedimentary gallium deposits, are the most important gallium resources that humans can exploit and utilize for a considerable period of time. Gallium mineralization and enrichment occur in different forms under varying physicochemical conditions. Under reducing conditions, the ionic radius of gallium in a 6-coordinate configuration is similar to that of elements such as Zn, Sn, Cu, Fe, and Sb in sulfide deposits, especially Zn. This leads to sphalerite in sulfide deposits becoming the primary enrichment carrier for gallium (Ren, 2006; Wen et al., 2020; Che et al., 2022; Zhang et al., 2022; Feng and Meng, 2024; Li and Song, 2025). Under oxidizing conditions, the geochemical properties of gallium are similar to those of aluminium and iron, especially aluminium, exhibiting strong lithophile properties, which allows gallium to participate extensively in various mineralization processes.

The most industrially significant associated/symbiotic gallium deposits in mainland China include three types: bauxite type (Luo et al., 2023), lead-zinc type (Deng et al., 2002), and coal type (Bai et al., 2007; Qin et al., 2009; Ding et al., 2023; Ning et al., 2023) (Table 3). These are described below.

3.2.1.1 Bauxite-type gallium deposit

According to the U.S. Geological Survey in 2024 (Li and Song, 2025; Xinlang Finance, 2025), global bauxite resources are estimated at between 55 billion and 75 billion tons, with a gallium metal exceeding 1 million tons, and are currently being utilized comprehensively. Global bauxite deposits are mainly distributed between 30°N and 30°S latitude in Africa (32%), Oceania (23%), South America and the Caribbean (21%), Asia (18%), and other regions (6%).

Table 3. Type and characteristics of gallium deposits in mainland China

Deposit type					Dominant deposit type/characteristics	Representative gallium deposit	Data source
Industrial	Genetic						
Independent	associated/symbiotic	Primary	Endogenous	Greisen	Ga-containing mica.	Less	Wen et al., 2020
				Pneumatolytic-hydrothermal	Nb, Ta-bearing alkaline granite	Ga-containing mica and feldspar	Dasongpo, Tengchong, Yunnan, China
					Pb-Zn polymetallic sulfide deposit	Ga-containing sphalerite	Fankou and Honggou Pb-Zn deposits in China
					Pyrite-type Cu deposit	Ga-containing sphalerite and chlorite	Northwest China
					Alunite deposit	Ga-containing alum stone	The Fanshan deposit, Zhejiang, China
					MVT	Including Pb, Zn, Cu, Ag, Ga, and As	Carbonatite Pb-Zn Deposit
				Intrusive	V, Ti magnetite deposit	Ga-containing titanium magnetite	Panzhihua V-Ti magnetite deposit
					Alkaline complex	Ga-containing nepheline	Less
				Pegmatite	Rare metal granite pegmatite	Ga-containing spodumene, lepidolite, feldspar	Pegmatite in Jiangxi, China
					alkaline granite pegmatite	Ga-containing nepheline, biotite, zeolite, feldspar	Less
				Metamorphic	Mica schist	Mica schist	Luozha complex in southern Tibet, China
			*PSH	Bauxite	Boehmite	Ga-containing boehmite	Guangxi, western Henan and Guizhou, China
			**EEM	SPCB***	Ga-Nb-REEs	Secondary paleoweathered basalt in Yunnan-Guizhou, China	
				Metamorphosed coal		Ga-containing coal	Shanxi, Inner Mongolia, China
			Exogenous	Sedimenary	Sedimentary iron deposit	Ga-containing hydroxide	Metamorphosed sedimentary Fe-bearing quartzite
					Bauxite deposit	Ga-containing boehmite	Guangxi, western Henan and Guizhou, China
					Coal	Ga-containing boehmite and kaolinite, etc.	The Junggar coal deposit in Inner Mongolia, China
					CCGMT*****		Yunnan and Guizhou, China
		Secondary	Sediment				

Note: *PSH - Primary secondary hybrid (joint) transitional type; **EEM - Endogenous-exogenous mixed (combined) transitional type; SPCB***: Secondary paleoweathering crust-type gallium polymetallic deposits in basalt; CCGMT*****: Carbonate-clay gallium multimetallic type.

Most bauxite deposits are lateritic and located in equatorial regions such as Guinea, Australia, Brazil, and India. Guinea holds the largest share of global reserves, followed by Vietnam, Australia, Brazil, and Jamaica, while China—mainly with karst-type bauxite—has smaller reserves and relies on imports for gallium production, making it sensitive to global market fluctuations.

Bauxite forms through weathering in warm, humid climates and contains 20-80 μg/g gallium (about 59 μg/g on average). Over 90% of primary gallium is recovered during alumina production. Due to similar geochemical behavior, gallium and aluminium accumulate together in bauxite, with gallium mainly substituting for aluminium in minerals such as gibbsite, diaspore, and boehmite. The Al/Ga ratio is commonly used to indicate enrichment.

Bauxite is classified as karst and/or lateritic. Karst bauxite contains 20-80 μg/g gallium, while lateritic bauxite contains 40-80 μg/g. Gallium is typically adsorbed in lateritic bauxite and may occur as GaO(OH) in karst bauxite, though overall contents are similar.

Gallium content in bauxite is generally 50-250 μg/g, 3-16 times higher than the crustal Clarke value of gallium. China's bauxite deposits are predominantly sedimentary, followed by cumulate, with lateritic bauxite being the least common. In bauxite dominated by gibbsite, gallium content is almost universally at industrial grade. These bauxite deposits were formed during the Carboniferous and Permian periods and are widely distributed in Shanxi, Guizhou, and Guangxi provinces and/or autonomous regions. Gallium content in western Henan bauxite ranges from 50-250 μg/g, with gibbsite being the primary gallium-bearing mineral, followed by kaolinite and iron-titanium minerals. Gallium grade in Guizhou bauxite is generally 122-127 μg/g, and the ore-bearing rock series is a combination of bauxite, along with iron ore, pyrite, refractory clay, and coal.

Regarding the origin of gallium in bauxite, Lu et al. believe that gallium in North China bauxite mainly originates from ancient continental aluminosilicate rocks rather than from the underlying carbonate basement (Zhao et al., 2017). Conversely, Wu believes that gallium mainly originates from the basement carbonate rocks (Zhang et al., 2022). Liu believes that gallium in Guizhou bauxite mainly originates from the argillaceous material in ancient island silicate rocks and basement carbonate rocks. In silicate rocks, gallium mainly substitutes for aluminium in feldspar. Feldspar easily transforms into kaolinite during lateritic transformation, with Ga and Al entering the kaolinite lattice together, and a small portion entering gibbsite. During weathering, the properties of gallium depend almost entirely on the solubility of kaolinite and gibbsite. In weathering solutions, Ga and Al generally exist in the forms of $Ga(OH)_3$ and $Al(OH)_3$. When the pH is 3-7, $Ga(OH)_3$ is more soluble than $Al(OH)_3$. During lateritic alteration, large quantities of gibbsite and kaolinite are formed in the acidic medium, resulting in significant iron loss, while Ga and Al remain stable within the residual weathered minerals. Most sedimentary bauxite deposits are formed by the transport and deposition of lateritic weathering crusts. Because gallium is more easily leached than aluminium, the upper Ga migrates downwards and accumulates in the lower honeycomb and earthy ores. This is likely why most gallium in western Henan bauxite deposits is hosted in earthy and honeycomb ores.

In a sense, this type of symbiotic/associated bauxite-type gallium deposit should be considered a mixed or transitional type of primary exogenous and secondary exogenous gallium deposits.

3.2.1.2 Coal-type gallium deposit

Presumably due to the adsorption of gallium by carbon, numerous studies (Bai et al., 2007; Qin et al., 2009; Ding et al., 2023; Ning et al., 2023; Feng and Meng, 2024; Li and Song, 2025) have shown that, although commercial gallium mining in coal mines has not yet been achieved due to technological limitations, Coal deposits contain over 10 million tons of gallium (industrial grade ~50 μg/g), with several super-large deposits identified in Inner Mongolia and Shanxi of China.

Gallium occurs in both inorganic and organic forms, mainly substituting in aluminium-bearing minerals like boehmite and kaolinite, though it can also be hosted in minerals such as illite, sphalerite, and feldspar. It is less abundant in organic matter and mainly associated with vitrinite.

Recovery is typically from coal combustion fly ash, but due to environmental concerns, low concentrations, and high costs, only China has achieved pilot-scale extraction. Thus, coal-hosted gallium is considered a potential future resource.

The industrial grade of gallium deposits in coal mines is 30 μg/g, while the gallium content in coal is generally 10-30 μg/g. Dai et al. (2006) reported gallium contents as high as 30-70 μg/g in the Junggar coalfield in Inner Mongolia, making it one of the newly discovered super-large gallium deposits in recent years.

The primary Ga-bearing mineral, gibbsite, was formed during peat accumulation when trihydrate colloidal solutions from ore-bearing weathered crust-type bauxite uplifted in the northern part of the basin were transported short distances into the peat swamp. It was dehydrated and coagulated through compaction during the peat accumulation stage and early diagenesis.

In some highly metamorphosed coals (such as the Daqingshan coalfield in Inner Mongolia), gallium is carried by gibbsite and kaolinite. To some extent, this associated/symbiotic coal-type gallium deposit is a mixed or transitional type of primary exogenous (sedimentary) and primary endogenous (metamorphic) gallium deposit.

3.2.1.3 Sediment-hosted massive sulfide type

Sphalerite can contain 0.01%-0.02% gallium, making lead-zinc deposits an important source, though actual recovery is limited by current technology. Gallium content is higher in low-temperature sphalerite (100-1000 μg/g) and much lower in high-temperature forms (<10 μg/g), and it may also occur in pyrite. Industrially, gallium is often recovered as a by-product of zinc sulfide processing.

Gallium content varies by deposit type, averaging 42 μg/g in Mississippi Valley-type (MVT) and 19 μg/g in volcanic-hosted massive sulfide (VHMS) deposits, with lower levels in other types. Although MVT and VHMS deposits make up a relatively small share of global lead-zinc resources, they are significant sources of gallium due to their higher concentrations.

3.2.2 Primary endogenous type

3.2.2.1 Volcanic-hosted massive sulfide type

Global zinc reserves are estimated at 1.9 billion tons, primarily located in Australia, China, Russia, and Peru. Despite these vast reserves, progress in extracting and utilizing gallium from zinc ore has been slow. Canada, Japan, Slovakia, and the United States have long recovered gallium from zinc scrap, and China has also begun recovering gallium from zinc smelting by-products. The main metallic minerals in lead-zinc deposits, such as galena, pyrite, and pyrrhotite, generally have very low gallium content, while sphalerite has higher levels, indicating that sphalerite is the most important Ga-bearing mineral. Not all lead-zinc deposits are Ga-rich. Magmatic lead-zinc deposits have very low gallium content. Ga-rich lead-zinc deposits are mostly hydrothermal sedimentary and/or sedimentary-modified types, such as the Fankou and Taolin deposits in mainland China, where the ore contains 30-60 μg/g of gallium, and the sphalerite contains more than 100 μg/g of gallium. These types of deposits generally have lower mineralization temperatures, and the sources of ore-forming materials are more complex than those of magmatic-hydrothermal deposits. Although gallium is chalcophilic, the fact that it is selectively enriched in certain deposits of a particular genetic type of lead-zinc deposit indicates that gallium enrichment in lead-zinc deposits is subject to more complex controls. The gallium content in MVT-type lead-zinc deposits varies considerably. For example, in the Fule deposit in the Sichuan, Yunnan, and Guizhou lead-zinc ore clusters, the gallium content in sphalerite ranges from 4.8 to 358 μg/g, with an average of 87 μg/g.

3.2.2.2 Metamorphosed (superimposed) type

This is a newly discovered symbiotic/associated gallium deposit. Located in the eastern Himalayan belt, the Lhozha magmatic-metamorphic complex intrudes into the southern Tibetan detached system (Gao et al., 2023). On the northeastern side of the intrusion, mica schist is xenografted by tourmaline-bearing leucogranite. The mica schist, mainly composed of phlogopite, chlorite, and minor biotite, contains high levels of Al_2O_3, K_2O, total FeO, MgO, and TiO, and is enriched in key metals such as Li, Rb, Cs, Ti, and Ga. Single-mineral chemical analysis indicates that the phlogopite in the mica schist is similar to that in the whole schist, also enriched in Li-Rb-Cs-Ga. These critical metals substitute for K in the phlogopite in isomorphous forms. Zircon geochronology results show widespread clastic ages and Cenozoic metamorphic events in the area. Previous studies suggest that the mica schist in the Lhozha area, originally a sedimentary rock, was xenografted and underwent low-grade metamorphism during the emplacement of the leucogranite.

The enrichment of rare metals thallium and gallium in metamorphosed sedimentary rocks of the Himalayan orogenic belt indicates that this region is expected to become one of the most important potential areas for the future mining of critical metals such as rare elements in mainland China. Globally, there is a need to strengthen the investigation and research on the mineralization potential of the critical metals in metamorphosed sedimentary rocks of all orogenic belts.

Other known gallium deposits associated with metamorphism include carbonate clay-type lithium-gallium-rare earth deposits (Wen et al., 2020a; Ma and Chen, 2024). However, current research on these deposits is still inadequate, and therefore, little is known about them thus far.

3.2.3 Secondary exogenous type

These gallium deposits include the weathered and eroded residual bauxite type and karst type mentioned above. These associated/symbiotic bauxite gallium deposits are not formed by a single mineralization process, but rather by a combination of secondary and primary geological processes; therefore, they are also referred to in this paper as combined and/or mixed transitional types (Table 3).

3.2.4 Primary/secondary and/or mixed endogenous/exogenous type

3.2.4.1 Carbonate-clay gallium multimetallic type (CCGMT)

The CCGMT deposit is characterized by its large mineralization scale, stable distribution, and low development and utilization costs (Wen et al., 2020a). Newly discovered clay-type lithium-REE polymetallic mineralized claystone strata in southwestern China include the Lower Carboniferous Jiujialu Formation (C1j) in Guizhou province and the Lower Permian Daoshitou Formation (P1d) in central Yunnan province. C1j, formed in the early to middle Early Carboniferous, is a lithological assemblage dominated by claystone, accompanied by bauxite claystone, ferruginous claystone, bauxite, and pyrite, with localized coal seams. It is an important bauxite-bearing stratum in Guizhou Province, China. P1d, formed in the Early Permian, is a coastal-lacustrine sedimentary assemblage consisting of sandstone and shale interbedded with limestone lenses, bauxite, and low-quality coal seams, generally 5-20 m thick, mainly distributed in the Kunming, Yuxi, Wuding, and Yiliang areas of central Yunnan. C1j and P1d claystones are classified into four types, developing from bottom to top: ① incompletely weathered iron-aluminous claystones during sedimentation and diagenesis, hard in texture and with high iron content; ② dense massive aluminous claystones; ③ oolitic aluminous claystones; ④ loose, earthy claystones, with strong near-surface weathering and leaching (Wen et al., 2020a).

In carbonate clay-type Li-Ga-REE deposits developed in the Yunnan-Guizhou provinces of mainland China, the ore-forming materials of Li-rich claystones have a relatively singular source, possibly originating from underlying impure carbonate rocks (Wen et al., 2020a; Wen et al., 2022). Due to limitations in mining conditions and extraction technology, the resources in carbonate clay-type lithium-gallium-rare earth deposits cannot yet be converted into reserves and cannot be truly put into production (Wang et al., 2022).

Studies of different types of Ga-rich deposits show that gallium generally tends to be enriched in a few specific minerals. In bauxite-type deposits, gallium is hosted in gibbsite; in lead-zinc ore-type deposits, gallium is mainly enriched in sphalerite; and in coal-type deposits, gallium is mainly found in gibbsite and diaspore. This seems to indicate that gallium enrichment has obvious mineralization specificity and mineral specificity.

3.2.4.2 Secondary paleoweathered crust-type gallium polymetallic deposits in basalt

The secondary paleoweathered crust of the basalts at the base of the Xuanwei Formation in the Yunnan-Guizhou region, located within the western and eastern metallogenic belts of the Upper Yangtze, is generally rich in metals such as niobium, rare earth elements, and gallium, all reaching industrial grades. This constitutes a rare metal enrichment layer, where rare earth elements and rare metals coexist, possessing enormous resource potential and significant economic value (Wen et al., 2020a).

The origin of the ore-forming materials in the Xuanwei Formation's niobium-gallium-rare earth deposits has been a long-standing point of contention in academic circles. The main viewpoints suggest: ① originating from the Kangdian Paleoland; ② from the acidic rocks at the top of the Emeishan Igneous Province beneath the Xuanwei Formation; ③ from the mixing of volcanic ash and hydrothermal fluids.

The Yunnan-Guizhou region possesses numerous areas of exceptionally high enrichment in rare earth elements and dispersed elements (Wang et al., 2020). Furthermore, this region widely distributes high-titanium, alkali-rich basalts, providing a rich ore-forming basis. Studies have shown that during the period of 257.2-254.6 Ma, claystones rich in rare and rare earth metals originated from the erosion zone within the Emeishan Large Igneous Province, and their metallic minerals mainly came from syenite, with a small amount from high-Ti basalt and felsic igneous rocks (Tian et al., 2023).

4. Gallium prospective area in mainland China

In recent years, with the development and advancement of detection technology, new Ga-rich deposits and/or mineralized areas have been continuously discovered. For example, gallium enrichment has been found in metamorphosed sedimentary rocks of the Himalayan orogenic belt. Furthermore, according to a report from China's Ministry of Natural Resources, a super-large rare earth metal weathered crust deposit containing 10,818 tons of gallium has been discovered in southern Yunnan, China.

It should be noted that although many gallium deposits have been discovered, very few actually meet the economic and technical standards for exploitation.

Researchers have concluded that the extraordinary enrichment of indium, germanium, gallium, niobium, and rare earth elements on the western margin of the Yangtze Plate in China has a certain material basis and internal mechanism, and have systematically proposed a "supergene weathered-sedimentary rare metal mineralization system," constructing a mineralization model for rare metals.

5. Discussion

Known gallium mineralization in mainland China exhibits diverse genetic and industrial types, including primary and secondary, exogenous and endogenous processes. There are also transitional and/or combined types formed by the combined effects of endogenous and exogenous, primary and secondary processes. Generally, one type initially enriches gallium, followed by further enrichment into mineralized deposits by subsequent geological

mineralization. In other words, its mineralization is characterized by multiple phases and stages, rather than being formed overnight by a single mineralization process.

The combined and superimposed alteration by weathering, erosion, sedimentation, igneous activity, and metamorphism is a major characteristic of gallium mineralization in mainland China. Because of this, it is sometimes difficult to classify a specific gallium mineralization into a particular genetic type, as they are often the result of the combined superposition of multiple geological processes from different geological periods.

Currently, most known gallium mineralization in China, especially the newly discovered ones, are concentrated in western China, particularly the Qinghai-Tibet Plateau and its surrounding areas. In other words, large-scale orogenic movements are the primary driving force behind the enrichment of numerous rare metals, including gallium, and rare earth element metals. An orogenic process often involves various scales and types of tectonic activity—igneous activity, metamorphism, sedimentation, and weathering and erosion. This is one of the main reasons why gallium mineralization is associated with multiple geological processes.

The known types of associated/symbiotic gallium deposits in mainland China, especially the genetic types newly discovered in the last two years, offer important insights for finding similar genetically derived gallium deposits in other parts of the world.
It is believed that in the near future, mainland China may be the first to discover independent gallium deposits in the Qinghai-Tibet Plateau and its surrounding areas, just as independent tellurium and selenium deposits were first discovered in the country (Yin and Shi, 2020; Yin, 2025).

Environments with multiple overlapping geological processes are most likely and suitable for occurrence in various orogenic belts. Therefore, orogenic belts are primary prospective areas for finding gallium and other rare metal deposits.

6. Conclusions

Globally known gallium deposits, especially associated/symbiotic gallium deposits, exhibit a wide variety of genetic types. The formation of these deposits is related to almost all known geological processes, such as orogenic movements, igneous magmatic activity, sedimentation, metamorphism, and even weathering and erosion.

Upon closer examination, the formation of many associated/symbiotic gallium deposits is not the result of a single geological process, but rather the result of two or more combined processes. Often, the first geological process initially enriches the associated/symbiotic gallium mineralization, and on this basis, a second and subsequent series of geological processes further enrich and modify the gallium mineralization. In other words, the economically viable mining scale of rare metals like gallium is the result of the combined enrichment by two or more geological processes.

In many cases, the mineralization of rare metals, including gallium, is the result of the combined effects of primary/secondary and exogenous/endogenous geological processes, rather than simply the result of one or a few endogenous mineralization processes.

For the enrichment of rare metals, the boundary between endogenous and exogenous mineralization is no longer clear. This is because the abundance of these metals in the Earth's crust is so low that they are difficult to concentrate into mineral deposits without a combination of endogenous and exogenous, or even primary and secondary, processes. For these reasons, orogenic belts are the optimal geological settings for finding mineralized zones of rare metals such as gallium.

References

01. Bai XF, Li WH, Chen YF and Jiang Y. 2007. Basic characteristics of trace element distribution in coal in China. *Coal Quality Technology*, (1): 1-4 (in Chinese with English abstract).
02. Che D, Zhang ZZ, Pan ZS and Xing EY. 2022. Status of rare and dispersed element minerals in strategic emerging industries and prediction of consumption demand. *Mining Research and Development*, 42 (12): 208-217 (in Chinese with English abstract).
03. Dai SF, Ren DY and Li SS. Discovery of super-large gallium deposit in Junggar, Inner Mongolia. *Science Bulletin*, 2006, 51 (2): 177-185 (in Chinese with English abstract).
04. Deng W, Liu ZD, Yang HY and Liu RD. 2002. Germanium and gallium resources and recovery in Fankou lead-zinc mine. *Nonferrous Metals*, (1): 54-57 (in Chinese with English abstract).
05. Ding GF, Lü ZF and Cao JC. 2023. Research progress on comprehensive utilization of coal-based gallium resources. *Comprehensive Utilization of Minerals*, (3): 119-126 (in Chinese with English abstract).
06. Feng QW and Meng YM. May 2, 2024. A national sentiment of gallium, though scattered, abundant in reality. https://mp.weixin.qq.com/s?__biz=MzUyMzM2ODkxNg==&mid=2247495245&idx=1&sn=2cef02758264f5feb78586cacaab9744&chksm=fbc8ce72a8bbc2a019d2c75839e064a767d02a1905eaa9d7ffe728c2884ea510c8a233f75a00&scene=27# (in Chinese). Trieved January 21, 2026.
07. Gao L, Zeng LS, Zhao LH, Yan LL, Li GG, Di YL, Xu Q, Wang YY, Wang HT and Tian YH. 2023. Metamorphic critical metal deposits—mica schist enriched in Li-Rb-Cs-Tl-Ga. *Journal of Petrology and Mineralogy*, 42 (1): 29-46 (in Chinese with English abstract).
08. Gunn G. 2014. *Critical Metals Handbook*. John Wiley & Sons.
09. Li DX and Wang J. 2020. Gallium—an emerging strategic mineral resource. *Popular Science and Culture of Natural Resources*, (04): 20-22. https://www.cgsjournals.com/article/id/gtzykpywh_GTKW202004005 (in Chinese). Trieved January 21, 2026.
10. Li HG and Song YY. March 3, 2025. The Magical and Precious "Gallium". *China Mining News*. https://www.pecmnr.cn/mobile/news.html?aid=5310689 (in Chinese). Trieved January 21, 2026.
11. Luo PQ, Fu Y, Tang B, Yao L, Liu GD, Pan ZF, Long Z and Liu Y. 2023. Distribution patterns, mineralization mechanisms and prospecting directions of gallium deposits in China. *Acta Geologica Sinica*, 44 (4): 599-624 (in Chinese with English abstract).
12. Ma Y and Chen XH. 2023. Progress in metallogenic theory and exploration of key rare minerals in my country. *Acta Geologica Sinica*, 97 (10): 3475-3492, DOI: 10.19762/j.cnki.dizhixuebao.2023363 (in Chinese with English abstract).

13. Ning SZ, Huang SQ, Yan XY, Dai GB, Zhu SF, Xu Q, Xu XT, Zhang L and Liu K. 2023. Prospects and research directions of coal-based germanium and gallium resources in my country. *China Mining*, 32 (11): 1-11 (in Chinese with English abstract).
14. Qin Y, Wang WF, Cheng AG, Liu XH and Zhao JL. 2009. Metallogenic prospects of gallium in coal in the first batch of nationally planned coal mining areas. *China Coal Geology*, 21 (1): 17-21+26 (in Chinese with English abstract).
15. Ren DY. 2006. *Trace Element Geochemistry of Coal*. Beijing: Science Press (in Chinese with English abstract).
16. Tu GZ, Gao ZM and Hu RZ. 2004. *Geochemistry and Mineralization Mechanism of Dispersed Elements*. Beijing: Geological Publishing House (in Chinese with English abstract).
17. Wen HJ, Zhu CW, Du SJ, Fan Y and Luo CG. 2020. Gallium (Ga), germanium (Ge), thallium (Tl) and cadmium (Cd) resources in China. *Chinese Science Bulletin*, 65 (33): 3688-3699. DOI: https://doi.org/10.1360/TB-2020-0267 (in Chinese with English abstract).
18.Xinlang Finance. July 25, 2025. https://baijiahao.baidu.com/s?id=1838601213875438733&wfr=spider&for=pc (in Chinese). Trieved January 23, 2026.
19. Yin JZ. 2025. Geology of the primary selenium deposits in Mainland China. *Naturalis Scientias*, 2 (1): 364-376. DOI: https://doi.org/10.62252/NSS.2025.1025. www.naturalisscientias.com.
20. Yin JZ and Shi HY. 2020. Mineralogy and Stable Isotopes of Tetradymite from the Dashuigou Tellurium Deposit, Tibet Plateau, Southwest China. *Sci Rep* 10, 4634. DOI: https://doi.org/10.1038/s41598-020-61581-3.
21. YiruShufang. November 2, 2024. Gallium, a strategic mineral in China. http://www.360doc.com/content/24/1102/17/40066813_1138311271.shtml (in Chinese). Trieved January 21, 2026.
22. Zhang LM, Zhang H, Liang Q, Wang XQ, Yu WL and Yan HY. Distribution and development of gallium resources and reflections on the development of gallium industry in China. *Mineral Exploration*, 2022, 13 (8): 1235-1240 (in Chinese with English abstract).
23. Zhao T, Qin PZ, Wang AJ, Wang GS, Li JW, Liu C and Liu YF. Analysis of gallium resource demand trend and reflection on the development of China's gallium industry. *Acta Geologica Sinica*, 2017, 38 (1): 77-84 (in Chinese with English abstract).

Data availability

The data that support the findings of this study are available from the author upon reasonable request.

Declaration of competing interest

The author declares that he has no competing financial interests or personal relationships that could have appeared to influence the work reported in this paper.

Use of AI tools declaration

The author declares that he has not used Artificial Intelligence (AI) tools in the creation of this article.

Original Article

A Theoretical Analysis of Dollar-Cost Averaging Under Different Index Price Trajectories

-- Mathematical Conditions, Price Trajectories, Volatility, Recovery, and Investor Behavior

Deliang Shi[1] Ⓛ

Abstract

Dollar-cost averaging (DCA) is the practice of investing a fixed dollar amount at regular intervals regardless of the current market price. This paper develops a simple theoretical framework for DCA under different index price trajectories. The analysis begins with a break-even condition: for a completed DCA program to be profitable at liquidation, the final asset price must exceed the investor's average cost per share. For equal-dollar contributions, this average cost is the harmonic mean of the purchase prices. The paper then examines linear and exponential growth, temporary declines followed by recovery, irregular market paths, and permanent impairment. A key clarification is made between profit as a percentage of cumulative contributions and an annualized money-weighted return. Under continuous equal-rate investing into an index that rises linearly from 100 to 110 over one year, ending wealth is approximately 1.0484 times total contributions, a 4.84% gain on contributed capital; this should not be called a 4.84% annualized return because the contributions were invested for different lengths of time. The framework further shows why DCA can benefit from temporary price weakness if recovery occurs, while permanent deterioration remains destructive. The practical implication is that long-term DCA is most coherent when applied to a broadly diversified asset with durable expected growth, low probability of permanent loss, and sufficient investor conviction to maintain the strategy through severe drawdowns.

Keywords: dollar-cost averaging; index investing; average cost; harmonic mean; volatility; drawdown; money-weighted return; investor behavior

---

Affiliation Info: [1] Independent Researcher, Vernon Hills, IL 60061, U.S.A.

Corresponding AurhorⓁ: Shi, D. L., PhD; Email address: deliangshi@gmail.com

Citation: Shi, D. L. 2026. A theoretical analysis of dollar-cost averaging under different index price trajectories

-- mathematical conditions, price trajectories, volatility, recovery, and investor behavior. *Naturalis Scientias*, 3: 676-685. DOI: https://doi.org/10.62252/NSS.2026.1038. www.naturalisscientias.com.

Copyright © 2026 by the author. Published by *Naturalis Scientias*. This is an open access article under the Creative Commons Attribution-NonCommercial 4.0 International (CC BY-NC 4.0) License. (https://creativecommons.org/licenses/by-nc/4.0/).

---

1. Introduction

Dollar-cost averaging is widely used in retirement plans and other periodic investment programs. Its defining feature is not an attempt to forecast short-term prices, but a rule: invest a fixed dollar amount on a predetermined schedule. Because a fixed contribution purchases more shares when prices are low and fewer shares when prices are high, DCA creates a distinctive relationship between the path of prices and the investor's accumulated cost.

This analysis begins with two observations. First, a DCA program is profitable at a chosen terminal date when the terminal price exceeds the accumulated average cost. Second, the psychological feasibility of continuing to invest depends heavily on confidence that the underlying asset can survive declines and resume long-term growth. To connect the mathematics with investment behavior, price histories are organized into five intuitive cases: an ideal low-buy/high-sell path, exponential growth, linear growth, irregular real-world behavior, and a best practical case involving a long-term-growing index with a low probability of permanent loss.

The framework combines intuitive price-path reasoning with formal mathematics. In particular, it distinguishes (i) gain relative to cumulative contributions, (ii) time-weighted asset return, and (iii) money-weighted investor return. This distinction matters because periodic contributions enter the market at different dates.

2. Mathematical framework

2.1 Equal-dollar periodic investment

Suppose an investor contributes the same amount C at n purchase dates. Let P_i denote the asset price at purchase i. The number of shares purchased at that date is $\frac{C}{P_i}$. Total shares accumulated are therefore:

$$Q = C \sum_{i=1}^{n} \frac{1}{P_i}$$

Total contributed capital is nC. The investor's average cost per share is:

$$P_{avg} = \frac{nC}{Q} = \frac{n}{\sum_{i=1}^{n} \frac{1}{P_i}}$$

Thus, for equal-dollar contributions, the average cost per share is the harmonic mean of the purchase prices. It is generally not the arithmetic mean.

2.2 Break-even and profit condition

Let P_f be the terminal price at which the accumulated position is valued or liquidated. Terminal wealth is QP_f, and profit is $QP_f - nC$. Since $nC = QP_{avg}$:

$$Profit = Q(P_f - P_{avg})$$

Therefore:

$$Profit > 0 \quad \Leftrightarrow \quad P_f > P_{avg}$$

This break-even relation is a terminal accounting identity, not a forecast that DCA must be profitable.

3. Linear growth: The 10% one-year example

Consider an index that begins at 100 and rises linearly to 110 over one year. Let t range from 0 to 1:

$$P(t) = 100(1 + 0.1t)$$

Assume contributions occur continuously at a constant rate and normalize total annual contributions to 1. The shares accumulated are:

$$Q = \int_0^1 \frac{dt}{100(1 + 0.1t)} = \frac{ln(1.1)}{10}$$

At the year-end price of 110, ending wealth is:

$$V = 110Q = \frac{110\ ln(1.1)}{10} \approx 1.04841$$

Hence the investor has approximately 4.84% more wealth than cumulative contributions. A rough midpoint estimate gives about 4.5%-5%; the continuous-contribution calculation gives 4.84% under these assumptions.

3.1 Why 4.84% is not an annualized return

Calling 4.84% an 'annual return' is potentially misleading. The first contribution is invested for almost the full year, while the last contribution is invested for almost no time. Dividing terminal profit by all contributions treats every dollar as though it had the same investment horizon.

A money-weighted return (IRR or XIRR, i.e. Internal Rate of Return or Extended Internal Rate of Return) accounts for the timing of each cash flow. If the asset follows a smooth return process consistent with a 10% annual return, the properly annualized investor return will be close to the asset's annual return; the lower 4.84% figure mainly reflects the fact that the average dollar was invested for only part of the year, as shown in Table 1.

Table 1: Index return vs DCA return

Measure	Approximate result	Interpretation
Index start-to-end return	10.0%	100 → 110
DCA gain / total contributions	4.84%	Ending wealth relative to all cash contributed
Annualized investor return	≈ underlying annual rate*	Must account for cash-flow timing

*Exact money-weighted return depends on the timing convention and discrete versus continuous contributions.

4. Linear versus exponential growth

A linear path adds a constant absolute amount over equal time intervals, whereas an exponential path compounds. For example, a 10% compounded process generates 100, 110, 121, 133.1, and so on, while a simple linear path might generate 100, 110, 120, 130. Over short intervals, exponential growth can be approximated by a linear function because $e^x = 1 + x$ for small x. Over long horizons, however, compounding creates increasingly large differences.

A broad equity index may therefore look approximately linear over a short interval, while long-run wealth accumulation is better understood through compounded growth. Actual index prices, however, are stochastic and are neither linear nor smoothly exponential.

5. Five price-trajectory cases for DCA

The five cases below separate mathematical attractiveness from psychological investability. The ideal mathematical path is not necessarily the easiest path to hold. A steadily rising market builds confidence but raises later purchase prices; a volatile market may create attractive purchase opportunities but tests investor conviction. The most useful long-term case therefore combines durable growth, recoverability after drawdowns, and a low probability of permanent loss (Figure 1).

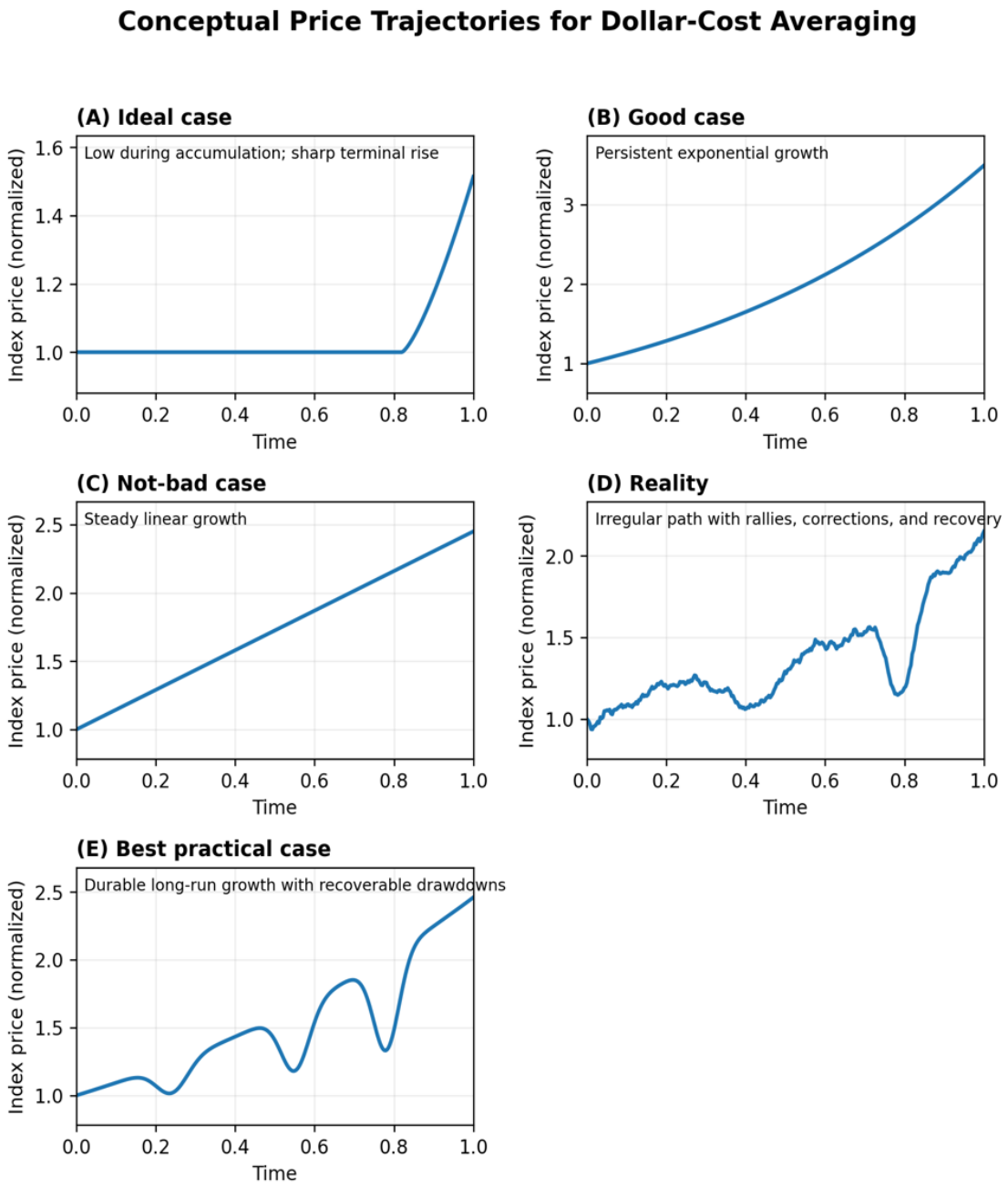


Figure 1. Five conceptual price trajectories for dollar-cost averaging. The curves illustrate qualitative investment cases rather than observed market data

5.1. Ideal case: buy very low, exit very high, as shown in Figure 1A

The mathematically attractive path is one in which most contributions occur at depressed prices and the terminal price is very high. Such a path maximizes shares accumulated per contributed dollar. Its weakness is behavioral and informational: a long period of low prices

can make it difficult to know whether the asset is temporarily undervalued or permanently impaired.

5.2. Good case: persistent exponential growth, as shown in Figure 1B

A steadily compounding asset reinforces investor confidence because new highs occur repeatedly. The disadvantage for DCA is that later contributions buy fewer shares. Nevertheless, a sufficiently high terminal price can dominate the higher purchase costs and produce strong long-run wealth accumulation.

5.3. Not-bad case: linear growth, as shown in Figure 1C

A steadily rising linear path has similar behavioral advantages but lacks the accelerating terminal value produced by compounding. Over a short horizon this can be a useful approximation; over long horizons it understates the economic significance of compound growth.

5.4. Reality: irregular and difficult to predict, as shown in Figure 1D

Actual markets combine rallies, corrections, crashes, recoveries, plateaus, and regime changes. The important question for DCA is therefore not whether the path is smooth, but whether the asset's long-run economic value and terminal price are sufficiently resilient relative to the investor's accumulated cost.

5.5. Best practical case: durable growth with low permanent-loss probability, as shown in Figure 1E

For a long-horizon investor, the most favorable practical target is a diversified asset with durable expected growth and a low probability of permanent destruction of capital. This condition is also behavioral: an investor who believes the asset can survive severe drawdowns is more likely to continue buying when DCA mathematically benefits most from lower prices.

6. Volatility, recovery, and the central asymmetry of DCA

DCA has an important asymmetry: temporary declines can be beneficial if they are followed by recovery, but permanent declines are harmful. The mechanism is mechanical.

When price falls, a fixed contribution purchases more shares. If the price later recovers, those low-cost shares contribute disproportionately to terminal wealth.

6.1. Simple recovery example

Table 2: recovery example

Stage	Price	Contribution	Shares purchased
Purchase 1	$100	$1,000	10
Purchase 2	$50	$1,000	20
Terminal valuation	$100	—	30 shares × $100 = $3,000

As shown in Table 2, total contributions are $2,000 and terminal wealth is $3,000, a 50% gain relative to contributed capital, even though the asset's start-to-end price return is 0%. This does not mean volatility automatically creates value. The result depends critically on the recovery to 100, as shown by the blue line in Figure 2.

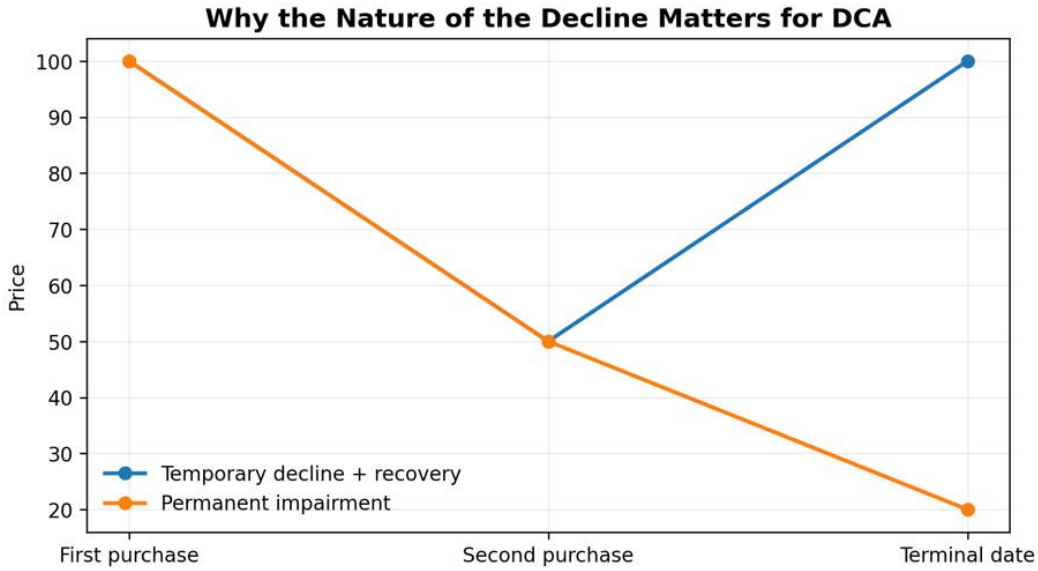


Figure 2. Temporary decline followed by recovery versus permanent impairment. Lower interim prices can improve DCA accumulation only when subsequent prices recover sufficiently. DCA can benefit from temporary price weakness, but it cannot rescue an asset from permanent impairment.

6.2. Permanent decline

If the same sequence were 100 → 50 → 20 with no recovery, the additional shares purchased at 50 would not convert the strategy into a success, as shown by the orange line in Figure 2. Repeated purchases can increase exposure to a deteriorating asset. Consequently, 'buying the dip' and DCA are only defensible when the underlying investment thesis remains valid.

7. Investor behavior and strategy persistence permanent decline

Investor confidence is a central part of the theory. A mathematically attractive strategy can fail in practice if the investor abandons it during a drawdown. DCA therefore has a behavioral dimension: a rules-based schedule may reduce the temptation to time each purchase, while diversification and confidence in the underlying asset may improve the probability that the investor continues the plan.

External research supports the relevance of this trade-off. Vanguard reports that, when an investor already possesses a lump sum, immediate lump-sum investment historically outperformed common cost-averaging approaches roughly two-thirds of the time, reflecting the opportunity cost of holding part of the capital in cash. At the same time, cost averaging may be attractive to highly loss-averse investors because it reduces initial market exposure and can make adherence easier (Finlay & Zorn, 2023).

This literature addresses a different question from paycheck-based periodic investing. When future savings are not yet available, investing each contribution as it arrives does not involve deliberately withholding an already-available lump sum. The distinction is essential when interpreting empirical comparisons between DCA and lump-sum investing.

8. Relationship to existing research

Academic research has often found that DCA sacrifices expected return relative to immediate lump-sum investment when all capital is available at the outset, because DCA delays exposure to assets with a positive expected risk premium. Knight and Mandell (1992) reported unfavorable results for DCA using analytical, historical, and Monte Carlo approaches. More recent formal work by Kirkby, Mitra, and Nguyen (2020) derives expected wealth and variance for DCA-type strategies and shows that DCA can reduce variance under suitable assumptions, but at the cost of lower expected returns.

Risk, however, is multidimensional. Trainor (2005) examined within-horizon exposure to loss and found that DCA can reduce the probability, magnitude, and duration of large interim losses relative to lump-sum investing. Thus, the choice between DCA and lump-sum investment cannot be summarized solely by average terminal return; it also depends on the investor's cash availability, loss tolerance, interim liquidity needs, and ability to maintain the strategy.

9. Refined propositions

Proposition 1 — Break-even condition. For equal-dollar DCA, terminal profit is positive if and only if the terminal price exceeds the harmonic-mean average cost of the purchased shares.

Proposition 2 — Contribution return is not annualized return. Profit divided by cumulative contributions is a useful accounting measure but is not a valid annualized return when contributions occur at different dates.

Proposition 3 — Path dependence. For a fixed terminal price, the sequence of intermediate prices affects the number of shares accumulated and therefore affects terminal DCA wealth.

Proposition 4 — Temporary weakness can help. Holding other factors constant, lower intermediate purchase prices can improve terminal DCA wealth when the asset subsequently recovers.
Proposition 5 — Permanent impairment dominates averaging. DCA cannot transform a permanently deteriorating asset into a sound investment merely by lowering average cost.
Proposition 6 — Asset selection and persistence are linked. A long-term DCA program is most robust when the underlying asset is sufficiently diversified and durable that the investor can rationally maintain contributions through major drawdowns.

10. Practical implications

The framework suggests that DCA should not be understood as a mechanism that guarantees profit or mechanically turns volatility into return. Its main mechanical benefit is the acquisition of more shares at lower prices. Whether this becomes economically valuable depends on subsequent prices.
For broad, diversified equity indexes, the rationale for long-term periodic investing is therefore stronger than for a single fragile company or a highly speculative asset. Diversification reduces idiosyncratic failure risk, while long investment horizons allow the investor to participate in economic growth. Even then, no index is guaranteed to rise, and historical resilience does not eliminate future risk.
The theory also discourages an overly simplistic preference for smooth price appreciation. A path with temporary declines may produce better DCA accumulation than a monotonic path with the same terminal price, provided recovery occurs. The key distinction is not 'volatility versus no volatility' but 'recoverable volatility versus permanent loss.

11. Practical implications

The analysis is intentionally stylized. It ignores taxes, transaction costs, dividends, inflation, bid-ask spreads, changing contribution amounts, interest earned on uninvested cash, sequence-dependent withdrawals, and stochastic changes in expected returns. The linear and exponential examples are deterministic illustrations rather than models of actual market dynamics.
Future work could test the propositions with historical total-return data for broad indexes, simulate stochastic price processes, compare monthly and biweekly contribution schedules, incorporate dividends and inflation, and measure outcomes using XIRR, terminal wealth, maximum drawdown, shortfall probability, and investor utility.

12. Conclusions

Dollar-cost averaging is best understood as a cash-flow rule whose outcome depends on both the terminal price and the path taken to reach it. For equal-dollar contributions, the relevant average purchase cost is the harmonic mean of purchase prices, and terminal profitability requires the final price to exceed that cost. In a one-year linear rise from 100 to

110 with continuous equal-rate contributions, terminal wealth is about 4.84% above cumulative contributions; this figure is not, however, the investor's annualized return.

The most important theoretical insight is the asymmetry between temporary and permanent declines. Temporary weakness followed by recovery allows fixed contributions to acquire more shares at favorable prices. Permanent impairment makes the same averaging mechanism destructive. Thus, the central requirement for a long-term DCA strategy is not the absence of volatility, but a credible basis for long-term growth and recovery. DCA benefits from recoverable weakness, but it cannot overcome permanent impairment.

References

01. Finlay M. and Zorn J. 2023. Cost averaging: Invest now or temporarily hold your cash? *Vanguard Research*.

02. Kirkby J. L., Mitra S. and Nguyen D. 2020. An analysis of dollar cost averaging and market timing investment strategies. *European Journal of Operational Research*, 286 (3): 1168–1186. https://doi.org/10.1016/j.ejor.2020.04.055.

03. Knight J. R. and Mandell L. 1992. Nobody gains from dollar cost averaging: Analytical, numerical and empirical results. *Financial Services Review*, 2 (1): 51–61. https://doi.org/10.1016/1057-0810 (92)90015-5.

04. Trainor W. J. Jr. 2005. Within-horizon exposure to loss for dollar cost averaging and lump sum investing. *Financial Services Review*, 14 (4). https://doi.org/10.61190/fsr.v14i4.4835.

05. Vanguard. 2026. The truth about cost averaging. *Vanguard UK Professional*.

Data availability

The data that support the findings of this study are available from the author upon reasonable request.

Declaration of competing interest

The author declares that he has no competing financial interests or personal relationships that could have appeared to influence the work reported in this paper.

Use of AI tools declaration

The author declares that Artificial Intelligence (AI) tools were used in the preparation of this article solely for language editing, including improvements to writing clarity and grammar. All original ideas, concepts, graphs, tables, analyses, and conclusions presented in this article are solely those of the author.

Original Article

Geology and Geochemistry of the Germanium Deposits in Mainland China

Jian Zhao Yin[1] Ⓛ

Abstract

Thanks to China's unique geological settings, such as its location at the intersection of the Indian, Eurasian, and Pacific tectonic plates, it possesses a wealth of rare earth elements and rare metals, making it virtually unparalleled globally. In today's society, where cutting-edge technologies heavily rely on various critical metals, this natural advantage is highly significant. However, for various reasons, the outside world is not fully aware of many of China's dispersed metal resources. This paper introduces the uses and resource overview of germanium (Ge), one of many critical mineral resources in mainland China, and summarizes its spatial and temporal distribution within the country, classifying its industrial and genetic types, and discussing the geology and geochemistry of various associated/symbiotic Ge deposits. China has a wide variety of associated/symbiotic Ge deposits of various genesis, including endogenic igneous mesothermal-epithermal deposits, as well as skarn, porphyry, and volcanic deposits. There are also mixed igneous-aqueous hydrothermal deposits, such as volcanic-sedimentary deposits, formed by the combined effects of endogenic and exogenic geological processes. Of course, as a major coal-producing country, mainland China also possesses numerous organic and inorganic sedimentary associated/symbiotic Ge deposits, such as coal-type, phosphate-type, and bauxite-type deposits. These internal and external associated/symbiotic Ge deposits on the mainland are not completely isolated but rather mutually reinforcing. For example, organic coal-type Ge mineralization involves, to some extent, igneous magmatic activity, such as providing ore-forming materials.

Keywords: Type, germanium (Ge) mineralization, rare metal, spatiotemporal distribution, geology and geochemistry, mainland China

---

Affiliation Info: 1 College of Earth Sciences, Jilin University, Changchun 130061, China

Corresponding AurhorⓁ: Yin, J. Z., PhD, Professor, geosciences, mineral exploration and mining; Email address: jzyin7@jlu.edu.cn

Citation: Yin, J.Z. 2026. Geology and Geochemistry of the Germanium Deposits in Mainland China. *Naturalis Scientias*, 3: 686-709. DOI: https://doi.org/10.62252/NSS.2026.1039. www.naturalisscientias.com.

Copyright © 2026 by the author. Published by *Naturalis Scientias*. This is an open access article under the Creative Commons Attribution-NonCommercial 4.0 International (CC BY-NC 4.0) License. (https://creativecommons.org/licenses/by-nc/4.0/).

---

1. Introduction

As a rare carbon group element with distinct non-metallic properties, the silvery-gray metal germanium (Ge) exhibits excellent semiconductor characteristics. This physical and chemical property gives it a crucial position and wide application in modern technology (Hu et al., 2000; Zhang et al., 2017; Geological Museum, 2025; Guanyan, 2025). In 2018, Ge was listed as one of the 35 critical minerals by relevant U.S. authorities. Although Ge is widely distributed in the Earth's crust, it is extremely dispersed, leading to a scarcity of Ge deposits. The mining and extraction of Ge are quite challenging and therefore difficult to obtain. Its scarcity and unique physical and chemical properties make Ge an indispensable strategic mineral resource or critical metal in high-tech industries and future energy development.

The strategic value of Ge lies in its irreplaceable and widespread application in several key technological fields. Ge is used in various fields, including semiconductor devices in high-tech industries, high-precision infrared optical components in aerospace measurement and control, fiber optic amplifier materials in fiber optic communication, and infrared optical equipment in defense and military industries such as night vision devices, infrared thermal imagers, high-precision military lenses, infrared radar, radiation detectors, and nuclear reaction spectrometers. Ge is also a key material in solar cells. It is also a chemical catalyst with important applications in the biomedical field (Hu et al., 2000; Zhang et al., 2002; Yuan et al., 2011; Geological Museum, 2025; Guanyan, 2025).

Ge is iron-, sulfur-, lithophilic, and organic-friendly. In nature, it mainly exists in dispersed compound forms in sphalerite, enargite, silver, lead, and iron ores (Hu et al., 2000; Yuan et al., 2011; Zhang et al., 2017). Currently, Ge is mainly recovered as a by-product during the processing of sulfide ores such as lead, zinc, copper, silver, gold, and iron, and/or through comprehensive recovery and utilization from fly ash after coal combustion. Almost all coal in nature contains Ge, but only a very small number form Ge deposits; most coals contain very little Ge (Ao et al., 2007; Yuan et al., 2011; Yuan et al., 2012; Zhang et al., 2017).

Lead-zinc ores with a Ge content greater than 0.001% and coal with a Ge content greater than 0.002% can be mined as Ge deposits. Global Ge resources are relatively scarce. As of 2010, the global basic reserves of Ge metal were approximately 8,600 tons (Wang, 2011; Zhang et al., 2017; Geological Museum, 2025; Guanyan, 2025). These reserves are mainly distributed in the United States (3,870 tons, accounting for 45% of the global total), China (3,526 tons, accounting for 41% of the global total), and Russia (860 tons), with the remainder distributed in countries such as Germany, Belgium, and Canada. China is the world's largest producer and exporter of Ge, supplying approximately 71% of the world's Ge consumption.

Global Ge production is highly concentrated in China, the United States, and Russia, whose combined output accounts for 75% of global production. In 2022, China's Ge production reached 151 tons, of which 130 tons were primary Ge, accounting for 86.09%. Secondary recycled Ge production was 21 tons, accounting for 13.91%. In 2023, global Ge metal

production was 138 tons, of which China produced 94 tons. Since 2004, China has been the world's largest Ge producer, playing a pivotal role in the global Ge market (Wang, 2011; Geological Museum, 2025; Guanyan, 2025). China possesses abundant Ge resources, a complete Ge industry chain, and leading smelting and separation technologies, giving it a significant competitive advantage in the global Ge market. However, China remains at the lower end of the Ge industry in terms of manufacturing and application: its production mainly focuses on the rough processing of Ge ingots and products, with development and utilization limited to primary products like Ge tetrachloride and Ge dioxide. Refining and deep processing are relatively low, and most products are exported (Zhao et al., 2019). China's output of primary Ge products accounts for more than 50% of the world's total.

While China's total Ge resources are relatively abundant, high-quality resources are scarce. China's Ge resources, especially its high-grade Ge-rich coal mines, are among the few high-quality resources in the world, with Ge often occurring alongside gallium in coal. However, due to the limited mining of the main mineral, the recovery rate of Ge is not high. The comprehensive utilization level of Ge associated with lead-zinc ores, except for a few individual deposits, is generally low.

Since China implemented an export licensing program for Ge and related mineral products on August 1, 2023 (Geological Museum, 2025; Guanyan, 2025), China's Ge exports have gradually declined over the past two years. In 2023, China's cumulative exports of Ge oxide and zirconium dioxide were 15,401 tons. Since 2024, due to shortages of lead and zinc smelting raw materials and China's export controls on Ge, the global Ge industry has experienced a persistently tight supply. Coupled with increased demand for Ge used in military infrared applications, satellite solar cells, drones, photovoltaics, and optical fibers, global Ge prices have nearly doubled since the beginning of the year. As of December 20, 2024, the price of Ge ingots closed at RMB 17,750/kg (around USD $2,631/kg), an increase of RMB 8,350 (around USD $1,238) from the beginning of the year; the price of Ge dioxide closed at RMB 12,250/kg (around USD 1,816/kg), an increase of RMB 6,000 (around USD $850) from the beginning of the year.

With the development of emerging industries and the increasing demands for military informatization, global demand for Ge will continue to grow. In the infrared and fiber optic fields, Ge applications will become more widespread. The widespread application of 5G communication technology will generate substantial demand for Ge used in fiber optics. The development of emerging industries such as autonomous driving and the Internet of Things will also drive demand growth for Ge. With the intensification of geopolitical competition among major powers and the higher requirements for national defense informatization, the demand and consumption of military infrared Ge for night vision devices, detectors, infrared thermal imagers, and radar will increase significantly. Demand for Ge in fields such as biomedicine and chemical catalysts will also continue to grow (Geological Museum, 2025; Guanyan, 2025). Countries and organizations such as the United States, the European Union, Canada, Australia, and Japan have all included Ge in their critical mineral lists for strict control.

China's export controls on Ge include an export licensing system. All export activities involving Ge, including raw materials, finished products, and products containing Ge, require prior export licenses from relevant departments. After obtaining an export license,

exporting entities must comply with specific restrictions on the quantity, price, and destination of Ge exports. Relevant departments will monitor export activities throughout the entire process to ensure compliance with national requirements. For exports without a license, exports exceeding the scope of the license, or other illegal activities, China will impose administrative penalties and even pursue criminal liability according to law (Geological Museum, 2025; Guanyan, 2025).

With technological advancements and the rise of emerging industries, the demand for Ge in fields such as semiconductors, fiber optic communications, and solar cells will continue to grow. It is believed that with the continued growth of global demand over time, the Ge industry will usher in a broader prospect. With increasing environmental awareness and advancements in related recycling technologies, the recycling rate of Ge will continue to improve, thereby reducing the mining of new Ge resources, reducing environmental pollution, and achieving sustainable resource utilization.

Given the important role of Ge and the significant proportion of Ge resources in China's global reserves, this paper, based on the collection, collation, and analysis of relevant research data on Ge deposits in mainland China, classifies their industrial and genetic types and summarizes their geological and geochemical characteristics.

2. Resource overview

Ge, a dispersed element, is a silvery-gray, brittle metal with an abundance of only 0.0007% in the Earth's crust (Hu et al., 2000; Geological Museum, 2025; Guanyan, 2025). China, possessing 41% of the world's Ge resources, supplies 71% of the world's Ge products. China's Ge resources are widely distributed (Figure 1), but are mainly concentrated in 14 provinces (autonomous regions), including Yunnan, Inner Mongolia, Jilin, Guizhou, and Gansu (Figure 2) (Zhao et al., 2019; Hu et al., 2000; Guanyan, Geological Museum, 2025; Guanyan, 2025). Inner Mongolia has the richest Ge resources, accounting for 46% of China's total reserves, while Yunnan accounts for 34%. However, the Ge grade in some of these areas is low, with poor exploitability, and some are even not economically viable under current economic and technological conditions.

Of the Ge deposits with proven resources in mainland China, there are 7 deposits associated with coal mines (Figure 3), accounting for 42% of the country's proven resources; at least 16 Ge deposits associated with lead-zinc mines, accounting for 29% of the country's proven resources; at least 1 Ge deposit associated with bauxite, accounting for 12.2% of the country's proven resources; 1 Ge deposit associated with iron ore, accounting for 3% of the country's proven resources; and 5 Ge deposits associated with copper deposits, accounting for 4% of the country's proven resource. There is also 1 Ge deposit associated with uranium and coal in coal mines (i.e., the Dazhai U-Ge deposit), accounting for 7% of the country's proven resources 2% (Hu et al., 1996; Wang et al., 1999; Hu et al., 2000; Qi et al., 2002a and 2002b; Wang et al., 2003; Zhang et al., 2003; Liu, 2005; Ao et al., 2007; Zhu et al., 2009; Wang et al., 2010; Yuan et al., 2011; Yuan et al., 2012; Zhang et al., 2012; Zhou et al., 2013; Han et al., 2014; Wang et al., 2016; Zhang et al., 2017; Liu et al., 2018; Zhao et al., 2019; Liu et al., 2023).

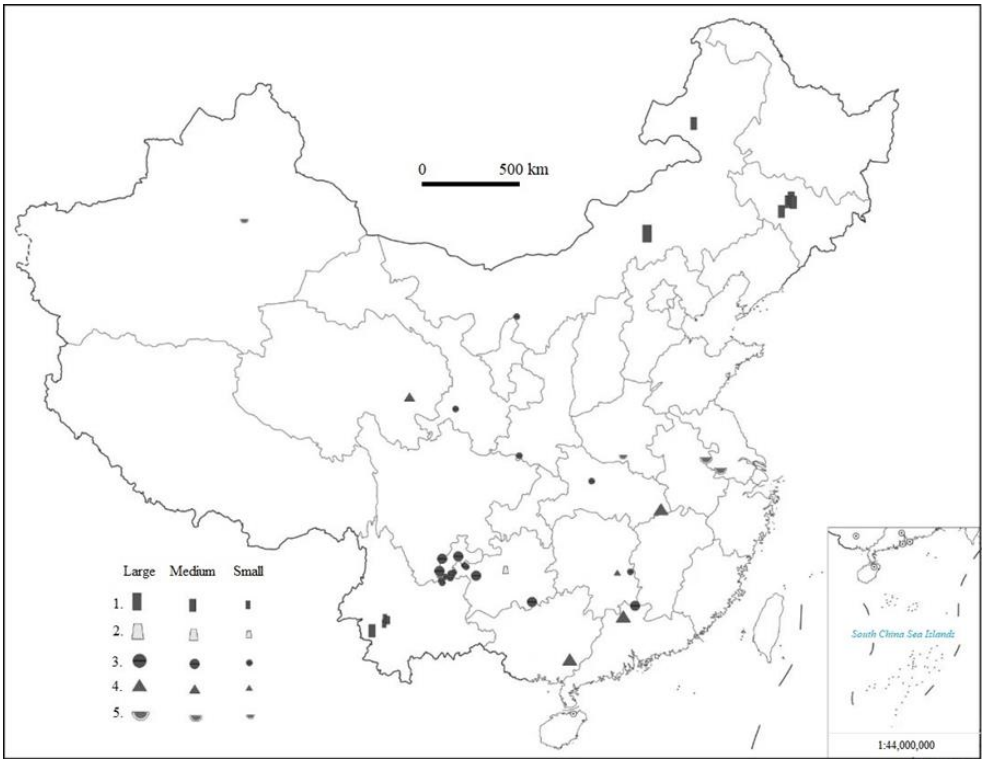


Figure 1. The known Ge deposits in mainland China (modified from Liu et al., 2023)

1. Exogenous/aqueous organic category including coal-Ge, oil shale and shale types; 2. Exogenous/aqueous inorganic category including volcano-sedimentary type, etc.; 3. Endogenous/igneous category including part of the mesothermal-epithermal types; 4. Endogenous/igneous category including hydrothermal/mesothermal-epithermal, porphyry, skarn, and part of the volcanic types; 5. Endogenous/igneous category including volcanic type

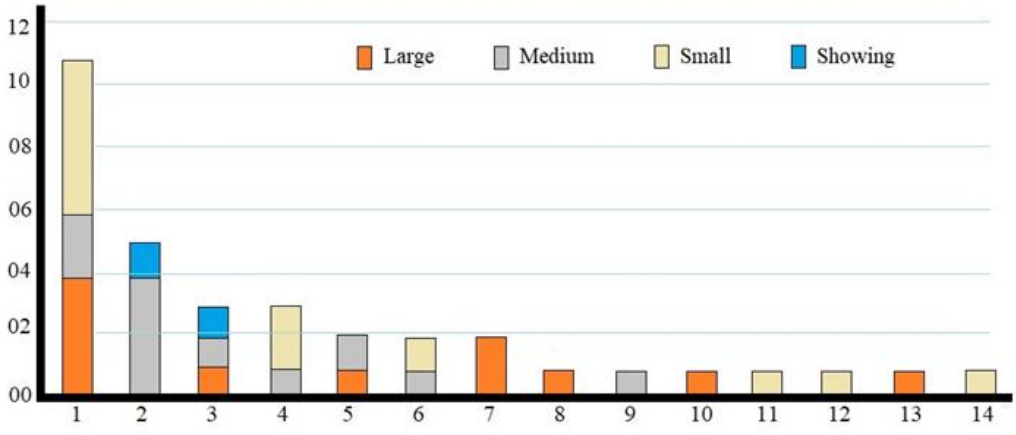


Figure 2. The number of known Ge deposits (showings) in various provinces and/or autonomous regions of mainland China (modified from Zhao et al., 2019)

1-Yunan; 2-Jilin; 3-Guizhou; 4-Gansu; 5-Sichuan; 6-Jiangsu; 7-Guangxi; 8-Shaanxi; 9-Qignhai; 10-Inner Mongolia; 11-Hubei; 12-Henan; 13-Guangdong; 14-Fujian



Figure 3. Coal-Ge deposits (showings) in mainland China (modified from Zhao et al., 2019)

China conducted a comprehensive survey of Ge resources in coal mines from the late 1950s to the early 1960s, discovering a series of Ge-bearing coal mines, mainly lignite. However, the Ge content in most coal mines in this major coal-producing country is low, making them unsuitable for industrial mining. Two Ge-bearing coal mines with independent mining value have been identified: the Bangmai Ge-bearing coal mine in the Lincang Neogene Basin of Yunnan Province and the Wulantuga Ge-bearing coal mine in the Mesozoic Basin of Inner Mongolia (Qi et al., 2002a; Ao et al., 2007; Zhu et al., 2009; Wang et al., 2016; Zhao et al., 2019).

Currently, China has four Ge mineral production bases in Yunnan, Inner Mongolia, Guangdong, and Jiangsu provinces. In 2014, China's Ge production was approximately 111.07 tons, an increase of 50 tons compared to 2005 (Wang, 2011). From 2005 to 2014, production increased approximately every three years. Production exceeded 100 tons for the first time in 2013. In 2011, China's Ge consumption surpassed Japan's, becoming the world's second-largest consumer. Ge consumption reached 32 tons in 2014, a 16.9-fold increase compared to 1.79 tons in 1987. Ge products produced in China include Ge tetrachloride, Ge oxide, Ge ingots, Ge single crystals, and organic Ge. In 2014, China's Ge consumption structure was as follows: infrared optics accounted for 69%, optical fibers for 19%, electronics and solar power generation for 6.3%, and others for 6.3%. Infrared optics is the main sector for Ge consumption in China.

Yunnan Province, located in the southwestern border region, is China's largest producer of Ge. Lincang City, relying on its lignite resources, is striving to build itself into the "Ge

Capital of Southern China," with Yunnan Lincang Xinyuan Ge Industry Co., Ltd. as its leading Ge enterprise. In addition, Chihong Zinc & Ge Co., Ltd.'s Huize Smelter processes Ge concentrate from the Huize lead-zinc mine. The joint venture, Yunnan Northern Chihong Optoelectronics Co., Ltd., produces high-purity Ge dioxide, zone-refined Ge, and downstream products. Some of Yunnan's Ge products are exported to Jiangsu, Sichuan, Hunan, and Wuhan. In 2014, Yunnan's local Ge production reached tens of tons.

Inner Mongolia, possessing China's largest Ge resources, is mainly supplied by State Grid. The group's subsidiary, Xilingol League Wulan Tuga Coal Co., Ltd., is responsible for mining. Its subsidiaries, Xilingol Tongli Ge Industry Co., Ltd. and Xilingol Mengdong Ge Industry Technology Co., Ltd., extract Ge from the flue gas after coal-fired power generation. Tongli Ge Industry, operating at full capacity, can produce tens of tons of Ge metal. Mengdong Ge Industry's capacity is approximately twice that of Tongli Ge Industry, and it also has downstream products. Ge mining in Inner Mongolia, China, is relatively concentrated, with stable output, and is increasing with the growth of Tongli Ge Industry and Mengdong Ge Industry. In addition, a certain amount of Ge is also produced in Guangdong, Jiangsu, Sichuan, Hunan, Hubei and Hebei provinces in China.

3. Spatiotemporal distribution

Known Ge deposits in mainland China are concentrated in the Sichuan-Yunnan-Guizhou Ge metallogenic belt, the Lincang coal-type Ge metallogenic belt in western Yunnan, the Xilingol coal-type Ge metallogenic belt in Inner Mongolia, and the Hami coal-type Ge metallogenic belt in Xinjiang (Figures 1-3). Among them, the average Ge content in the Ge-rich coal seams of the Naomohu coalfield in the Hami coal-type Ge metallogenic belt reaches 202×10^{-6}. The Hulunbuir coal-type Ge deposit in Inner Mongolia is located in the Yimin coalfield of the Hailar Basin. The Ge anomaly is mainly developed in interbedded rock, and the Ge resource is estimated to exceed 4,000 t. The Ge content of the main coal seams is generally between 50×10^{-6} and 200×10^{-6} (Wang, 1999). The average Ge content in the Shengli Coalfield of Inner Mongolia reaches 244×10^{-6}, and in the Baiyinwula Coalfield of Sunite Left Banner, it reaches 290×10^{-6}. Ge can be recovered from the coal ash after coal combustion at pithead power plants (Wang, 1999; Zhao et al., 2019). In the Ordos Basin coalfield, the average Ge content in the Xiaotagou Coalfield reaches 613×10^{-6}, in the Changtan Coalfield 327×10^{-6}, and in the Kongduigou Coalfield 301×10^{-6}.

The Sichuan-Yunnan-Guizhou Ge metallogenic belt contains numerous lead-zinc deposits, along with associated/symbiotic large amounts of rare metals such as Ga, Ge, and Cd, making it one of China's important rare metals producing areas. Currently, most Ge recovery in mainland China comes from Ge-rich sphalerite, with a recovery rate of around 60%. These deposits include the Daliangzi and Tianbaoshan lead-zinc mines in Sichuan, the Huize and Fule lead-zinc mines in Yunnan, and the Shanshulin, Niujiaotang, and Qingshan lead-zinc mines in Guizhou. All of these lead-zinc ores contain the dispersed element Ge (Wang et al., 2010; Zhang et al., 2012; Zhao et al., 2019).

Ge in the Lincang coal-type Ge metallogenic belt of western Yunnan is found in the Bangmai lignite-bearing clastic basin, which is based on Indosinian granite. It includes two

deposits, Dazhai and Zhongzhai, both with independent development value (Qi et al., 2002a and 2002b).

The Fankou lead-zinc deposit is a typical sedimentary-reformed Ge deposit in the northern Guangdong Ge metallogenic belt (some argue it is of hydrothermal origin), with a Ge resource of approximately 1,000 tons. Ge mainly occurs in sphalerite through isomorphous substitution with zinc (Wang et al., 2003; Chen et al., 2014).

Most known Ge mineralization in coal-bearing areas of mainland China occurred during the shrinking stages of rift basins or depressions, with favorable sedimentary environments including peat bogs and swampy lakeshores. For example, the coal-bearing strata of the Yimin coalfield are the Damoguaihe Formation and the Yimin Formation, products of the shrinking stage of the Hailar Basin, with the sedimentary environment gradually shifting from shallow lacustrine islands and lakeshores to shallow lake-swampy environments. The coal-bearing strata of the Shengli coalfield are the Lower Cretaceous Tengger Formation and the Saihantala Formation, corresponding to the uplift and shrinkage stage of the Erlian Basin in the Late Cretaceous, with the main sedimentary environment being swampy lakes.

Ge mineralization in the Sichuan-Yunnan-Guizhou metallogenic belt is controlled by tectonic and stratigraphic factors. The discovered deposits have numerous ore-bearing strata, ranging from the Neoproterozoic to the Paleozoic, with dolostone as the dominant lithology. The main ore bodies are layered, quasi-layered, vein-like, pocket-like, and/or lenticular. Ge mineralization associated with igneous activity includes porphyry, skarn, and epithermal deposits. The discovered deposits are mostly located at plate boundaries in areas of frequent tectonic and magmatic activities. The left-lateral strike-slip fault zone of the Lancang River constrained the formation and evolution of the Lincang-Bangmai Basin, hydrothermal activity within the basin, and the enrichment, mineralization, and spatial distribution of Ge (Wang et al., 2001). The mineralization epoch is concentrated in the Late Triassic to Late Cretaceous.

Ge mineralization in mainland China occurred from the Proterozoic to the Cenozoic, but was concentrated between the Mesozoic and Cenozoic. The Yanshanian period was the most developed, followed by the Himalayan and Indosinian periods. Large-scale associated/symbiotic Ge mineralization mainly developed during the Yanshanian and Himalayan periods. Ge mineralization associated with lead-zinc deposits mainly developed during the Yanshanian period, followed by the Indosinian period. Coal-type Ge mineralization mainly developed during the Jurassic and Cretaceous periods, with some development in the Late Tertiary (Wang et al., 2014; Zhao et al., 2019), but was relatively concentrated in the Mesozoic.

The formation of coal-type Ge deposits is complex, and the exact timing is difficult to determine. However, most researchers believe that Ge entered coal-bearing basins around the same time as coal formation, namely, concentrated in the Cretaceous and Neogene periods (Liu et al., 2023). Specifically, coal-type Ge deposits in the Hailar, Songliao, and Erlian basins of Northeast China formed during the Cretaceous, while the Lincang coal-type Ge deposits in Yunnan Province formed during the Neogene.

Ge mineralization in carbonate rocks is characterized by multiple phases and stages. The formation age of the ore-bearing strata covers a broad period from the Sinian to the Late Permian. However, isotopic geochronological results show that the majority of deposits were formed in the Late Paleozoic to Early Middle Paleozoic (Liu et al., 2023). For example, the ^{40}Ar-^{39}Ar age of sphalerite fluid inclusions in the Fanxian lead-zinc deposit is

(265.8±1) Ma; the Rb-Sr age of sphalerite in the Huize lead-zinc deposit is (226±6.4)～(223.5±3.9) Ma; the Rb-Sr age of sphalerite in the Qiping lead-zinc deposit is (321.7±5.8) Ma; and the Rb-Sr and Sm-Nd ages of sphalerite in the Maozu lead-zinc deposit are (190.5±5.0) Ma and (196±13) Ma, respectively. Wu et al. (2019) believe that there were two major mineralization events in the Sichuan-Yunnan-Guizhou region, at 382–328 Ma and 245–205 Ma. Among them, the mineralization events of the Middle to Late Triassic were of greater scale.

Ge mineralization related to igneous activity mainly occurred in the Late-Middle Miocene, such as the Chengmenshan copper polymetallic deposit in Jiangxi Province, where the intrusive body age is 139.1–144.5 Ma, and the Re-Os age of molybdenite in the ore body is (140±2) Ma. The diagenetic age of the Youmapo tungsten-molybdenum deposit is 109.7–100.7 Ma. The Re-Os isotopic isochron age of molybdenite in the ore body is (100.1±3.3) Ma. The Sm-Nd age of garnet in the Tongyugou copper polymetallic deposit is 216.3±1.5 Ma. Marine volcanic Ge deposits mainly formed in the Proterozoic and Early Paleozoic. However, the known number of such deposits is relatively small, and precise mineralization age data are lacking. Only the ages of the host rocks for some deposits can be collected, such as the smallest detrital zircon age of the ore-bearing strata of the Liushan Formation in the Dongchuan volcanic copper deposit in Yunnan, which is 1,220 Ma. The ore-bearing strata of the Liushanyan copper-zinc deposit are the Liushan Formation of the Erlangping Group, in which the age of the spilite porphyry is 517±84 Ma.

From the perspective of the spatiotemporal evolution of Ge mineralization in mainland China, the Huize Pb-Zn-Ge deposit is the most representative in the Sichuan-Yunnan-Guizhou Ge metallogenic belt. The mineralization occurred during the Indosinian-Yanshanian period, mainly in the late Indosinian period, with some extending into the early Yanshanian period (Han et al., 2014). The mineralization age of the Fankou Pb-Zn-Ge deposit in the northern Guangdong Ge metallogenic belt is approximately in the late Early Cretaceous, with a relatively long duration (Zhu et al., 2013). Similar in genesis to the Fankou Pb-Zn-Ge deposit, the Beishan Pb-Zn-Ge deposit in Guangxi was formed from mineralized hot brine produced during the formation of the Devonian-Permian basin due to compaction and dehydration. This hot brine migrated to favorable locations during the Yanshanian period and precipitated to form minerals (Liu et al., 2018). Coal-type Ge mineralization is relatively young. The Xilingol coal-type Ge metallogenic belt in Inner Mongolia is Cretaceous, the Hami coal-type Ge metallogenic belt in Xinjiang is Jurassic, the Lincang coal-type Ge metallogenic belt in western Yunnan is mainly Neogene, and the Hulunbuir coal-type Ge metallogenic belt is mainly Late Jurassic and Early Cretaceous.

Ge mineralization is commonly found in lead, zinc, silver, copper, and molybdenum sulfides and in coal seams. In lead-zinc ores, Ge typically exists as an isomorphism within the zinc sphalerite lattice. Under strong reducing and low-temperature conditions, Ge^{4+} transforms into Ge^{2+}, with an ionic radius similar to Zn^{2+}, making it easier to enter the zinc sphalerite lattice (Liu, 2005). The Ge grade in coal seams varies considerably, primarily concentrated at the top and/or bottom. The Ge in the coal seams of the Lincang Bangmai Basin in Yunnan Province likely originates primarily from surrounding metamorphic rocks, granites, and the basin's basement strata (Zhu, 2009). However, Hu et al., based on the spatial distribution patterns of coal-type Ge mineralization and siliceous rocks, the sulfur isotope composition of pyrite, the grade variation patterns of Ge in coal seams, and the geochemical characteristics of siliceous rocks (Hu et al., 1996 and 2000), believe that Ge

mainly originates from hydrothermal solutions, and that the Ge in these solutions is primarily supplied by the Ge-rich granites at the basin's basement (Zhang et al., 2003).
Overall, about half of China's proven Ge resources are associated with coal mines, while the majority of the remainder is associated with non-ferrous metal minerals such as lead-zinc deposits. Ge can be found in various deposits from different eras, including endogenic hydrothermal polymetallic deposits, Ge-bearing organic rock deposits, and sedimentary reformed deposits, with the first two being the most prevalent, accounting for 64% of all Ge resources. China's high-grade coal-type Ge is a rare and high-quality resource in the world.

4. Type and characteristics

Some Chinese scholars have classified associated/symbiotic Ge deposits in the country into three main types (Wang, 2011): mesothermal-epithermal polymetallic associated/symbiotic Ge deposits, Ge-bearing organic rock deposits, and sedimentary reformed Ge deposits. They concluded that Ge mineralization in mainland China is mainly composed of mesothermal-epithermal deposits and Ge-bearing organic rock deposits, accounting for 64% of all Ge deposit types. Other Chinese researchers have further elaborated (Ao et al., 2007) that mesothermal-epithermal polymetallic deposits are the most common type of associated/symbiotic Ge deposit, with typical examples including the Kuangshanchang, Qilinchang, and Yulu lead-zinc deposits in Yunnan. Ge-bearing organic rock deposits refer to deposits where Ge is co-occurring and/or associated with coal, oil shale, and black shale. The Bangmai Ge deposit in Lincang, Yunnan, is a rare, independently mineable Ge deposit within coal-bearing strata in mainland China and even the world (Zhu, 2009), with large-scale reserves. The Wulantuga coal-type Ge deposit in the Shengli coalfield of Inner Mongolia has resources approaching 3,000 tons. Sedimentary reformed type Ge deposits, such as the Maomaochang-Zhazichang lead-zinc deposit in Guizhou, have Ge content in zinc oxide reaching 390 g/t. Hydrothermal replacement Ge mineralization is generally small in scale, such as the Shizhuang lead-zinc deposit in Yunnan and the Luoyang iron deposit in Fujian (Yuan et al., 2011 and 2012; Zhou et al., 2013; Zhang et al., 2014).
Some other researchers classify Ge deposits in mainland China into coal-bearing Ge deposits occurring in coal-bearing sediments, such as the Wulantuga coal-Ge deposit in Shengli Coalfield, the Wumuchang coal-Ge deposit in Yimin Coalfield, the Dazhai coal-Ge deposit in Lincang, and the Yingcheng coal-Ge deposit. Carbonate rock-hosted Ge deposits are the most numerous and have the most mature recovery and utilization technologies. These include porphyry, skarn, and epithermal deposits, which are magmatic-hydrothermal Ge-rich deposits related to magmatic-hydrothermal activity. This includes volcanic-type Ge deposits, encompassing both marine and terrestrial volcanic rock deposits, as well as other sedimentary Ge deposits besides coal-bearing Ge deposits, such as associated Ge in bauxite and phosphate deposits.
Clearly, these classifications are rather rough. Some types have no connection to their “origin” or their genesis is unclear. They also lack in-depth research and analysis of known Ge deposits in the country, hindering overseas researchers from understanding their true nature.
Based on a detailed review of existing research literature on Ge deposits in mainland China, this paper classifies currently known associated/symbiotic Ge deposits in the country into

three main categories: endogenous, exogenous, and a mixture of both (Table 1). The former are closely related to igneous activity and can be further subdivided into mesothermal-epithermal, skarn, porphyry, volcanic, and volcanic sedimentary types. The exogenous types are closely related to sedimentary and hydrothermal activity and can be further subdivided into organic coal deposits, inorganic bauxite deposits, and phosphate deposits. At the same time, it was predicted that mainland China might become the first in the world to discover independent Ge deposits in and around the Qinghai-Tibet Plateau. These are briefly described below.

Table 1. Type and representative Ge deposit in mainland China

Type					Representative deposit	Data source
Industrial	Genetic			MA[1]		
Symbiotic/Associated	Endogenous	Igneous	M-E[2]	Pb-Zn-Ge	Luoba in Gansu, Huidong in Sichuan, and Huize in Yunnan, etc.	Gao, 1963
				Pb-Zn-Ag-Ge	Huidong in Sichuan, and Yingde in Guangdong, etc.	Luo et al., 1963
				Cu-Sn-Ge	Qinjia in Guangxi, etc.	Wang, 1988
				Cu-Zn-Ge	Liushanyan (Dahe) in Henan, etc.	Lu et al., 2000
				Cu-Ge	Xiaohankou in Hubei, etc.	Qi, 2002
				Ag-Pb-Ge	Xialadi in Gansu, etc.	Xue et al., 2006
				Zn-Ge	Nanmushu in Shaanxi, and Woqianchang in Yunnan, etc.	Wang et al., 2015
				Pb-Zn-P-Ge	Huize in Yunnan, etc.	Lin et al., 2016
				Pb-Zn-S-Ge	Beishan in Guangxi, etc.	Wang et al., 2016
				Wu-Mo-Ge	Youmapo in Guangxi (Ge reserves: 319 tons), etc.	Huang et al., 2018
				Cu-Ge polymetallic	Jiujiang in Jiangxi, etc.	Zhao et al., 2019
			Volcanic	Cu-Fe-Ge	Lanniping & Shijiangjun in Yunnan, Tongyugou in Qinghai, etc.	Weng et al., 2020
				Cu-Zn-Ge	Dahe, Tongbai in Henan, etc.	Duan et al., 2022
				Ag-Pb-Ge	Xialadi in Gansu, etc.	Liu et al., 2023
				W-Cu-S-Ge	Caihuagou in Xinjiang, etc.	Xue et al., 2024
				Cu-Ge polymetallic	The Volcanic basin in Lishui, Jiangsu etc.	Gegological Museum, 2025
				Fe-Mn-Ge	The Volcanic basin in Lishui, Jiangsu etc.	Guanyan, 2025
				Fe-Ge	The Volcanic basin in Lishui, Jiangsu etc.	Huang et al., 2026
			Skarn	Cu-S-Ge	Jiujiang in Jiangxi, etc.	Liu et al., 2026
				S-Ge	Shangpu, Laiyang in Shandong, etc.	You et al., 2026;
				Fe-Ge-Ga	Fujian, etc.	
			Porphyry	Cu-Ge polymetallic	Late Yanshan quartz porphyry in Jiangxi, etc.	
	E&XH[3]	I&A[4]	VS[5]	Fe-Ge-U	The Volcanic basin in Lishui, Jiangsu etc.	
	Exogenous	Aqueous	Organic	Coal-Ge	Inner Mongolia's Ulantuga, Yunnan's Dazhai & Bangmai, etc.	
				Oil shale	No related mineral deposit has been developed yet	
				Shale	No related mineral deposit has been developed yet	
			Inorganic	P-Ge	Huize in Yunnan, etc.	
				Bauxite-Ga-Ge	Xiaoshanba in Guizhou, etc.	
				Pb-Zn -Ge	Kuangshanchang in Yunnan, etc.	
Independent			No findings yet, but the future looks promising.			

Note: MA[1] - Mineralization assemblage; M-E[2] - mesothermal-epithermal; E&XH[3] - Endogenous and exogenous hybrid; I&A[4] - Igneous and Aqueous hybrid; VS[5] - volcano-sedimentary.

4.1 Endogenous igneous

The endogenous igneous associated/symbiotic Ge deposits discovered in mainland China mainly include the following genetic types.

4.1.1 Mesothermal-epithermal

This type of Ge deposit includes what previous researchers called carbonate rock hosted types. Classifying genetic types based on the host rock is clearly inappropriate. Practice has shown that mineralization of different genetic types in the same region can occur entirely within the same host rock. In fact, these Ge mineralization hosted in carbonate rocks are genetically closely related to hydrothermal fluids generated by magmatic activity, and should be classified as magmatic mesothermal-epithermal deposits. Based on currently published data, this type of Ge mineralization is the most numerous in mainland China, and its recovery and utilization technology is relatively mature. Mesothermal-epithermal Ge deposits are mainly distributed in the Sichuan-Yunnan-Guizhou metallogenic belt and the Nanling metallogenic belt. The Sichuan-Yunnan-Guizhou region is the area with the densest distribution of this type of Ge deposit, with representative deposits such as several large and medium-sized Ge deposits in Huize and Qiping. The host rock alteration of this type of deposit is generally weak, with the main alterations including calcitization and dolomitization, followed by ankeritization and silicification. Based on their main mineral composition, these deposits can be further subdivided into numerous subcategories, such as Pb-Zn-Ge, Pb-Zn-Ag-Ge, Cu-Sn-Ge, Cu-Zn-Ge, and Ag-Pb-Ge (Table 1). The primary minerals in mesothermal-epithermal Ge mineralization are mainly sphalerite, galena, and pyrite, with minor amounts of chalcopyrite, stibarsen, and dufrenoysite. Secondary minerals include smithsonite, cerussite, anglesite, limonite, and hemimorphite. The minerals are mainly found in massive, banded, vein-like, disseminated, and fine veinlet forms. Ge is primarily found in sphalerite and smithsonite. Vein minerals are mainly dolomite and calcite, with some deposits containing quartz, barite, fluorite, sericite, gorse, carbonaceous minerals, and asphalt.

While some deposits contain high levels of Ge, sphalerite formed at low temperatures remains the primary carrier of hydrothermal Ge mineralization. Direct substitution and/or coupled substitution between elements are likely the main mode of Ge entry into sphalerite. Studies have shown a good correlation between Ge and copper content in sphalerite; Ge^{4+} and Cu^{2+} can isomorphously substitute Zn^{2+} in the sphalerite lattice through coupling, and combinations of In^{3+} and Ge^{4+} can also substitute Zn^{2+}. The phenomenon of Ge^{4+} substituting for Zn^{2+} and/or Ge^{2+} substituting for Zn^{2+} has been observed in the Uss River Pb-Zn-Ge deposit.

Ge in hydrothermal Ge deposits may originate from the basement and/or ferruginous rocks in adjacent areas. In the Sichuan-Yunnan-Guizhou region, Ge abundance in both the basement and cap-rock is lower than in the crust, but the Ge background value in the basement is higher than in the cap-rock. Sedimentary Ge-rich phosphate deposits and ferruginous Ge mineralization are developed near the basement strata, such as the Dajing lead-zinc-phosphate deposit and the Lanniping Cu-Ge deposit. In some regional deposits, such as the Fule and Qiping lead-zinc deposits, the sulfide lead isotope characteristics are similar to those of the Kunyang Group in the basement, indicating that the basement is a source of ore-forming materials for some deposits. Although the Ge background value in the Emeishan Wuluite and Xuanwei Formation is lower than that in the basement, it is higher than that in the adjacent upper and lower strata, suggesting a potential to provide certain ore-forming materials.

The fluids found in Ge-rich deposits in China are characterized by low temperature (100–150 °C) and moderate salinity (w(NaCleq) = 10%–30%). The fluids mainly originate from basin brines, but some deposits exhibit characteristics of deep crustal fluids. Generally, the Ge content in lead-zinc deposits gradually increases as the fluid temperature decreases. However, when multiple generations of sphalerite exist, the Ge content in early-generation sphalerite is not necessarily lower than that in later-generation sphalerite due to factors such as the residual Ge content in the fluid, the content of ore-forming coupling/competing elements, temperature, and pH. For example, in the Huize lead-zinc deposit, three generations of sphalerite (Sp1, Sp2, and Sp3) develop from high to low temperature, but the Ge content, from high to low, is Sp3 > Sp1 > Sp2. In the Wusihe Ge-rich lead-zinc deposit, the Ge content in the Sp1 sphalerite, which formed at a higher temperature, is higher than that in the Sp2 sphalerite, which formed at a lower temperature. Meng (2026), through his study of sphalerite in two typical Ge-rich lead-zinc deposits in the Sichuan-Yunnan-Guizhou metallogenic region of China—the Huize deposit in Yunnan and the Wusihe deposit in Sichuan—concluded that the sphalerite in the Huize deposit is divided into three phases: early dark brown (Sp1), middle yellowish-brown (Sp2), and late reddish-brown (Sp3). The sphalerite in the Wusihe deposit has two phases: sedimentary (Sp1) and hydrothermal (Sp2). The mineral assemblage of the Huize deposit is relatively simple: the ore minerals are mainly pyrite, sphalerite, galena, and jamesonite, while the gangue minerals are mainly calcite, dolomite, and clay minerals. The ore minerals of the Wusihe deposit are mainly pyrite, sphalerite, galena, and jamesonite, while the gangue minerals are mainly dolomite, quartz, apatite, rutile, and pitch. The sphalerite in the Huize lead-zinc deposit has a relatively simple structure and is relatively clean internally, with no exsolution minerals or independent Ge minerals present. It is inferred that Ge mainly exists as isomorphous minerals within the sphalerite. The sphalerite in the Wusihe lead-zinc deposit has a more complex structure, with pyrite visible as fine thread-like inclusions within the sphalerite, and numerous internal impurities, including micron-nano-sized sulfonate minerals, galena, and germanite (GeO_2). It is inferred that Ge may exist simultaneously as independent minerals, nanoparticles, and isomorphous minerals. Scanning electron microscopy revealed abundant jordanite and geocronite within both the Huize and Wusihe lead-zinc deposits. Electron probe microanalysis showed that the average Ge content of sulfonate minerals in the Huize lead-zinc deposit was 0.05%. A new mineral, ruizhongite, was discovered in the Wusihe lead-zinc deposit. The Ge content in sphalerite within the Kuangshan and Qilin sections of the Huize lead-zinc deposit is roughly the same: late-stage reddish-brown Sp3 (average Ge 151.64 ppm) is richer in Ge than dark brown Sp1 (average Ge 32.93 ppm) and yellowish-brown Sp2 (average Ge 45.73 ppm), and there is no significant correlation between sphalerite color and Ge enrichment under transmitted light. The Ge content in sphalerite from the hydrothermal mineralization period of the Wusihe lead-zinc deposit is relatively high, ranging from 0.87 to 2,305.29 ppm, with an average of 319.34 ppm. The Wusihe lead-zinc deposit sphalerite contains a large number of independent minerals of Ge at the micron-nano scale, as well as galena and sulfide minerals. Low to medium temperature, low sulfur fugacity, weak alkalinity, and high Cu activity in the fluid are likely the main reasons for the formation of Ge-rich sphalerite in the Huize lead-zinc deposit. High Cu and Ag activities, high oxygen fugacity, high sulfur fugacity, and acid-neutral conditions in the fluid are likely the main reasons for the formation of Ge-rich sphalerite and other Ge-rich minerals in the Ussghe lead-zinc deposit. Sun et al. (2025) found that the Ussghe lead-zinc deposit, during its hydrothermal

phase, contained a stage I of darker-colored sphalerite and a stage II of lighter-colored sphalerite, with average visual reflectance values of 16.126% and 16.187%, respectively; average dominant reflectance wavelengths of 474.179 nm and 474.164 nm, respectively; average reflectance saturation values of 0.048 and 0.043, respectively; and average Ge contents of 244.33×10^6 and 43.22×10^6, respectively. Ge exists isomorphously in the sphalerite and is more readily enriched in sphalerite with high reflectance saturation. The substitution mechanism of Ge is related to Cu and Ag. The reflectance color index of Ge-rich sphalerite indicate an upper limit of mineralization temperature of 203.0-293.0 ℃, while the trace element characteristics indicate a lower limit of mineralization temperature of 83.3-199.0 ℃. The deposit is genetically classified as a Mississippi Valley-type (MVT) lead-zinc deposit.

4.1.2 Volcanic

Known volcanic-type associated/symbiotic Ge mineralization in mainland China can be classified into various mineralization assemblages based on their main mineral types, including Cu-Zn-Ge, Ag-Pb-Ge, Cu-Fe-Ge, W-Cu-S-Ge, Cu-Ge polymetallic deposits, and so on (Table 1). These discovered deposits are mostly located in areas with frequent tectonic-magmatic activity at plate boundaries, with mineralization epochs concentrated in the Late Triassic to Late Cretaceous. Representative deposits include the Liushanyan (Dahe) Cu-Zn-Ge deposit in Tongbai County, Henan Province; the Shijiangjun deposit in Dongchuan County, Yunnan Province; the Tongyugou Cu-Ge deposit in Qinghai Province; and the Cu-Ge-Sr polymetallic deposit in the Dongshantou volcanic basin in Lishui County, Jiangsu Province.

These Ge deposits can be further subdivided into marine volcanic and terrestrial volcanic. Globally, Ge deposits associated with marine volcanic activity are mainly a few Kuroko ore deposit or black ore deposits in Japan and Spain, among others. The number of such deposits discovered in mainland China is extremely small, with the main metallogenic epochs being the Paleoproterozoic and Early Paleozoic.

The known but controversial Paleoproterozoic marine volcanic Ge deposits in mainland China are primarily Ge-rich Dongchuan-type copper deposits. The ore bodies in these deposits are mainly hosted in volcanic rocks. Taking the Lanniping copper deposit as an example, the host rocks include metamorphosed tuff, diabase, gabbro, biotite-altered rocks, gray-siliceous rocks, and tuffaceous dolomite rocks in the transition zone between the Yinling Formation and the Luoxue Formation. The ore bodies include copper ore bodies and copper-iron ore bodies, mostly occurring in layered to quasi-layered formations. The main minerals are bornite, chalcopyrite, tetrahedrite, hematite, chalcocite, and magnetite. Hu (2010) reported 47 t of associated/symbiotic Ge in copper deposits, but the specific grade and occurrence state are unclear.

Early Paleozoic Ge-rich deposits in mainland China include the Liushanyan copper-zinc deposit and the Caihuagou tungsten-copper-pyrite deposit (Table 1). The ore bodies of these deposits are mainly hosted in acidic volcanic rocks. The Liushanyan copper-zinc deposit formed in a back-arc environment, with the ore-bearing strata being the Erlangping Group, belonging to the intraplate-enlarged back-arc basin submarine volcanic sedimentary metamorphic spilite porphyry (Zeng, 2012). The Caihuagou copper-sulfur polymetallic deposit occurs in marine rhyolite.

Typical galvanic-type massive sulfide deposits exhibit distinct vertical zoning. The mineral assemblage, from top to bottom, consists of a barite zone (barite content greater than sulfide), a Kuroko ore zone or a lead-zinc ore zone (rich in sphalerite), a chalcopyrite ore zone (rich in copper ore), and a pyrite ore zone. The alteration of the surrounding rocks, from the central to the periphery, consists of sericitization and chloritization zone, montmorillonitization zone, and zeolite zone. The main minerals include pyrite, sphalerite, chalcopyrite, and galena. Ge-bearing minerals include sphalerite (up to 370×10^{-6}), renierite, Ge-bearing bornite, and Ge-bearing colusite. The gangue minerals are mainly quartz, sericite, barite, gypsum, scleroderma, and chlorite.

Whether it's the Liushanyan or Caihuagou deposits, the ore bodies are all tectonically controlled to a certain extent, exhibiting complex morphologies, including banded, lenticular, or vein-like forms. The alteration and mineralization of the surrounding rocks near the ore are more intense than those further away. The intensity of alteration and mineralization in each deposit gradually decreases from top to bottom. Taking the Caihuagou sulfur-copper polymetallic deposit as an example, the top of the deposit consists of layered and quasi-layered polymetallic sulfide ore bodies formed by volcanic eruption and sedimentation, while the bottom consists of banded and veinlet pyrite bodies formed by volcanic-hydrothermal alteration. The main alterations in the Caihuagou sulfur-copper polymetallic deposit include silicification, baritization, sericitization, chloritization, and pyritization, with higher intensity baritization and pyritization near the ore bodies. The mineral structure is mainly semi-anthromorphous to anhedral granular, with massive, sparse to dense disseminated textures. Minerals include pyrite, magnetite, chalcopyrite, bornite, and sphalerite.

In China, continental volcanic/subvolcanic Ge mineralization is mainly distributed in the Lishui Volcanic Basin of Jiangsu Province, with discovered deposits including Wanshoushan, Nanshantou, and Dongshantou. These Ge deposits are associated with large-scale volcanic eruptions in the Early Cretaceous (Meng et al., 2022), and the ore-bearing formations are fluvial-lacustrine sediments occurring between two eruptive cycles. The main host rocks are iron-bearing siliceous rocks. Ore bodies occur mostly as stratiform, flattened, and irregular shapes, clearly controlled by tectonics and stratigraphy. The main mineral type is Ge-containing iron-manganese ore, followed by Ge-containing iron ore, etc.

The Wanshoushan deposit is located in the Erdingshan-Lujia'ao overturned anticline, and the ore bodies are controlled by an east-west trending fracture zone (You et al., 2026). There are a total of 35 ore bodies, one of which is a continuous, gently undulating, irregular vein-like ore body, 900 meters long, 0.59-17.10 meters thick, with an average thickness of 5.42 meters, and a depth of 105-360 meters. The remaining 34 smaller ore bodies are mostly located above and parallel to the main ore body, exhibiting vein-like or lenticular shapes, 5-64 meters long, with a maximum thickness of 4.5 meters, generally less than 1 meter. The ore minerals are mainly Ge-bearing hematite, with minor amounts of specularite, trace amounts of magnetite and limonite. The ore has a colloidal structure, exhibiting oolitic, botryoidal, crust-like, and brecciated textures. The ore contains 0.001%-0.0168% Ge, generally 0.003%, with the usable ore averaging 0.0035% Ge. Ge is found in hematite, and its grade is directly proportional to the iron content. Generally, when the iron content is greater than 5%-10%, the Ge content can reach the cut-off grade, i.e., above 0.001%; when the iron content is greater than 10%-15%, the Ge content can reach 0.002%.

The Ge mineralization in the Nanshantou-Shizishan area of the volcanic basin in Lishui County, Jiangsu Province, is closely related to the spatial relationship of the small intrusive

bodies exposed in the area, and may have a genetic relationship (You et al., 2026). The volcanic breccia in the area was likely formed by volcanic eruptions deposited in shallow water; therefore, the strata in the area are volcanic sedimentary rocks. From April 1960 to March 1963, relevant investigations found that the Ge grade in the iron ore was close to the Ge cut-off grade, basically meeting the requirements for Ge ore, thus confirming that the deposit is a Ge deposit.

4.1.3 Skarn

Studies have shown that Ge does not exhibit significant selective enrichment in different intrusive and volcanic rocks; that is, its background values are not significantly different, with slight enrichment only observed in some highly differentiated or volatile-rich rock bodies. Ge-rich rocks discovered in mainland China are typically late-stage intermediate-acidic facies within complex intrusive bodies. For example, the ore-forming rock body of the Youmapo skarn tungsten-molybdenum deposit is a late-stage muscovite granite from the Yanshan period complex intrusive body, containing accessory minerals such as fluorite, ilmenite, and sulfides, and exhibiting high silica, high fluorite content, and low oxygen fugacity. The ore-forming rock body of the Chengmenshan skarn-type copper polymetallic deposit is a late-stage quartz porphyry from a Yanshan period intermediate-acidic shallow-to-hypershallow complex intrusive body. The ore-forming intrusion of Saishitang-Tongyugou is a late-stage granodiorite from a Late Triassic complex.

Skarn-type Ge mineralization is often not isolated, but rather occurs in conjunction with porphyry and/or even mesothermal-epithermal Ge mineralization, forming a multi-genetic Ge metallogenic series. A typical example is the Chengmenshan skarn-type copper polymetallic deposit in Jiangxi Province, which is essentially a coexistence of skarn and porphyry types.

Jiang et al. (2020) reported that the Ge content of the raw ore in a skarn-type Ge-Ga-Fe deposit in Fujian Province reached 52×10^{-6} (measured by plasma mass spectrometry at the Guangdong Provincial Institute of Mineral Resources). Guo et al. (2021) reported the discovery of a small amount of copper ore samples with relatively high Ge content in carbonate metasomatic ore bodies in the Chengmenshan copper polymetallic deposit. This data was obtained using electron probe microanalysis.

4.1.4 Porphyry

Internationally, Ge-rich ore bodies genetically linked to igneous activity are mostly distributed in the marginal zones of porphyry systems, and these ore bodies are often vein-like and/or brecciated, exhibiting distinct medium-to-low temperature mineralization characteristics. Influenced by mineralization type and ore-forming element assemblages, Ge in these deposits is found in a wide variety of minerals. For example, in porphyry-hydrothermal vein-type Cu-Mo-Au deposits, Ge may be enriched in bornite, enargite, domeykite, and covellite, while in hydrothermal vein-type Ag-Pb-Zn deposits, Ge is mainly enriched in sphalerite, and so on.

Similar to other genetic types, porphyry-type Ge mineralization is not isolated but often occurs alongside skarn-type and igneous-hydrothermal Ge mineralization within the same

tectonic-magmatic-stratigraphic system. Sometimes, these endogenous and exogenous Ge mineralizations even coexist, forming a relatively complete metallogenic series.

4.2 Igneous and aqueous mixed

Igneous and aqueous mixed Ge mineralization often occurs in volcanic basins. Similar mixed endogenous and exogenous mineralizations of other minerals also frequently occur in volcanic basins. A typical example is the Nanshantou Fe-U-Ge deposit in the volcanic basin of Lishui County, Jiangsu Province, China.
Volcanic basins are often sites where igneous and aqueous activities coexist and thrive, thus providing an optimal environment for the combined occurrence of endogenous and exogenous mineralization.

4.3 Exogenous aqueous

In fact, it is a type of Ge mineralization related to sedimentation. According to its main mineral composition, it is divided into two major categories: organic and inorganic.

4.3.1 Aqueous organic

Aqueous organic Ge mineralization refers to those occuring primarily in natural fossil fuels, such as coals. Currently, the most abundant and exploited Ge resources of this type are mainly Ge deposits in coal-bearing sediments; therefore, this paper refers to them as coal type.

- **Coal type**

China's discovered coal-type Ge deposits include the Shengli Coal Mine-Wulantug Deposit, the Yimin Coal Mine-Wumanchang Deposit, and the Lincang Dazhai, Caiba, and Yingcheng Coal Mine Deposits.

Studies have shown that the spatial distribution of Ge ore bodies in different coal deposits varies due to factors such as the location of Ge-rich magmatic/volcanic rocks and the migration pathways of Ge-rich hydrothermal fluids. For example, in the Lincang coal-Ge deposit, Ge-rich sections are mainly distributed in the first coal-bearing section near the basin basement (Hu et al., 2000). In the Wulantuga coal-Ge deposit, the Ge-rich No. 6-1 coal seam is located near the western edge of the basin. The enrichment locations of Ge also differ at the coal seam scale. For instance, in the Lincang Basin, the Ge enrichment pattern conforms to Zilbermints' law, mainly distributed in the top and bottom plates of Ge-bearing coal seams; while in the Shengli Coal Mine, the Ge-rich ore body in the No. 6-1 coal seam is mainly distributed in the middle of the coal seam.

Coal-type Ge deposits are mainly composed of low-rank lignite and long-flame coal. In addition to common organic components, the ore also contains silicate minerals such as quartz, plagioclase, and illite, as well as sulfides such as ferrous ore. Ge in coal is mainly

enriched in the organic matter, but the relationship between the enrichment degree of Ge and the petrographic composition of the coal is still unclear. For example, in high-grade Ge-rich coal mines, samples from the Lincang area are dominated by humic components, with a content of 88.5%-99.5%, while the inertinite content is only 0%-8.3%. However, in the Wulantuga Ge mine samples, the humic component content is only 33.1%-69.8%, while the average inertinite content is as high as 52.5%. Among the organic components, except for trace amounts of Ge detected in some hydrothermal pyrite, most minerals do not contain Ge.

Extensive research indicates that Ge in coal-type Ge deposits mainly originates from intermediate-acidic intrusive rocks, volcanic rocks, or volcanic clastic rocks adjacent to coal-bearing basins. Among these, the Ge-rich rocks in the Lincang area consist of a stock-like set of two-mica granite, dating to the Middle to Late Triassic. The rock mass is rich in potassium and silicon but poor in iron and titanium, representing a product of magmatic fractionation and crystallization under post-collisional conditions. The rock mass contains 3.5×10^{-6} Ge, exhibiting a relatively high Ge leaching rate. However, there is limited research on Ge-rich rock masses in the Wulantuga and Yimin areas. Qin (2001) found that the w(Ge) of the western monzogranite and diorite samples from the Wulantuga coal-type Ge deposit was above 15×10^{-6}. Du et al. (2009), after conducting geochemical tests on various intrusive rocks and volcanic rocks surrounding the same deposit, found that only in the silicified Late Jurassic rhyolitic conglomerate lava was a relatively high Ge content (approximately 5×10^{-6}).

Clearly, even so-called aqueous coal-type Ge mineralization is not purely a result of sedimentary processes, but is closely related to igneous activity; that is, it is the result of the combined effects of endogenous and exogenous geological processes, with each intertwined.

The entry of Ge from its source region into the coal-bearing basin and its eventual mineralization is a complex process, influenced by various factors such as paleogeography, paleoclimate, and igneous activity. Furthermore, hydrothermal activity within the basin is also a crucial condition for the formation of Ge deposits. For example, the overall trace element variation of siliceous rock interlayers and the underlying two-mica granite in the Lincang coal mine are similar, indicating that the hydrothermal fluids that formed the siliceous rocks carried a large amount of trace elements, including Ge, from the granite. In the Wulantuga coal-type Ge deposit, Ge enrichment benefits from non-magmatic N_2-bearing alkaline hydrothermal fluids and mixed hydrothermal fluids from other sources. In the Hunchun coalfield in the eastern Yingcheng Basin, Guo et al. (2019) used SEM-EDS to find quartz and pyrite filling fractures in some Ge-rich coal samples, indicating that Ge enrichment in this deposit may also be related to hydrothermal activity.

Huang et al., through statistical analysis of Ge content data from a large number of coalfield exploration data, concluded that the average Ge content in major coalfields in Northeast China is 1-5 μg/g, which is close to the average Ge content in Chinese coal mines. In the Shengli coalfield, where the typical coal-type Ge deposit Wulantuga is located, and the Yimin coalfield, where Wumuchang is located, the average Ge content in coal is 2.63 μg/g and 3.30 μg/g, respectively, which are not significantly different from the average Ge content in Chinese coal mines. The enrichment of Ge in coal is characterized by small-scale

accumulation, with hydrothermal minerals commonly found in the enriched areas, indicating that hydrothermal intrusion provides favorable conditions for Ge enrichment in coal.

- **Oil shale**

There is currently no published research on this topic, although this type of statement exists.

- **Shale**

There is currently no published research on this topic, although this type of statement exists.

4.3.2 Aqueous inorganic

These types of Ge mineralization include bauxite, phosphate, iron, and lead-zinc placer deposits. Reported non-coal sedimentary Ge-rich deposits include the Xiaoshanba bauxite deposit and some phosphate deposits. The metallogenic geological setting and ore-bearing strata of these deposits are not strongly correlated with the degree of Ge enrichment, and the Ge in most of these deposits has not been recovered and utilized, making their development and utilization prospects unclear.

- **Bauxite type**

The Xiaoshanba bauxite deposit is located in northern Guizhou Province and is a sedimentary diaspore bauxite deposit. The ore-bearing strata are the Jiujialu Formation of the Lower Carboniferous. The main minerals are earthy bauxite, semi-earthy bauxite, gravelly oolitic bauxite, and massive bauxite. As of 2009, the cumulative Ge resource was 1,623.81 t. Ye et al. (2008) conducted ICP-MS tests on various types of bauxite ore samples in this deposit and found that the sample with the highest Ge content was earthy bauxite, but it had not yet reached the current minimum industrial grade requirements.

- **Phosphate type**

Sedimentary phosphate deposits of Ge represent another potential source of Ge. Studies indicate that approximately one-third of phosphate deposits in mainland China contain various associated metals, including Ge. Taking the Huize area as an example, the locations of phosphate deposits in the region are often close to hydrothermal Ge mineralization. Some phosphate deposits and Ge mineralizations are even integrated into the same exploration area, such as the Dashuijing lead-zinc and phosphate exploration area. Studies by Zhang et al. (2015) on Shifang-type phosphate deposits suggest that Ge and other dispersed elements may be enriched in phosphate rocks and sulfur-phosphorus-aluminum-strontium deposits. Although current research on the geochemical behavior of Ge in phosphate deposits is limited, its organic affinity allows it to accumulate to a certain extent

during phosphorogenesis under suitable environment. The main phosphorus-bearing layer in the Huize area is the Lower Cambrian Yuhucun Formation, which is also one of the potential source layers for Ge in the region. Therefore, although the exploitability of Ge in phosphate rock is still unclear, the Ge-generating potential of phosphate rock in Huize area is still worth further attention.

5. Discussion

Based on the three-tiered metallogenic belts, researchers have divided Ge deposits in mainland China into 15 Ge-forming belts according to their spatial distribution patterns (Liu et al., 2023). Coal-type Ge mineralization is distributed in the Neogene basins and Songliao Basin on the western side of the Greater Khingan Mountains, involving the Hailar Basin Ge-forming belt (Ge1), the Erlian Basin Ge-forming belt, and the Songliao Basin Ge-forming belt. Neogene coal-type Ge deposits are mainly found in the Lincang Basin Ge-forming belt.

Mesothermal-epithermal Ge mineralization is concentrated in the Sichuan-Yunnan-Guizhou region along the western margin of the Yangzi Platform, including the Upper Yangzi-Eastern Yunnan-Southern Sichuan-Guizhou metallogenic belt and the Upper Yangzi-Eastern (folded belt) metallogenic belt-Hunan-Hubei-Southern Guizhou metallogenic sub-belt. Other Ge mineralizations and Ge-rich deposits of this type are scattered along the northern margin of the Yangzi Platform and the western margin of the North China Platform, including the Ordos western margin Ge belt, the eastern upper Yangzi Ge belt, the northern Nanling Ge belt, the Huanjiang Ge belt, and the Nanling-Yunkai Ge belt.

Skarn-type and porphyry-type Ge mineralizations are distributed along the northern margin of the Yangzi Platform, the western margin of the Cathaysia Block, and the central and western sections of the Qinling-Qilianshan-Kunshan orogenic system, involving the Yangtze River mid-lower reaches Ge belt, the Nanling-Yunkai Ge belt, and the Qinling-Dabie-Xinghai Ge belt. In addition to the aforementioned Sichuan-Yunnan-Guizhou Ge-bearing belt and the middle and lower reaches of the Yangtze River Ge-bearing belt, sedimentary and volcanic Ge-rich deposits also include the North Qinling Ge-bearing belt and the Baluntai Ge-bearing belt. Aqueous sedimentary Ge deposits are concentrated in the Sichuan-Yunnan-Guizhou Ge-bearing belt and the Xiaoshanba Ge-bearing belt.

With increasing attention to Ge and continuous investment in its exploration, it is believed that more Ge mineralized areas and belts, and even independent Ge mineralized belts or deposits, will be discovered in mainland China.

6. Conclusions

The known associated/symbiotic Ge deposits in mainland China exhibit diverse genetic types, including endogenic igneous mesothermal-epithermal deposits, skarn-type, porphyry-type, and terrestrial and marine volcanic deposits. There are also aqueous

sedimentary deposits, such as organic coal-type Ge deposits, and inorganic bauxite and phosphate Ge deposits.

It is important to note that, in the context of Ge mineralization in this country, endogenic and exogenic sedimentary deposits are not independent or isolated, but rather exhibit mixed or combined mineralization.

Even within endogenic igneous Ge mineralization itself, each specific genetic type is not isolated but coexists and thrives. For example, porphyry, skarn, volcanic, and mesothermal-epithermal deposits, and even some exogenic sedimentary deposits, often occur together within the same tectonic-magmatic-sedimentary system, forming a relatively complete Ge metallogenic series. Therefore, finding one type of Ge mineralization in this area can lead to the discovery of other related types, improving prospecting efficiency.

Even organic coal-type Ge deposits are not formed in isolated, purely aqueous sedimentary formations, but are closely related to and/or connected with igneous activity. At the very least, igneous activity provides the ore source and/or ore-forming fluids and dynamics.

In terms of mineral types, Ge mineralization can be associated/symbiotic with many other metals such as Pb, Zn, Cu, Fe, W, Mn, Ag, and even non-metals such as S and P. Of course, among these associated/symbiotic minerals, coal and related sediments are also crucial.

References

01. Ao WH, Huang WH, Ma YY, Sun L and Wan H. 2007. Characteristics and utilization status of germanium resources in coal in China. *Resources and Industries*, 9(5): 16-18 (in Chinese with English abstract).
02. Chen YC, Wang DH, Xu ZG and Huang F. 2014. An overview of metallogenic and Mesozoic magmatic metallogenic laws in South China. *Geotectonics and Metallogeny*, 38 (2): 219-229 (in Chinese with English abstract).
03. Duan PP, Wang WF and Ma MY. Distribution characteristics of trace elements in germanium-rich coal of Wulantuga in coal of different density grades. *Coalfield Geology and Exploration*, 2022, 50 (11): 9. DOI: 10.12363/issn.1001-1986.22.03.0204 (in Chinese with English abstract).
04. Gao HL. 1960. *Report on the Results of the Inspection Work of Nanshantou Germanium Mine in Lishui County, Jiangsu Province in 1963*. Geophysical Prospecting Team of Jiangsu Metallurgical Geological Exploration Corps (unpublished in Chinese).
05. Geological Museum, Guilin University of Technology. May 12, 202. China's Strategic Mineral - Germanium.https://www.kepuchina.cn/article/articleinfo?ar_id=600576&business_type=100&classify=0 (in Chinese). Trieved January 30, 2026.
06. Guanyan Tianxia. February 20, 2025. Research Report on the Development Status and Investment Prospect Forecast of China's Germanium Industry (2024-2031). https://www.chinabaogao.com/baogao/202401/684043.html (in Chinese). Trieved January 30, 2026.
07. Han RS, Wang F, Hu YZ, Wang XK, Ren T, Qiu WL and Zhong KH. 2014. Study on the metallogenic tectonic dynamics and geochronological constraints of Huize-type (HZT) germanium-silver-lead-zinc deposits. *Geotectonics and Metallogeny*, 38 (4): 758-771 (in Chinese with English abstract).
08. Hu RZ, Bi XW, Ye ZJ, Su WC and Qi L. 1996. Preliminary study on the genesis of germanium deposits in Lincang. *Acta Mineralogica Sinica*, (2): 97-102 (in Chinese with English abstract).

09. Hu RZ, Su WC, Qi HW and Bi XW. 2000. Geochemistry, occurrence, and mineralization of germanium. *Bulletin of Mineralogy, Petrology and Geochemistry*, (4): 215-217 (in Chinese with English abstract).
10. Huang SQ, Zhang JQ and Zhang HL. 2018. Distribution characteristics and enrichment control factors of germanium in coal in coal-bearing areas of Northeast China. *Coal Geology and Exploration*, 46 (3): 6-10 (in Chinese with English abstract).
11. Huang WH, Ma YY, Sun L, Wan H, Tang XY, Du G, Wu W, Qin SL and Finkelman RB. 2026. Characteristics of germanium-rich coal and metallogenic environment in Wulantuga coalfield, Shengli, Inner Mongolia. *The Third National Symposium on Metallogenic Theory and Prospecting Methods* (in Chinese with English abstract).
12. Lin KQ, Huang WH, Wang YZ and Chen L. 2016. Distribution law and mineralization mechanism analysis of germanium-rich coal in Wumuchang area of Yimin coalfield. *China Coal Geology*, 28 (2): 6. DOI: 10.3969/j.issn.1674-1803.2016.02.01 (in Chinese with English abstract).
13. Liu F. 2005. *Metallogenic Mechanism and Occurrence State of Germanium in Large Lead-Zinc Deposits in Huize, Yunnan*. Beijing: Chinese Academy of Geological Sciences.
14. Liu H, Zhang CQ, Ji XJ, Guo ZL, Lou DB, Wu Y, Zhang YF and Li YL. 2022. Study on the differential enrichment regularity of germanium, a rare element, in sphalerite of the Huize lead-zinc deposit in Yunnan Province. *Mineral Deposits*, 41 (5):1057-1072. DOI: 10.16111/j.0258-7106.2022.05.011 (in Chinese with English abstract).
15. Liu JN, Ding JH, Chen BH and Yin JN. 2023. Summary of metallogenic regularity of germanium in China. *Mineral Deposits*, 42 (2): 267-286. DOI: 10.16111/j.0258-7106.2023.02.003 (in Chinese with English abstract).
16. Liu XH, Tang CX, Wu XM, Shi J and Zhou X. 2018. Study on the type and metallogenic model of lead-zinc pyrite deposits in Beishan, Guangxi. *Bulletin of China Metals*, (2): 203-204 (in Chinese with English abstract).
17. Lu JL, Zhuang HP, Fu JM and Liu JZ. 2000. Sedimentary environment, diagenetic processes and hydrothermal activity and enrichment of germanium in the Lincang super-large germanium deposit. *Geochemistry*, 2000, 29 (1):7. DOI: 10.3321/j.issn:0379-1726.2000.01.006 (in Chinese with English abstract).
18. Luo SF. 1963. *Report on the Results of Germanium Mineral Exploration Work in Nanshantou and Dongshantou, Lishui County, Jiangsu Province in 1963*. Geophysical Exploration Team of Jiangsu Metallurgical Geological Exploration Corps (unpublished in Chinese).
19. Meng SN. 2026. *Study on the Occurrence State of Germanium in Sphalerite--Taking the Huize and Wusihe Lead-Zinc Deposits in the Sichuan-Yunnan-Guizhou Mining Area as Examples*. Master's Thesis. Chengdu University of Technology (in Chinese with English abstract).
20. Qi HW. 2002. *Terrestrial Hydrothermal Sedimentation and the Genesis of Super-large Germanium Deposits—a Case Study of the Lincang Germanium Deposit*. Dissertation (in Chinese).
21. Qi HW, Hu RZ, Su WC and Qi L. 2002a. Genesis of carbonaceous siliceous limestone in Lincang germanium deposit and its relationship with germanium mineralization. *Geochemistry*, (2): 161-168 (in Chinese with English abstract).
22. Qi HW, Hu RZ, Su WC and Qi L. 2002b. Geochemistry of rare earth elements in lignite from Lincang germanium deposit. *Geochemistry*, (3): 300-308 (in Chinese with English abstract).
23. Sun SQ, Chen CH, Zhao WH, et al. 2025. Mineral typological characteristics and germanium substitution mechanism of germanium-rich sphalerite in the southwestern margin of the Yangtze Platform. *Rock & Mineral Analysis*, 44 (2). DOI: 10.15898/j.ykcs.202406210138 (in Chinese with English abstract).
24. Wang GZ, Hu RR, Fang WX and Tao XF. 2001. Belt slip deformation of the Lancang River fault and its relationship with the Lincang germanium deposit. *Acta Mineralogica Sinica*, DOI: CNKI:SUN:KWXB.0.2001-04-020 (in Chinese with English abstract).

25. Wang L, Peng SL, Long YZ and Shu GL. 2003. The formation of lead-zinc mines in Fankou, Guangdong Province is mainly due to complex mineralization. *Journal of Guilin University of Technology*, (2): 149-153 (in Chinese with English abstract).
26. Wang LM. 1999. Geological characteristics and exploration work of the Ulan Tuga germanium deposit in Xilingol League, Inner Mongolia. *Inner Mongolia Geology*, (3): 16-20+15 (in Chinese with English abstract).
27. Wang TH, Huang WH and Yan DY. 2015. Enrichment law and geochemical characteristics of germanium deposit in Wulantuga, Shengli coalfield, Inner Mongolia Autonomous Region. *Proceedings of the 15th Annual Meeting of the Chinese Society of Mineralogy, Petrology and Geochemistry (5)* (in Chinese with English abstract).
28. Wang TH, Huang WH, Yan DY and Tang XY. 2016. Research progress on metallogenic models of large coal-germanium deposits in China: a case study of the Lincang, Yunnan and Ulantuga coal-germanium deposits in Inner Mongolia. *Frontiers in Geology*, 23 (3): 113-123 (in Chinese with English abstract).
29. Wang WC. Extraction of metallic germanium from Nanshantou germanium-iron ore. *Modern Transportation and Metallurgical Materials*, 1988 (S1): 61-65 (in Chinese with English abstract).
30. Wang Y. 2011. Supply and demand analysis of metallic germanium. *China Metal Bulletin*, (7): 42-43 (in Chinese with English abstract).
31. Wen HJ, Zhu CW, Du SJ, Fan Y and Luo ZG. 2020. Gallium, germanium, thallium, and cadmium resources in China. *Chinese Science Bulletin*, 65 (33): 12 (in Chinese with English abstract).
32. Wu JT, Li GM, Li YB, Wei JH, Wang HF and Li P. 2019. Progress in geochronological study and metallogenic tectonic background of MVT lead-zinc deposits in the border area of Sichuan, Yunnan and Guizhou. *Geological Science and Technology Information*, (4): 134-144 (in Chinese with English abstract).
33. Xue BG. 2026. Complex genesis of the super-large Huize germanium-rich lead-zinc deposit. *Yunnan Geology*, 25 (2): 17. DOI: CNKI:SUN:YNZD.0.2006-02-003 (in Chinese with English abstract).
34. Xue G, Wang XH, Dao Y, Zhou JX, Xing C, Xiao GQ, Su XY, Cao XM, Dong T and Li R. 2024. A summary of the metallogenic regularity of germanium resources in Yunnan Province. *Acta Geoscientica Sinica*, 45 (4). DOI: 10.3975/cagsb.2024.052402 (in Chinese with English abstract).
35. You JB. 2026. Supplementary report on geological exploration of germanium deposit in Nanshantou, Lishui County, Jiangsu Province. https://xueshu.baidu.com/ndscholar/browse/detail?paperid=1v1804k0614u0rj0ew4n0ae0tu479080&site=xueshu_se. Trieved February 1, 2026 (in Chinese).
36. Yuan Y, Zhu XY and Li ST. 2012. Content, distribution patterns and comprehensive utilization status of associated rare metals in lead-zinc mines in my country. *Mineral Deposits*, 31 (S1): 965-966 (in Chinese with English abstract).
37. Yuan Y, Zhu XY and Wang YL. 2011. A review of the distribution and occurrence status of associated rare and dispersed elements in lead-zinc deposits in my country. *Acta Mineralogica Sinica*, 31 (S1): 316-317 (in Chinese with English abstract).
38. Zhang CQ, Wu Y, Wang DH, Chen YC, Rui ZY, Lou DB and Chen ZH. 2014. Brief introduction on metallography of Pb-Zn deposits in China. *Acta Geologica Sinica*, 88 (12): 2252-2268 (in Chinese with English abstract).
39. Zhang M, Gu XX, Fu SH, Si RJ and Li FY. 2003. Geochemical properties of germanium and germanium deposits. *Bulletin of Mineralogy, Petrology and Geochemistry*, 22 (1): 82-87 (in Chinese with English abstract).
40. Zhang SJ, Ji GY, Wang N, Jiang AL and Shang L. 2017. Current status of germanium resources in China and its sustainable development strategies. *Mineral Resources Protection and Utilization*, (2): 6-12 (in Chinese with English abstract).

41. Zhang YX, Zhu CW, Fu SH, Zhou GF, Qin YR, Fan HF, Wen HJ. 2012. Study on enrichment regularity of germanium in lead-zinc deposits in Sichuan, Yunnan and Guizhou regions. *Acta Mineralogica Sinica*, 32 (01): 60-64 (in Chinese with English abstract).
42. Zhao T, Wang DH, Liu C, Li DX and Zhou FY. 2019. Metallogenic regularity and current status of germanium mining in China. *Acta Geologica Sinica*, 93 (6): 1245-1251. DOI: 10.19762/j.cnki.dizhixuebao.2019182 (in Chinese with English abstract).
43. Zhou Y, Duan QF, Cao L and Gan JM. 2013. Enrichment patterns of dispersive elements in MVT-type lead-zinc deposits in western Hunan and western Hubei. *Acta Mineralogica Sinica*, 33 (S2): 189-190 (in Chinese with English abstract).
44. Zhu XL. 2009. Geological conditions and distribution patterns of germanium in coal. *Science and Technology Information Development and Economy*, 19 (32): 153-154 (in Chinese with English abstract).
45. Zhu XY, Wang JB, Liu SB, Wang YL, Han Y, Zhen SM and Guo NN. 2013. Metallogenic age of the Fankou MVT lead-zinc deposit in Guangdong — evidence from SHRIMP dating of zircon from diabase. *Acta Geologica Sinica*, 87 (2): 167-177 (in Chinese with English abstract).

Data availability
The data that support the findings of this study are available from the author upon reasonable request.

Declaration of competing interest
The author declares that he has no competing financial interests or personal relationships that could have appeared to influence the work reported in this paper.

Use of AI tools declaration
The author declares that he has not used Artificial Intelligence (AI) tools in the creation of this article.

Original Article

Mathematical, Physical, and Chemical Interpretations of Structural Control and Contributions to Mineralization-Taking Global Gold Deposits as an Example

Jian Zhao Yin[1Ⓛ] , Kuinuan Li[2], Hongyun Shi[3], Haoyu Yin[4], and Yuhong Chao[5]

Abstract

Using the gold provinces in the North China Platform and western Canadian orogenic belt as examples, this article concludes that gold metallogenic series often correspond to the structures in that area. Structures at different hierarchical levels within the same system play distinct roles in deposit formation: the first-level deep-large structures are often channels for the rise of rock-forming materials and their carriers, and control countless gold belts on the earth's surface. The secondary structures control gold fields and/or deposits of different sizes. The third-level structures control the ore bodies of a specific deposit. The mechanical properties of structures, their activity periods, and development of structural rocks influence timing and stages of mineralization, as well as intensity and structure/texture of the deposits. The deep-seated mechanisms underlying structural control of mineralization align with principles of mathematics, physics, and chemistry. The localized dissipative structures resulting from tectonic activity drive the final stages of mineralization. The essence of mineralization is the result of steady-state instability developing into a non-equilibrium dissipative structure. The structures facilitate the conduction, extraction, further enrichment, and upward intrusion of deep ore-bearing fluids through physical effects like seismic pumping, expansion, and re-fracture of mineralized zones. Deep and large faults also contribute to certain mutations in the ore-forming fluid entering the nonlinear low-pressure expansion zone, which causes hydrothermal boiling and a rapid nonlinear decrease in the solubility of the ore fluid. Chemically, the low-pressure expansion spaces formed by these structures act as vast reactors, in which mineralizing materials from different sources undergo violent physichemical reactions. This melting reactor both changes the temperature and pressure of the fluid and leads to drastic changes in chemical conditions such as oxygen fugacity, pH, and electrolyte balance, thus creating conditions for the formation of deposits. Some structures such as epigenetic faults intersect and divide each other to create differences in the bottom topography, hydrodynamics, hydrogeochemistry, and physichemistry in the basin. These variations create favorable space for the accumulation of large quantities of minerals, contributing to the formation of large and/or super-large deposits.

Keywords: tectonic and/or structural hierarchy system; gold metallogenic series; localized dissipative structure; nonlinear coherence effects; physical effects; physicochemical differences

---

Affiliation Info: 1 College of Earth Sciences, Jilin University, Changchun 130061, China; 2 Henan Faende Mining Co., Ltd., Luoyang 471700, China; 3 Xiamen Zijin Mining and Metallurgy Technology Co. Ltd., Xiamen 361101, China; 4 Guinea Westfield Mining Company, Plaza Diamant, kipe, Commune de Ratoma, Conakry-Guinee; 5 Engineering Geology Brigade, Jiangxi Bureau of Geology, Nanchang 330002, China

Corresponding AurhorⓁ: Yin, J. Z., PhD, Professor, geosciences, mineral exploration and mining; Email address: jzyin7@jlu.edu.cn

Email Address: Kuinuan Li, yybh1983@163.com; Hongyun Shi, shi_hongyun@zijinming.com; Haoyu Yin, yinhaoyu11@163.com; Yuhong Chao, 435975944@qq.com

Citation: JZ Yin, KN Li, HY Shi, HY Yin and YH Chao. 2026. Mathematical, physical, and chemical interpretations of structural control and contributions to mineralization-taking global gold deposits as an example. *Naturalis Scientias*, 3: 710-738. DOI: https://doi.org/10.62252/NSS.2026.1040. www.naturalisscientias.com.

Copyright © 2026 by the author. Published by *Naturalis Scientias*. This is an open access article under the Creative Commons Attribution-NonCommercial 4.0 International (CC BY-NC 4.0) License. (https://creativecommons.org/licenses/by-nc/4.0/).

1. Introduction

The formation of gold deposits is subject to multivariate ore-controlling factors, including complex structural systems with different levels, various igneous rocks with multi-period and multi-cycle origins, and a vast stratigraphic space with different physical and chemical properties following long periods of sedimentation. These ore-controlling factors can either provide migration channels for ore-forming materials and their carriers, are themselves the sources of ore-forming materials, provide the necessary physical and chemical conditions for the enrichment of ore-forming materials, or ultimately provide storage space for the precipitation and placement of ore-forming materials.

Among the three major metallogenic geological conditions mentioned above, structure, especially faults, is undoubtedly the most eye-catching, and to some extent, the most important. With various levels and different mechanical properties of faults, rock-forming and mineralizing materials such as igneous rocks occur, differentiate, and evolve, form ore-bearing fluids, and enrich to eventually form mineral deposits (Yin and Shi, 1995; Yin, 2019a; Wang et al., 2022; Yin and Shi, 2026 a & 2026b).

Therefore, summarizing and discussing the temporal and spatial distribution patterns and genetic relationships between structure and gold mineralization, especially the deep-seated mutual achievement mechanism between the two, has very important significance to both theoretical and practical mining. After all, the formation of a considerable proportion of hard rock gold, especially endogenous gold deposits, is closely related to structure. The survey, exploration, and development of gold deposits are also inseparable from the in-depth study and understanding of structure.

The authors' research, exploration, and development experience in the early Precambrian blocks and volcanic basins of the major gold provinces in the North China Platform, including Hebei, Liaoning, Henan and Shandong, in addition to gold deposits in the Mesozoic orogenic belt of western Canada, is combined with relevant research results of other scholars. This paper summarizes the close temporal, spatial, and causal connection between gold mineralization and structure, and explores the deep-seated intrinsic relationship between the two from the perspectives of mathematics, physics, and chemistry.

2. Examples of the relationship between structure and gold Mineralization

Although no two hard rock gold deposits in the world are exactly the same, almost all endogenous gold deposits around the world still have many commonalities. For example, the formation of these gold deposits is inseparable from the control and/or contribution of various geological structures. Below, we will take some typical gold provinces in China and Canada, thousands of miles apart, as examples to explain the close temporal and spatial relationship between structure and gold mineralization, so as to provide geological facts for the discussion of the internal mechanism of structure control and contribution to gold mineralization later in this article.

2.1. The gold province in the northern margin of North China Platform

In the thousands of years of Chinese civilization, Hebei Province, where the North China Platform is located, and its surrounding provinces of Liaoning, Inner Mongolia, Shanxi, Henan and Shandong, has been important gold-producing areas for successive Chinese dynasties. Historically the focus was mainly the development and utilization of extremely high-grade placer gold deposits. Among them, Hebei Province is a typical representative. Take as an example Zhangjiakou gold province in Hebei Province, which is located on the northern edge of the North China Platform. This area still has a large number of gold deposits of different sizes, and gold mining sites are scattered and numerous (Figure 1).

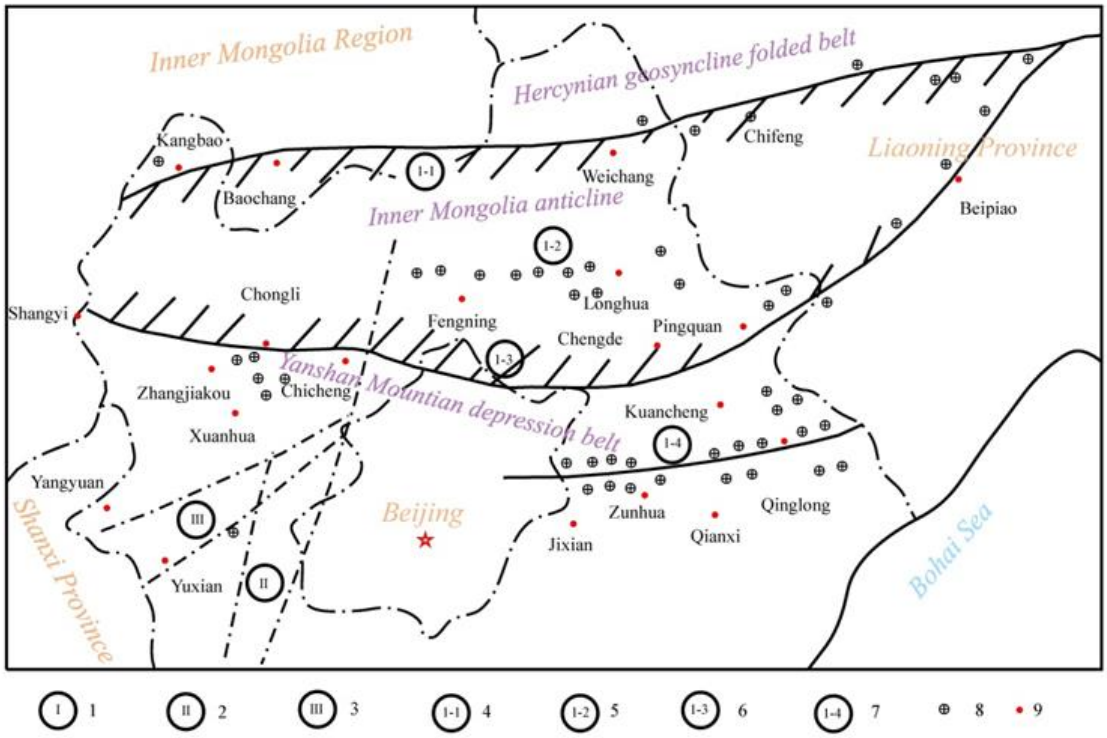


Figure 1. Spatial relationship between faults and gold deposits in the Zhangjiakou gold province of the North China Platform

1. East-West fault zone; 2. North-Northeast fault zone; 3. Northeast fault zone; 4. Kangbao-Weichang-Chifeng fault zone; 5. Fengning-Longhua fault zone; 6. Chongli-Chicheng-Pingquan-Beipiao fault zone; 7. Zunhua-Qinglong fault zone; 8. Gold deposits; 9. Settlements

Zhangjiakou gold province is located in the convergent part between the Inner Mongolian axis (anticline) and the Yanshan geosyncline folded belt of the North China Platform. Most of the over 100 lode gold deposits in the region are located within a 1,500 square kilometer triangular area among the towns of Xuanhua, Chicheng, and Chongli, and are thus called a gold triangle (Figures 2-3) (Song et al., 1994; Yin and Shi, 1995; Xu et al., 2014; Yin et al., 2021; Yin et al., 2023). The emergence of these gold deposits is closely related to the extremely developed faults and folds of different levels in the local area. Together with many gold deposits in eastern Hebei, Inner Mongolia, and western Liaoning, they are confined between and on both sides of two giant east-west fault tectonic zones on the

northern edge of the North China Platform (Figures 1-3). Among the numerous gold deposits in the area, the largest and most representative are the Xiaoyingpan, Dongping, and Zhangquanzhuang gold deposits (Wang, 1986; Dong, 1989; Hu et al., 1990; Zhang, 1990; Xu et al., 2014; Yin et al., 2021; Yin et al., 2023), followed by the Hougou, Shuijingtun, and Hanjiagou gold deposits (Figure 2) (Li, 1992; Li and Peng, 1994; Wang et al., 2021; Zhen et al., 2021). The Xiaoyingpan, Dongping and Zhangquanzhuang gold deposits also represent three different types of gold mineralization (Yin et al., 2021; Yin et al., 2023).

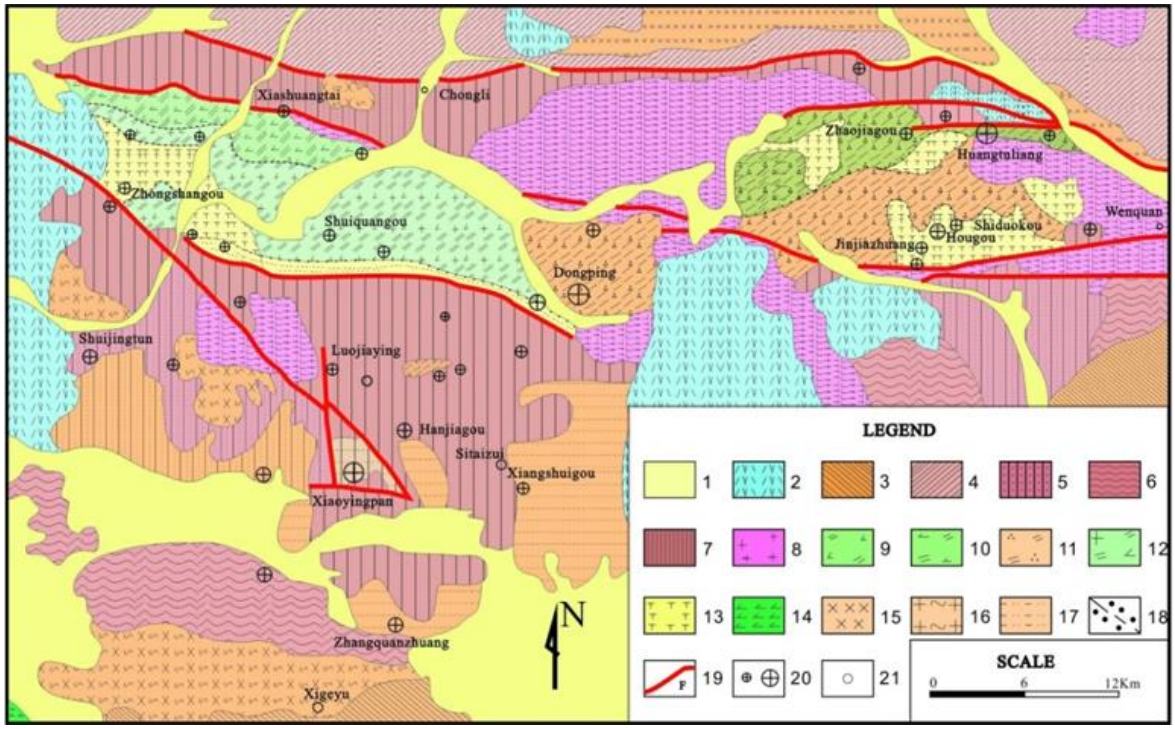


Figure 2. Simplified geological map of the gold deposits in the Zhangjiakou gold province (after Yin et al., 1995; 2021 & 2023)

1. Quaternary sediments; 2. Tuff conglomerate, sandstone and breccia of the hanging Jurassic system; 3. Sandstone, siltstone and dolomite of the Proterozoic Changcheng system; 4. Metamorphic granulite of the late Archean Hongqiyingzi Group; 5. Metamorphic granulite of the Aijiagou Formation of the Archean Sanggan Group; 6. Gneiss of the Shuidizhuang Formation of the Archean Sanggan Group; 7. Metamorphic granulite of the Jiagouhe Formation of the Archean Sanggan Group; 8. Granite of the Yanshan orogeny; 9. Amphibolite monzonite of the Hercynian orogeny; 10. Pyroxene amphibolite monzonite of the Hercynian orogeny; 11. Quartz monzonite of the Hercynian orogeny; 12. Amphibolite adamellite of the Hercynian orogeny; 13. Syenite of the Hercynian orogeny; 14. Pyroxenite of the Hercynian orogeny; 15. The Proterozoic granite-gneiss; 16. The Archean granite-gneiss; 17. The Archean metamorphic mica quartz diorite; 18. Marginal migmatization zone of the monzonite; 19. Fault and/or fault zone; 20. Small to large size gold deposits; 21. Town and/or village

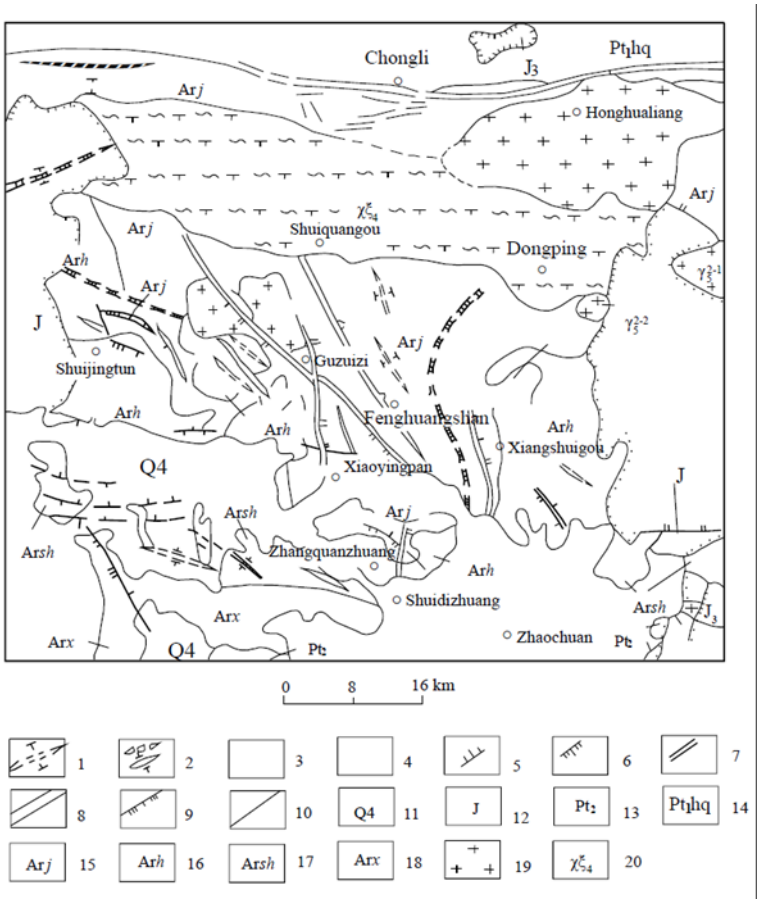


Figure 3. Structural outline of the Zhangjiakou gold province

1. Yanshanian syncline; 2. Early Precambrian third stage antediluvian folds; 3. Early Precambrian second stage reverse antediluvian folds; 4. Early Precambrian first stage reversed complex syncline (form) folds; 5. Himalayan fault zone; 6. Yanshanian fault zone; 7. Archean fault zone revived in the Yanshanian; 8. Deep and large fault zone since the Archean; 9. Archean fault zone; 10. Faults of unknown nature; 11. Quaternary; 12. Jurassic volcanic-sedimentary rocks; 13. Mesoproterozoic Changchengian marine sedimentary rocks; 14. Lower Proterozoic Hongqiyingzi Group; 15. Archean Sanggan Group Jiangouhe Formation metamorphic rocks; 16. Archean Sanggan Group Huajiaying Formation metamorphic rocks; 17. Archean Sanggan Group Shudizhuang Formation metamorphic rocks; 18. Metamorphic rocks of the Xigeyu Formation of the Archean Sanggan Group; 19. Yanshanian granite (porphyry); 20. Hercynian alkaline complex (unclassified)

2.1.1. Regional Structure

Zhangjiakou has a long geological history and complex geological structure. The Archean Sanggan Group metamorphic rocks have undergone multiple stages of tectonic action, forming different types and forms of geological structures (Figure 3) (Yin and Shi, 1995; Yin, 2019a; Wang et al., 2022; Yin and Shi, 2026 a & 2026b).

Regional fold

The metamorphic rocks of the Sanggan Group underwent three folding deformations in the Early Precambrian (Song et al., 1994; Yin and Shi, 1995). The first phase of folding formed a giant compound syncline in the metamorphic rocks of the Sanggan Group, with an axis nearly east-west, an axis plane dipping south, and strata reversed from south to north,

forming the basic structural framework of the Zhangjiakou area. Most researchers believe that this phase of folding occurred in the Archean, contemporaneous with the high-amphibolite-granulite metamorphic event in the region, and slightly earlier than the occurrence of the Chongli-Chicheng deep fault. The second-stage folds are a group of NW-NWW-trending, compound inverted anticlines, with axial planes inclined to the northeast or even lying flat. The sizes of the folds in this stage vary. The secondary tight folds with a scale of 10-100 m on both sides of the main anticline are extremely developed. The second-stage folds predate the migmatization of the area, which occurred at 2500-2400 Ma. The third-stage folds are a group of axially northwest or northwest-west-oriented compound folds formed by NE-SW compressional stress, which appear as wavy fold bundles widely distributed throughout the area, either parallel to each other or arranged in a staggered pattern. Their sizes vary, and a single anticline generally extends for 2-7 km. Among them, the backbone fold in this area is also the largest with the Hanjiagou anticline, which extends nearly 20 km along the axial direction (Figure 4). The Hanjiagou anticline is a wide and gentle wavy fold with a dip angle of about 30 degrees on both wings. The wavelength is generally several times greater than the wave height, and the axial plane is nearly vertical. It is one of the most clearly exposed and best preserved fold structures in the area.

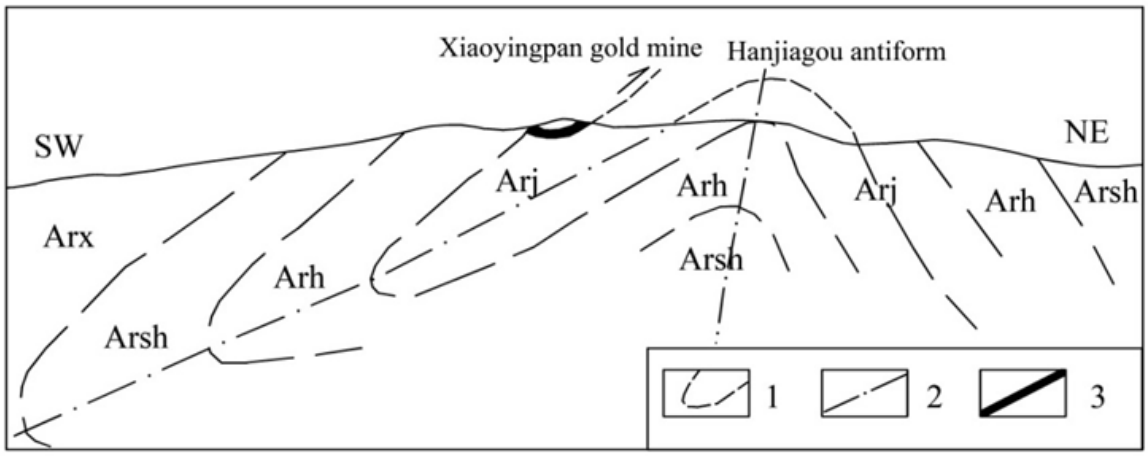


Figure 4. Ore-hosting structure of the Xiaoyingpan gold deposit in the Zhangjiakou gold province (Yin and Shi, 1995; Wang et al., 2022)]

1. Schistose of the host rock; 2. The fold axis plane; 3. Gold-bearing quartz vein/ore body

Regional fault

There are many faults and/or fault zones in the area, which can be divided into east-west faults, northwest faults and northeast faults according to their strike direction (Figures 1-3). The gold belt and ore fields are mainly controlled by the east-west Chongli-Chicheng deep fault, and the gold deposits and ore bodies are located in the secondary fault systems on both sides of the deep fault. The intersection of faults in different directions is often where gold deposits are concentrated. This is also one of the common characteristics of almost all endogenous gold deposits in the world.

• **East-west fault:** The Chongli-Chicheng deep fault zone, which is more than 500 kilometers long and 1-5 kilometers wide, is the most important first-order fault and gold-controlling structural zone in the North China Platform. As the dividing line between the Inner Mongolia axis and the Yanshan platform folded belt, the fault zone starts through Shangyi, Shizuizi, Chongli, Zhenningbao to

Chicheng in the west and turns north through Chengde and Beipiao to merge with the Kangbao-Weichang-Chifeng fault zone, forming an important gold metallogenic zone in northeastern China. The fault zone is composed of a series of densely parallel high-angle reverse faults, compression and crushing zones, and ductile shear zones. The rock strata close to the fault zone are nearly upright and some small mylonite belts are developed along the layers. The fault surface is roughly south-dipping, and the alteration foliation on both sides is strong. The rocks in the fault zone generally contain 0.01-0.40 g/t of gold, with the highest at 0.87 g/t (Yin and Shi, 1995). There are a series of Archean and Hercynian basic-ultrabasic rock bodies of varying sizes on both sides of the fault zone. Gravity field measurements have shown that the fault zone cuts deep below the Moho surface. The depth of the Moho surface in the Chongli area is 42-43 km (Dong, 1989; Song et al., 1994; Yin and Shi, 1995). This is a deep fault zone that has been active from the Archean Era through the Himalayan Period. The series of structures derived from it not only control a series of magmatic activities, but also control deformation, metamorphism, migmatization, and sedimentation of different ages and scales on both sides. All these geological processes provide power, heat, mineralizing materials, ore fluid migration channels, and ore-bearing space for the activation, migration, and enrichment of gold in this area, and ultimately create many different types of gold deposits in the Zhangjiakou gold province (Figure 5). On both sides of this fault zone stretching for more than 200 km, especially within 30 km on its south side, from the Erdaobei gold mine in Shangyi in the west to the Tulongshan gold mine in Chicheng in the east, there are more than 100 gold deposits and gold showings distributed intermittently (Figures 1-2).

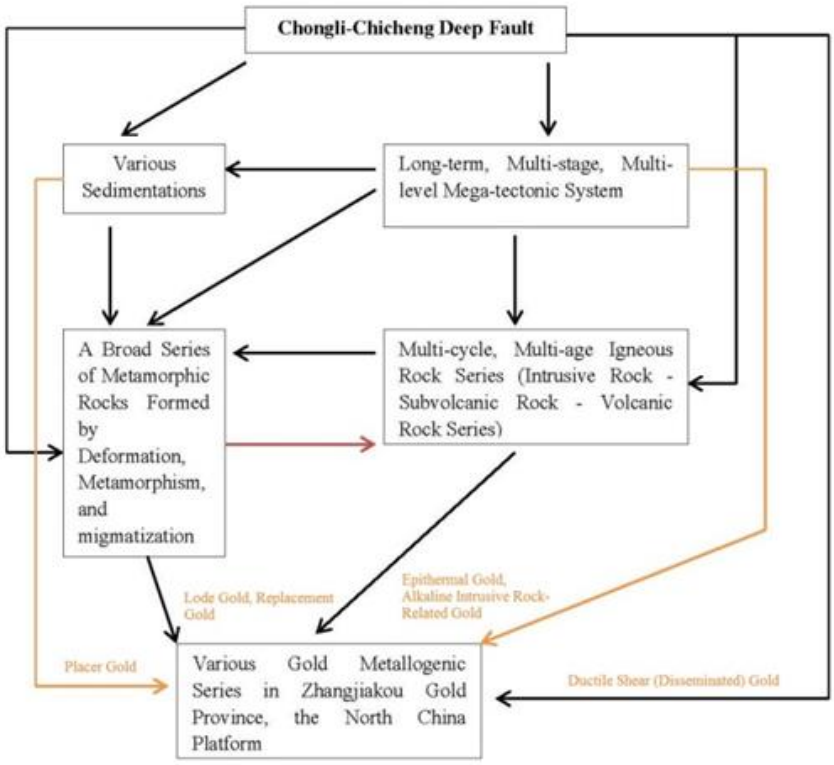


Figure 5. The extensive impact of the Chongli-Chicheng deep fault zone and its control over the Zhangjiakou gold province

The fault zone is mainly composed of early mylonite rocks, late tectonic breccias, marine sedimentary rocks of the lower part of the Mesoproterozoic Changcheng Group, and tectonic rocks of the Jurassic. Some sections are limonite-mineralized, and thin quartz veins are interspersed and filled along the fault zone. The mylonite is mainly composed of sericite, light red potassium feldspar, and quartz, the latter possessing an obvious wire drawing structure. These rocks with strong tectonic foliation are often distributed around some rigid blocks. The structure and rock deformation of the fault zone indicate that it has a history of multi-period and multi-stage activities (Wang, 1986; Dong, 1989; Hu et al., 1990; Zhang, 1990; Song et al., 1994; Yin and Shi, 1995; Xu et al., 2014). Its main activity periods are: the early stage, including the ductile shear thrust during the Late Archean Wutai Movement; the middle stage of the Proterozoic Jixian Movement, was revived and dominated by ductile-brittle thrust activities; the Hercynian stage, characterized by brittle deformation and the formation of a large number of tectonic breccias, accompanied by the emplacement of basic and ultrabasic rock bodies. Finally, the late stage, comprised of the Mesozoic and Cenozoic periods, was characterized by brittle normal fault activities.

• **NW-trending fault**: The northwest-trending faults are the most widely distributed, large-scale, and frequently active group of faults in the area. According to the occurrence, they can be divided into two groups: one group strikes NW310°-340°, dips to the northeast, and has a dip angle of 50°-80°. It is mainly distributed in the Zhangquanzhuang-Xiangshuigou area, containing many gold-bearing quartz veins and filled with various igneous dykes. The other group strikes NWW280°-310°, dips to the south, and has a dip angle of 60°-70°, which is mostly consistent with the occurrence of the strata. The faults are filled with gold-bearing quartz veins with very few igneous dykes. It is mainly distributed in the Shuijingtun-Sitaizui area. In the Xiaoyingpan-Zhangquanzhuang area, more than 200 gold-bearing quartz veins and intermediate-basic dykes distributed in the northwest are widely developed. This fact shows that the northwest-west-trending faults in the area have important mineralization and prospecting significance. The northwest-trending faults that are closely related to mineralization have the following characteristics: larger-scale faults often show traces of multi-stage activities, and the structures are inherited and accompanied by multi-stage hydrothermal superposition. Before gold mineralization, they were characterized by compression and torsion, and during the mineralization period, they were tensile and tension-torsion. The deposits and ore bodies are often controlled by secondary feather-shaped fissures. The various types of igneous dykes contained within them, including gabbro, diabase, lamprophyre, diorite porphyry, granite porphyry, and quartz porphyry, are mostly very developed due to the influence of later structures, and polymetallic mineralization is common. The top and bottom plates and surrounding rock of the fault are well hydrothermally altered, and sericitization, silicification, chloritization, and pyritization are common.

• **North-south fault**: According to their formation age and structural characteristics, the North-South fault can be divided into two categories: one is a large-scale multi-stage active fault, extending 3-7 km; the fracture zone constituting the fault is relatively wide at 20-30 m on average, with the widest area at 50-100 meters with an inclination of 50°-70°. It is filled with gold-bearing quartz veins or dykes and has developed various alterations, which were revived in the Yanshan orogeny and destroyed the existing ore bodies and/or cut through the dykes. The second category is the product of the Yanshan orogeny, with a small scale and obviously cuts various early geological bodies and ore bodies.

There are many ductile thrust structures and a klippe group in the area, some of which are closely related to the formation of gold deposits. For example, the main controlling ore structure of the Xiaoyingpan gold deposit discussed below is a typical representative of this type of ductile thrust structure.

2.1.2. Ore-bearing structure

The main ore-bearing structure of Xiaoyingpan gold deposit is a gentle wavy compression-shear structure, with an overall trend of 46° northeast, a dip to the southeast, and an average dip of 4° (Figure 6). The gently dipping gold-bearing quartz vein, i.e. the fault, is bounded by different lithologies of the hanging and foot walls: the hanging wall is composed of the older Archean Huajiaying Formation metamorphic rocks (Ar*h*), while the footwall belongs to the younger Jiangouhe Formation metamorphic rocks (Ar*j*). Most researchers theorized that (Wang, 1986; Dong, 1989; Hu et al., 1990; Zhang, 1990; Li, 1992; Song et al., 1994; Xu et al., 2014) this structure is an interlayer sliding or detachment zone. It is a compressive structure formed by relative sliding between the metamorphic rock layers of the Huajiaying Formation and Jiangouhe Formation of the Archean Sanggan Group during the compression and folding process. It was later filled with gold-bearing ore fluid to form the main ore body of the Xiaoyingpan gold deposit.

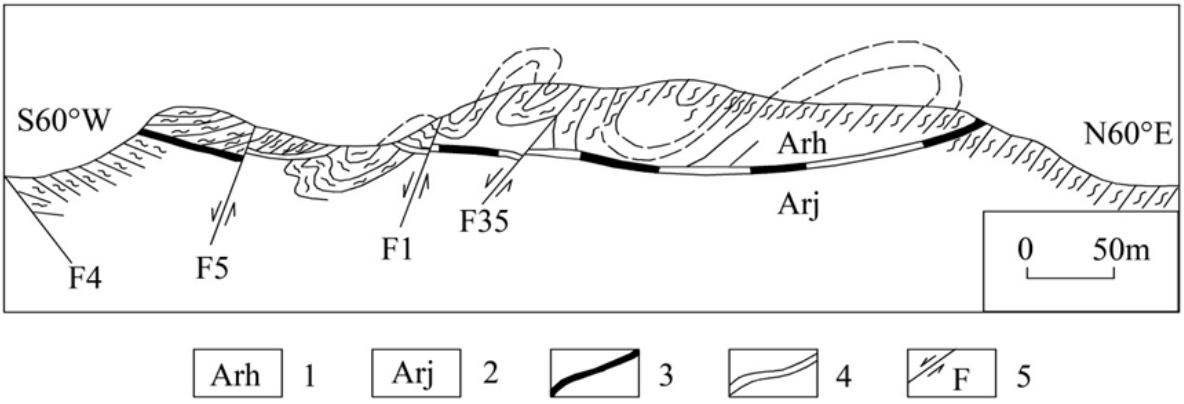


Figure 6. Cross section of the main ore-hosting structure of Xiaoyingpan gold deposit and its relationship with the surrounding rocks of both the hanging wall and the foot wall

1. Metamorphic rocks of the Huajiaying formation of the Archean Sanggan group; 2. Metamorphic rocks of the Jiangouhe formation of the Archean Sanggan group; 3. Gold-bearing quartz vein/ore body; 4. Altered rocks; 5. Fault

Field observations and studies have shown that the structure is mainly composed of mylonite rocks and is strongly altered, and the gold-bearing quartz veins are strictly confined within the mining area. The more than 30 gold-bearing quartz veins exposed on the surface that were originally identified were later proven to belong to the same vein belt through systematic exploration and were strictly controlled by the uneven compressional structure with convex and concave separations. After a detailed field study of this ore-bearing structure, the author of this article concluded that it is not an interlayer sliding zone or a slip zone, but a typical thrust-nappe ductile shear zone. The evidence is as follows: The overall occurrence of this large-scale gently inclined quartz vein-type ore body is not consistent with the overall occurrence of the gneissosity of the metamorphic rock strata in

the mining area, nor is it consistent with the trend of the folds in the area. No matter what kind of superposition the folds developed in the area have experienced, their trends are all NW, EW, and SN, and there are no NE-trending folds. The overall occurrence of the main ore body of the Xiaoyingpan gold deposit strikes 46 degrees north and dips to the southeast. Obviously, it is impossible for the existing fold structure to form such an occurrence of the ore body through interlayer sliding. Statistics of more than 500 occurrences of ore bodies in different parts of the mining area show that the dip angle of the ore body is generally 3°-5°, and locally 17°-21°. Statistics on the occurrence of the strata above and below the ore bodies in the area show that the strata in the mining area generally have an inclination of 20°-40° and can reach 50°-60° or even steeper locally. Obviously, the ore bodies and strata are in an oblique relationship, which is also proved by field observations. This oblique relationship cannot be explained by the view of interlayer sliding (debonding) zones.

It is almost universally recognized by relevant researchers that the turning end of a fold is often a favorable location for mineralization. This favorable location includes two main parts: the collapsed location and the compression cracks, especially the tension cracks. If the main mineralization structure of the Xiaoyingpan gold deposit is indeed a slip structure in the process of folding, then there should be ore bodies filled in the collapsed location and/or structural cracks at the turning end, but neither drilling nor open pit exploration have found the existence of such ore bodies. This proves instead that the mineralization structure is not an interlayer slip structure in the process of folding. Field drilling and open pit exploration also confirm the uneven mineralization structure, with a height difference of 20-30 m between the ore layers at the crest and trough and a wavelength difference of about 100 m, while the ore body is still continuous in the same layer (Song et al., 1994; Yin and Shi, 1995). It is hard to imagine that the ore-bearing space created by the interlayer sliding (decollement) during the folding process can create such a huge single ore body. As previously mentioned, the hanging and foot walls' lithology of the ore-bearing quartz veins is different, and the secondary small soft wrinkles and fold structures are developed in the metamorphic rocks of the hanging wall but not in the foot wall (Figure 6). If the structure where the ore body is located is indeed the interlayer sliding (decollement) between Arh and Arj, then the ore body should only be produced in this position. The reality is that this structure is only the location where the main ore body of the mining area is located. The gold ore body is not only produced in the contact zone between the Huajiaying Formation of the Sanggan Group and the Jiangouhe Formation metamorphic rocks, but are also produced in single Arh or Arj metamorphic rocks. This obviously cannot be explained by the interlayer sliding (decollement) structure between Arh and Arj to explain its ore-control mechanism.

Some researchers believe that the ore-bearing structure of the Xiaoyingpan gold deposit is part of the Qingbiankou-Xiaoyingpan thrust structure (Li, 1994). The two wings of this ductile thrust-nappe structure are tightly closed and small folds and secondary faults with inclined or upright axial surfaces are well developed, resulting in an intense deformation zone. A series of isoclinal inverted folds are developed in the middle zone between the root and the frontal zones. The axial surfaces of these folds are inclined to the root zone, and secondary faults are developed. The thrust-nappe structure is a rear-edge thrust fault system that is imbricate fan-shaped and has forward extension characteristics. . Blastomylonites are developed in the Dongwangshan-Zhoudingtun-Geyubao area, which are the product of early ductile thrust deformation and later transformation such as static recrystallization. Its external system is the Archean granulite facies terrane, which is a component of the early

deeper crust that was exposed to the surface through thrust uplift. Its scale is estimated to be more than 100 km, and the thrust distance may be several kilometers. This thrust structure has the characteristics of multiple periods of activity, and it may be revived in the later period (Zhang, 1984; Xu et al., 1997; Wang et al., 2021; Zhen et al., 2021).

Thrust faults are well developed in the Huajiaying Formation (Ar*h*), the main ore body's hanging wall in the Xiaoyingpan gold deposit. As secondary structures of the hanging wall, these thrust faults are either oblique to the surrounding rock or occur along the layer and become interlayer faults. In this regard, the main ore-bearing structure of the area cannot be consistent or parallel to the occurrence of the surrounding rock, otherwise its secondary faults will not occur along the layer. This proves from one aspect that the main ore-bearing structure is not what has previously been called an interlayer sliding. Both these small-scale thrust faults and the main ore body are upturned about 25° north, and the occurrence gradually slows down towards the south. In the Sandaogou open-pit mining area of the Xiaoyingpan deposit, you can see almost vertical strata and ore-bearing layers upturned to the north. This shows that the overall movement direction of the thrust structure is from south to north. The remaining scratches, steps, and directional mylonite structures on the hillside to the west of the Sandaogou mining area also confirm this.

Mylonite is widely developed in both the hanging and foot walls of the ore-bearing structure in the Xiaoyingpan West mining area, especially in the foot wall. This indicates that the thrust nappe structure is a ductile shear zone. There is also sugar-like quartz with slight iron staining and yellow-brown and brown in the mining area, and the quartz grains are of different sizes. According to Bonnemaison and Houssou et al (Bonnemaison, 1986; Houssou et al., 2017), this kind of extremely fine, milky white or even colorless and transparent sugar granular quartz, which sometimes has a jasper- or chalcedony-like appearance, is composed of microcrystalline quartz (1 - n μm) aggregates. This microcrystalline quartz aggregate is the result of the reprecipitation of silicon dioxide after the original existing mineral-free milky white quartz formed a solution through mylonitization. Essentially, the mineral-free quartz vein plays the role of sugar granular quartz matrix. Sugar granular quartz is a "lithology" that is conducive to capturing gold and is the result of ductile shear. In other words, sugar granular quartz can be used as an identification mark for the existence of ductile shear zones.

In summary, the ore-bearing structure of the Xiaoyingpan gold deposit is a gently inclined, thrust-nappe ductile shear zone. The general direction of the thrust is from south to north. From a regional perspective, along with the aforementioned first-stage closed isoclinal folds, a series of thrust-nappe ductile shear zones developed in the Zhangjiakou area. In addition to the above-mentioned Xiaoyingpan main ore-bearing and Chongli-Chicheng giant thrust-nappe ductile shear zones, there are also the Shizuizi-Xishuangtai and Dalingbao-Tianjiayao thrust-nappe structures. In this geological environment where thrust-nappe action is generally developed, the possibility of the development of thrust-nappe ductile shear zones in the Xiaoyingpan area is far greater than interlayer sliding.

Based on the interaction between different geological phenomena in the field and the characteristics of the Xiaoyingpan gold deposit's main ore-bearing structure, and by comparing them with faults at different stages in the region while accounting for the isotopic ages of existing geological events (Table 1), it should be effective to examine the formation age and development evolution of the ore-bearing structure.

Table 1. The key geological events in Zhangjiakou gold province

Major Geological Events in the Region		Relative Geological Period	Isotopic age
		Early → Late	Ma
Early	Volcano-sedimentary processes and mafic and ultramafic intrusions	….	>2800
	High-amphibolite-granulite metamorphism (Chongli-Chicheng	….	2790 ± 155
	(deep fault begins to be active)		
	Regional migmatization	….	2500-2400
	Amphibolite-facies retrograde metamorphism	….	2400
	Greenschist-amphibolite retrograde metamorphism	….	1800-1500
	Localized migmatization	….	600-450
	Main dike emplacement	….	380-242
	Alkaline complex emplacement	….	273-203
	Mineralization of major gold deposits	….	260-150
Late	Part of the porphyritic granite emplacement	…	188-156
Data source	Zhang, 1984; Wang, 1986; Zhang, 1986; Gao & Gao, 1988; Dong, 1989; Hu et al., 1990; Zhang & Wang, 1990; Zheng, 1990; Gao, 1991; Li, 1992; Hu, 1994; Li and Peng, 1994; Wu, 1995; Yin and Shi, 1995; Mo, 1996; Wu, 1997; Xu et al., 1997; Niu et al., 2009; Zhao et al., 2010; Liu, 2014; Xu et al., 2014; Zhen et al., 2021		

Through a detailed study of the Xiaoyingpan gold deposit and regional structures, some researchers have concluded that its main controlling structure is one of a series of faults that occurred with the first phase of folding. In other words, the ore-bearing structure of the deposit occurred during the Wutai Movement at the end of the Archean Era (Ye and Qian, 1994; Bai, 2018). Judging from the deformation characteristics of the ore-bearing structure and its hanging rock strata, it is similar to the Chongli-Chicheng giant thrust nappe ductile shear zone. Therefore, the author agrees with this view. Judging from the different fillings in the fault zone, this is also a multi-stage active fault zone. The fault has since been reactivated, and the gold-bearing quartz veins have been strongly broken and transformed.

The main ore-bearing structure of the Xiaoyingpan gold deposit is a fault that occurred in the late Archean and was active many times across different geological periods. The three main evolutionary stages of the fault and their characteristics are as follows: ① Early ductile deformation began in the late Archean, and thus the characteristic mylonite is formed. The rock is transformed from high amphibolite phase to granulite phase through ductile shearing to greenschist phase. The typical mineral combination is sericite + chlorite + quartz ± feldspar. ② The mid-term brittle-ductile or ductile-brittle deformation stage occurred in the Hercynian period. Uneven strain occurred in the area due to the differences in the rock types that underwent tectonic activation in different sections, some of which were continuous non-uniform strains while others were discontinuous non-uniform strains. In this way, hardening occurred through plastic deformation in some sections, where the rock's mechanical properties changed from toughness (plasticity or viscosity) to brittleness. This caused the ductile shear zones formed under the same time, space, and physical and chemical conditions to show different characteristics of toughness or brittleness in different sections. Fractures in brittle sections lead to the filling of quartz veins, or the pre-existing quartz veins are fractured and gold-bearing hydrothermal fluids flow in to form quartz vein-type ore bodies. In the ductile stage or section, sugar-like gold-bearing quartz veins and altered rock-type gold mineralization are formed. This also explains why there are two types of gold ores in the Xiaoyingpan deposit. ③The late transformation that occurred in the early Yanshan orogeny was brittle deformation, which was mainly manifested in the

strong crushing and transformation of the existing ore body, causing dislocation and complicating its occurrence. At the same time, white quartz and carbonate veins without ore were generated. This post-ore-forming transformation stage created good conditions for the late oxidation and secondary enrichment of the ore in the mining area, and also created conditions for the formation of local placer gold deposits.

In summary, the main ore-bearing structure of the Xiaoyingpan gold deposit has multi-stage and multi-phase activity characteristics and exhibits different structural properties. This structural feature leads to multi-stage and multi-phase gold mineralization, as well as different mineralization styles, namely quartz vein, replacement, and oxidized secondary enrichment.

The Dongping gold deposit in Zhangjiakou area is related to a large-scale alkaline complex intrusion (Figures 2-3). Its ore bodies and veins are also clearly controlled by various structures (Figures 7-8) (Song and Guo, 1992; Yin, 1994i; Li and Jin, 2000; Zhang et al., 2000; Jiang et al., 2012; Wang et al., 2021; Chao et al., 2022).

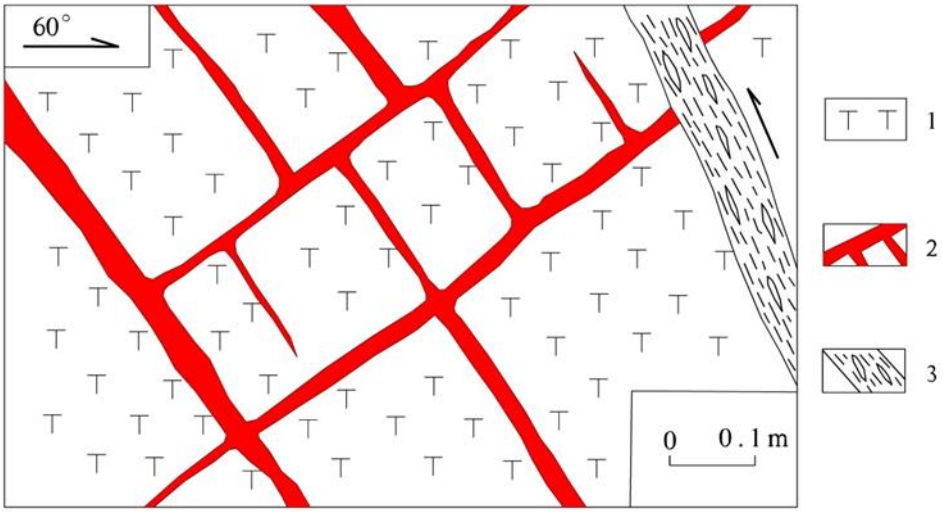


Figure 7. Sketch map of grid-like quartz stockwork veins in Dongping gold mine (#36 Drift, 1503 Level; after Yin and Shi, 1995 and Chao et al., 2022)

1. potassium feldspar altered monzonite; 2. grid-like quartz stockwork vein (Q1); 3.fault

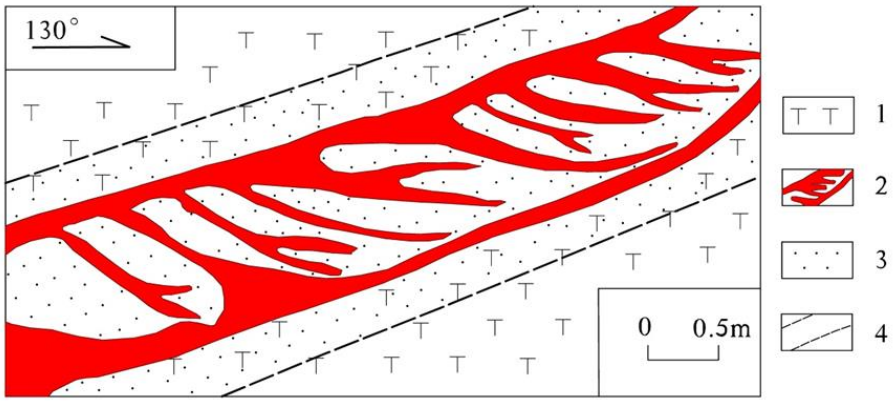


Figure 8. Sketch map of quartz vein (Q3) formed in the third paragenetic stage in Dongping gold deposit (on the roof, 1464 Level; after Yin and Shi, 1995 and Chao et al., 2022)

1. monzonite; 2. quartz vein (Q3); 3. potassium feldspar altered monzonite; 4. ore body range

2.2. Gold deposits and structures in the Mesozoic orogenic belt on the west coast of Canada

The Cariboo gold mining district, located in the east-central region of British Columbia, Canada, has been a historically significant gold rush district on the Pacific coast of western North America since at least 1858. Large-scale gold rush mining occurred in this region prior to the 1930s, since which exploration and mining of hard rock gold have been the main focus. To this day, it is still an important gold-producing area in North America with hard rock gold as the main exploration and mining target. At the same time, placer gold mining of different scales still flourishes. During the Great Depression in the 1920s, the Cariboo gold mining district thrived in spite of the broader severe economic decline. The British Columbia government even had plans to move the provincial government to Barkerville, a small town that was the epicenter of the Cariboo gold mining district. Although this move did not come to fruition, Barkerville, which is still famous for its role in the BC gold rush, has become a provincial park and is still favored by tourists from all over the world. Among the many projects in the park, the most popular one is the gold panning show. The luckiest tourists will harvest a small amount of real gold nuggets among the "fool's gold" pyrite that was put in the sediment beforehand.

According to relevant statistics, recorded gold production from the Cariboo gold mining district totals some 5.0 million ounces, including an estimated 3.0 million ounces from placer mining from 101 creeks and rivers, and 2.0 million ounces from lode gold mining (Yin, 2018a; Yin, 2019a).

The mining district lies approximately 80 km east of Quesnel, 120 km southeast of Prince George, and 500 km north of Vancouver. It is situated within the Quesnel Highlands on the eastern edge of the Interior Plateau. The highlands have an average width and length of approximately 50 km and 160 km respectively (Yin and Daignault, 2007 & 2008). The Quesnel Highlands are the remnants of a rolling plateau formed initially from bedrocks lain down as the ancient North American Plate moved westwards, colliding with offshore seabed and island groups. The bedrocks were then overlain by lava flows emanating from Chilcotin volcanoes that filled the lowlands between the Coast and Cariboo Mountains. These remnants rise gradually from roughly 1,500 m above sea level in the west to more

than 1,900 m above sea level in the east, and become progressively more dissected with elevation. Located between the Coast and northern Rocky Mountains, the district is within the Southern Cordillera region, as defined by the Geological Survey of Canada for the purpose of describing seismic risk (Bowman, 1889; Johnston and Uglow, 1926; Richards, 1948).

Situated within the Cariboo gold belt (Figure 9), the district encompasses (from northwest to southeast) the former producing Hardscrabble tungsten-gold mine and the Mosquito Creek (MGM), Aurum, and Island Mountain gold mines (IGM), located on the northwest of the Jack of Clubs Lake. The IGM (1934-1967) and MGM (1980-1983) produced 603,800 ounces of gold from approximately 1.35 million tons of quartz-type ore with an average grade of 12.0 g/t gold and replacement ore with an average grade of 23.0 g/t gold. The Cariboo Gold Quartz mine (CGQ), situated on southeast of the Jack of Clubs Lake (Figures 9), produced 1.68 million tons grading 12.7 g/to gold from 1933 to 1959, primarily from quartz veins. Additionally, the belt also contains the Bonanza Ledge gold mine, the Cariboo Thompson gold & silver mine, and the Cariboo Hudson gold mine (Skerl, 1948; Struik, 1986; Rhys, 2001; Yin, 2009 & 2010).

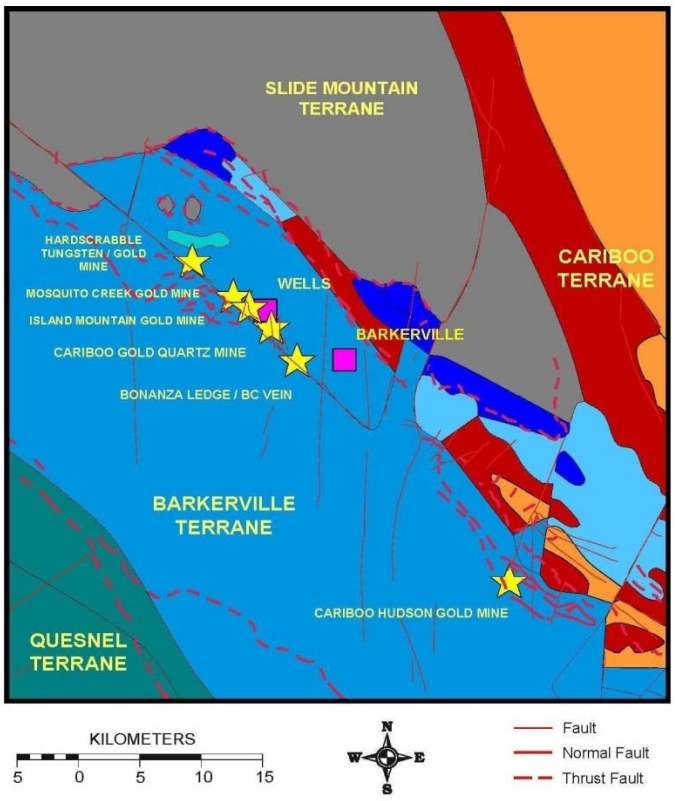


Figure 9. Regional geology of the Cariboo gold mining district (After Yin, 2018a)

The region lies within the Barkerville terrane consisting of a late Proterozoic and/or Paleozoic sequence of continental shelf and slope deposits developed adjacent to the craton

of Ancestral North America, and includes clastic sedimentary rocks along with lesser amounts of volcanic rocks and carbonates. As part of the Omineca belt of the Canadian Cordillera, it is structurally the lowest exposed stratigraphic sequence in area, and is more deformed and metamorphosed than adjacent terranes (Rhys, 2001; Yin, 2009 & 2010). Rocks of the Snowshoe group in the district have been metamorphosed to lower greenschist facies, generally of lower metamorphic grade than other sequences in the Barkerville terrane. Rocks of the Barkerville terrane were subjected to an early period of ductile deformation that resulted in westward-directed, asymmetrical folds plunging shallowly to the northwest. Post metamorphic open folds with upright cleavage are superimposed on earlier structures. During the late Cretaceous to early Tertiary, the terrane was disrupted by northwest trending dextral strike-slip faults such as the Willow fault, a major strike-slip fault of unknown displacement that has been mapped through Mount Tom, Island Mountain, Cow Mountain and Richfield Mountain in the Barkerville area (Struik, 1986). The north striking cross faults are an important control for the gold vein mineralization (Rhys, 2001). Stratigraphic position, host rock lithologies, and proximity to north-striking fault zones are important guides to the different styles of gold mineralization recognized in the district. Historical production has been from mesothermal pyrite-bearing quartz vein systems that cut turbiditic rocks, and from semi-massive to massive pyrite replacement type bodies that occur in carbonate-rich rocks structurally higher but stratigraphically lower in the sequence (Skerl, 1948; Struik, 1986; Rhys, 2001). The area is underlain by a northwest striking, moderately northeast dipping sequence of rocks on the steep, overturned limb of a southwest-verging antiform (Figures 9), which in turn, is on the northeast flank of the Island Mountain anticlinorium. Structure in the district is briefly discussed as follows (Rhys, 2001; Yin, 2011):

•**Deformation and folding**: at least three phases of folding and fabric development occur in the region and are responsible for the major regional map patterns. The early deformation event records significant, ductile penetrative shortening. Deformation 2 is associated with a spaced to penetrative northeast-dipping foliation. The youngest deformation results in spaced, northwest trending, and steeply dipping crenulation cleavage in the region.

•**Faults**: faults and shear zones developed in the region are of several generations and orientations. These include the north trending and moderate to steep east-dipping faults; for example, the No. 1, Rainbow, Sanders, Lowhee, Goldfinch, Waoming and Marie faults. The strike faults are a northwest-trending, and moderate to steep northeast-dipping (45° - 80°) set of faults, likely the oldest in the area; one of the most important strike faults is the BC fault zone, localized mainly in the BC Argillite Unit and occupied by the BC quartz vein.

There are five principal types of lode gold deposits in the district; namely, auriferous pyrite replacement, including replacement in limestone and in calcareous clastic rock; pyrite-quartz vein/veinlet lode gold, including strike vein, diagonal vein, orthogonal vein, and quartz veinlets; basalt-hosted auriferous pyrrhotite-pyrite lode gold; and associated gold in porphyry copper styles (Table 2) (Yin, 2018a & 2019a).

Table 2. Lode gold deposit type in the Cariboo gold mining district (Yin, 2018a & 2019a)

Lode gold type	Sub-type	Representative gold deposit
Auriferous pyrite replacement	Limestone hosted	Mosquito Creek, Aurum, Island and Cow Mountain gold deposit
	Clastic rock hosted	Bonanza Ledge gold deposit on the Barkerville Mountain
Basalt-hosted gold-bearing pyrrhotite-pyrite lode gold	N/A	QR gold deposit
Auriferous pyrite-quartz vein/veinlet lode gold	Strike quartz vein	BC Vein on Barkerville & Cow Mountains
	Diagonal quartz vein	Hardscrabble W-Au Mine, Island, Cow and Barkerville Mountains
	Orthogonal quartz vein	Island, Cow and Barkerville Mountains; Cariboo Thompson & Cariboo Hudson Gold Mines
	Quart veinlet	Island, Cow and Barkerville Mountains
Associated gold in porphyry copper	N/A	Mount Polly porphyry copper

As the most important type of gold deposit in the area, quartz vein-type gold mineralization is completely controlled by faults of different properties and occurrences. Most important in this case refers to gold deposits with the largest mineralization scale, the most gold produced, and are still being explored and mined today.

3. Close spatiotemporal relationship between structure and gold mineralization

By examining the relationship between different types of gold deposits and structures around the world, we can generally establish the following common rules: the two have the same or very similar temporal and spatial distributions, and they are also inseparable in space. The tectonic system's scale, level, stress type, and activity period determine the scale of gold belts, ore fields, deposits, and ore bodies, and even the type of gold mineralization.

Within the same fault system, faults of different levels play different controlling roles in the formation of gold deposits, and can be viewed as having their own division of labor. The first-level deep faults in the fault zone not only control the formation of mineralization parent rocks closely related to the formation of gold deposits, but also directly or indirectly control the migration of mineralization materials and gold-bearing fluids, and ultimately direct the formation and distribution of the gold deposit belt in the area (Figure 1-3,5,9). Secondary faults control the distribution of different gold fields in the same gold belt. As for tertiary faults, they specifically control the formation and distribution of specific deposits in a certain gold field.

There is no doubt that the empty areas at the turning ends of the folds and associated cracks and fractures are also favorable locations for the production of gold deposits and gold ore bodies. The Ø-shaped structure formed by the intersection of linear and circular structures is also a favorable location for gold mineralization (Yin, 1996). Depending on the sizes of the circular and the linear structures, the Ø-shaped structure at their intersection controls either some gold ore fields (large-scale Ø-shaped structure) or some gold deposits (small-scale Ø-shaped structure).

Similar to the above-mentioned Ø-shaped structures, the intersection of two or more linear structures and depending on their size the intersection of linear structures and folds, also control the formation of gold ore fields and/or deposits. Similarly, the intersection of two or more ring structures is also a favorable condition for the formation of gold mineralization. The scale of these ring structures also determines the scale of the relevant gold ore fields and/or deposits, and by association determines the output form of the relevant gold ore bodies.

The mechanical properties of faults or fissures at different levels (tensile, compressive, compression-torsion, tension-torsion, shear, brittle, ductile, brittle-ductile or ductile-brittle, etc.) also control the scale and output pattern of gold mineralized belts, ore fields, ore deposits, and to an extent ore structure and texture.

The number of fault activities also controls the scale and output pattern of the same gold belt, ore field, ore deposit, and ore body to a certain extent. Similarly, the number of fault system activities also controls more specific gold mineralization elements such as the stage, mineralization intensity, and ore structure to a certain extent.

In short, structural association indirectly or directly controls the occurrence, development, and completion of gold mineralization by controlling the three major diagenetic processes closely related to mineralization, especially igneous activities.

4. Discussion: the deep mechanism between structure and mineralization

Fundamentally speaking, the ultimate question of mineral deposit research is a very complex and extremely difficult one to answer: Where is the deposit, and why is it here instead of elsewhere? The traditional mineral deposit theory gives a vague and general description: given a certain tectonic position and a specific structural-magmatic-sedimentary background, certain P, T, Eh, pH, mineralizers and their concentrations and other factors control the formation of mineral deposits. This is an answer largely without substance.

Theoretically, the answers to all problems in nature ultimately come down to a series of scientific principles based on mathematics, physics, and chemistry.

However, the complexity of the ore forming control factors in nature is difficult to accurately summarize using the same language of mathematical and physical formulas and/or chemical reaction equations. Among the many ore-controlling factors, some variables seem to be certain, while others exist in a state of non-integer dimension: the ore-forming hydrothermal system is a complex nonlinear, non-equilibrium system.

Due to the existence of certain nonlinear fluctuation factors, it is impossible to fully and meticulously characterize the variables of a mineralization process under current scientific and technological conditions. In a specific mining area, even between structures of the same level and type, there will be differences in mineralization capacity due to the different surrounding rock conditions. One part is completely mineralized, another part is locally mineralized, and even more parts are not mineralized at all. Even under the same surrounding rock conditions, two structural systems, or even different parts of the same

structural system, can result in two completely different results of mineralization or non-mineralization due to some very inconspicuous factors.

Nevertheless, in-depth exploration of the intrinsic mechanism of structural control over gold mineralization still has very important economic value and theoretical significance.

According to the dissipative structure theory, a nonlinear open system far from equilibrium will constantly exchange matter and energy with the outside world. When the change of an individual parameter in the system reaches a certain threshold, the system will undergo a mutation, i.e., a non-equilibrium phase transition through fluctuations, and transform from the original chaotic disordered state to an ordered state in time, space, or function [58]. Geologists have studied the branch theories of dissipative structure formed by nonlinear dynamics, such as bifurcation, cynergetics, and catastrophe theory (Yu, 1981 & 1987; Li, 1989; Wu and Lin, 1992; Yang et al., 1993; Yin, 1996), in addition to the non-equilibrium and nonlinear problems that are common in geological processes. They point to the transformation from mineralization to mineral deposits, which is essentially the result of the development of dissipative structures from steady-state instability to a state far from equilibrium ((Yu, 1981 & 1987).

The occurrence of mineralization results from the development of localized dissipative structure and length of coherence. There are a large number of nonlinear coherent effects in the fault system. When the ore-forming fluid reaches some nonlinear low-pressure expansion zones, mutation phenomena cause hydrothermal boiling, nonlinear rapid decrease in solubility, cross-catalysis, and convergence between alteration and mineralization, which are all obvious nonlinear coherent effects. The fault-ore-forming system is a dissipative structure far from equilibrium, which provides the necessary conditions for mineralization.

The formation of dissipative structure requires two conditions that are internal and external to the system: internal conditions that constitute the self-organization conditions of dissipative structure, and external conditions such as certain mineralization forces that trigger and maintain the occurrence of self-organization, including magmatic events, geothermal gradients, and the maintenance of certain material compensation guarantees. The generation of dissipative structure is the result of thermodynamic instability caused by order parameters exceeding a certain critical value. At this time, even a small disturbance can cause the state of the system to transition to the dissipative structure branch (Figure 10). This branching phenomenon destroys the original uniform symmetry of the system, which are the so-called symmetry-breaking instabilities. The essence of mineralization is the combination of conditions and transformational mechanism of the non-equilibrium steady-state instability without ore into a dissipative, ore-forming structure.

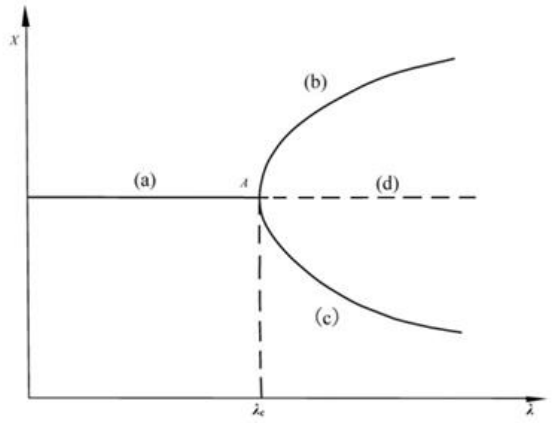


Figure 10. Stability and bifurcation of solutions of reaction-diffusion equations (After Yu, 1987)

X represents the amplitude of the solution of the equation, and the solid line and the dotted line represent the stable solution and the unstable solution, respectively; λ_c is the critical value of λ; *A* is the branch point; a and d represent thermodynamic branch, b and c represent its branches

Ore accumulation is spatially localized, i.e., the localization of dissipative structures. The emergence of prospective mineralization areas is a reflection of localized dissipative structures. Whether various mineralization factors can enter a coordinated state together is the key to mineralization. When a large amount of minerals enter the localized dissipative structure, they are precipitated and mineralized due to the action of state attractors, i.e., expansion zones or favorable ore-controlling spaces. Some ore-bearing spaces have accumulated minerals many times, and some ore-forming hydrothermal fluids have pulsed up and formed minerals many times. This inheritance can occur between multiple mineralizations over a long period of time, such as tens or hundreds of millions of years. The ore source exists for a long time in the mineralization concentration area, and localized dissipative structures appear many times in favorable spatial locations under the action of multiple external forces. This favorable space can be as large as a mineralization belt or as small as a specific ore-gathering structure.

In short, the control of structure on gold and other mineralization is essentially the formation of localized dissipative structures that are conducive to the occurrence of gold deposits. The formation of any mineralization zone on earth is the result of the development and evolution of a grand dynamic system in geological history. It is a unified whole of geological-metallogenic processes and their time-space structures that have been formed and constantly changed. The spatial zoning of strata, structures, igneous rocks, and ore deposits, the formation of mineralization zones, and the establishment of mineralization periods all come from the self-organization process occurring in a macroscopic homogeneous system and the resulting time-space ordered structure, namely dissipative structure.

The dynamic response of the geochemical system to disturbances both inside and outside the system and its relative stability are the root causes of the system's self-organization process and the formation of ordered space-time structures. The emergence of multiple

non-equilibrium steady states (where the space-time symmetry of the system remains unchanged) in the geochemical cycle of crustal evolution, the occurrence of periodic chemical oscillations (time-ordered structure "limit cycle", time asymmetry) in the process of magma crystallization, and the division of regional mineralization prospect areas (space-ordered structure "localized dissipative structure", space asymmetry) are open physical and chemical systems in a non-equilibrium state. They generally undergo dynamic evolution, self-organization processes, and form space-time dissipative structures. They are generated because the system's local time and space domains do not respond in time to inside and outside disturbances and are pushed away from equilibrium, thus causing the non-equilibrium steady state to become unstable. The multi-order of successive bifurcation of dissipative structures determines the formation of mineralization zones on the earth's surface (Yu, 1981 & 1987; Li, 1989; Wu and Lin, 1992; Yang et al., 1993; Yin, 1996).

The identification procedure of ore-aggregating dissipative structures is to identify and find open systems for energy and material exchange. More specifically, it is to find deep structures and rising channels of magma and fluids, and discover the ore-forming forces that ensure the supply of materials and energy, such as geothermal anomalies, magma, and tectonic activities. It's also important to look for ore-forming "attractors" such as expansion zones and favorable ore-controlling spaces, and traces of nonlinear coherence effects or specific alteration and geochemical element combinations, and pay special attention to their scale and intensity. The length of coherence can then be reviewed to estimate the potential of ore deposits. The length of coherence refers to the linear length of the system that breaks symmetry and forms a dissipative structure when the rise and fall increases at the critical point and the steady state become unstable.

Large structures are often closely related to the formation of large and super-large mineral deposits. Large structures that penetrate the entire crust and even reach the mantle lithosphere provide energy for geological processes such as magmatic activity. Changes in the thermal state of the crust or lithosphere, such as the rise of mantle plumes, can also cause the activation of existing large structures. The continuity of large faults and the decompression induced by faults will cause deep superheated materials to melt due to pressure release, thereby further inducing diagenesis and mineralization. Some special types of faults, such as the ductile shear system deep in the crust, not only provide some metamorphic fluids, but also help to extract mineralizing materials from the surrounding rocks under reducing conditions and tectonic pumping. The brittle-ductile tectonic conversion system in the middle of the crust and the open brittle fracture network system in the upper crust provide channels for ore fluid convection and places for ore-forming materials to precipitate, thus forming shear zone-type ore bodies related to fragmented mylonite and vein-like ore bodies related to open fracture systems, respectively [65-66].

Many micro-disseminate type gold deposits in the Yunnan, Guizhou, and Guangxi Provinces of China are generally believed to have been formed on the basis of initial gold enrichment during syngenetic sedimentation, followed by subsequent enrichment through hydrothermal transformation along faults, such as replacement and filling.

In the relatively active period of some faults, such as syngenetic faults, the faults assist the conduction of ore-bearing fluids through seismic pumping, expansion, and re-rupture of mineralized zones. When the applied stress is close to the rock's breaking strength, the

expansion effect causes a series of microcracks in the rock that are parallel or approximately parallel to the fault plane, thereby increasing the fault's conductivity. If the fluid potential gradient is parallel to the fault plane, the fluid will flow preferentially along the syngenetic fault zone. Usually, the expansion effect is strongest in the area of maximum tensile stress. Re-rupture of mineralized zones occurs in the middle and late stage of diagenesis, which reconnects the cracks blocked by cement and enhances the fault's ability to conduct fluids and heat energy. The seismic pumping effect was first proposed by Scholz in 1974 (Zhai et al., 1997).

Fault movement releases stress in the fault zone, compresses the rock back to its pre-expansion state, and the fluid that originally filled the expansion gap is squeezed out and flows upward along the fault zone. The driving, drainage, excretion, and mineral accumulation of hydrothermal fluids by syngenetic faults are necessary conditions for the formation of hydrothermal sedimentary deposits. Syngenetic faults of different orientations and scales intersect and divide large basins to produce secondary small basins, resulting in differences in the bottom topography, hydrodynamics, hydrogeochemistry, and physical chemistry in the basin, thus creating a favorable space for the accumulation of large amounts of minerals.

The main fault belt in south China’s Yunkai gold province also clearly controls the distribution of gold mineralization belts (Chen, 1994). Approximately 95% of the 130 gold deposits are located in various faults. The shape and occurrence of gold deposits are generally similar to specific sections of the fault structure, or depend on the shape and occurrence of its secondary fault. Brecciated gold ore is developed in fault breccia or compression fracture zones of brittle fracture, and the brecciated ore is mostly the surrounding rock from both sides of the structure. Gold mineralization is mostly developed in cementing materials including siliceous, iron-manganese, etc. Vein gold ore is often produced in brittle fractures or in secondary fractures beside them. The gold ore structure in the ductile fault is mainly banded and disseminated, and the ore structure includes mylonitic structure and anisotropic granular structure. The bands in banded gold ore are primarily formed by the directional arrangement of minerals such as quartz, mica, and calcite that have been elongated due to plastic deformation. The intensity of gold mineralization is positively correlated with the intensity of fault activity. In structures with large fault scale, developed tectonic rocks, and multi-stage activity characteristics (especially those with early ductility and late brittleness), the intensity of gold mineralization is strong. Otherwise, it is weak.

Fault zones are mutation zones of rock mechanical properties and physical and chemical conditions. Where pores and cracks are developed, rock and mineral particles are small but the surface area is large, which will have a greater absorption function for ore-bearing hydrothermal fluids. This is conducive to the interaction between the ore-bearing hydrothermal fluids and tectonic rocks to produce alteration and mineralization. With the continued action of geo-stress and the further development of tectonic rocks, the migration, convergence, and precipitation of ore-bearing hydrothermal fluids will continue. If the fault is revived, multi-stage and multi-epoch gold mineralization may occur.

The Dongwujiazi and Paishanlou gold deposits in western Liaoning Province are close to each other and belong to the eastern section of the North China Platform’s northern margin.

and are both produced in late Archean metamorphic rocks. However, as a representative of quartz vein-type gold deposits, the Dongwujiazi gold deposit is quite different from the ductile shear zone-type represented by the Paishanlou gold deposit in terms of mineralization mechanism, age, and characteristics. Some researchers believe (Zhou et al., 2015) that the difference in local tectonic environment has caused these two different types of gold deposits. This sharp contrast can be well explained based on the "wave conduction" theory.

The three major faults in the northwest Shandong Province of China control more than 80% of the gold reserves in Jiaodong gold province (Liu, 2015). The tectonic stress field in the mining area was characterized by NW-W compression before mineralization, resulting in a NNE-trending compressional fault zone; during the mineralization period, it was characterized by NW-W extension, with two groups of faults in the nearly N-S and NE directions opening and being filled with ore fluids; after mineralization, it was characterized by NNW-W compression, forming a grid-like structural fluid-conducting system (Chen, 2010). The secondary faults of the Tanlu fault are the ore-controlling and ore-guiding structures of the Jiaodong gold province. The shallow tension-shear fractures produced by the right-lateral strike-slip faults in the late Yanshanian period are ore-containing structures. The expansion effect caused by the tension-fracture deformation is the driving force for the "pumping" of deep ore fluids to invade and fill (Zhao et al., 1996). The structure of the Jiaodong gold province in the mineralization period has the characteristics of multi-level ore control. The NEE-trending Taishan-type structure controls the distribution of the Jiaodong gold province, and the NNE-trending regional shear zone controls the output location of the gold ore field. The nature of the fault controls the gold mineralization style. The occurrence of the fault zone controls the inclination and lateral inclination of the ore body. The migration characteristics of the hanging and foot walls of the shear structure and the combination of faults control the distribution pattern of the veins. The structural deformation lithofacies zone controls the geochemical characteristics of the structure. The structure in the main mineralization stage shows the characteristics of stress relaxation and tension (Lu et al., 2007).

The latest research reveals that the multiple eruptions of the Icelandic volcanic system between 2023 and 2024 did not come from a single magma reservoir, but from multiple reservoirs with different chemical compositions (Simon et al., 2024). This shows the complexity and dynamics of the mid-crustal magma domain, and is of great significance to build a more accurate and profound understanding of the mineralization mechanism of magma. For a long time, scientists generally believed that most basalt eruptions on oceanic islands and mid-ocean ridges were supplied by a single magma reservoir located in the middle crust or shallow crust, and therefore believed that the magma had been fully mixed underground before the eruption. The materials produced by the Icelandic volcanic eruption possess significant heterogeneity in chemical composition. The differences in the isotopic ratios of K_2O/TiO_2, $^{87}Sr/^{86}Sr$, and $^{143}Nd/^{144}Nd$ and the ratios of incompatible elements all point to the existence of multiple magma reservoirs with different chemical compositions beneath the Icelandic volcano. Additionally, changes in the geochemical characteristics of rocks in different eruption events indicate that these magma reservoirs are not static, but instead undergo complex dynamic evolution processes, including magma injection, mixing, and differentiation.

From this, it can be inferred that deep faults cause the melting and mixing of rocks of different compositions at different depths in the earth's crust, further promoting chemical reactions between these substances, thereby greatly promoting the occurrence and development of various mineralizations and the formation of mineral deposits.

6. Conclusions

The “dissipative structure” reframes mineralization as a mathematical and physical problem, linking it to the stability and bifurcation of reaction–diffusion equations that describe its time evolution. Mineralization is essentially the transformation of a non-equilibrium, non-mineralized state into a stable dissipative structure, driven largely by geological features such as faults.

Beyond serving as pathways and storage for ore-forming materials, faults influence mineralization through key physical and chemical effects. Deep, large faults cause decompression, triggering melting, magmatic activity, and mineralization. They also facilitate fluid movement through seismic pumping, fracturing, and expansion. Long-term tectonic activity sustains geothermal anomalies, hydrothermal systems, and favorable geochemical conditions, while repeated fault activity enhances the accumulation and enrichment of ore materials, increasing the likelihood of large gold deposits.

Deep faults also induce crustal melting and mixing of rocks at different depths, creating conditions for chemical reactions, migration, and re-enrichment of ore-forming materials. Within fault systems, different levels play distinct roles: major deep faults act as channels for magma and mineralizing materials, forming specific types of gold deposits depending on rock composition, while smaller faults control the distribution of ore fields, deposits, and ore bodies.

Finally, structural characteristics—such as mechanical properties, activity, and rock types—govern the intensity and stages of mineralization. Post-mineralization tectonic processes further reshape deposits, often transforming primary gold deposits into placer deposits.

References

01. Bai, HJ. 2018. Research on the characteristics of ore-controlling structures in the Xiaoyingpan-Hanjiagou gold ore field in Hebei Province. The 5th National Symposium on Ore Field Structure and Deep Ore Prospecting Prediction. Geological Society of China.
02. Bonnemaison M. 1986. Gold-bearing quartz veins: a special case of gold shear-zone. Chronic of Mining Researc, 482: 55-56.
03. Bowman A. 1889. Report on the geology of the mining district of Cariboo, British Columbia. Geological Survey of Canada, Annual Report for 1887- 1888, V. 3, pt. 1, pp. 1-49c.
04. Chao YH, Yin JZ and Yin YH. 2022. The paragenetic stage of the Dongping gold deposit in the northern margin of the North China Platform. European Journal of Applied Sciences, 10 (6). DOI: https://doi.org/10.14738/aivp.106.13391.

05. Chen HY. 2010. Study on Metallogenic Structure and Structural Geochemical Prospecting of Wangershan Gold Deposit in the Northwest Jiaodong. Guilin University of Technology, Doctoral dissertation. DOI:10.7666/d.y1717620.
06. Chen SW. 1994. The fault controlling actions on the gold deposits in Yunkai area, Guangdong China. Journal of Precious Metallic Geology, 3 (1): 32-37. DOI: 10.13686 /j.cnki .dzyzy (in Chinese with English abstract).
07. Dong JL. 1989. Genesis of gold deposits in the northern Hebei & western Liaoning Provinces, China. Geology and Prospecting, (9): 22~23 (in Chinese with English abstract).
08. Gao L and Gao F. 1988. Retrograde metamorphism of Archean granulite in Zhangjiakou-Yihua area and evidence from Rb-Sr isochron ages. Journal of Hebei Institute of Geology, 1988; (24): 11-19.
09. Gao M. 1991. Geochemistry of the Archean granulite facies metamorphic rocks in the Zhangjiakou-Xuanhua region, China. Geology and Exploration, (9): 16~22 (in Chinese with English abstract).
10. Houssou NN, Allialy EM, Kouadio J-L F and Gnanzou A. 2017. Structural control of auriferous, mineralization in the Birimian: Case of the Agbahou deposit in the region of Divo, Côte d'Ivoire. International Journal of Geosciences, 8 (2). DOI: 10.4236/ijg.2017.82008.
11. Hu XD. 1994. "Granite-Greenstone Terrane Gold Deposit Type Ore-Controlling Conditions and Mineralization Prediction" Research Report. Tianjin Institute of Geology and Mineral Resources, Ministry of Geology and Mineral Resources.
12. Hu XD, Zhao JN and Li SB. 1990. Gold mineralization in the Archean metamorphic rocks in the Zhangjiakou-Xuanhua region, China. Journal of the Tianjin Institute of Geology & Minerals, (22): 2~9 (in Chinese with English abstract).
13. Jiang XM, Fan BH and Li SZ. 2000. Structural characteristics of the Dongping gold mine in Hebei Province. Geological Prospecting, DOI: CNKI: SUN: DZZK.0.2000-04-008.
14. Johnston WA and Uglow WL. 1926. Placer and vein gold deposits of Barkerville, Cariboo District, British Columbia. Geological Survey of Canada, Memoir 149.
15. Li HY and Peng L 1994. Mineralization mechanism of the Chongli-Chicheng gold-bearing shear zone in the
north-western Hebei Province. Geology and Resource, (3): 169-175.
16. Li JL. 1989. Practical significance of dissipative structure and earth integrated field theory. Bulletin of Mineralogy, Petrology and Geochemistry, (2): 3. DOI: CNKI:SUN:KYDH.0.1989-02-018.
17. Li R. 1992. Geology, geochemistry and metallogenic model of the Hougou gold deposit in Hebei Province, China. Geology and Prospecting, (3): 46~50 (in Chinese with English abstract).
18. Li SZ and Jin GC. 2000. Geological characteristics and structural ore-controlling role of the Dongping gold deposit, Hebei Province. Acta Geoscientia Sinica, (1): 45-52. DOI: CNKI:SUN:DQXB.0.2000-01-006.
19. Liu W. 2015. Study on Geological Characteristics and Ore-controlling Rules of the Zhaoyuan-Muping Fault Zone in the Northwest Jiaodong. Doctoral dissertation, China University of Geosciences (Beijing).
20. Liu WJ. 2014. Research on Mineralization Characteristics and Mineralization of Gold Deposits in Northern Hebei. Doctoral dissertation, China University of Geosciences (Beijing).
21. Lü GX, Sun ZF, Zheng XL et al. 2007. Study on the multi-level ore-controlling law of the structural system in the concentrated area of Jiaodong gold deposits. Geotectonica et Metallogenia. 31 (2): 12. DOI: 10.3969/j.issn.1001-1552.2007.02.009.
22. Mo CH. 1996. Study on the mineralization and enrichment mechanism of gold in the main gold deposits in Zhangjiakou area. Bulletin of Mineralogy, Petrology and Geochemistry, (4): 4. DOI: CNKI: SUN:KYDH.0.1996-04-005.

23. Niu SY, Sun AQ, Wang, BD, Gao CJ, Wei MH, Yang LJ, Xie XM and Wang XZ. 2009. Analysis of mineralization and deep prospecting potential of Zhangxuan Manzhi structure. Geotectonics and Mineralization, 33 (4): 8. DOI: 10.3969/j.issn.1001-1552.2009.04.009.
24. Rhys D. 2001. Lode gold in the Cariboo: the Bonanza Ledge discovery of International Wayside Gold Mines. 2001 Cordilleran Roundup Abstracts, p. 20-21.
25. Richards F. 1948. Cariboo Gold Quartz mine. In: Structural Geology of Canadian Ore Deposits, Canadian Institute of Mining and Metallurgy 1948; p. 162-168.
26. Simon WM and Alberto C et al. 2024. A dynamic mid-crustal magma domain revealed by the 2023 to 2024 Sundhnúksgígar eruptions in Iceland. Science, 386 (6719): 309-314. DOI: 10.1126/science.adp8778.
27. Skerl AC. 1948. Geology of the Cariboo Gold Quartz mine, Wells, B.C. Economic Geology, 43: 571-597.
28. Song GR and Guo NL. 1992. Ore-controlling geological factors and mineralization model of Dongping gold deposit. Geology and Resources, 1 (2): 110-114.
29. Song R, Wang Y and Wang Z. 1994. Geology of the Lode Gold Deposits in Hebei Province, China. Beijing: Geological Publishing House (in Chinese).
30. Struik LC. 1986. Imbricated terranes of the Cariboo Gold belt with correlations and implications for tectonics in southeastern British Columbia. Canadian Journal of Earth Sciences, 23: 1047-1061.
31. Wang JP, Yin JZ, Chao YH, Yin YH, Xiang SP and Shi HY. 2022b. Structural control of gold deposits in the northern margin of the North China Platform. European Journal of Applied Sciences, 10 (6): 29-37. DOI:
10.14738/aivp.106.13390.
32. Wang SQ. 1986. Genetic research of the gold deposits in the Zhangjiakou-Xuanhua region, China. Journal of Peking University (Nature Science Edition), (4): 81~89 (in Chinese with English abstract).
33. Wang ZK, Jiang X, Wang Y and Shang MY. 2021. Geological and geochemical comparison of Xiaoyingpan and Dongping gold deposits in Zhangjiakou area. Geology and Exploration, (7): 14-20 (in Chinese with English abstract).
34. Wu FU and Lin Q. 1992. Application and review of the dissipative structures in geology. Journal of Changchun University of Geology, 22 (1): 31-38. 01): 33-40. DOI: CNKI:SUN:CCDZ.0.1992-01-005.
35. Wu SF. 1995. A brief analysis of the ore-controlling effect of remote sensing line-ring structures in the concentrated gold mineralization area of Zhangjiakou. Gold Geology, 1 (2): 4. DOI: CNKI:SUN:HJDZ.0.1995-02-008.
36. Wu ZH. 1997. Deformation characteristics and ore-controlling effect of Chongli-Longhua-Fuxin tectonic belt in northern Yanshan Mountains. Chinese Journal of Geomechanics, 3 (2): 9.
37. Xu H, Liang R, Zhao J, Yang Y and Liang Y. 2014. Geological characteristics of the gold triangle region and its prospecting target, Hebei Province, China. Mineral Exploration, 5 (1): 14~20 (in Chinese with English abstract).
38. Xu ZQ, Zhang JX and Xu HF. 1997. Ductile shear zones and dynamics of China's main continental mountain chains. Beijing: Geological Publishing House.
39. Yang RH, Shen QW and Yang PA. 1993. Application of fractal method in revealing the rock-controlling and ore-controlling conditions of basement. Journal of Changchun University of Geology, (1): 102-107. DOI: CNKI:SUN:CCDZ.0.1993-01-015.
40. Ye FG and Qian XL. 1994. Study on ore-controlling structure of Xiaoyingpan gold deposit in Xuanhua. Mineral Deposits, 13 (4): 8. DOI: CNKI:SUN:KCDZ.0.1994-04-007.
41. Yin JZ. 1994i. Research on the types of gold deposits in the north-western Hebei Province, China. Journal of Precious Metallic Geology, 3 (3): 176-185 (in Chinese with English abstract).
42. Yin JZ. 1996. On the Paragenetic Model and Mineralizing Mechanism of the Dashuigou independent tellurium deposit in Shimian County, Sichuan Province, China-the Only Independent

Tellurium Deposit in the World. Chongqing: Chongqing Publishing House, 190 pp (in Chinese with English abstract).
43. Yin JZ. 2009. Assessment Report on the 2008 Exploration Program on the Cariboo Gold Project, Wells, British Columbia. British Columbia Ministry of Energy, Mines and Petroleum Resources Assessment Report.
44. Yin JZ. 2010. Assessment Report on the 2009 Drill Program on the Cariboo Gold Project, Wells, British Columbia. British Columbia Ministry of Energy, Mines and Petroleum Resources Assessment Report.
45. Yin JZ. 2011. Assessment Report on the 2010 Drill Program on the Cariboo Gold Project, Wells, British Columbia. British Columbia Ministry of Energy, Mines and Petroleum Resources Assessment Report.
46. Yin JZ. 2018a. Metallogenic series of gold deposits in the Cariboo gold mining district, British Columbia, Canada. Earth Sciences, 7 (1): 17-22. DOI: 10.11648/j.earth.20180701.14.
47. Yin JZ. 2019a. Structure controls on gold deposits in the Cariboo Gold Mining District, British Columbia, Canada. GSA Annual Meeting in Phoenix, Arizona, USA, 51 (5). DOI: 10.1130/abs/2019am-330823.
48. Yin JZ, Liu Y and Shi HY. 2021. Chemical and physical characteristics of quartz from gold deposits in the North China platform: relationship to gold mineralization. Acta Geochim 2021; 40, 998–1022. DOI; https://doi.org/10.1007/s11631-021-00487-x.
49. Yin JZ and Daignault P. 2007. Report on the 2006 Exploration Program on the Cariboo Gold Project, Wells, British Columbia. British Columbia Ministry of Energy, Mines and Petroleum Resources Assessment Report.
50. Yin JZ and Daignault P. 2008. Report on the 2007 Exploration Program on the Cariboo Gold Project, Wells, British Columbia. British Columbia Ministry of Energy, Mines and Petroleum Resources Assessment Report.
51. Yin JZ and Shi HY. 1995. Geology of Gold Ore Deposits in Zhangjiakou-Xuanhua Region, Hebei Province, China. Beijing: Geological Publishing House, China. pp 131 (in Chinese with English abstract).
52. Yin JZ and Shi HY. 2026a. Quantitative indices of ore-bearing potential in porphyry polymetallic deposits and their modern exploration methods. Iran J Sci. https://doi.org/10.1007/s40995-026-01989-0.
53. Yin JZ and Shi HY. 2026b. Types and metallogenic indices of porphyry (Cu) polymetallic deposits based on tectonic settings. AIMS Geosciences, 2026, 12(3): 704-737. doi: 10.3934/geosci.2026028.
54. Yin JZ, Sun Y, Yin HY, Shi HY, Sparling J, Chao YH and Xiang, SP. 2023. Correlations between trace elements in pyrite and gold mineralization of gold deposits on the North China platform. Acta Geochim, 42: 1079-1103. DOI: https://doi.org/10.1007/s11631-023-00636-4.
55. Yu CW. 1981. Mechanisms of ore formation and primary dispersion at the Dexing porphyry copper deposit, Jiangxi, and their implications in geochemical exploration. In: Proceedings of the 8th International Geochemical Exploration Symposium, Journal of Geochemical Exploration, 15 (1-3): 115-137.
56. Yu CW. 1987. Ore-forming process and dissipative structures. Acta Geologica Sinica, (4): 54-67. DOI: CNKI:SUN:DZXE.0.1987-04-004 (in Chinese with English abstract).
57. Zhang CH and Wang QC. 1990. Early Precambrian Metamorphism in Hebei Province, China. Beijing: Geological Publishing House 1990.
58. Zhang GR, Xu JH, Wei H, Song CG, Zhang YB, Zhao JK, He B and Chen DL. 2012. Study on the structure-alteration-fluid mineralization of the deep-peripheral Dongping gold deposit in northern Hebei Province. Acta Petrologica Sinica, 28 (2): 637-651.
59. Zhang QS. 1984. Geology and Metallogeny of the Early Precambrian in China. Changchun: Jilin People’sPublishing House （in Chinese with English abstract).

60. Zhang YX. 1986. Archean Geology and Metamorphic Iron Ore deposits in Eastern Hebei Province, China. Beijing: Geological Publishing House.
61. Zhai YS, Deng J and Li XB. 1999. Essentials of Metallogeny. Beijing: Geological Publishing House, 286pp (in Chinese with English abstract).
62. Zhai YS, Zhang H, Song HL et al. 1997. Macroscopic Structures and Superlarge Ore Deposits. Beijing: Geological Publishing House, 180pp (in Chinese with English abstract).
63. Zhao LS, Wu YB and Ye R. 1996. Study on the metallogenic structure-geochemical dynamics of the Jiaodong gold deposits. Modern Geology, 10 (2): 5. DOI: CNKI:SUN:XDDZ.0.1996-02-009.
64. Zhao S, Zhang FX and Niu SY. 2010. Study on the ore-controlling structure of the Shuijingtun gold deposit in Zhangjiakou. In: National Seminar on Ore Field Structure and Geological Prospecting Theory and Methods. Geological Society of China.
65. Zhen SM, Wang DZ and Bai HJ. 2021. Paleozoic-Mesozoic magmatic tectonic activities and gold mineralization in the Zhangjiakou-Xuanhua area on the northern margin of the North China Craton. Acta Petrologica Sinica, (6). DOI: 10.18654/1000-0569/2021.06.01.
66. Zheng YD. 1990. Structural research on the Dongping gold deposit in Chongli County, Hebei Province, China. Geology and Prospecting Review, (2): 20~27 (in Chinese with English abstract).
north-western Hebei Province. Geology and Resource, 1994. (3): 169-175.
67. Zhou YH, Zhang J, Wang HB, Zhao DF and Shao J. 2015. Control of local tectonic environment evolution on gold mineralization: A case study of Dongwujiazi and Paishanlou gold mines in western Liaoning. Geology and Resources, (6): 545-553.

Data availability

The data that support the findings of this study are available from the author upon reasonable request.

Declaration of competing interest

The author declares that he has no competing financial interests or personal relationships that could have appeared to influence the work reported in this paper.

Use of AI tools declaration

The author declares that he has not used Artificial Intelligence (AI) tools in the creation of this article.

Original Article

Genetic Types and Geology of Cesium Deposits in Mainland China

Jian Zhao Yin[1] Ⓛ

Abstract

Thanks to the diverse geological settings formed during the long geological evolution process, mainland China ranks among the best in the world in terms of critical metal resources, including cesium. Based on previous research results, this article determines the genetic types of existing cesium deposits in mainland China and summarizes different types of geological characteristics. The known cesium deposits in mainland China are all associated/paragenetic deposits, and no independent cesium deposits have been discovered so far. These cesium mineral resources include endogenous deposits closely related to tectonic and magmatic activities, exogenous deposits related to weathering, erosion and sedimentation, and mixed endogenous and exogenous deposits formed by a combination of endogenous and exogenous geological processes. Endogenous cesium deposits include granitic pegmatite type, igneous hydrothermal type, alkaline granite and carbonate type, granite type and pegmatite type. Endogenous and exogenous mixed types include hot spring type, various brine types (surface water body subtype, deep brine subtype and oil and gas field subtype) and coal type. Exogenous types include sedimentary clay, granite weathering crust and moraine peat types. These cesium mineralizations mostly occurred in the Yanshanian period of the Mesozoic and the Himalayan period of the Cenozoic, and less frequently in the Paleozoic. They are significantly spatially controlled by the Tethys-Himalaya, Altay-Western Junggar and South China multi-stage orogenic belts. Cesium mineralization is often symbiotic and/or associated with rare metals such as rubidium, lithium, niobium and tantalum. Generally speaking, the known cesium ore resources in mainland China are relatively scattered and of low grade, but have high comprehensive utilization potential.

Keywords: genetic type; geology; endogenous, mixed endogenous and exogenous geological processes, exogenous; cesium deposit; mainland China

---

Affiliation Info: 1 College of Earth Sciences, Jilin University, Changchun 130061, China

Corresponding AurhorⓁ: Yin, J. Z., PhD, Professor, geosciences, mineral exploration and mining; Email address: jzyin7@jlu.edu.cn

Citation: Yin, J.Z. 2026. Genetic types and geology of cesium deposits in Mainland China. *Naturalis Scientias*, 3: 739-762. DOI: https://doi.org/10.62252/NSS.2026.1041. www.naturalisscientias.com.

Copyright © 2026 by the author. Published by *Naturalis Scientias*. This is an open access article under the Creative Commons Attribution-NonCommercial 4.0 International (CC BY-NC 4.0) License. (https://creativecommons.org/licenses/by-nc/4.0/).

---

1. Introduction

Cesium and its compounds are widely used in fields such as atomic clocks, catalysts, chemical reagents, electrolytes, camera tubes, high-pressure mercury lamps, scintillation counters, analytical chemistry, bioengineering, medicine, and optical glass. As a key material for manufacturing high-precision timing devices and atomic clocks, cesium finds extensive application in telecommunications, navigation, and scientific research (Dong and Xiao, 2005; Gao et al., 2023; Zhiyan Consulting, 2025; Baike Baidu, 2026). Applications in emerging fields include aerospace ion thrusters, magnetohydrodynamic (MHD) generators for new energy, missiles, spacecraft, thermionic power generation, solar cells, LEDs, lasers, photodetectors, glass-ceramics, DNA separation, and the information industry. In China, the application of cesium is primarily concentrated in traditional industrial sectors, such as catalysts and the chemical industry.

Cesium is a soft, lightweight metal—indeed, the softest of all metals—with a Mohs hardness of only 0.2 and good ductility; it has a melting point of 28.4 °C and a boiling point of 669.3 °C. Pure metallic cesium is golden-yellow in color, exhibits excellent photoelectric properties, and is chemically highly reactive. Due to its chemical instability, cesium does not occur in nature in its elemental form but rather exists in the form of salts (Fan et al., 2007; Liu, 2013; Sihan Industry Research Institute, 2025; Zhiyan Consulting, 2025; Baike Baidu, 2026).

Like many other rare elements, cesium is primarily found in pegmatites and frequently occurs in association with rare metals such as rubidium, lithium, beryllium, niobium, and tantalum. Pollucite is the mineral with the highest natural cesium content and serves as the principal raw material for cesium extraction. It is predominantly found in lithium-rich granitic pegmatites, often co-occurring with minerals such as lepidolite, analcime, petalite, spodumene, and quartz (Zhao et al., 2006; Liu, 2013; Wu, 2023; Li et al., 2025; Wen et al., 2025; Baike Baidu, 2026; Zhao et al., 2026). Globally, major pollucite-bearing pegmatite belts are distributed across the Winnipeg–Lake Nipigon metallogenic province of the Canadian Shield, the Zimbabwe Craton, the Karibib metallogenic belt in Namibia, and the Pilbara metallogenic belt in Western Australia. Cesium-bearing brines are found in Chile and China, while cesium-bearing thermal springs occur in Germany, India, and China.

Based on extensive published literature, this paper focuses on the current status of research and development regarding cesium resources in China; it classifies the genetic types of known cesium deposits and provides a preliminary discussion of their geological characteristics and formation mechanisms.

2. Current status of cesium resources

2.1 Internationality

Global cesium resources are scarce, with over 90% of the total volume concentrated in three countries: Canada, Zimbabwe, and Namibia. Currently, resources suitable for large-

scale mining are concentrated in three major deposits: the Tanco mine in Canada, the Bikita mine in Zimbabwe, and the Sinclair deposit in Australia. Global pegmatite-hosted cesium resources are estimated at approximately 217,100 tonnes (Liu, 2013; Tong, 2014; Zhang et al., 2021; Gao et al., 2023; Li and Hou et al., 2025; Zhiyan Consulting, 2025; Zhao et al., 2026). Among these, Canada's Tanco mine is the only currently operating mine where pollucite is the primary ore, and it holds the world's largest reserves of pollucite. The ore features a high grade, with an average cesium oxide content of 23.3%. Tanco holds 117,200 tonnes of unmined cesium ore resources (containing 16,200 tonnes of cesium oxide) and approximately 3.5222 million tonnes of cesium tailings resources (containing about 26,000 tonnes of cesium oxide), bringing the mine's total cesium oxide resource to 42,200 tonnes. The Bikita mine in Zimbabwe is another major global source of pollucite. Since its discovery in 1911, Bikita has produced significant quantities of metals, including cesium, lithium, and tantalum. The Sinclair deposit in Australia is a recently discovered pollucite deposit, with identified cesium ore resources totaling 7,110 tonnes at a cesium oxide grade of 16.4%, containing 1,166 tonnes of cesium oxide (Gao et al., 2023; Li and Hou et al., 2025; Zhiyan Consulting, 2025).

2.2 China

China ranks high globally in terms of prospective cesium resources; however, its proven reserves are limited. Most deposits are associated/paragenetic minerals characterized by relatively poor ore quality and high development costs, resulting in a current reliance on imports for production. In 2023, China's production of cesium (including cesium compounds) stood at 537 tonnes, a year-on-year increase of 6.76% (Li et al., 2025; Li and Hou et al., 2025; Zhiyan Consulting, 2025).

China's cesium mining industry has evolved through five distinct stages: The initial stage (1950s–1970s) saw exploration, mining, and processing activities primarily serving national defense and the nuclear industry; operations were small-scale with limited technical capabilities, relying heavily on imported equipment and technology. During the 1980s and 1990s, as the Reform and Opening-up policy progressed, China intensified its efforts to explore and develop critical mineral resources; cesium exploration advanced, infrastructure for mining and processing was gradually established, and technical capabilities improved. From the 2000s to the 2010s, rapid technological advancement drove increased cesium application in high-tech sectors, leading to significant progress in technological innovation and industrial chain expansion; breakthroughs in mining and processing technologies expanded the scope of exploration. Between 2010 and 2020, fueled by rising global demand and China's rapid growth in high-tech fields, the industry developed a comprehensive value chain—spanning upstream resource exploration and mining, midstream processing and refining, and downstream high-value-added applications—while the industry scale continued to grow. Concurrently, Chinese enterprises began participating in global cesium resource development. Since the 2020s, driven by further technological progress and stricter environmental regulations, the industry has entered a phase of high-quality development characterized by a shift toward high-end, intelligent, and green operations (Gao et al., 2023; Li et al., 2025; Li and Hou et al., 2025; Sihan Industry Research Institute, 2025).

Cesium deposits in China primarily occur in various brines, granites (in the broad sense) and pegmatites, magmatic-hydrothermal deposits, sedimentary clays, hot springs, and weathered granite crusts (Dong and Xiao, 2005; Liu, 2013; Tong, 2014; Mei et al., 2022; Tang and Wu, 2022; Gao et al., 2023; Li and Wang et al., 2023; Niu et al., 2023; Tan et al., 2023; Yu et al., 2023; Ding et al., 2024; Xue et al., 2024; Zhao et al., 2024; Zhu et al., 2024; Li and Hou et al., 2025; Zhao et al., 2026; Fig. 1).

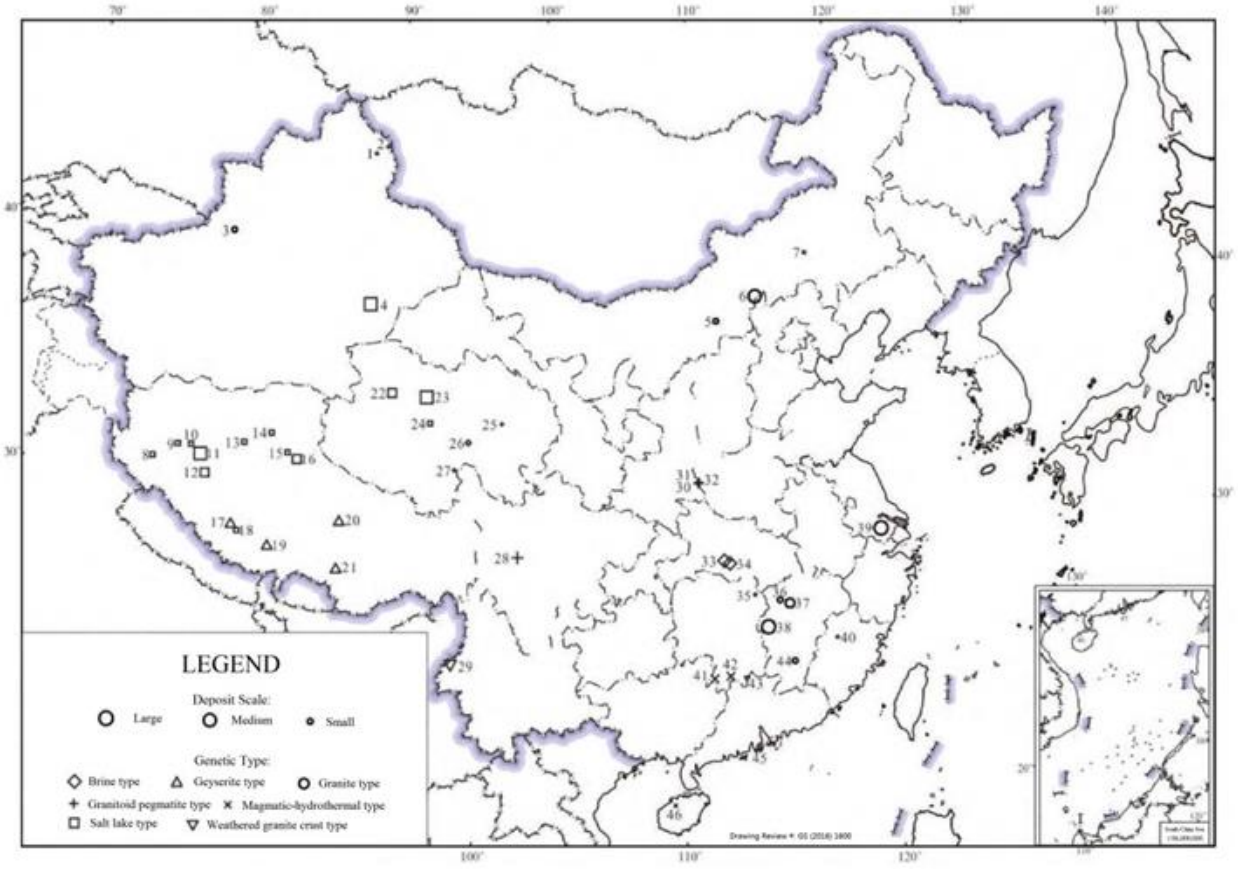


Figure 1. Distribution of cesium deposits in mainland China (modified from Chen et al., 2023)

1-Keketuohai; 2-Bieyesamasi; 3-Boziguoer; 4-Lop Nur; 5-Zhaojinggou; 6-Jiabusi; 7-Weilasituo; 8-Rebangcuo; 9-Niercuo; 10-Bieruozecuo; 11-Mamicuo; 12-Zhabuye; 13-Guping lake; 14-Maerguo; 15-Kongkongchaka; 16-Eyacuo; 17-Dagejia; 18 Semi; 19-Sagalangga; 20-Gulu; 21-Bulangxionggu; 22-Dachaidan; 23-Chaerhan; 24-Dabuxun; 25-Shinaihai; 26-Xiaoliangshan; 27-Caolong: 28-Jiajika; 29-Xinqi; 30-Guanpo; 31-Nanyangshan; 32-Caijiagou; 33-Jiangling; 34-Qianjiang; 35-Renli; 36-Jianxiaguo; 37-Yashan; 38-Siyisi; 39-Shananbang; 40-Xikeng; 41-Xiangyuan; 42-Xianghuapu, 43-Heshangtian; 44-Dongxi; 45-Beijiandao; 46-Fengshou

China previously mined the Koktokay cesium deposit in Xinjiang. However, since the closure of the Koktokay No. 3 Mine in 1999, there have been no domestic, standalone pollucite deposits available for mining. Currently, China continues to develop cesium resources by recovering cesium associated with tailings from lepidolite-based lithium extraction. The supply of high-quality pollucite raw materials relies primarily on imports (Wu et al., 2023; Li and Hou et al., 2025; Zhiyan Consulting, 2025; Baike Baidu, 2026).

Overall, China's cesium resources are relatively scarce; they consist entirely of associated/paragenetic deposits characterized by lower ore quality, extraction difficulties, and limited economic viability. Geographically, lepidolite-hosted cesium deposits in Jiangxi Province represent a significant type of cesium resource in China; these deposits are typically associated with granites or pegmatites, with lepidolite serving as the primary cesium-bearing mineral. Although the cesium grade in these deposits is not high, the reserves are relatively substantial. Additionally, other types of cesium deposits, such as brine-hosted resources, exist in mainland China and are available for future development.

Jiangxi Dongpeng New Materials Co., Ltd. and Jiangxi Tungsten Industry Group Co., Ltd. hold significant positions in the domestic development and processing of cesium ore in China. Xinjiang Nonferrous Metal Industry Group Co., Ltd. and Xianghuangqi Mengjin Mining Development Co., Ltd. have gradually enhanced their competitiveness in the cesium sector through technological innovation. In recent years, Chinese enterprises have made remarkable progress in cesium mining and processing technologies; extraction efficiency and resource utilization rates have risen sharply, precision separation and energy-efficient technologies have continued to evolve, and the production efficiency and purity of cesium compounds have further improved. In 2023, China's production of cesium compounds reached 537 tonnes, a year-on-year increase of 6.76% (Zhou et al., 2024; Li and Hou et al., 2025; Zhiyan Consulting, 2025). As the applications of cesium and its compounds expand across high-tech sectors—including atomic clocks, nuclear energy, semiconductors, and fiber-optic communications—the demand for cesium ore is poised to rise steadily.

While vigorously exploring and developing domestic cesium deposits, mining companies in mainland China are also actively expanding their access to overseas cesium resources. For instance, in 2023, Sinomine Resource Group Co., Ltd. completed the 100% acquisition of equity in the Tanco mine (Canada) and the Bikita mine (Zimbabwe), and secured the exclusive right to purchase the entire output of pollucite resources from the Sinclair mine (Australia), thereby consolidating its position in the global cesium industry (Zhiyan Consulting, 2025; Baike Baidu, 2026). Established in 1999, Sinomine Resource Group has achieved a full industry chain layout—spanning from resource extraction to the production of fine chemical products—through acquisitions such as Dongpeng New Materials, the Tanco mine, and the Bikita mine. Currently, Sinomine controls over 80% of global pollucite resources and accounts for 80% of cesium salt production and supply. The company's Tanco mine in Canada is the only currently operating mine in the world where pollucite is the primary ore. As of the first half of 2024, the Tanco mine held 116,100 tonnes of cesium resources, with a cesium oxide content of 42,100 tonnes, representing more than half of the world's total cesium reserves. The associated pollucite at the Bikita lithium deposit in Zimbabwe offers the potential to further expand the resource base for lithium, cesium, and tantalum. Following the commissioning of the mine's pollucite processing line, Sinomine's production capacity for cesium and rubidium salts is projected to increase from 1,000 tonnes to 1,500 tonnes, with full production capacity expected to be reached by 2027.

Starting with an analysis of the industry chain and establishing a data foundation for cesium, Gao et al. (2023) employed sectoral demand forecasting and input-output analysis to conclude that China's domestic cesium consumption is poised for a period of rapid

growth; China's cesium demand is projected to reach 1,000-1,100 tonnes in 2025, signaling a significant expansion in the market.

3. Types and geology of cesium deposits in Mainland China

Similar to known cesium deposit types elsewhere in the world, all cesium deposits discovered in mainland China are associated/paragenetic deposits; no independent cesium deposits have yet been identified. According to relevant statistics (Zhou et al., 2021), hard-rock cesium resources in mainland China are primarily distributed in Jiangxi Province, with reserves reaching 140,000 tonnes (Cs_2O). Genetically, these deposits fall into various categories—endogenic, exogenic, and mixed types (Table 1)—which are discussed individually below.

3.1 Endogenous cesium deposit

Endogenic deposits are mineral deposits formed by internal geological processes—such as tectono-magmatic activity, metamorphism, and/or the movement of gases and fluids—driven by the Earth's internal thermal energy. Endogenic cesium deposits in mainland China include granite-pegmatite, magmatic-hydrothermal, alkaline granite, carbonatite, granite, and pegmatite types (Fig. 1 and Table 1).

3.1.1 Granitic pegmatite type

Granitic pegmatite-type cesium deposits in China are primarily found in the following regions: northern and southern Xinjiang (including the Koktokay area in Altay); the Kangding, Jinchuan, and Shiqu areas of Sichuan; the Yichun and Shichang areas of Jiangxi; the Chenzhou and Hengyang areas of Hunan; northern Guangdong; the Suzhou area of Jiangsu; as well as Qinghai and Yunnan (Li et al., 2013; Liu, 2013; Tong et al., 2014; Mei et al., 2022; Tang and Wu, 2022; Gao et al., 2023; Li et al., 2023; Niu et al., 2023; Tan et al., 2023; Ding et al., 2024; Li and Hou, 2025). The majority of these deposits are located in Xinjiang, with a smaller number found in provinces such as Yunnan and Sichuan (Li and Hou et al., 2025).

Geotectonically, granitic pegmatite-type cesium deposits in mainland China are predominantly situated within and/or near orogenic belts such as the Altay, West Kunlun, and Songpan-Ganze belts. For instance, the Koktokay Cs-polymetallic metallogenic belt in Altay, Xinjiang, is located at the margin of the Altay orogenic belt.

These deposits typically occur in the exocontact zones of granite bodies and/or in their immediate vicinity. Cesium and associated metals like rubidium tend to become enriched during the late stages of magmatic fractional crystallization; the primary cesium-bearing minerals are pollucite and lepidolite. This is currently the only type of cesium deposit suitable for stable, economic exploitation. Their formation is linked to the crystallization of

residual magma during the pneumatolytic-pegmatitic stage. Such deposits are characterized by high grades, with cesium content in pollucite reaching up to 21.2% (Zhang et al., 2021).

Representative deposits include the Jiajika Cs-bearing polymetallic deposit in Sichuan, as well as the Dahongliutan and Bailongshan Cs-bearing polymetallic deposits in the West Kunlun region of southern Xinjiang (Han et al., 2021; Peng et al., 2024). Research by Hou et al. (2018) indicates that the Cs content in the two-mica granite of the Jiajika Rb-Cs deposit in Sichuan reaches 136×10^{-6}, signifying abundant reserves and immense potential for exploration and development. Fan et al. (2007) reported a Cs content of 85.2×10^{-6} in the pegmatites of the Bailongshan polymetallic deposit, with Cs concentrations of 442×10^{-6} in muscovite and 40.8×10^{-6} in spodumene. These data suggest that Cs in the Bailongshan deposit is primarily enriched in minerals such as muscovite (Li and Hou et al., 2025).

3.1.2 Magmatic-hydrothermal type

Igneous-hydrothermal cesium mineralization is widely distributed across provinces and regions such as Inner Mongolia, Sichuan, Chongqing, Yunnan, Hubei, Hunan, Jiangxi, Guangdong, Gansu, Shaanxi, Shandong, and Zhejiang. Researchers have further subdivided deposits of this genetic type into pneumatolytic-hydrothermal, medium-to-low-temperature hydrothermal, and high-temperature hydrothermal subtypes (Hou, 2023; Li et al., 2024; Liu et al., 2024; Tang et al., 2024; Zhang et al., 2024; Zi et al., 2024).

These deposits are closely associated with tectono-magmatic activity. Cesium mineralization typically develops at the tops of intrusive bodies, within faults inside the intrusions, in folded structures of the wall rock, above fault zones, and within late-stage lithofacies of the intrusions. The intensity of rare-metal mineralization—including that of cesium—correlates positively with the intensity of hydrothermal metasomatism. Cesium commonly co-occurs or is associated with tin, tungsten, lithium, niobium, and tantalum. The mineralization is primarily hosted in potassium-bearing minerals such as K-feldspar, amazonite, (ferroan) lepidolite, biotite, and muscovite. Its formation is linked to processes including the crystallization of residual magma and hydrothermal fluids, as well as metasomatism (including skarnization).

Representative igneous-hydrothermal cesium deposits include the Yujiacun deposit in northern Yunnan (Zhang et al., 2024), the large-scale Tengchong-Xinqi hydrothermal deposit, the Geyuan high-to-medium-temperature hydrothermal deposit in Hengfeng County (Jiangxi), the Bamianshan medium-to-low-temperature hydrothermal filling-type deposit (Xu et al., 2011; Jia et al., 2019), as well as the Shihuiyao and Zhaojinggou deposits (Inner Mongolia), Zhengchong deposit (Hunan), Tiantangshan deposit (Guangdong), and Guobaoshan deposit (Gansu) (Fig. 1 and Table 1).

Table 1. Genetic types, geology, and distribution of cesium deposits in China

Type			Geology	Place of origin	Data source
Endogenic	Granitic pegmatite		Predominantly found near orogenic belts such as the Altai, West Kunlun, and Songpan-Ganzi regions, and commonly occur in the external contact zones of granite bodies or their vicinity. The primary Ce-bearing minerals include pollucite and lepidolite.	Jiangxi, Hunan, Sichuan, Xinjiang, Guangdong, Yunnan, Qinghai, and Jiangsu, etc.	Shen, 2002; Zhao et al., 2006; Fan et al., 2007; Zhao et al., 2008-2010; Xu et al., 2011; Li et al., 2013; Liu, 2013; Tong et al., 2014; Zhang and Li, 2014; Luo et al., 2017; Hou et al., 2018; Jia et al., 2019; Han et al., 2021; Li et al., 2021; Liu et al., 2021; Xiong et al., 2021; Xu et al., 2021; Yu et al., 2021; Mei et al., 2022; Tang and Wu, 2022 & 2024; Yan et al., 2022; Chen et al., 2023; Dai et al., 2023; Gao et al., 2023; Hou, 2023; Li et al., 2023; Niu et al., 2023; Pan et al., 2023; Tan et al., 2023; Wang et al., 2023; Yi et al., 2023; Yu et al., 2023; Zhou et al., 2023; Chen et al., 2024; Ding et al., 2024; Li et al., 2024; Peng et al., 2024；Wang et al., 2024; Xue et al., 2024; Zhang et al., 2024；Zhao et al., 2024; Zhou et al., 2024; Zhu et al., 2024; Li and Hou et al., 2025; Wen et al., 2025; Zhao et al., 2026
	Magmatic-hydrothermal		Typically develop at the tops of rock bodies and frequently occur in association with Sn, W, Li, Nb, and Ta. Primarily hosted in K-bearing minerals such as K-feldspar, amazonite, (ferroan) lepidolite, biotite, and muscovite.	The Inner Mongolia, Hunan, Guangdong, Gansu, Sichuan, Chongqing, Hubei, Shandong, and Yunnan, etc.	
	Alkaline granite and carbonatite		Granite-hosted Nb-Ta deposits with associated Ce primarily formed in orogenic belts dating from 750 to 190 million years ago; the ore-hosting rocks include carbonatites and alkaline granites.	The 414 deposit in Jiangxi, the Limu deposit in Guangxi, and the Jianfengling deposit in Hunan.	
	Granite		Occurring in the South China tectonic-metallogenic belt, the eastern segment of the Yangtze suture zone, and the metallogenic belt on the western slope of the Greater Khingan Range.	Xinjiang, Inner Mongolia, Hunan, Jiangxi, Gansu, etc.	
	Pegmatite		It occurs in areas such as the Tianshan metallogenic belt, the South China metallogenic belt, the Greater Khingan Range metallogenic belt, and the southern part of the Qinling fold belt.	Inner Mongolia, Gansu, Hunan, and Jiangxi, etc.	
Superimposed endogenic-exogenic	Brine	Including surface waters, underground brines, and oilfield brine subtypes.	Occuring within geothermal zones associated with Cenozoic rift valleys and fault-controlled basins in the Qinghai-Tibet Plateau; the associated minerals include opal, hydromica, chalcedony, and cristobalite, alongside Ce-bearing brines and siliceous rocks. Surface brine-type deposits are controlled by the Bangong Co–Nujiang Tectonic Zone and the Northern Qaidam Suture Zone; subsurface brine-type deposits occur in South China and the Jianghan Basin; and oilfield brine-type deposits are found in the Qaidam Basin and the Jianghan Basin.	Surface water types include salt lakes such as Qarhan in Qinghai and Zabuye Tsaka in Tibet; underground brine types include the Qianjiang depression in Hubei; and oilfield brine types include Weiyuan in Sichuan and the Jianghan Plain in Hubei.	
	Coal seam		It has been found in many coalfields across mainland China.	Northeast, North, Northwest, and Central-South China	
	Hot spring		It is commonly found in the vicinity of the Yarlung Zangbo Suture Zone, such as in the southern Tibet region.	Gulu Hot Spring and Semi Hot Spring, Tibet	
Exogenic	Weathered granite crust		The weathered crust of the Cenozoic Baihuanao alkali-feldspar granite in western Yunnan is a rare, super-large, multi-commodity deposit of Rb, Cs, Y, Sc, quartz, and albite.	Tengchong in Yunnan, Xiaojiang in Hunan, etc.	
	Sedimentary clay		They are predominantly located on the Qinghai-Tibet Plateau and occur in association with brine-type deposits; they are found in regions such as Xinjiang, Tibet, and the Qaidam Basin in Qinghai. Their	Salt lakes in northern Tibet; the surroundings and beds of salt lakes such as Balunmahai in the Qaidam Basin.	
	Glaciogenic peat		Currently, in mainland China, it is found only in Jiangxi Province.	The 414 Ore Deposit in Yichun, Jiangxi	

3.1.3 Alkaline granite and carbonatite types

Alkaline granite- and carbonatite-hosted Nb-Ta-Cs deposits primarily formed within orogenic belts dating from 750 to 190 Ma; the associated ore-bearing rocks include carbonatites and alkaline granites (Chen et al., 2024; Li et al., 2024; Li and Hou et al., 2025).

These deposits have been discovered in provinces and regions such as Jiangxi, Hunan, and Guangxi. Representative examples include the 414 deposit in Yichun (Jiangxi), the Limu deposit (Guangxi), and the Jianfengling and Xianghualing deposits (Hunan) (Zhou et al., 2021; Li et al., 2024; Li and Hou et al., 2025; Yichun, 2026). Notably, the formation of the super-large Ta-Nb-rare metal 414 deposit in Yichun, Jiangxi—discovered in 1969—is linked to the Early Yanshanian Yashan granite stock. The deposit covers a mineralized area of 2.8 square kilometers and comprises three sections: Yinziling, Gongrencun, and Zhulouchong. Proven reserves of tantalum, lithium, rubidium, and cesium at the site are classified as super-large scale, while niobium reserves are large-scale. Mining operations began in 1970; the site is one of Asia's largest open-pit Ta-Nb-Li mines and is operated by Jiangxi Tungsten Industry Group Co., Ltd.

3.1.4 Granite type

Granite-hosted cesium deposits in mainland China are relatively widely distributed, occurring in provinces and autonomous regions such as Xinjiang, Tibet, Gansu, Inner Mongolia, Jiangxi, Jiangsu, Guangdong, Hunan, and Sichuan. These deposits are primarily located within the South China tectonic-metallogenic belt, the eastern segment of the Yangtze suture zone, and the metallogenic belt on the western slope of the Greater Khingan Range; the host rocks are predominantly highly fractionated, rare-metal-bearing granites that are peraluminous and rich in muscovite and albite.

Such granite-hosted cesium deposits generally exhibit a trend of extraordinary rubidium enrichment, whereas cesium enrichment is not particularly pronounced (Li and Hou et al., 2025).

Representative deposits include Bijiashan in the West Kunlun Mountains, Gari'atong in Nagqu (Tibet), Guobaoshan in Gansu, Shihuiyao and Zhaojinggou in Inner Mongolia, Songshugang and Yichun 414 in Jiangxi, and No. 107 in Conghua (Guangdong). Overall, these deposits possess substantial reserves and a broad distribution. Cesium-bearing minerals primarily include amazonite, lepidolite, and biotite (Xu et al., 2021; Chen et al., 2024; Tang and Wu, 2024; Wang et al., 2024).

3.1.5 Pegmatite type

Similar to the aforementioned granite-hosted cesium deposits, pegmatite-hosted cesium deposits in mainland China are relatively widely distributed, occurring in regions such as Xinjiang, Tibet, Gansu, Hunan, Inner Mongolia, Jiangxi, Jiangsu, Guangdong, and Sichuan.

To some extent, there is a close spatiotemporal association or and/co-occurrence between pegmatite-hosted and granite-hosted cesium mineralization in mainland China.

These deposits are found in areas including the Tianshan metallogenic belt, the South China metallogenic belt, the Greater Khingan Range metallogenic belt, and the southern part of the Qinling fold belt. Their formation is linked to the crystallization of residual magma during the pneumatolytic-pegmatitic stage. Representative deposits include Jing'erquan and Zhangbaoshan in Hami, Xinjiang; Bayangaole in Inner Mongolia; and Chuanziyuan in Pingjiang, Hunan (Xu et al., 2021; Chen et al., 2024; Tang and Wu, 2024; Wang et al., 2024).

3.2 Superimposed endogenic and exogenic cesium deposits

3.2.1 Quaternary hot-spring type

Quaternary hot-spring-type cesium-rubidium mineralization is commonly found along the Yarlung Zangbo Suture Zone and its surrounding areas, such as southern Tibet. While cesium concentrations in hot spring waters are generally low, anomalous enrichment of rare elements occurs in certain unique springs (Li and Hou et al., 2025). Geothermal spring waters and associated deposits (such as sinter) in southern Tibet exhibit significant enrichment of rare metal elements like Li, Rb, and Cs (Zhao et al., 2008–2010; Niu et al., 2023; Xue et al., 2024); these elements are subsequently transported into the salt lakes of the Tibetan Plateau via surface runoff and groundwater (Liu et al., 2021; Li et al., 2023; Zhou et al., 2023; Li et al., 2024).

The Gulu hot spring cesium deposit in Nagqu City, Tibet (Fig. 2), represents a rare global example of a hot-spring-type siliceous sinter cesium deposit, formed primarily from siliceous sinter. Analytical results (Zhao et al., 2010) indicate that cesium concentrations in the deposit reach up to 2,286 ppm, with over 50% of samples exceeding the industrial grade threshold. The area remains characterized by active hydrothermal activity, and cesium concentrations within the siliceous sinter continue to rise.

Zhao et al. (2010) termed this type of rare-metal mineralization on the Tibetan Plateau "sinter-type cesium deposits" and distinguished between two mineralization styles: the Dagejia type and the Gulu type. The former (e.g., the Dagejia cesium deposit) is dominated by hydrothermal mineralization with a subordinate biological component, whereas the latter (e.g., the Gulu and Buchonglanggu cesium deposits) is dominated by biological mineralization with a subordinate hydrothermal component.

The Gulu hot-spring-type cesium deposit, which reaches medium scale, is located in the Gulu area of Nagqu County, Tibet (Zhao et al., 2009). Ore textures include coarse-porous, brecciated, cataclastic-platy, fine-porous, massive, and oolitic forms, while structures include granular, colloform, biogenic, dissolution, cubic, encrusting, spherical, and tubular types. Biogenic structures are ubiquitous across all stages of sinter formation. Opal is the primary constituent mineral of the sinter, though the specific type of opal varies by stage; Opal-CT and quartz characterize stages 2 and 3, whereas only Opal-A appears in stages 4 and 5. The opal contains up to 97.48% SiO_2, up to 3.2% $\Sigma(CaO+Na_2O+MgO)$, and up to

3.57% Cs_2O. From the early to late stages, SiO_2 content shows a marked decrease, while cesium content shows an increasing trend. The average cesium content in stages 2 through 4 falls below the industrial cutoff grade (500 ppm) (Zhao et al., 2009).

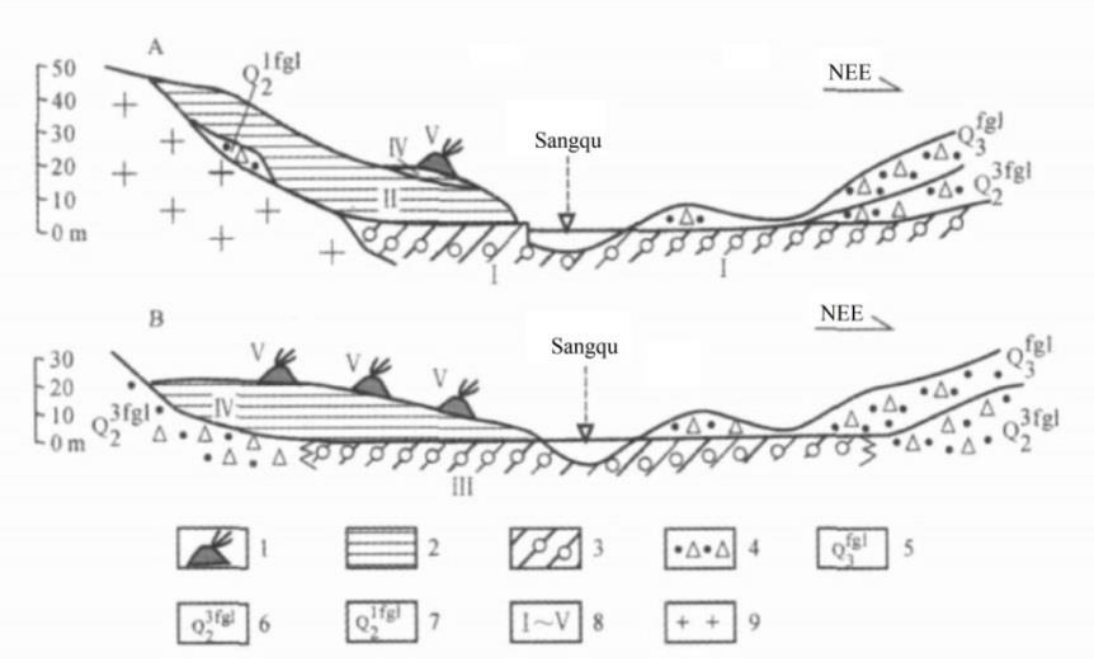


Figure 2. Cross section of the Gulu geothermal field, Tibet (after Zhao et al., 2009)

1-Siliceous sinter cone; 2-Siliceous sinter terrace; 3-Matrix-supported conglomerate; 4-Glaciofluvial deposits; 5-Glaciofluvial deposits of the Laqu Glaciation; 6-Glaciofluvial deposits of the Paran Glaciation; 7-Glaciofluvial deposits of the Ningzhong Glaciation; 8-Numbering of tufa sequences I–V; 9-Neogene granite

The Dagejia hot-spring-type cesium deposit is situated at the southern end of the N-S trending Dajiacuo-Dajiamangcuo rift, located between the Indus-Yarlung Zangbo Suture Zone to the north and the Bangong-Nujiang Suture Zone to the south. It represents a unique modern hot-spring-type cesium deposit in Tibet; the cesium content in its sinter reaches as high as 11,632 ppm, and preliminary estimates place its resource volume at 14,459.42 tonnes, classifying it as a super-large deposit (Zhang and Li, 2014). Zhao et al. (2006) classified the deposits of the Dagejia hot-spring-type cesium deposit into six units: Unit I consists of grayish-white travertine, while Units II through VI are composed of sinter, with colloidal and granular opal as the primary minerals. These spring deposits formed during the periods of 403-202 ka, 99 ka, 39-25 ka, 17-4 ka, and the present day. The ores of the Dagejia deposit contain abundant quartz, whereas the late-stage deposits consist entirely of opal (Zhao et al., 2008). Granular opal is present throughout the sequence, whereas colloidal opal appears primarily in the late stages. Early-stage ores exhibit cauliflower-like, coarse-grained massive, and coarse-porous textures, as well as dissolution structures resulting from dehydration; in contrast, late-stage ores display fine-grained massive and fine-porous textures. The presence of the diatom genus denticula in the third stage indicates

low-temperature conditions. From the early to late stages, the SiO_2 content in the ore shows a decreasing trend, while the combined content of (Na_2O + Al_2O_3 + K_2O + CaO) and the Cs_2O content show increasing trends.

3.2.2 Brine-type

Brine-type cesium deposits are categorized into three subtypes: surface water (including various salt lakes and closed seas), subsurface brine, and oil-gas field brine. They primarily occur in geothermal fields associated with Cenozoic rift and fault-controlled basins in the hinterland of the Qinghai-Tibet Plateau. Cesium-bearing minerals and materials include granular and colloidal opal, hydromica, cristobalite, potash salts, cesium-bearing brines, carnallite, and siliceous rocks. Cesium and rubidium typically become enriched and precipitate during the final stages of salt lake evolution. The surface brine subtype is controlled by the Bangong Co-Nujiang Tectonic Zone and the North Qaidam Suture Zone, occurring in southern Xinjiang, the Northern Tibetan Plateau, and the Qaidam Basin. The subsurface brine subtype occurs in South China and the Qianjiang Sag tectonic zone of the Jianghan Basin. The oil-gas field brine subtype is found in the Qaidam Basin and the Mangya and Qianjiang Sags of the Jianghan Basin. Their formation is linked to deep-seated magmatic activity and/or surface evaporation, concentration, and sedimentation processes. With the exception of the Jianghan Plain, most of these cesium-mineralized zones are located in sparsely populated, remote plateau regions with poor accessibility.

The surface brine subtype is distributed across southern Xinjiang, Tibet, and Qinghai, controlled by tectonic fault-controlled basins within the Qinghai-Tibet Plateau (Luo et al., 2017; Liu et al., 2021; Wang et al., 2023; Yi et al., 2023). Current research on cesium-rubidium resources in salt lakes on the Chinese mainland focuses primarily on Hoh Xil (Kekexili), the Northern Tibetan Plateau, and the Qaidam Basin. Representative salt lakes in the Qaidam Basin include Qarhan Salt Lake, certain lakes in northern Hoh Xil, and the "Four Lakes of Western Qaidam" (Xiong et al., 2021). Most lakes in northern Hoh Xil exhibit varying degrees of cesium-rubidium enrichment; notably, Lexiewudan Lake shows cesium and rubidium concentrations of 0.95 mg/L and 2.47 mg/L, respectively (Zhu et al., 2024)—levels significantly higher than those found in other natural water bodies. In the Hongshui River and deep-seated thermal springs—which serve as the recharge water systems for the lake—cesium concentrations reach 0.30 mg/L and 18.78 mg/L, respectively, while rubidium concentrations reach 0.30 mg/L and 11.52 mg/L. These figures indicate that the recharge systems in the area, particularly the deep-seated thermal springs, are significant sources of cesium and rubidium within the region. Research by Zhao et al. (2009) indicates that while the trend of cesium and rubidium enrichment in the upper reaches of the Na River is not pronounced, the intercrystalline brines of the Xitaijinaier and Yiliping salt lakes exhibit cesium concentrations of 0.20 mg/L and 0.12 mg/L, and rubidium concentrations of 8.00 mg/L and 6.02 mg/L, respectively. The study suggests that the anomalous enrichment of cesium and rubidium in the Na River basin is linked to high-temperature circulating groundwater undergoing water-rock reactions involving deep-seated magmatic fluids and ore-bearing host rocks. In the vicinity of the Bangong Co-Nujiang tectonic zone on the Northern Tibetan Plateau—including Zhabuye, Mami Co, and Jibu Chaka, as well as shallow and peninsular lakes in the Qiangtang

endorheic region—cesium concentrations exceed 2 mg/L (Hou, 2023). Notably, the Mami Co salt lake exhibits a cesium concentration as high as 18.55 mg/L; it is one of the salt-lake-type cesium-rubidium deposits that attracted early attention and was targeted for development. Research by Zhou et al. (2024) indicates that cesium and rubidium in the salt lakes of the Qinghai-Tibet Plateau are still in the concentration phase; these deposits hold broad application prospects and represent a potential resource characterized by large volumes and relatively simple extraction processes.

Deep-seated brine-type cesium-rubidium deposits are primarily distributed in South China, specifically near the Jiangling and Qianjiang depressions; while their distribution is concentrated, the number of such deposits is limited (Li and Hou et al., 2025). Typically situated within sedimentary basins (Hou, 2023), these cesium deposits are few in number but rich in resources, all classified as large-scale cesium-rubidium deposits. According to Yu et al. (2021), the cesium ion concentration in the deep-seated brine-hosted lithium-polymetallic deposit of the Jiangling Basin can reach 32.08 mg/L, indicating immense resource potential.

The oil-and-gas field subtype represents a relatively new—and consequently less studied—category of brine-hosted cesium deposits. Current research in mainland China on this subtype focuses primarily on the Nanyishan anticline within the Mangya Sag of the western Qaidam Basin, as well as on Paleogene oil and gas fields in the Qianjiang Sag of the Jianghan Basin (Li and Hou et al., 2025). Studies by Fan et al. (2007) and Li et al. (2013) indicate that the average Rb^+ concentration in oil and gas fields such as Nanyishan and Youquanzi in the western Qaidam Basin reaches 45.2 mg/L (though data regarding cesium are unavailable). As a byproduct of oil and gas extraction, these resources hold significant utilization value.

3.2.3 Coal type

It is an established fact that numerous coal deposits in mainland China contain various rare metals, including gallium, germanium, and cesium (Yin, 2026c, 2026d, etc.). The concentrations of these critical metals—enriched in both the coal and the resulting fly ash—can match or even exceed those found in traditional ore deposits, positioning them as potential major sources for these metals in the future.

Focusing on the Xintian coal mine in the western section of the Pingle Depression, Jiangxi Province (Fig. 3), Dai et al. (2023) employed techniques such as scanning electron microscopy-energy dispersive spectroscopy (SEM-EDS), the TESCAN Integrated Mineral Analyzer (TIMA) system, X-ray fluorescence (XRF) spectrometry, and inductively coupled plasma-mass spectrometry (ICP-MS). Their study revealed that the critical metal cesium is enriched in both the coal seams and the underlying host rock (with an average content of 18 ppm, or 20 ppm Cs_2O). Cesium likely occurs through isomorphous substitution—replacing Rb and K in feldspar crystal lattices or K in illite within clay minerals—or is adsorbed onto clay minerals alongside lithium.

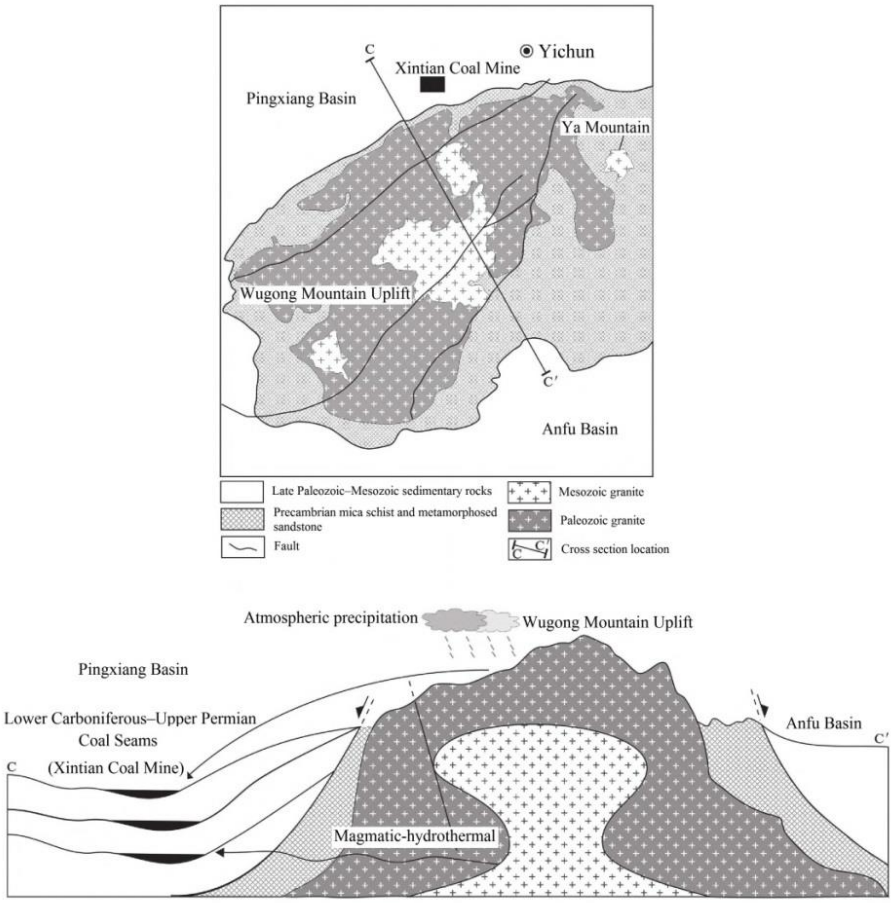


Figure 3. Distribution of magmatic rocks in the Wugongshan Uplift along the southern margin of the Pingxiang Basin, Jiangxi (top); and geological map of the Pingle Coalfield, Jiangxi, along with the metallogenic model for coal-hosted cesium deposits (bottom) (both adapted from Dai et al., 2023)

The coal in the Xintian Coal Mine is composed primarily of organic matter and kaolinite, followed by quartz, feldspar, and illite, with minor amounts of magnetite, tremolite, rutile, and apatite. By comparing critical metal contents with those in global coal mines and sedimentary rocks, and by integrating data on Al_2O_3/TiO_2 ratios, rare earth element characteristics, and the regional tectonic-magmatic history of the Xintian mining area, Dai et al. (2023) proposed that the cesium (Cs) in this coalfield likely originated from terrigenous clastics derived from the weathering of Paleozoic granites along the southern margin of the Pingxiang coal-bearing basin; subsequent modification by Cs-rich magmatic-hydrothermal fluids during the Yanshanian period further enriched Cs within the coal measures (Fig. 3). The Pingle Depression Zone is situated at the junction of the Yangtze Platform and the Cathaysia Block; its southern and northern boundaries are defined by the Pingxiang-Guangfeng and Yifeng-Jingdezhen regional faults, respectively, placing it in direct contact with the Neoproterozoic Wugongshan Uplift and the Mesoproterozoic Jiuling Uplift (Fig. 3).

Mineralogical and elemental geochemical studies conducted by Yan et al. (2022)—using techniques such as X-ray diffraction (XRD), scanning electron microscopy with energy-dispersive spectroscopy (SEM-EDS), inductively coupled plasma mass spectrometry (ICP-MS), and X-ray fluorescence (XRF)—on coal measure samples from the Nadu Formation in the Baise Basin, Guangxi, indicate that the minerals within these Paleogene coal seams are predominantly illite, kaolinite, and quartz. Compared to the global average for low-rank coals, the coal seams in the Baise Basin are enriched in Rb, Sb, and Cs. Specifically, coal seams in the western part of the basin are relatively enriched in Rb and Cs, whereas those in the eastern part are relatively enriched in Sb, Cs, and U. Cs is enriched not only within the coal itself but also in the roof strata, floor strata, and partings, with concentrations in the latter three being significantly higher than in the coal. Correlation analysis indicates that Cs is primarily associated with clay minerals. SEM observations reveal that the clay minerals are largely terrigenous clastics, suggesting that the input of terrigenous clastics into the sedimentary source area may be a key factor contributing to the Cs anomaly. The correlation coefficient between Cs and ash content is 0.98, indicating a significant inorganic affinity for Cs. The positive correlations of Cs with K_2O (0.45), SiO_2 (0.46), and Al_2O_3 (0.64) suggest an association with aluminosilicates and indicate that Cs may be hosted in clay minerals.

3.3 Exogenic cesium deposit

Exogenic mineral deposits are secondary deposits formed at the Earth's surface—comprising the upper lithosphere, hydrosphere, atmosphere, and biosphere—through the interaction of exogenic geological processes driven primarily by solar energy. The ore-forming materials originate mainly from endogenic deposits exposed at the surface. These deposits are created under ambient temperature and pressure conditions through processes such as weathering, transport, sedimentation, and/or biochemical enrichment. They include the aforementioned brine-type and coal-hosted cesium deposits, as well as sedimentary clay-type, weathered granite crust-type, and glaciogenic peat-type deposits, which are discussed below (Fig. 1 and Table 1).

3.3.1 Sedimentary clay type

These deposits are distributed across the Qinghai-Tibet Plateau and frequently occur in association with brine-type cesium deposits. They are found in regions such as Xinjiang, Tibet, and the Qaidam Basin in Qinghai. Their formation is linked to the evaporation, concentration, and sedimentation processes of surface-water-subtype cesium deposits.

In a study on the mineralization processes of salt lakes in the Qaidam Basin and metal ion concentrations in surface brines, Li et al. (2023) observed a significant decline in cesium and rubidium levels—with cesium showing a particularly anomalous depletion—resulting in a brine composition characterized by high rubidium and low cesium. However, cesium concentrations in the majority of thermal spring samples feeding the salt lakes were comparable to those of lithium and significantly higher than those of rubidium; this suggests that cesium in the surface brine may have been removed from the water column

through adsorption onto clay minerals. Relevant studies (Cornell, 1993; Park et al., 2021) indicate that lacustrine environments contain abundant clastic sediments, where fine-grained clays possess large specific surface areas and exhibit preferential adsorption of Rb^+ and Cs^+. The depletion of cesium and rubidium in surface brines may therefore be attributed to adsorption by lacustrine sediments. Analyses conducted by Li et al. (2023) and Pan et al. (2023)—covering surface-water-subtype cesium deposits in northern Tibet, salt lake bottom sediments, and clay samples from drill cores in the Qaidam Basin—revealed significant enrichment of cesium and rubidium in lacustrine clay minerals, with concentrations ranging from 234.5 to 1,357.8 ppm and 225.6 to 365.0 ppm, respectively. Ding et al. (2024) found that in the surface clay sediment layers surrounding the Balunmahai Salt Lake in the Qaidam Basin, Cs and Rb concentrations ranged from 5.94 to 12.4 ppm and 58.7 to 128 ppm, respectively, showing a strong positive correlation with elements such as potassium and lithium. According to data from Li and Hou, et al. (2025), the potential resources of cesium (Cs_2O) and rubidium (Rb_2O) in the Qaidam Basin are 31,300 tonnes and 357,200 tonnes, respectively.

Representative clay-type cesium-rubidium deposits are found in the salt lakes of northern Tibet, as well as in the surrounding areas and lakebeds of salt lakes such as Balunmahai in the Qaidam Basin.

3.3.2 Weathered granite crust-type

In a 2002 paper, Shen reported that the weathered crust of the Cenozoic Baihuanao alkali-feldspar granite in western Yunnan constitutes a rare, super-large, multi-component deposit of Rb, Cs, Y, Sc, quartz, and albite, with Ta, Nb, Sn, and W available as recoverable by-products. Primary magmatic activity was the dominant factor in the formation of the parent rock for this weathered crust-type polymetallic deposit. Key characteristics of the deposit include massive reserves, a wide range of valuable components, and immense economic potential, alongside ease of mining, beneficiation, and smelting. A drawback, however, is that the grades of the valuable components—with the exception of Rb—are relatively low.

3.3.3 Moraine-peat type

In mainland China, occurrences are currently known only in Jiangxi Province—specifically, secondary cesium deposits located on the surface and in the vicinity of the large-scale "414" primary alkaline granite-hosted cesium-polymetallic deposit in the Yichun area. However, information regarding this secondary cesium deposit is currently very limited.

4. Discussion

The diverse geological structural units across mainland China—spanning various geological eras and including platforms, geosynclines, and orogenic belts—have shaped a

complex geological setting and a wide array of associated mineral resources. This diversity underpins the country's world-leading position in the reserves of numerous rare metal minerals, including cesium.

This geological diversity and complexity have resulted in a wide variety of cesium deposit types across the mainland; indeed, cesium deposits of virtually every genetic type can be found on this continent, which boasts a complex geological evolutionary history.

Mainland China hosts endogenous cesium deposits—such as pegmatite, hydrothermal, and granite types—as well as deposits formed through the combined action of endogenic and exogenic processes, including hot spring, brine, and coal-seam types. Additionally, there are exogenic cesium deposits, such as sedimentary clay, weathered granite crust, and moraine-peat types. Among these, brine-type deposits can be further subdivided into surface water, deep-seated brine, and oil-gas field subtypes. Naturally, based on the physical state of mineralization, these cesium deposits can also be broadly categorized into solid and liquid types.

It is generally considered that cesium mineralization in mainland China is closely associated with highly fractionated, peraluminous granites and extensional or transtensional tectonic settings resulting from continent-continent collision. Cesium becomes enriched in late-stage residual magmatic melts/hydrothermal fluids or in evaporative salt lake systems; it typically occurs via isomorphous substitution within minerals such as lepidolite and amazonite, whereas discrete cesium minerals—such as pollucite—are rare.

Brine-type cesium resources are primarily found on the Tibetan Plateau and in surrounding regions, including Tibet, Xinjiang, Qinghai, Sichuan, and Yunnan. Hard-rock cesium deposits are distributed widely across the country; beyond the tectonically active Tibetan Plateau and its periphery, solid-state cesium deposits of various scales and types occur across all cardinal directions—from west to east, south to north, northeast to southwest, and northwest to southeast. Known cesium deposits are concentrated in the Altay region of Xinjiang, the Songpan-Ganzi terrane of western Sichuan, the Nanling-Jiangnan Orogenic Belt, the Qaidam Basin, and the salt lake regions of northern and western Tibet. Chen et al. (2023) delineated ten cesium metallogenic belts across mainland China, with Jiangxi, Henan, Qinghai, Tibet, and Xinjiang holding the largest cesium resources.

Regardless of their genetic type, cesium deposits are generally closely linked to tectono-magmatic activity. Even in cases of so-called supergene (exogenic) cesium mineralization, active involvement of tectono-magmatic processes is frequently observed. Research indicates that the source material—specifically the cesium metal—for various types of cesium deposits is closely related to high degrees of magmatic fractionation and hydrothermal activity. Studies also suggest that ancient metamorphic rocks serve as another important source stratum for cesium. Furthermore, research indicates a close link between cesium deposit formation and specific stratigraphic units (Wen et al., 2025). Certain strata rich in mica-group minerals exhibit relatively high cesium content, as the layered structure of mica minerals can accommodate cesium ions. Additionally, feldspar-rich strata can release cesium during geological processes such as alteration and weathering, subsequently leading to mineralization under favorable geological conditions. Chen et al. (2023) determined that the metallogenic ages of cesium deposits in mainland China are concentrated in the Mesozoic (150–100 Ma, Yanshanian) and Cenozoic (<65 Ma,

Himalayan) eras, with fewer occurrences in the Paleozoic (Fig. 4). Pegmatite-type deposits predominantly belong to the Indosinian–Early Yanshanian periods; whereas surface-water and hot-spring subtypes largely result from Quaternary supergene enrichment. Spatially, cesium mineralization is significantly controlled by the Tethys-Himalaya, Altay-West Junggar, and South China polyphase orogenic belts, and the deposits frequently occur in association with rare metals such as lithium, rubidium, niobium, and tantalum. No independent cesium deposits have been discovered in China to date; over 90% are associated/paragenetic deposits. Overall, these cesium resources are characterized by being dispersed and low-grade, yet possessing high potential for comprehensive utilization. Metallogenic patterns are jointly constrained by the degree of magmatic evolution, tectono-fluid activity, and paleoclimate.

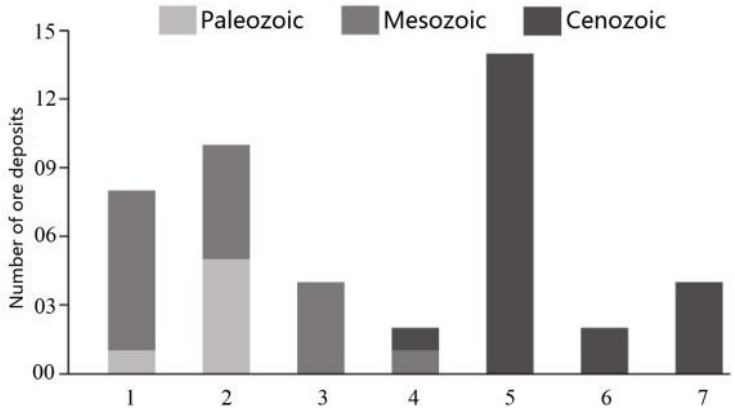


Figure 4. Statistics on the metallogenic ages of cesium deposits in mainland China (after Chen et al., 2023)

1-Granite type; 2-Granitic pegmatite type; 3-Magmatic-hydrothermal type; 4-Weathered granite crust type; 5-Salt lake type; 6-Brine type; 7-Siliceous sinter type

Among the various genetic types of cesium deposits, those currently holding the greatest industrial value are the granite-pegmatite type (e.g., Koktokay in Xinjiang and Jiajika in Sichuan), the granite type (e.g., the large-scale but low-grade lepidolite-granite-hosted cesium deposits in South China), and the surface-water brine type (e.g., Qarhan in Qinghai and Zabuye Salt Lake in Tibet); these are followed by the magmatic-hydrothermal type and the weathered granite crust type.

Jiangxi and Henan are the two provinces in mainland China with the most abundant cesium resources. Granite-pegmatite and granite-hosted mineralization represent the primary deposit types in these regions.

The combined action of endogenic and exogenic mineralization processes is essential for the formation of many cesium deposits. Even the Quaternary hot-spring-type and surface-water-subtype cesium mineralization found on the Qinghai-Tibet Plateau—which appear superficially to be products of purely exogenic processes—actually result from deep-crustal magmatic activity (driven by the collision between the Indian and Eurasian plates) that

transported cesium to specific surface locations (Zhao et al. 2010); subsequent evaporation and sedimentation processes then led to further cesium enrichment in surface waters (specifically salt lakes) and their lacustrine sediments.

5. Conclusions

Thanks to its diverse geological settings, mainland China possesses various types of associated/paragenetic cesium resources and holds a competitive global position, even though no independent cesium deposits have been discovered to date. These cesium occurrences include deposits of endogenic origin closely linked to tectono-magmatic activity (such as pegmatite, granite, and igneous-hydrothermal types); deposits formed by the combined action of endogenic and exogenic processes (such as Quaternary hot spring, brine, and coal-measure types); and various exogenic deposits (such as sedimentary clay, weathered granite crust, and glacial till-peat types).

In terms of physical state, cesium deposits in mainland China include both solid forms and—particularly in the Qinghai-Tibet Plateau and surrounding regions—numerous liquid brine and/or Quaternary hot spring types. Although these brine-type cesium deposits appear superficially to be purely exogenic, many are actually closely linked to endogenic processes—specifically tectono-igneous activity—and are thus the product of combined endogenic and exogenic geological forces.

Pegmatite- and granite-type cesium deposits currently represent the most important types for exploitation in mainland China, while the brine subtype associated with surface water bodies represents a significant potential target for future development.

The Mesozoic Era was the primary period for the formation of hard-rock cesium deposits in mainland China, whereas the Cenozoic Era was the principal period for the formation of brine-type cesium deposits.

References

01.Baike Baidu. 2026. Cesium ore. 2026. https://baike.baidu.com/item/%E9%93%AF%E7%9F%BF%E7%9F%B3/57258649?fromModule=search-result_lemma (in Chinese). Retrieved February 20, 2026.

02. Chen BH, Li P and Liu JN. 2023. Metallogenic regularity of caesium deposits in China. *Geology in China*，51 (6): 1946-1959. DOI: 10.12029/gc20220321002.

03. Chen ZW, Yuan C and Lin ZF et al. 2024. Genesis of the Jiangjunshan amazonite granites and the related rubidium enrichment mechanism in the Chinese Altai, Xinjiang (in Chinese with English abstract). *Geotectonica et Metallogenia*, 48 (6): 1394-1420.

04. Cornell RM. 1993. Adsorption of cesium on minerals: a review. *Journal of Radio analytical and Nuclear Chemistry*, 171 (2): 483-500.

05. Dai JF, Li ZH, Xu DR, Zou YJ, Xiao FQ, Mi ZH and Zhang J. 2023. Enrichment characteristics and genesis mechanism of critical metal cesium in Xintian coal mine of Pingle Depression, Jiangxi,

China. *Journal of Earth Sciences and Environment*, 45 (5): 1162-1175. DOI: 10.19814/j.jese.2023.06038.

06. Ding CW, Ma YL and Chen JZ et al. 2024. Mineralogy and geochemical characteristics of rare elements in clays from Balun Mahai Salt Lake of Qaidam Basin (in Chinese with English abstract). *Journal of Salt Lake Research*, 32 (3): 32-39.

07. Dong P and Xiao RG. 2005. Application of cesium salts and resource evaluation of cesium (alkali metal) deposits (in Chinese with English abstract). *China Mining Magazine*, (2): 30-34. DOI: 10.3969/j.issn.1004-4051.2005.02.010.

08. Fan QS, Ma HZ and Tan HB et al. 2007. Hydrochemical anomaly and resources evaluation of the oil field brines in the typical area of Western Qaidam Basin (in Chinese with English abstract). *Journal of Salt Lake Research*, (4): 6-12.

09. Gao XR, Jia HX, Li TJ, Li WD and Wang AJ. 2023. Outlook on the Demand for Rubidium and Cesium Resources in China (in Chinese with English abstract). *Acta Geoscientica Sinica*, 44 (2): 279-285. DOI:10.3975/cagsb.2022.122501.

10. Han CM, Xiao WJ and Fang AM et al. 2021. Metallogenic regularity and metallogenic series of West Kunlun and its adjacent areas (in Chinese with English abstract). *Acta Petrologica Sinica*, 37 (12): 3615-3644.

11. Hou JL, Li JK and Zhang YJ et al. 2018. Li isotopic composition and its constrains on rare metal mineralization of Jiajika two mica granite, Sichuan Province. *Earth Science*, 43 (6): 2042-2054.

12. Hou YL. 2023. Overview of geological research on rubidium deposits in China and implications for mineral exploration (in Chinese with English abstract). *West China Exploration Engineering*, 35 (2): 117-119, 123.

13. Jia EH, Tang JR and Liu YQ. 2019. Geological characteristics and genesis of the Bamianshan deposit, Zhejiang (in Chinese with English abstract). *World Nonferrous Metals*, (11): 125-126.

14. Li H, Huang F and Zhou WJ et al. 2024. Resource characteristics, metallogenic regularity and prospecting direction of precious metal minerals in Guangxi (in Chinese with English abstract). *China Mining Magazine*, 33 (8): 225-237.

15. Li JS, Li TW and Ma HZ et al. 2013. Investigation of the chemical characteristics and its geological significance of the Tertiary oilfield brine in the western Qaidam Basin (in Chinese with English abstract). Hydrogeology & Engineering Geology, 40 (6): 28-36.

16. Li QK, Wang JP and Fan QS et al. 2023. Rubidium and cesium enrichment in lacustrine sediments from Tibetan Salt Lakes: a potential resource (in Chinese with English abstract). *Acta Geologica Sinica*, 97 (10): 3410-3420.

17. Li YL, Miao WL and He MY et al. 2023. Origin of lithium-rich salt lakes on the Western Kunlun Mountains of the Tibetan Plateau: evidence from hydrogeochemistry and lithium isotopes. *Ore Geology Reviews*, 155: 105356.

18. Li Z, He M Y and Wen X et al. 2024. Multi-isotopic composition (Li and B isotopes) and hydrochemistry characterization of the Lakko Co-Li rich salt lake in Tibet, China: origin and hydrological processes (in Chinese with English abstract). *Journal of Hydrology*, 630: 130714.

19. Li Z， Lou FS and Xiong YY et al. 2025. Main types, geological characteristics and metallogenic regularity of typical lithium deposits in South China (in Chinese with English abstract). *China Mining Magazine*, 34 (10): 254-266. DOI: 10.12075/j.issn.1004-4051.20241666.

20. Li ZY, Hou DB and Chang H et al. 2025. Research progress on the types, distribution, genesis, enrichment regulation, separation and extraction techniques of rubidium and cesium resources in China (in Chinese with English abstract). *China Mining Magazine*, 34 (2): 265-283. DOI: 10.12075/j.issn.1004-4051.20242316.

21. Liu CL, Yu XC and Yuan XY et al. 2021. Characteristics, distribution regularity and formation model of brine-type Li deposits in salt lakes in the world (in Chinese with English abstract). *Acta Geologica Sinica*, 95 (7): 2009-2029.

22 Liu L. 2013. Current status of rubidium and cesium resources and technology in China (in Chinese with English abstract). *Xinjiang Nonferrous Metals (Supplement 1)*: 158-165. DOI： 10.16206/j.cnki.65-1136/tg.2013.s1.073.

23. Liu XC, Zhang L and Huang FF et al. 2024. Unraveling typical magmatic-hydrothermal ore deposits: progresses of the experimental metallogeny (in Chinese with English abstract). *Bulletin of Mineralogy, Petrology and Geochemistry*, 43 (6): 1171-1181.

24. Luo YB, Zheng MP and Ren YQ. 2017. Metallogenic correlation of special salt lake and hydrothermal, Qinghai-Tibet Plateau, China (in Chinese with English abstract). *Science & Technology Review*, 35 (12): 44-48.

25. Mei YX, Pei RF and Wei R et al. 2022. Critical minerals and energy resources security (in Chinese with English abstract). *China Mining Magazine*, 31 (11): 1-8.

26. Niu XS, Liu XF and Lv YY et al.2023. Origin mechanism of thermal springs and their supply of minerals to the salt lake (Li-Rb-Cs) in the Tangqung Co watershed of Tibet (in Chinese with English abstract). *Geology in China*, 50 (4): 1163-1175.

27. Pan T, Chen J and He MY et al. 2023. Characterization and resource potential of Li in the clay minerals of Mahai Salt Lake in the Qaidam Basin, China (in Chinese with English abstract). *Sustainability*, 15 (19): 14067.

28. Park SM, Kim JG and Kim HB et al. 2021. Desorption technologies for remediation of cesium-contaminated soils: a short review. *Environmental Geochemistry and Health*, 43 (9): 3263-3272.

29. Peng JJ and Lin K. 2024. Knowledge graph analysis of mineralization laws research of lithium ore (in Chinese with English abstract). *China Mining Magazine*, 33 (9): 228-235.

30. Shen GF. 2002. Weathering crust of the Baihuanao granite: A potential super-large deposit of Rb, Cs, Y, Sc, quartz, and albite (in Chinese with English abstract). *Bulletin of Mineralogy, Petrology and Geochemistry*, 22 (3): 182-184. DOI: 10.3969/j.issn.1007-2802.2002.03.007.

31. Sihan Industry Research Institute. September 29, 2025. Recoverable resources of cesium and rubidium are highly concentrated, and upstream producers hold a monopolistic position (in Chinese). https://caifuhao.eastmoney.com/news/20250929142122729562360. Retrieved February 21, 2026.

32. Tan HB, Shi ZW and Cong PX et al. 2023. The spatial distribution law of B, Li, Rb and Cs elements and supernormal enrichment mechanism in Tibet geothermal system. *Sedimentary Geology and Tethyan Geology*，43（2）：404-415.

33. Tang GQ and Wu CZ. 2022. Rubidium and cesium: the unparalleled duo of rare metals (in Chinese with English abstract). *Bulletin of Mineralogy, Petrology and Geochemistry*, 41 (5): 1073-1077.

34. Tang GQ and Wu CZ. 2024. The main genetic types and metallogenic potential of hard-rock rubidium deposits in Xinjiang (in Chinese with English abstract). Bulletin of Mineralogy. *Bulletin of Mineralogy, Petrology and Geochemistry*, 43 (1): 102-126.

35. Tong CL. 2014. Geological characteristics of the Cs-Rb rare metal deposit in Danzhou, Hainan (in Chinese with English abstract). *Mineral Resources and Geology*, 28 (6): 7.

36. Wang YT, Du JG and Lei RX et al. 2024. Fluid characteristics and mineralization process of cryptoexplosive breccia-type Li-Rb ore body in Weilasituo deposit, Inner Mongolia. *Earth Science*, 49 (12): 4318-4334.

37. Wang ZD, Shi Z and Tong HK et al. 2023. Analysis and countermeasures study of guarantee capability of salt lake resources in Qinghai Qaidam Basin. *China Mining Magazine*, 32 (2): 38-42.

38. Wen PF, Zhu Q and Zou XH et al. 2025. Research on the characteristics and development utilization of global cesium mineral resources (in Chinese with English abstract). *China Mining Magazine*, 34 (2): 438-448. DOI: 10.12075/j.issn.1004-4051.20242269.

39. Wu JJ. 2023. Applications of the rare metals rubidium and cesium and their compounds in China (in Chinese with English abstract). *Xinjiang Nonferrous Metals*, 46 (5): 55-56.

40. Xiong ZH, Zhang JW and Wang SJ. 2021. Countermeasures of ecological and environmental protection for Qarhan Salt Lake resource exploitation (in Chinese with English abstract). *China Mining Magazine*, 30 (3): 113-117.

41. Xu SK, Xia XH and Yan F et al. 2011. Mineralization temperature of Bamianshan new type fluorite deposit of Zhejiang (in Chinese with English abstract). *China Non-Metallic Minerals Industry*, (2): 48-52, 57.

42. Xu SQ, Xue CJ and Feng J et al. 2021. Geological characteristics and prospecting direction of the Bijia Mountain rubidium deposit in the Western Kunlun Mountains (in Chinese with English abstract). *Xinjiang Geology*, 39 (2): 220-228.

43. Xue F, Tan HB and Zhang XY et al. 2024.Ources, enrichment mechanisms, and resource effects of rare metal elements-enriched geothermal springs in Xizang, China (in Chinese with English abstract). *Scientia Sinica (Terrae)*, 54 (11): 3513-3537.

44. Yan XY, Wang Q, Zhang R, Liang Y and Zhao L. 2022. Controlling factors on enrichment of cirtical element cesium in Paleogene coals from the Baise Basin. *Journal of China Coal Society*, 47 (5): 1865-1875.

45. Yichun. 2026. Yichun tantalum-niobium deposit. https://baike.baidu.com/item/%E5%AE%9C%E6%98%A5%E9%92%BD%E9%93%8C%E7%9F%BF%E5%BA%8A/7934480. Trieved May 29, 2026.

46. Yi JZ, Wang XY and Lin DC et al. 2023. Suggestions for green development of mining industry in Tibet against the background of a new round of strategic breakthrough in mineral exploration (in Chinese with English abstract). *China Mining Magazine*, 32 (7): 45-49.

47. Yin JZ. 2026c. Type and origin of the gallium deposits in Mainland China. *Naturalis Scientias*, 3: 662-675. DOI: https://doi.org/10.62252/NSS.2026.1037.

48. Yin JZ. 2026d. Geology and geochemistry of the germanium deposits in Mainland China. *Naturalis Scientias*, 3: 686-709. DOI: DOI: https://doi.org/10.62252/NSS.2026.1039.

49. Yu X, Liu C and Wang et al. 2021. Origin of geothermal waters from the Upper Cretaceous to Lower Eocene strata of the Jiangling Basin, South China: constraints by multi-isotopic tracers and water-rock interactions. *Applied Geochemistry*, 124: 104810.

50. Yu XC, Wang CL and Huang H et al. 2023. Sources and genesis of lithium in Paleogene oilfield brines from the Qianjiang Sag, Jianghan Basin (in Chinese). *2023 Joint Annual Meeting of Chinese Geosciences*.

51. Zhang BS and Li ZQ. 2014. Study on the cesium deposit in the Dagejia Area, Tibet. Proceedings of the 2014 Joint Annual Meeting of Chinese Geosciences — Session 55: Eastern Tethys Collisional Orogeny and Metallogenesis.

52. Zhang LJ, Li XH and Zheng YH et al. 2024. Study on the metallogenic conditions and models of the Yujiacun gold-silver polymetallic deposit in Northern Yunnan (in Chinese). *China Mining Magazine*, 33 (4): 252-260.

53. Zhang XW, Xin TY and Liu JX et al. 2021. Analysis on the current situation of global cesium resources and its comprehensive utilization technology. *Conservation and Utilization of Mineral Resources*, 41 (5): 7-11.

54. Zhao CT, Chen L and Li QK et al. 2024. Sources and enrichment processes of rubidium and cesium in the Nalengele River and its terminal lakes, Qaidam Basin (in Chinese with English abstract). *Journal of Salt Lake Research*, 32 (5): 10-18.

55. Zhao YY, Fan XT and Han JY et al. 2009. Geologic and geochemical features and ore forming process for hot spring cesium deposit of Gulu area, Nagqu region, Tibet, China. *Geological Bulletin of China*, 28 (7), 933-954. DOI: 10.3969/j.issn.1671-2552.2009.07.014.

56. Zhao YY, Han JY and Guo LH et al. 2008. Mineralogy, ore fabric characteristics, and geological significance of the Targejia hot-spring-type cesium deposit (in Chinese with English abstract), Tibet. *Acta Petrologica Sinica*, 24 (3): 12. DOI: CNKI:SUN:YSXB.0.2008-03-012.

57. Zhao YY, Li ZQ and Nie FJ et al. 2026. Preliminary study on the metallogenesis of the Targejia hot-spring-type cesium deposit, Tibet (in Chinese with English abstract). *The 9th National Conference on Mineral Deposits*.

58. Zhao YY, Nie FJ and Hou ZQ et al. 2006. Geological characteristics and formation age of hot spring cesium deposit in Targejia area, Tibet (in Chinese with English abstract). Mineral Deposits, 25 (5): 613-619. DOI: 10.1611/j.0258-7106.2006.03.007.

59. Zhao YY, Zhao XT and Li ZQ et al. 2010. Types and metallogenic characteristics of Quaternary cesium deposits in Tibet (in Chinese with English abstract). Mineral Deposits, 29 (Special issue): 399-400. DOI: 10.16111/j.0258-7106.2010.s1.208.

60. Zhao YY, Zhao XT and Ma ZB et al. 2010. Chronology and significance of the Gulu hot spring type cesium deposit in Xizang. *Acta Geologica Sinica*, 84 (2): 211-220.

61. Zhiyan Consulting. Outlook for 2025! Analysis of resource distribution, production, and key enterprises in China's cesium industry: Global cesium resources are scarce, with Sinomine Resource Group controlling over 80% of global mineral assets (in Chinese). https://finance.sina.com.cn/stock/relnews/cn/2025-03-06/doc-inensmtt3788289.shtml. Retrieved February 20, 2026.

62. Zhou J, Li B and He M et al. 2023. Hydrochemical characteristics and sources of lithium in carbonate-type salt lake in Tibet. Sustainability, 15 (23): 16235.

63. Zhou X, Zhao YY and Chen WX. 2024. Rubidium and cesium resources current status, enrichment pattern and extraction technology in salt lakes of Qinghai-Xizang（Tibet） Plateau, China. *Geological Review*, 70 (2): 705-716.

64. Zhou Y, Tian SF and Dong H. 2021. Evaluation and analysis of the exploitative intensity of mineral resources in Jiangxi Province (in Chinese). *China Mining Magazine*, 30 (12): 30-37.

65. Zhu ZY, Kong FC and Lei ZC et al. 2024. Distribution characteristics and formation mechanisms of rubidium and cesium in the water bodies of the Northern Hoh Xil Region. Journal of Salt Lake Research, 32 (5): 19-28.

66. Zi YM, Tian SH and Chen XY et al. 2024. Potassium and magnesium isotope fractionation during magmatic differentiation and hydrothermal processes in post-collisional adakitic rocks and its indicative significance: a case study of the Qulong porphyry copper deposit, Southern Tibet. *Earth Science Frontiers*, 31 (3): 150-169.

Data availability

The data that support the findings of this study are available from the author upon reasonable request.

Declaration of competing interest

The author declares that he has no competing financial interests or personal relationships that could have appeared to influence the work reported in this paper.

Use of AI tools declaration

The author declares that he has not used Artificial Intelligence (AI) tools in the creation of this article.

Original Article

"Historical Records" Born of Earth and Fire

—Messages from the Ancestors of the Chinese Nation on "Qin and Han Ancient Bricks," and Collector-Connoisseur Zhang Yanwei

J.Z. (Jet) Yin[1]

Abstract

This "Qin-Han grey brick"—originating from the ancient Central Plains along the Yellow River—bears images on its reverse side that go beyond the depictions of Fuxi and Nuwa (identified by collector and connoisseur Mr. Yanwei Zhang) found in the upper section. The designs in the middle and, particularly, the lower sections conceal significant information regarding the ancestral figures of Chinese mythology—specifically Pangu, the deity who wielded a giant axe to cleave heaven and earth and bring order to the cosmos. The serpentine motif situated between the upper figures (Nuwa and Fuxi) and the lower figure (Pangu) serves a dual purpose: it corroborates ancient legends describing Pangu as having a human body with a serpent's head and depicting the intertwining bodies of Nuwa and Fuxi, while also illustrating the ancestral lineage connecting the elder Pangu below to the younger generation of Nuwa and Fuxi above—despite ongoing, unresolved debate regarding the precise generational gap between these two groups of figures. In addition to interpreting the profound symbolism of these patterns through scholarly references, this article introduces Mr. Yanwei Zhang. For over thirty years, he has devoted his time, money, and energy—with unwavering focus—to the collection, rubbing, and study of Qin and Han bricks and tiles in a corner of the Central Plains. He is a dedicated independent scholar who has poured his personal resources into this lifelong pursuit, as well as an artist, calligrapher, and bearer of the intangible cultural heritage of stone and brick rubbing techniques who has spent decades educating the youth and kids. We must also acknowledge the courage, sense of responsibility, and keen insight of the Nanjie School principal; in today's materialistic society, she unhesitatingly provided a space for Mr. Zhang to house his extensive collection of Qin and Han bricks and tiles, thereby enabling the transmission of traditional Chinese culture to successive generations of young students.

Keywords: Pangu, Nüwa and Fuxi—ancestral figures of the Chinese nation; grey bricks from the Qin and Han dynasties; Yanwei Zhang; Nanjie School

---

Affiliation Info: 1 College of Earth Sciences, Jilin University, Changchun 130061, China

Corresponding Aurhor: Yin, J. Z., PhD, Professor, geosciences, mineral exploration and mining; Email address: jzyin7@jlu.edu.cn

Citation: Yin, J.Z. 2026. "Historical records" born of earth and fire—messages from the ancestors of the Chinese nation on "Qin and Han ancient bricks," and collector-connoisseur Yanwei Zhang. *Naturalis Scientias*, 3: 763-776. DOI: https://doi.org/10.62252/NSS.2026.1042. www.naturalisscientias.com.

Copyright © 2026 by the author. Published by *Naturalis Scientias*. This is an open access article under the Creative Commons Attribution-NonCommercial 4.0 International (CC BY-NC 4.0) License. (https://creativecommons.org/licenses/by-nc/4.0/).

土与火结合而来的“史记”

--“秦汉古砖”上华夏始祖们的信息及收藏鉴赏家张彦伟

J.Z. (Jet) Yin

摘要

一块儿源自华夏大地黄河流域古老中原的“秦汉青砖”，其背面除收臧鉴赏家张彦伟先生本人解读出来的上部伏羲女娲图案外，其中部尤其是下部的“奠基性”图案隐藏着远古神话传说中华夏始祖的重大信息，即那位用一柄巨斧开天辟地澄清玉宇的盘古。上（女娲伏羲）、下（盘古）图案中间的蛇形图案，既印证了盘古蛇首人身、女娲伏羲交尾的古老传说，又点明了下部老一辈的盘古与上部年轻世代女娲伏羲之间的血脉传承关系，尽管目前关于这两组人物之间辈分差异几何存在巨大争议且尚无定论。本文在引经据典解读该图案所隐含重大信息的同时，推介了 30 余年来投入大量时间、金钱和精力在中原大地的一隅心无旁骛地沉醉于秦砖汉瓦收藏、拓片和研究的张彦伟先生，一个几乎倾其个人所有皓首穷究独立开展秦砖汉瓦收藏与解读的民间学者，一位数十年如一日教书育人的美术家和书法家、金石传拓技艺非遗传承人。也不得不感谢南街学校校长的勇气、担当和独具慧眼，在物欲横流的当今社会，能够义无反顾地给张彦伟先生提供一片天地，收纳他琳琅满目的秦砖汉瓦藏品、向一代又一代年轻学子们传承华夏传统文化。

关键词：盘古，女娲和伏羲，华夏始祖，秦汉青砖，张彦伟，南街学校

1. 引言

在华夏灿烂的文明史上，最为今人熟知和称道的传递早期先民文明与文化的遗产之一，当属那些大家耳熟能详的金石碑刻及清末开始发现并进行研究的甲骨、尤其是它们所承载的华夏先民试图传给我们这些后人的各种文字、图案和图画信息。

实际上，除金石碑刻和甲骨外，古人还充分利用他们周围常见的泥土和火并将二者完美地结合起来，在赋予这些火与土相结合的产品一定文化属性后，留给我们后人。是的，这些火与土的文化产品，就是我们如今并不陌生的陶器、砖瓦和瓷器。其中最值得一提的，自然是带有文字、符号（或纹饰）和图案的古老陶器和秦砖汉瓦之类。

需要说明的是，正如笔名第二自然所指出的那样（2019），,所谓“秦砖汉瓦”并非简单的“秦朝的砖，汉代的瓦”，而是泛指秦汉时期登峰造极的建筑材料砖块和瓦当。秦砖以“颜色青灰、质地坚硬、制作规整、浑厚朴实和形制多样”闻名于世。这些砖瓦样式别致，质量更是让后人叫绝：“敲之有声，断之无孔”。秦砖质量之所以如此之好，与秦始皇施行的“物勒工名，以考其诚”制度有关。砖瓦的制

造者需要把自己的名字刻在上面，一旦出现质量问题便可依名追责，严重者甚至被砍头。秦砖的制作工艺也很厉害，以至于现代人无法复原出来。有学者分析，当年烧制秦砖需高达 1000 摄氏度以上的高温，且对烧制时间和温度都有严密而精准的把控，难度非常高。曾有现代学者用类似工艺烧制较小尺寸的大方砖以降低难度，但多次试验均未成功。

通过当时的临颍县文管所所长袁振炎先生，我和张彦伟先生相识于 2023 年的春天。此后几乎每次回到这片我自己一直十二分钟爱的故乡热土、我的出生地，都会油然到这个虽处喧嚣闹地但依旧保持自己独特安静气质的秦砖汉瓦收藏馆，来这里感受华夏先民超然的工匠精神，将火、土和文化三者有机集合起来的磅礴智慧，在那个绝对慢节奏的时空中心无旁骛专心于一件事儿的静气，汲取先贤大德们默默中赋予秦砖汉瓦的不凡灵气。

对历史上曾属于大名鼎鼎的颍川古郡且群星灿烂人才辈出的这块土地，我一直怀有特殊感情，并部分地将我的这些深情寄托在我于 2022 年春天完成并出版的长篇历史小说《龙脊》中，那里面也提到很多值得我敬仰的先贤和先人。《龙脊》已经是 4 年前的事情也可以说是过去式了。如今，同样位于这片土地上的张彦伟先生的这家独立秦砖汉瓦收藏馆，成为我新的精神寄托和心灵所系。

这篇文章，是我对张彦伟先生这家私人馆藏品之一的初步探讨及对其主人即张彦伟先生的初步介绍。确切地说，是我对这家秦砖汉瓦馆藏之一藏品的初步体会和研判。考虑到包括本文涉及的这块古老青砖在内的所有藏品暂时还没有现代同位素测年数据和/或可资对比的拉曼光谱扫描资料，本文将这块张彦伟先生收集自汝南郡某古老县域的秦汉古老青砖，暂时统一称之为“汝南古砖”，以便行文。

2. 已知信息外的隐藏密码

2026 年 5 月 16 日上午，我和另一友人在南街学校主楼 4 楼参观张彦伟先生琳琅满目的收藏及或黑白或橘红色的相关拓片时，看到一块一端有些许残缺、但背面图案内容颇值得进一步玩味的古青砖（图 1）。当时张先生在这块青砖的注释标签上写有“伏羲女娲画像砖”字样，并向本文笔者和同行的当地友人进行了讲解。

当张先生问笔者青砖下方图案的可能含义时，笔者根据图案人物手持大斧的形象及中间的蛇形图案，想起从小就耳熟能详的华夏传说中的盘古开天地故事：自从盘古开天地……于是提出这个图案，应该是千百年来华夏传说中的始祖盘古，那位舞动巨斧将混沌世界清轻者上浮（为天）浊重者下沉（为地）的盘古。古砖中间的蛇形图案，既与下部的奠基性图案盘古有关，也与上面此前张先生本人解读的伏羲女娲图案相连，有承上启下的纽带作用。关于这一点，将在本文下节通过经典史籍资料进一步论述、说明。



图 1. “汝南古砖”背面图案拓片（左）及影像（右）（均由汉砖收藏家张彦伟制作并拍摄）

图案中大斧在盘古怀抱中的位置及斧头朝向，或许暗示盘古不是左撇子。确切地说，是当时这块儿汉砖制造者理解中的先祖盘古，可能不是左撇子。本文对此先不下结论，而是抛砖引玉式地提出这一问题，供读者朋友们进一步讨论、研究、详查。

将盘古的形象放在下部，而将女娲和伏羲的放在上部，暗示着盘古时代的更久远或辈分更高、有华夏始祖或奠基人的意味；上面的女娲和伏羲，相对盘古要年轻一些，算是盘古的后代或晚辈。至于两组人物之间究竟相差多少代则很不好说，古籍文献上也莫衷一是各说各话。关于这一点，下面还会进一步讨论。

至于这块汉砖正面的图案则比较简单明了（图 2）。：两位怀抱冷兵器戈或戟的兵丁门人，正守在那里履行他们养家糊口枕戈待旦的平凡职责。关于这一点无需多言，也不是本文的主题。当然，二人各自右手所持之小长方形物究竟是啥，目前也无明确结论。本文作者推测可能是一种类似古代大臣们上朝时的笏板即记事板、提醒自己需要注意的事项之类。



图 2. “汝南古砖”正面拓片（左）及影像（右）（均由汉砖收藏家张彦伟制作并拍摄）

有文献说（笏板，2026），笏板长约 2 尺 6 寸中宽 3 寸（旧制，短于今天的 2 尺 6 寸），分别用玉、象牙、竹或木等制成。最早在商朝就可能已开始使用了，是中国古代官员使用时间最长的一种办公用品。古时大臣朝见君王时执笏以记录君命，或将要对君王上奏的要点记在笏板上以防遗忘。《释名》载：“笏，忽也，备忽忘也。”《礼记•玉藻》说：“凡有指画于君前，用笏；造受命于君前，则书于笏。”笏板的其它作用是挡住自己的脸以彰显龙威，面见天子时眼睛要望着笏板以表示对天子的敬意。笏板在中国古代也是地位的象征。唐武德四年后，五品官以上执象牙笏、六品以下官员执竹木笏。形状也有规定，三品以上的笏前拙后直，五品以上的前拙后屈，后又改为上圆下方。明代规定五品以上官员执象牙笏，五品以下不执笏。清朝笏板被废弃使用。古代官员原则上一人只用一只笏，但公务繁忙的官员则允许用好几个，并用称作笏囊的袋子装起来，还用一个随从背着笏囊一同上朝。如唐代张九龄为相时因年迈体弱便开始用随从背笏囊，未料后来竟成被众官员们群起仿效

的时尚。这些背笏囊的随从，就很接近现代官员的秘书团队了。古人没发明纸张前，私用的“笏”还起着书籍的功能，称“牍”。

此时，中原大地这一隅的时空正值不燥不凉的美好季节，南街学校大门外西南方南街村幼儿园围墙内东北角那株杏树及其附近的松树正枝繁叶茂，杏儿则泛着诱人的金黄（图 3）。

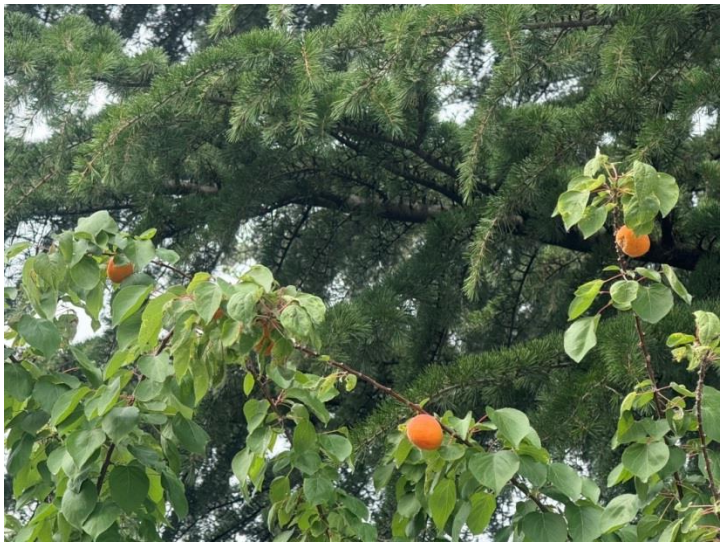


图 3. 河南临颍南街村幼儿园围墙内东北角的杏子（本文作者拍摄）

南街村这一大名响彻华夏大地乃至海外的古老土地四周广饶田野中的冬小麦正由青转黄（图 4），即将进入繁忙但愉快的收获季节。



图 4. 黄淮大平原上渐次成熟的冬小麦（本文作者拍摄）

如诗如画般仓廪实现代文明社会的实现，是数百万年来人类的先祖们茹毛饮血筚路蓝缕一步步走来、含辛茹苦传承并发展才逐渐取得的。

3. “汝南古砖”的身份来源

同样来自古老郡县颍川古郡河南临颍的土著人张彦伟先生的“秦砖汉瓦”收藏，集中于河南尤其是该省的中南部，南到南阳、北到许昌或安阳、西到洛阳、东到开封与周口一带。本文涉及的“伏羲女娲画像砖”即本文特称的“汝南古砖”（图 1 和 2），由张彦伟于 2009 年辗转收获于南邻的另一古老郡县汝南郡一农户手中。

这个时间，显然不是“汝南古砖”的具体出土时间，而是此次的转手收购时间。至于这块古砖已经被转手了多少次，已基本是一个谜一样的问题了。

张先生提供的“汝南古砖”的具体尺寸如下：（残）高 48 厘米，宽 22 厘米，厚 14 厘米。

古砖背面画像下部呈半蹲状的雄性人物浑圆壮硕，四肢粗壮有力，头部装饰山形斗笠或其它含义的头饰，左肩扛有大斧。上方人首蛇身的伏羲女娲手持仙草作交尾状。两组人物中部有一龟甲线条分明的玄武画像，四肢作爬行状。伏羲女娲上部原有一马，可惜残缺。

这类前期主要被赋予金钱属性的特殊商品，其最大缺失是具体出土时间和具体出土位置。这是这类特殊文物的最大损失，且基本是几乎完全无可弥补的重大损失。试想，如果知道其具体出土位置并加以科学考古挖掘，或许会有更多及更大发现。因为像这种信息如此丰富等级如此之高的青砖，普普通通的古人是用不起也不会用的。能够使用信息量如此之大的青砖者，身份显然不一般。

假若“汝南古砖”出土于某个墓葬，为何墓主人要将远古传说中华夏始祖们的形象烧制到青砖上随葬？仅仅是为了对神话传说中的古人致敬吗？还是墓主人与这些神话传说中的先祖有某种渊源？也或许这个墓葬本来就可能是盘古或伏羲与女娲俩人的？如此等等。按照当前流行的“一起都有可能”的原则，所有上述疑问都无法排除，即都有可能。

果真如此，就不得不万分遗憾地说：目前这块“无本之木无源之水”的大青砖“汝南古砖”，原本可能是敲开传说中华夏始祖盘古、女娲和伏羲出处的敲门砖，或进一步了解他们的钥匙之一。

这种可能不是不存在。越来越多的研究证实并得到人们的普遍认可，盘古、女娲和伏羲的后代、“三皇五帝”之一的姬姓黄帝就出生在汝南郡北边不远的轩辕丘即如今的新郑一带，而他传说中的妻子（元妃）、即被后人奉为“先蚕”圣母的嫘

祖（又名累祖，《山海经》中写作“雷祖”），不但出生在汝南北界的西平（西陵氏之女），后来还长期在西平北邻的沙澧河即如今的漯河一带活动。

《史记:五帝本纪》载:“黄帝居轩辕之丘，而娶于西陵之女，是为嫘祖。嫘祖为黄帝正妃，生两子，其后皆有天下。其一曰玄嚣，是为青阳，青阳降居江水。其二曰昌意，降居若水。"战国《世本·卷一帝系篇》:“"黄帝居轩镜之丘，娶于西陵氏之子，谓之嫘祖，产青阳及昌意。”神话传说中把她说成养蚕吐丝方法的创造者。北周以后更被祀为"先蚕”(蚕神)。

4. 典籍中的盘古、女娲和伏羲

无名氏在其题为“史籍中关于‘盘古’的记载”一文中（2026），大致总结了盘古的历史资料。华夏历史上有众多史料和小说，也先后提到盘古、女娲和伏羲之间的大致时间脉络。

《开辟演义》即《开辟衍绎通俗志传》第一回就是盘古氏开天辟地，第九回是伏羲画卦定天下，第十一回是女娲兴兵诛共工、第十三回则是众所周知的女娲氏炼石补天。这一时间顺序，大致反映了三个神话人物之间的年代先后，即盘古在先，女娲和伏羲在后。

唐代欧阳询等编修的类书《艺文类聚》引《五运历年纪》载：“天气蒙鸿，萌芽兹始，遂分天地，肇立乾坤，启阴感阳，分布元气，乃孕中和，是为人也。首生盘古，垂死化身；气成风云，声为雷霆，左眼为日，右眼为月，四肢五体为四极五岳，血液为江河，筋脉为地里，肌肉为田土，发髭为星辰，皮毛为草木，齿骨为金石，精髓为珠玉，汗流为雨泽，身之诸虫，因风所感，化为黎氓。”《艺文类聚》第十一卷帝王部一，列有燧人氏和帝女娲氏。《五运历年纪》由三国时期的徐整辑录上古重要历史著作而成。

这两部书证实了本文作者在本文开篇的推断，即“首生盘古”，盘古是女娲和伏羲的先辈。

肖琳指出（2017），三国时原吴国太常卿徐整弃官游历至桐柏时，为当地盛传历史久远的创世大神盘古开天辟地所吸引，遂作《三五历纪》和《五运历年记》。这两本书也因此成为目前所知记载盘古开天辟地之说最早的古文典籍。但关于创世大神盘古出现的确切时间却无定论。有学者认为盘古之说可溯于西周，《六韬•大明》云：召公对文王曰，盘古之宗不可动也，动者必凶。也有学者认为盘古之说始于春秋，如《山海经•大荒北》记载：西北海之外赤水之北有章尾山。有神，人面蛇身而赤，直目正乘，其瞑乃晦，其视乃明，不食不寝不息，风雨是谒。是烛九阴，是烛龙。烛龙是盘古的另一名号。

这里需要注意的是，盛传创世大神盘古开天辟地的桐柏，与其北边“汝南古砖”的发现地直线距离不过数十千米。二者之间或许通过盘古存在某种神秘关联，比如

“汝南古砖”的原始拥有者听说了桐柏的盘古传说，便制作了大砖表示纪念；或者盘古及其部落，原本就在更容易耕种收获繁衍生息沃野千里的大平原汝南-颍川一带活动（图 4）、或者就在那里开天辟地，只是后来传到了南边山区的桐柏一带，等等。

祖冲之所著《述异记》记载：元者，本也。始者，初也，先天之气也。此气化为开辟世界之人，即为盘古；化为主持天界之祖；即为元始。

《历代神仙通鉴•卷一》说：盘古将身一伸，天即渐高，地便坠下。而天地更有相连者，左手执凿，右手持斧，或用斧劈，或以凿开。自是神力，久而天地乃分。二气升降，清者上为天，浊者下为地，自是混沌开矣。

这一文献，证实了本文作者基于“汝南古砖”背面画像所做的上述推断，即盘古不是左撇子。

《开辟衍绎通俗志传》还载：天地合闭……就像个大西瓜，合得团团圆圆的，包罗万物在内，计一万零八百年，凡一切诸物，皆溶化其中矣。止有金木水火土五者混于其内，硬者如瓜子，软者如瓜瓤，内有青黄赤白黑五色，亦溶化其中。合闭已久，苦不得开。却得一个盘古氏，左手执凿，右手执斧，犹如剖瓜相似，辟为两半。上半渐高为天，含青黄赤白黑，为五色祥云；下半渐低为地，亦含青黄赤白黑，为五色石泥。硬者带去上天，人观之为星，地下为石，星石总是一物。若不信，今有星落地下，若人掘而观之，皆同地下之石。然天下亦有泉水，泉水无积处，流来人间，而注大海。

《开辟衍绎通俗志传》附录《乩仙天地判说》载：天人诞降大圣。曰浑敦氏，即盘古氏，初天皇氏也。龙首人身，神灵，一日九变，一万八千岁为一甲子……

值得注意的其中的“龙首人身”之说。这里的所谓龙，可以理解为蛇，与“汝南古砖”上女娲伏羲和盘古之间的那个蛇形图案相合（图 1）。

《开辟衍绎通俗志传》又说：毗多崩娑那奉西方佛祖之命下界开天辟地,此即盘古氏。盘古伸直身体,天渐升高,地随之下堕,然后左手执凿,右手执斧,将天地相连之处劈凿开,自此混沌初开,乾坤始奠,天下万国四大部洲得以开辟洪蒙,人亦从水火之中解脱。盘古之后有三皇五帝……伏羲氏立天下政治,用仓颉所造的文字取代上古初民的结绳记事之法,并得河图洛书,划定八卦。伏羲氏之妹女娲继兄位号称女皇。共工氏不服,兴兵作乱。女娲兴兵诛共工氏,战于不周山。共工战败,头触不周山而死。他撞倒不周山,于是天柱折,地维倾,女娲炼五色石将天补好,又立鳌足将天支撑,自此天倾西北,地陷东南……

这里明确指出盘古、女娲和伏羲之间的关系，盘古早得多，后生的女娲和伏羲为兄妹。

《古今图书集成•岁功典》卷八十三引《补衍开辟》说：代(世)所谓盘古氏者，神灵，一日九变，盖元混之初，陶融造化之主也。今赣之会昌有盘古山，本盘固名。其湘乡有盘古保，而雩都有盘古祠，盘固之谓也。按《地理坤鉴》云：“龙首人身。”而今成都、淮安、京兆皆有庙祀。事具徐整《三五历纪》及《丹壶记》。至唐袁天纲推言之《真源赋》，谓元始应世，万八千年为一甲子。荆湖南北今以十月十六日为盘古氏生日，以候月之阴暗，云其显化之所宜，有以也。

《元丰九域志》载：“广陵有盘古冢、庙”，殆亦神假者。

晋张华编撰的《广博物志》记载：昔盘古氏之死也，头为四岳，目为日月，脂膏为江海，毛发为草木。秦汉间俗说：盘古氏头为东岳，腹为中岳，左臂为南岳，右臂为北岳，足为西岳。先儒说：盘古氏泣为江河，气为风，目瞳为电。古说：盘古氏喜为晴，怒为阴。吴楚间说：盘古氏夫妻，阴阳之始也。今南海有盘古氏墓，亘三百里，俗云后人追葬盘古之魂也。桂林有盘古祠，今人祝祀，南海有盘古国，今人皆以盘古为姓。盘古氏，天地万物之祖也，而生物始于盘古。

这里明确指出，开天辟地的盘古或盘古氏，就是华夏之始祖。

《路史•前纪一》罗苹注：昔二气未分，螟涬鸿蒙，未有成形，天地日月未具，状如鸡子，混沌玄黄，已有盘古真人，天地之精，自号元始天王，游乎其中。复经四劫，天形如巨盖，上无所系，下无所依，天地之外，辽瞩无端，玄玄太空，无响无声，元气浩浩，如水之形，下无山岳，上无列星，积气坚刚大柔服维天地浮其中，展转无方。若无此气，天地不生。天者，如龙旋回云中，复经四劫，二仪始分，相去三万六千里，崖石出血成水，水生元虫，元虫生滨牵，生刚须，刚须生龙。元始天王在天中心之上，名曰玉京山，山中宫殿并金玉饰之，常仰吸天气，俯饮地泉，复经二劫，忽生太元玉女，在石涧积血之中，出而能言，人形具足，天姿绝妙，当游厚地之问，仰吸天气，号曰太元圣母，元始君下游见之，乃与通气结精，招还上宫。当此之时，二气絪缊，覆载气息，阴阳调和，无热无寒，天得一以清，地得一以宁，并不复呼吸，宣气合会相成自然饱满。大道之兴，莫过于此，结积坚固，是以不朽。金玉珠者，天地之精也。服之能与天地相毕。

清代马骕撰写的《绎史》记载：盘古之君，龙首蛇身，嘘为风雨，吹为雷电，开目为昼，闭目为夜。死后骨节为山林，体为江海，血为淮渎，毛发为草木。

综上所述，盘古即盘古氏，浑敦氏或混沌氏，初天皇氏，毗多崩娑那，神灵，元始天王，等等，是中国传说中开天辟地创造人类世界的始祖。

张启华认为（2026），盘古和伏羲女娲是祖孙关系。

易中天先生认为（2016），女娲的名字最早出现于《楚辞•天问》。在《山海经》和画像石中，女娲和伏羲都是人首蛇身，且二者的蛇尾相互缠绕在一起呈准备传宗接代之状。这倒是与“汝南古砖”背面上部和中部之间的蛇形图案相符。而所谓“龙首蛇身”的文字记载，最早见于东汉王逸的《楚辞章句》，图画形象最早见于汉画像石。换言之，女娲为蛇是汉代的说法，并无原始依据。女娲应为女蛙，即青

蛙。女娲手捧月亮，伏羲手捧太阳。女娲和伏羲都不是具体的人，而是分别代表母系和父系氏族社会文化的符号。女娲的伟大发明是生殖崇拜，伏羲的则是请神吃饭。前者是因人死亡太多，后者则是人饥饿所致。“伏羲琴瑟，女娲笙簧。女娲天皇，伏羲地皇；女娲天圆，伏羲地方。”

在当时那种生产力极其低下的时空里，容易耕种的大平原便成为先民们的首选，即所谓的问鼎中原（图 4），于是就有了汝南的大青砖即“汝南古砖”。

易中天又说（2016）：神话和传说，都是民族的童年记忆，无不隐含着某种文化秘密和梦想。神的历史就是人的历史，是人类自我认识的心灵史。只要抹去神秘的色彩，我们就能打开迷宫，依稀看见一些真实的东西。

5. 收藏鉴赏家张彦伟

在他个人的小红书（号码：95065722722）介绍中，张彦伟先生的 Profile 是这样的：美术教书人，汉画守护者。致力于让汉画“活”起来。分享研究汉画心得、美学赏析、趣味解读。一起感受汉代工匠的磅礴想象力。

某种意义上，这种 profile 是其主人对自己精神追求的确切定位，或其希望的人生理想生活状态，而不全是现实生活简历。

在现实世界中，张彦伟先生是河南省漯河市南街村学校的美术老师。他本文提供给本文作者的个人介绍是：张彦伟，高级教师，中国汉画学会会员，省骨干教师，金石传拓技艺非遗传承人，河南省教育学会美术书法专业委员会会员，河南省民间文艺家协会会员，（河南省漯河市）临颍县首席科普专家。2019 年 9 月，受邀参加第十一届全国少数民族传统体育运动会民族大联欢非遗展演；2022 年被评为“2022 年度全省优秀文物保护员”。工作单位：河南省漯河市临颍县南街学校。

从 1995 年开始，张彦伟利用周末、节假日和寒暑假，以临颍为中心走村串户，只要见到农户家院墙上、甚至老砖堆砌的厕所上带有图案和/或文字的古砖，便想办法买回去进行拓片、研究、解读。通过三十余年的含辛茹苦收集、抢救和整理，把 480 余件画像砖、铭文砖、古陶器、汉画像砖石拓片无偿捐献出来，在南街学校及该校校长张红女士的大力支持下，在南街学校创建了“南街学校汉画艺术馆”，受到广大师生和周围居民的喜爱和欢迎。

6. 讨论

人们常说的“秦砖汉瓦”，并不意味着千年前的古砖一定是秦代的，有精美图案的瓦当只能是汉代的。而是对那个年代击之发音乐之声的火与土有机结合且含有一定文化信息的砖瓦之统称。换言之，秦汉之际都可以出产类似“汝南古砖”这种大青砖。

在缺乏同位素测年数据和拉曼光谱比对资料的情况下，“汝南古砖”这块画像砖也有可能是秦代的，也可以笼统称之为“秦汉古砖”。考虑到汝南悠久的历史，尤其是其孕育了华夏历史上罕见的以另一种形式开天辟地的旷世奇人李斯：帮秦灭六国，参与制定法律，统一车轨、文字、度量衡制度，建立郡县制、奠定了中国两千多年政治制度的基本格局，这是完全有可能的。也就是说，张先生收藏的很多所谓“汉砖”，理论上都有可能是秦代的。

当务之急是趁着时间还不是那么久远，抽丝剥茧尽快找出“汝南古砖”的具体出土位置，进而通过科学挖掘找出其原始拥有者的身份，甚至通过挖掘获得其主人更多更确切的资料和更多实物信息。万一主人是盘古或女娲和伏羲的墓葬或生前活动地点呢？

关于“汝南古砖”的另一种可能是，秦汉时期某个有血脉情怀的先人，出于对盘古和/或女娲及伏羲等华夏先祖的敬仰、怀念或纪念，特意为他们设立的类似于后人衣冠冢的墓葬。这一可能性，远较盘古或女娲伏羲原始墓冢的可能性为大，毕竟火和土结合制砖的出现，要比传说中盘古和女娲伏羲的出现晚得多。

还有一种可能，“汝南古砖”来自秦汉时期某个纪念盘古、女娲和伏羲的寺庙，而不一定是上述某个墓葬。

还有一种可能，这块古砖的原始出处并不在汝南，而是周围某个地方，如上面提及的盘古开天地传说很盛行的更南部一些的桐柏。只是后来获得这块砖的人为了赚钱谋生，将它贩卖到了汝南。仅就这一点来说，称之为“汝南古砖”并不准确或科学，更应该称之为“秦汉古砖”。

笔者 1995 年春在景德镇市与校友、地质学家出身的景德镇市矿管局局长毛炎超面谈时，热情豪迈的他提出：瓷器文化，本质上就是火与土的文化。实际上，华夏的秦砖汉瓦文化，又何尝不是如此？何尝不是火、土和文化有机结合后的伟大文明产物？只是在时间上，秦砖汉瓦的火与土文化，比瓷器的火与土文化早得多而已。

7. 结论

“汝南古砖”背面画像下部的人物，当为传说中“开天辟地”的华夏始祖盘古，那把大斧是证据之一。盘古画像处于女娲伏羲画像下方，意味着他奠基人的地位，即其历史地位高于、年龄也早于华夏神话传说中补天的女娲和发明八卦的伏羲氏。

下（盘古）、上女娲伏羲之间的蛇形图案，既印证了传说中盘古“龙首蛇身”和女娲伏羲“人首蛇身”的信息，同时也证明了其它岩画或砖画中传出的女娲伏羲交尾的信息不虚。

更为重要的是，上、下两组画像之间的蛇形图案，传递出盘古与女娲伏羲这两代、乃至他们之间和数代和女娲伏羲之后，无数华夏先民代代相传生生不息的血脉乃至基因联系。

至于“汝南古砖”正面画像中两位守卫大门兵丁右手所持之小长方形物，当为流传了数千年之久的古老办公记事本或提示板，笏板。一来表明两位门卫很勤于职守，但也说明当时守卫制度很严，必须严格照章办事一丝不苟。

最后但也是最重要的一点，就是衷心感谢南街学校及其校长张红女士的独具慧眼及伟大的家国情怀，感谢他们勇于担当提供场地和资金开辟这块难得的充满文明气息的秦砖汉瓦馆，为这方古老大地增添了又一抹亮色、乃至绚丽色彩。

参考文献/References

01. 陈梦雷，蒋廷锡. 清（中国）. 《古今图书集成》. https://wenku.baidu.com/tfview/1d02b22832126edb6f1aff00bed5b9f3f90f7275.html?fr=launch_ad&utm_source=360ss-WD&utm_medium=cpc&keyword=%E5%8F%A4%E4%BB%8A%E5%9B%BE%E4%B9%A6%E9%9B%86%E6%88%90%E7%9B%AE%E5%BD%95&utm_account=SS-360tg01&qhclickid=18828eaded673d41&_wkts_=1779335942658. Trieved May 21, 2026.
02. 第二自然. 2019-10-14. 现代人无法还原的“秦砖汉瓦”. https://baike.baidu.com/article/91d7722a17280d4fb01e1f44.htm. Trieved May 22, 2026.
03. 笏板. https://baike.so.com/doc/5964037-32349483.html. Trieved May 19, 2026.
04. 嫘祖.https://baike.so.com/doc/30505622-32300306.html. Trieved May 22, 2026.
05. 李斯的生平简介. https://wenda.so.com/q/1375192948066577?src=180&q=%E6%9D%8E%E6%96%AF%E7%AE%80%E4%BB%8B. Trieved May 22, 2026.
06. 罗泌. 南宋（中国）. 《路史》. https://bkso.baidu.com/item/%E8%B7%AF%E5%8F%B2. Trieved May 21, 2026.
07. 马驌，王利器. 清（中国）. 2002.《绎史》. 北京：中华书局.
08. 欧阳询，令狐德棻，陈叔达，裴矩，赵弘智，袁朗等. 唐（中国）. https://baike.so.com/doc/5584827-5797421.html. Trieved May 20, 2026.
09. 《山海经•海内经》.战国（中国）. https://baike.so.com/doc/24970230-25927381.html. Trieved May 22, 2026.
10. 司马迁. 汉（中国）. 《史记•五帝本纪》. https://wenku.so.com/tfd/944b55c49fcfcdf7ff3cb0b9d888bae2?src=360ss&ocpc_id=125406&plan_id=2713803455&group_id=2482963016&keyword=%E3%80%8A%E5%8F%B2%E8%AE%B0%C2%B7%E4%BA%94%E5%B8%9D%E6%9C%AC%E7%BA%AA%E3%80%8B&aivip_extjson=%7B%22360ocpc%22%3A%7B%22accountid%22%3A%223330293484%22%2C%22keywordid%22%3A%2265849148724%22%2C%22creativeid%22%3A%2210996016355%22%2C%22groupid%22%3A%222482963016%22%2C%22planid%22%3A%222713803455%22%2C%22query%22%3A%22%E3%80%8A%E5%8F%B2%E8%AE%B0%C2%B7%E4%BA%94%E5%B8%9D%E6%9C%AC%E7%BA%AA%E3%80%8B%22%7D%2C%22pcsem%22%3A%7B%22medium%22%3A%22dianjingps%22%2C%22sputag%22%3A%22sssstttt%22%2C%22aibid%22%3A%22aaaabbbb%22%2C%22retentionstrategy%22%3A%22rrrrssss%22%7D%7D&qhclickid=e15605d6b9a0a147. Trieved May 22, 2026.
11. 王存，曾肇和李德刍. 北宋（中国）. 《元丰九域志》. https://baike.so.com/doc/6705634-6919619.html. Trieved May 21, 2026.
12. 无名氏. 史籍中关于盘古的记载. https://wenku.baidu.com/view/d6377ca652e79b89680203d8ce2f0066f53364d0.html?fr=income3-

doc-search&_wkts_=1778915322309&wkQuery=%E3%80%8A%E5%8F%B2%E8%AE%B0%E3%80%8B%E4%B8%AD%E5%85%B3%E4%BA%8E%E7%9B%98%E5%8F%A4%E7%9A%84%E8%AE%B0%E8%BD%BD&needWelcomeRecommand=1. Trieved May 16, 2026.
13. 肖琳.《三五历纪》及姊妹篇《五运历年记》和《神谱》所载创世神话. 2007. https://www.docin.com/p-1277861462.html.《新西部》：（20）：213-214. Trieved May 21, 2026.
14. 徐人瑞，程瑶，徐道，程毓奇和胥紫来. 明清（中国）.《历代神仙通鉴》. https://baike.so.com/doc/5710117-5922838.html. Trieved May 21, 2026. 历代神仙通鉴》.https://wenku.so.com/tfd/22c31fa710d2fe04b9957e75210e30d6?src=360ss&ocpc_id=139916&plan_id=1505876098&group_id=1669479000&keyword=%E3%80%8A%E5%8E%86%E7%A5%9E%E4%BB%99%E9%80%9A%E9%89%B4%E3%80%8B&aivip_extjson=%7B%22360ocpc%22%3A%7B%22accountid%22%3A%223575869317%22%2C%22keywordid%22%3A%2271512786908%22%2C%22creativeid%22%3A%2210285865341%22%2C%22groupid%22%3A%221669479000%22%2C%22planid%22%3A%221505876098%22%2C%22query%22%3A%22%E3%80%8A%E5%8E%86%E7%A5%9E%E4%BB%99%E9%80%9A%E9%89%B4%E3%80%8B%22%7D%2C%22pcsem%22%3A%7B%22medium%22%3A%22dianjingps%22%2C%22sputag%22%3A%22ssssttt%22%2C%22aibid%22%3A%22aaaabbbb%22%2C%22retentionstrategy%22%3A%22rrrrsss%22%7D%7D&qhclickid=836aaee792bb5e14. Trieved May 21, 2026.
15. 易中天. 2016.《易中天中华史.祖先》（The History of China 01）. 杭州：浙江文艺出版社.
16. 张华. 晋（中国）.《广博物志》. https://www.shidianguji.com/ens/book/SK2000/chapter/1kf2gxw8niu4q. Trieved May 21, 2026.
17. 张启华。2026-02-19.盘古开天辟地女娲抟土造人伏羲创制八卦：他们三个是什么关系？ https://mbd.baidu.com/newspage/data/videolanding?nid=sv_14151408666435501306&sourceFrom=share. Trieved May 19, 2026.
18. 周游.明崇祯（中国）.《开辟演义》（《开辟衍绎通俗志传》）. https://book.gushikan.com/book/63.html. Trieved May 20, 2026.
19. 周游. 明崇祯（中国）.《开辟衍绎通俗志传》. https://www.kekeshici.com/xiaoshuo/mingqing/65587.html. Trieved May 21, 2026.
20. 祖冲之. 南朝（中国）.《述异记》. https://baike.so.com/doc/5710117-5922838.html. Trieved May 21, 2026.

Data availability

The data that support the findings of this study are available from the author upon reasonable request.

Declaration of competing interest

The author declares that he has no competing financial interests or personal relationships that could have appeared to influence the work reported in this paper.

Use of AI tools declaration

The author declares that he has not used Artificial Intelligence (AI) tools in the creation of this article.

Original Article

Types and Metallogenic Mechanism of Rubidium Deposits in Mainland China

Jian Zhao Yin[1] Ⓛ

Abstract

Mainland China holds a dominant global position in terms of rubidium resources; while rubidium mineralization of various types has been discovered across many regions, most occurrences are low-grade associated/paragenetic deposits that are difficult to develop and process. Genetically, the country's known rubidium deposits fall into three categories: endogenic, exogenic, and those formed by the superposition of endogenic and exogenic processes. The endogenic category encompasses types such as pegmatites (broadly defined), granites (broadly defined), magmatic-hydrothermal systems, crypto-explosive breccias, alkaline igneous rocks, porphyries, skarns, and volcanic rocks. Deposits formed by the superposition of endogenic and exogenic mineralizations include brines, Quaternary hot springs, and coal-hosted deposits. Exogenic deposits consist of weathered granite crusts and minor placer-type occurrences. Rubidium mineralization is closely linked to tectono-magmatic activity. Key ore-controlling factors include, but are not limited to: magmatic fractional crystallization and hydrothermal metasomatism; the degree of magmatic differentiation; the intensity of magma melt-fluid interaction and crustal contamination; oxygen fugacity and the remelting of crustal material; alteration intensity; the involvement of fluxing and incompatible elements; and the influx of mantle-derived material (including its quantity and/or extent). For liquid-phase deposits—specifically brine types—additional ore-controlling factors include hot spring temperatures, etc.

Keywords: genetic type; geology; rubidium deposits; endogenic/exogenic type; type formed by the superposition of endogenic and exogenic geological processes; mainland China

---

Affiliation Info: 1 College of Earth Sciences, Jilin University, Changchun 130061, China

Corresponding AurhorⓁ: Yin, J. Z., PhD, Professor, geosciences, mineral exploration and mining; Email address: jzyin7@jlu.edu.cn

Citation: Yin, J.Z. 2026. Types and metallogenic mechanism of rubidium deposits in Mainland China. *Naturalis Scientias*, 3: 777-802. DOI: https://doi.org/10.62252/NSS.2026.1043. www.naturalisscientias.com.

Copyright © 2026 by the author. Published by *Naturalis Scientias*. This is an open access article under the Creative Commons Attribution-NonCommercial 4.0 International (CC BY-NC 4.0) License. (https://creativecommons.org/licenses/by-nc/4.0/).

---

1. Introduction

Rubidium and cesium exhibit high chemical reactivity and excellent photoelectric properties; consequently, they are widely used in traditional sectors such as photoelectric conversion devices, optical crystals, optical glass, catalysts, specialty glass, biochemistry, and medicine. Owing to these outstanding physicochemical properties, they also serve indispensable roles in emerging high-tech industries and the defence sector. Currently, the application of rubidium in optical technologies, synthetic catalysis, and specialty glass and ceramics represents a leading frontier in the development of emerging industries (Sun, 2013; Sun et al., 2013; Wang et al., 2024; Wang et al., 2025).

Benefiting from diverse and favorable geological settings, mainland China possesses abundant and widely distributed rubidium resources, encompassing both solid-state deposits and various liquid (hot spring) brine-type deposits (Sun, 2013; Sun et al., 2013; Wang et al., 2024).

The rare metal rubidium is a key material for the development of strategic emerging industries under China's "13th Five-Year Plan" (Hou, 2023). Over the past two decades, there has been a surge in exploration and research regarding rare and critical metals—including rubidium—across mainland China, leading to breakthroughs in numerous areas.

Drawing on the latest research by Chinese scholars, this paper classifies the genetic types of rubidium deposits in mainland China, summarizes the geological characteristics of these various deposit types, and offers a preliminary discussion on their formation mechanisms.

2. Characteristics and current status of rubidium resources

Rubidium deposits in mainland China are primarily distributed across 12 provinces and autonomous regions—including Jiangxi, Xinjiang, Hunan, Sichuan, Yunnan, Tibet, Qinghai, Shaanxi, Henan, and Guangdong (Fig. 1)—and are predominantly of super-large and large scale (Sun et al., 2015; Sun et al., 2019; Gao et al., 2023).

Tectonically, rubidium mineralization in mainland China primarily occurs within rare-metal metallogenic belts such as the eastern segment of the Jiangnan Uplift, the Wugongshan–Northern Wuyishan belt, the central Nanling belt, the Central Zhejiang–Wuyishan belt, the Kangdian region, the Altay region, and the northern margin of the North China Craton. Granite-hosted and (granite-) pegmatite-hosted deposits constitute the main types of rubidium deposits in the country, though they are predominantly associated/paragenetic resources. The fundamental pattern of inherent scarcity regarding rubidium resources in mainland China has not yet undergone substantial change (Sun et al., 2019). In the first half of 2025, 38 new mineral deposit sites were discovered nationwide, representing a year-on-year increase of over 30% (Yi, 2025). Significant breakthroughs were achieved in the exploration for strategic/critical metals—including uranium, rubidium, gold, cobalt, and manganese—with the discovery of a number of large-scale and super-large deposits. Notably, the addition of 3.37 million tonnes of rubidium resources in Xinglong County,

Hebei Province—reaching a super-large scale—has further consolidated China's dominant global position in rubidium resources.

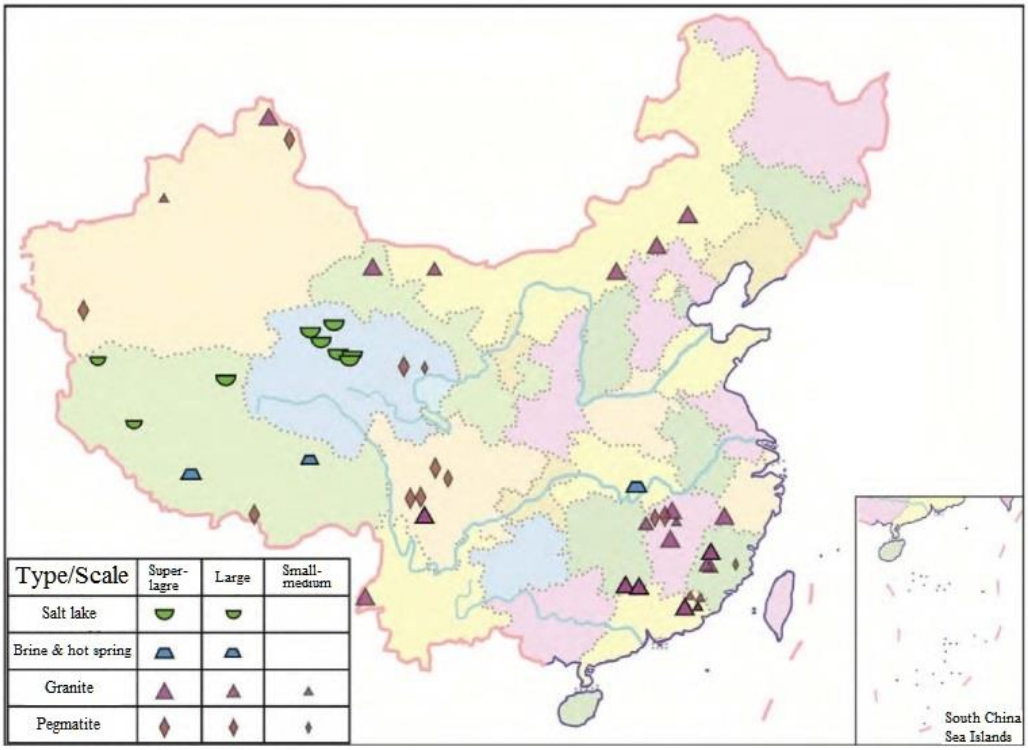


Figure 1. Distribution map of rubidium (and cesium) deposits in China (after Gao et al., 2023)

Although mainland China possesses abundant rubidium resources—a critical metal—almost all currently known deposits are granite-hosted associated resources characterized by low grades, difficult extraction, and processing challenges. High-grade, easily processed granite-pegmatite-hosted rubidium deposits—featuring ore minerals such as zinnwaldite, lepidolite, and pollucite—are extremely limited (Wu et al., 2021; Tang and Wu, 2024). The metallogenic ages of associated/paragenetic rubidium deposits in mainland China are concentrated within specific periods, and no independent rubidium deposits have yet been discovered (Sun et al., 2013).

Rubidium primarily occurs in pollucite, lepidolite, microcline, and roscoelite, with some occurrences in Nb-Ta-Mn minerals and biotite. It mainly substitutes for potassium via isomorphous replacement in minerals such as biotite, muscovite, and K-feldspar. Gangue minerals include quartz, K-feldspar, and mica (Sun, 2013; Xing, 2020).

Rubidium resources in mainland China consist primarily of solid hard-rock deposits, with reserves (as Rb_2O) totalling 1.16 million tonnes (Wang et al., 2024). While acid-based extraction from solid ores is currently the dominant method for industrial-scale production, solvent extraction and ion exchange hold immense promise for processing liquid-phase

rubidium resources. Wang et al. (2024) highlight the significant development potential of surface and subsurface brine-type rubidium resources; they recommend intensifying resource surveys and exploration, advancing technologies for the comprehensive beneficiation of low-grade solid and liquid ores, and expanding the application scope and functional capabilities of rubidium products.

Meanwhile, Sun et al. (2013) suggest that China prioritize the exploration and development of high-grade mica-hosted rubidium deposits, while also focusing on rubidium recovery from existing mine tailings and strengthening research into beneficiation processes and comprehensive utilization.

3. Genetic types and their geology

There is currently a broad consensus within the industry in mainland China that rubidium mineralization within the country can be classified into several types—including granite-hosted, (granitic) pegmatite-hosted, greisen-hosted, magmatic-hydrothermal, salt lake, subsurface brine, weathered granite crust, and placer types—with hard-rock mineralization (specifically granite and granitic pegmatite types) predominating; the Yanshanian period represents the most significant era of mineralization (Shen et al., 2003; Hou, 2023). While different hard-rock rubidium mineralization types exhibit distinct prospecting indicators, most are closely associated with albitization, amazonitization, and micatization, and are rich in volatile-bearing minerals such as fluorite and tourmaline. These endogenic rubidium deposits are closely linked to Yanshanian granites and often display horizontal and vertical zonation (Shen et al., 2003).

Based on publicly available data regarding rubidium deposits in mainland China, this paper reclassifies their genetic types, paying particular attention to specific details. For instance, mineralization previously termed "greisen-type" is, in reality, altered granite and is thus fully subsumed into the broad category of granite-hosted deposits. As there is no fundamental difference between salt lake and subsurface brine types, they are collectively categorized as "brine-hosted" deposits, further subdivided into surface water body and deep brine subtypes; additionally, an oil-and-gas-associated subtype has been added, alongside a Quaternary hot spring type, which ranks at the same hierarchical level as the brine-hosted category. The hard-rock category has been expanded to include skarn, porphyry, and volcanic rock types, while the solid-state category now includes the weathered granite crust type (Table 1); these are briefly described below.

3.1 Endogenic rubidium deposit

This type of rubidium mineralization is closely associated with tectono-magmatic activity; indeed, many deposits of rare and dispersed metals in mainland China are closely linked to tectono-magmatic activity within orogenic belts (Fig. 1 and Table 1).

Table 1. Genetic types and geology of rubidium deposits in Mainland China

Type		Geology	Origin/representative deposit	Data source
Endogenous	Pegmatite (broad sense)	In all pegmatite dikes—including microcline pegmatites, muscovite granite pegmatites, and muscovite-albite-spodumene pegmatites; Rb primarily occurs in minerals such as microcline and muscovite.	The Jiajika polymetallic deposit in Sichuan; numerous pegmatite dikes across the Qinghai-Tibet Plateau, Xinjiang, Sichuan, and the Eastern Qinling Mountains; the Shihuiyao deposit in Inner Mongolia, etc.	Du, 1983; hao, 1987; Wang, 2009; Liu et al., 2010; Sun, 2013; Duan et al., 2016; Xu et al., 2016; Sun et al., 2017; Yang, 2017; Guo, 2019; Yu et al., 2019; Zhang, 2019; Li, 2020; Wang et al., 2020; Xue et al., 2020; Kong et al., 2021; Chen et al., 2022; Fan et al., 2022; Liu, 2023; Xie et al., 2023; Chen et al., 2024; Fang et al., 2024; Li et al., 2024; Qin et al., 2024; Wang et al., 2024; Wen et al., 2024; Ban et al., 2025; Du et al., 2025; Li et al., 2025; Liang et al., 2025; Wang et al., 2025; Xie et al., 2025; Zhu et al., 2025; Cheng et al., 2026; Sha, 2026; Yin, 2026c, 2026d and 2026e; Yuan, 2026
	Magmatic-hydrothermal	These include hydrothermal vein types—such as quartz veins, often coexist and/or are associated with mineralization types such as quartz veins, explosive breccias, porphyry deposits, and skarns.	Inner Mongolia's Vilasto deposit, Xilinhot's Shihuiyao, northern Guangdong, the Qinghai-Tibet Plateau, and Sichuan's Jiajika, etc.	
	Cryptovolcanic breccia	The formation of crypto-explosive breccias is closely linked to the intense accumulation and explosive release of magmatic-hydrothermal fluids; consequently, some classify them as belonging to the magmatic-hydrothermal category.	The Weilasituo deposit in Inner Mongolia, among others.	
	Granite (broad sense)	Granite-hosted Rb deposits—which represent the most economically valuable Rb resource—encompass a wide variety of types, including albitized and K-feldspathized granites, granite-hosted disseminated deposits, greisenized granites, metamorphosed granites, autometamorphosed granites, alkaline or alkali-feldspar granites, monzogranites, fine-medium grained monzonites, fine-grained muscovite granites, coarse-grained to pegmatitic granites, microgranites, fine-grained muscovite-spodumene granites, and even (muscovite) albitites; these deposits are predominantly found within Mesozoic folded orogenic belts.	The Qinghai-Tibet Plateau and surrounding areas, Tengchong and Gejiu in Yunnan, Inner Mongolia, Zhengchong in Hunan, Tongcheng in Hubei, northern Guangdong, Xianglushan in Guangxi, and Jiajika in Sichuan, among others.	
	Alkaline igneous rock	Ferro-sodic alkaline basic rocks, ferro-potassic trachyte, ferriferous alkaline diabase and gabbro, alkaline (ferriferous) picrite, tephrite, alkaline syenite, and albitite, etc.	Areas such as Dongchuan in eastern Yunnan, as well as Henan and Shaanxi.	
	Porphyry	These include quartz porphyry and granite porphyry; Rb mineralization occurs primarily within quartz porphyry dikes and their contact zones with the surrounding rock, with Rb substituting for other elements within muscovite or biotite, and the mineralization is closely associated with silicification and sericitization.	Rb deposits such as those in Jianning (Fujian), Zhengchong (Hunan), and Ningguo (Anhui).	
	Skarn	Skarn-type Rb mineralization associated with syn-collisional granites frequently co-occurs or is associated with various other metals, forming a concentration zone of ferrous, non-ferrous, and rare (or even rare-earth) metal mineralization.	Polymetallic mineralization in Diantan, Tengchong, Yunnan, etc.	
	Volcanic	Occurs in rhyolite porphyry.	Siziwang Banner, Inner Mongolia.	
Superposition of endogenous and exogenous factors	Hot spring	It is commonly found along the Yarlung Tsangpo Suture Zone on the Qinghai-Tibet Plateau and in surrounding regions, such as southern Tibet, Sichuan, and Yunnan.	It is commonly found on the Qinghai-Tibet Plateau and in surrounding areas such as Sichuan and Yunnan.	
	Brine	Including surface water subtypes such as salt lakes, as well as underground brine subtypes and oil and gas field subtypes.	It is commonly found on the Qinghai-Tibet Plateau and in surrounding areas such as Sichuan and Yunnan.	
	Coal	Various rare metals are present in many coalfields across mainland China.	They are found in the Northeast, Northwest, North China, Central-South, and Southwest regions, among others.	
Exogenous	Weathered granite crust and placer	The Dayangtian rubidium deposit in Tengchong, Yunnan, features a weathering-crust type rubidium deposit near the surface; the primary rubidium-bearing minerals include potassium feldspar, albite, and mica.	Tengchong, Yunnan, and other areas.	

3.1.1 Porphyry-type

These include rock types such as quartz porphyry and granite porphyry. For instance, in the rubidium deposit near Dongkeng Village, Jianning County, Fujian Province, the host rocks consist primarily of quartz porphyry, with subordinate amounts of cataclasite and granite porphyry. The average Rb_2O grade is approximately 0.13%, with associated tin; the delineated rubidium resource is currently classified as large-scale. The rubidium ore bodies occur mainly within quartz porphyry dikes and their contact zones with the country rock, and are strictly controlled by NE-trending faults (dipping northwest with steep attitudes) (Yang, 2017; Li, 2020). The country rocks comprise the Tianjingping Formation leptynite and Caledonian-age migmatite; mineralization is closely associated with silicification and sericitization. Within the ore, rubidium occurs via isomorphous substitution for K^+ in altered K-feldspar, muscovite, and biotite (Yang, 2017). The ore-forming materials originated from Caledonian basement rocks characterized by high background levels of Rb and Sn; these materials were mobilized, transported, and enriched within shallow fault

zones and porphyry contact zones by Late Yanshanian (approx. 140–100 Ma) magmatic-hydrothermal processes. The deposit is classified as a porphyry-contact metasomatic Rb-Sn deposit, closely linked to intermediate-acidic magmatism associated with the large-scale extensional tectonic setting of the Yanshanian period in South China.

The Zhengchong Rb-polymetallic deposit in Hunan Province, located in the central section of the Nanling Rb metallogenic belt, is a super-large, Rb-dominant rare-metal deposit associated with highly fractionated granite (Fig. 2). The ore bodies are hosted within a zinnwaldite-bearing porphyry body; phenocrysts include quartz, zinnwaldite, and topaz, with zinnwaldite serving as the primary Rb-bearing mineral (Liu, 2023). The micas in this porphyry are almost exclusively zinnwaldite, with muscovite being rare; the high F content in the zinnwaldite and relatively low F content in the topaz reflect characteristics of a magmatic origin. Monazite within the fine-grained greisenized porphyry exhibits a high average Th content of up to 7.0 wt.%, alongside Th/Ce, Y/LREE, Ca/Ce, and Si/Ce ratios indicative of a magmatic origin. The whole-rock Y/Ho ratio of the greisenized porphyry approximates that of chondrites (240.01), serving as a petrological marker for Rb-Li-Cs rare-metal exploration in the region. This porphyry likely underwent three superimposed stages of in-situ crystallization, leading to the extreme enrichment of incompatible elements and the eventual formation of an Rb-Li-Cs rare-metal deposit.

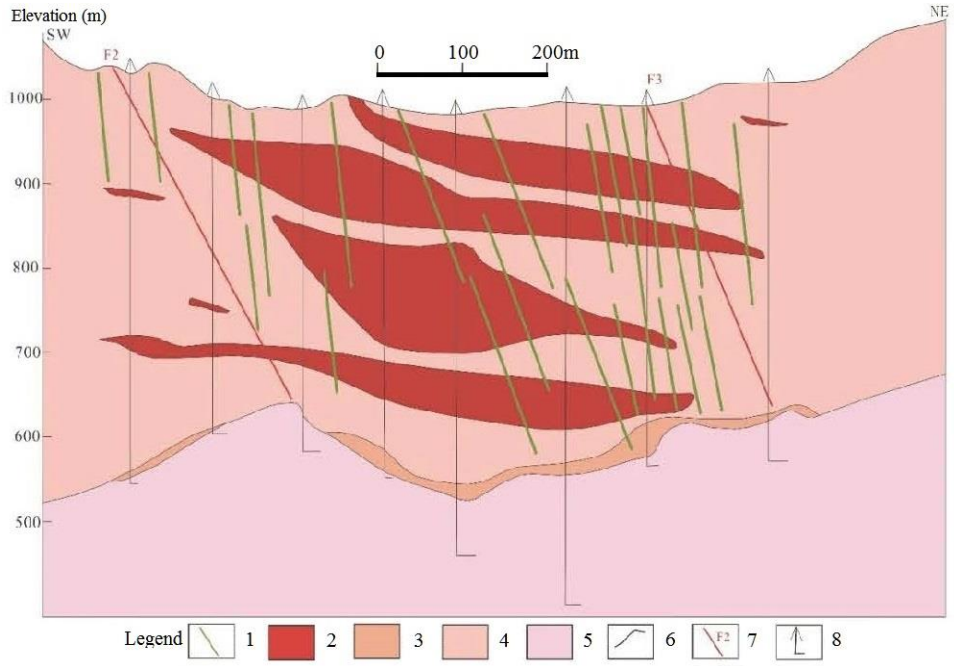


Figure 2. Section of the Zhengchong greece porphyry Rb polymetallic deposit in Hunan, China (average grade: Rb_2O 0.225%, Li_2O 0.557%, Cs_2O 0.012%. Quoted from Wen et al., 2024)

1-Quartz-vein type tungsten deposit; 2-Greisen-type lithium deposit; 3-Granite-type lithium deposit; 4-Porphyritic biotite granite; 5-Medium- to fine-grained alkali-feldspar granite; 6-Geological boundary; 7-Fault; 8-Drill hole

The Xiwukou rubidium deposit, located in the Jiangnan Uplift Belt, is the first critical metal deposit discovered in Ningguo, Anhui Province, in recent years; the associated magmatic rock is granite porphyry (Chen et al., 2022). Two types of rubidium ore bodies are present: Ore Body I occurs as a lens at the top of the granite porphyry body, with phengite content reaching 70% and a grade of 0.25%; Ore Body II occurs at the contact zone between the granite porphyry and the surrounding strata, with a grade of 0.21%. Both types of ore bodies share a mineral assemblage of phengite and quartz. Electron probe micro-analysis (EPMA) and laser ablation inductively coupled plasma mass spectrometry (LA-ICP-MS) studies on the ore-forming intrusion and the major minerals within the ore bodies reveal that the average Rb contents in plagioclase, K-feldspar, and biotite from the granite porphyry are 3.10×10^{-6}, 872×10^{-6}, and 1328×10^{-6}, respectively; while the average Rb contents in phengite from Ore Bodies I and II are 2544×10^{-6} and 2686×10^{-6}, respectively. Crystal-chemical calculations indicate that rubidium enters the phengite crystal lattice via $Rb^{+} \rightarrow K^{+}/Na^{+}$ substitution—existing in the form of isomorphous replacement. The ore-forming magma of the Xiwukou deposit is characterized by high background Rb values and fluorine content. Mineral crystallization enriched Rb in the residual magma; during the transition from the magmatic to the hydrothermal stage, the high F content caused the framework silicate structure of the original magmatic system to transform into a layered structure, thereby facilitating the crystallization of abundant Rb-rich phengite and ultimately leading to the formation of the rubidium ore bodies.

3.1.2 Magmatic-hydrothermal + explosive breccia type

The formation of crypto-explosive breccia is essentially driven by the intense accumulation and high-pressure explosive release of magmatic fluids (gases and liquids). Consequently, researchers classify crypto-explosive breccia-hosted rubidium mineralization within the broader category of magmatic-hydrothermal systems.

The Weilasituo deposit in Inner Mongolia hosts three types of ore bodies: alkali-feldspar granite-hosted Sn-Rb, crypto-explosive breccia-hosted Li-Rb, and quartz vein-hosted Sn. The crypto-explosive breccia-hosted ore body is situated between the other two types. Focusing on quartz crystals and their fluid inclusions within the crypto-explosive breccia ore, Wang et al. (2024) employed techniques such as quartz cathodoluminescence, microthermometry of fluid inclusions, laser Raman spectroscopy, and in-situ oxygen isotope analysis. Their findings indicate that the quartz crystals underwent three growth stages: Q1, Q2, and Q3. While fluid inclusion salinity remained similar between stages Q1 and Q2, homogenization temperatures decreased and quartz oxygen isotope values became lighter, signalling an increased influx of meteoric water. The Weilasituo crypto-explosive breccia-hosted ore resulted from crypto-explosive activity at the top of the intrusion; as depressurized magmatic-hydrothermal fluids ascended, they mixed to varying degrees with meteoric water, triggering the precipitation of Li-rich micas and the associated Li-Rb mineralization.

In essence, the Weilasituo crypto-explosive breccia-hosted ore represents a form of granite-related or magmatic-hydrothermal Rb-polymetallic mineralization, albeit one where fluid-gas interactions have altered the ore's texture and structure.

3.1.3 Skarn-type

The Diantan skarn belt in Tengchong is situated at the junction of the Lhasa Block and the Indian Plate; it represents a concentration zone of skarn-type Fe-Cu-Pb-Zn and rare-metal mineralization associated with Early Cretaceous syn-collisional granites. Research by Cheng et al. (2026) indicates that the rubidium (Rb) ore bodies within the Diantan skarn belt typically occur alongside iron ore bodies within the skarn bodies and are accompanied by polymetallic mineralization involving Cu, Pb, Zn, Sn, W, and Mo. Seventeen major Rb ore bodies occur as stratiform, lenticular, and/or vein-like bodies, reaching lengths of up to 808.0 m; individual drill-hole intercepts show thicknesses of 1.02–11.28 m and average Rb grades of 0.040%–0.113%. Both the iron and rubidium resources are classified as large-scale deposits. Electron probe micro-analysis (EPMA) data for phlogopite show contents of SiO_2 (40.91%–41.39%), MgO (26.42%–26.87%), Al_2O_3 (14.30%–14.65%), K_2O (10.11%–10.45%), Na_2O (0.17%–0.19%), FeO (2.03%–2.27%), and TiO_2 (0.06%–0.11%). In-situ trace element analysis reveals Rb contents of 2,485–2,641 ppm; Rb, Sn, Cs, Ba, Li, B, Pb, Zn, Ga, and Nd are relatively enriched, whereas Sc, V, Cr, Co, Ni, Cu, Sr, and Zr are relatively depleted. Rare earth element (REE) contents are extremely low (41.9–253.2 ppb). The rubidium is hosted within phlogopite and formed during the late stage of skarn evolution. The Tengchong-Diantan skarn-type Fe-polymetallic ore belt extends over 40 km from north to south and is approximately 20 km wide from east to west. Phlogopite is present in several skarn-type deposits within the belt—such as the Tongchangshan Pb-Zn deposit—indicating potential for rubidium exploration.

3.1.4 Granite type

Granite-hosted rubidium deposits are known by various, albeit closely related, terms—such as albitized granite, K-feldspar-altered granite, disseminated granite-hosted, metamorphosed granite, autometasomatic granite, and greisen types (Du, 1983)—as well as alkaline granite, monzogranite, and medium-to-fine-grained monzonite types.

Granite-hosted rubidium deposits represent the most economically valuable rubidium resource (Xie et al., 2023). As a vital resource base for national strategic minerals and critical metals, granite-hosted rubidium deposits in the Qinghai-Tibet Plateau are predominantly located within Mesozoic folded orogenic belts and associated with large-scale faulting; alteration processes—specifically albitization, greisenization, and amazonitization—are closely linked to mineralization. Numerous granite-hosted and pegmatite-hosted rubidium (or rubidium-polymetallic) deposits with large- to super-large-scale resource potential have been identified in the Qinghai-Tibet Plateau (Xie et al., 2023).

In Hunan, granite-hosted mineralization involving lithium, rubidium, niobium, tantalum, and other rare metals is concentrated in the Early Yanshanian (Jurassic) and Late Yanshanian (Late Cretaceous) periods; for instance, the monazite U-Pb age of the Zhengchong Li-Rb-Cs deposit in Hunan is 148–150 Ma (Wen et al., 2024), while the mineralization age of the Shihuiyao granite-hosted Rb-polymetallic deposit in Inner Mongolia is 144.7 Ma (determined via $^{40}Ar/^{39}Ar$ geochronology; Sun, 2013).

Granite-hosted rubidium mineralization occurs in association not only with other rare and non-ferrous metals but sometimes with non-metallic mineral resources as well. For

instance, the recently discovered super-large rubidium deposit in Tongcheng, Hubei Province, is hosted within greisenized granite used for ceramics; this deposit is situated in the greisenized granite along the northeastern margin of the Mufushan granite batholith (Xue et al., 2020).

The primary rubidium-bearing minerals at the Dayangtian rubidium deposit in Tengchong, Yunnan Province, are K-feldspar, albite, and mica (Du et al., 2025). The ore-forming materials originated from acidic magma enriched in rare and non-ferrous metals; post-magmatic fluids, formed as the magma ascended along fault structures, facilitated the further enrichment of rubidium. The sedimentary wall rocks—comprising the Gaoligongshan Group and Carboniferous clastic rocks—served as an effective cap rock, successfully retaining the rubidium-bearing fluids and ultimately leading to the formation of the granite-hosted rubidium deposit.

The Shihuiyao Rb-Nb-Ta deposit in Xilinhot, Inner Mongolia, is a large rare-metal polymetallic deposit associated with alkaline granite. The principal niobium and tantalum minerals in the ore include manganocolumbite, columbite-tantalite, manganocolumbite-tantalite, manganotantalite-cassiterite, and microlite (Duan et al., 2016). This deposit resulted from the combined effects of early-stage magmatic crystallization and late-stage hydrothermal metasomatism, with the latter representing the primary mineralization stage for niobium, tantalum, and rubidium. Mineralization is closely linked to albitization and greisenization; the ore bodies are hosted within altered granite and are strictly controlled by northeast-trending structures. Albitized and greisenized granites serve as direct indicators for prospecting these rare metals.

Granite-hosted rubidium polymetallic mineralization rarely occurs in isolation; it is frequently associated with other rare metals, rare earth elements, base metals, ferrous metals, and even non-metallic minerals. Such mineralization often exhibits distinct zoning patterns. A prime example is the Liangyuan Nb-Ta-Rb-W polymetallic deposit, situated at the intersection of the east-west trending Nanling tectonic-magmatic belt and the northeast-trending Wuyishan tectonic belt. This deposit represents one of the most significant breakthroughs in recent years regarding the exploration and assessment of quartz-vein type tungsten deposits, greisen-type Nb-Ta-Rb-W deposits, and granite-hosted Nb-Ta-Rb polymetallic deposits in northern Guangdong Province (Fan et al., 2022). Four new Nb-Ta-Rb-W ore bodies have been discovered, with resources comprising 3,425.72 tonnes of Nb_2O_5 (average grade 0.0108%), 1,428.99 tonnes of Ta_2O_5 (average grade 0.00449%), 8,205.14 tonnes of WO_3 (average grade 0.25%), and 61,398.73 tonnes of associated Rb_2O (average grade 0.0987%). The Liangyuan deposit features quartz-vein type tungsten polymetallic ore bodies and greisen-type Nb-Ta-Rb-W ore bodies in its shallower sections, while granite-hosted Nb-Ta-Rb ore bodies occur at greater depths. Zircon SHRIMP U-Pb dating indicates that the formation age of the greisen ranges from 163.6 to 159.2 Ma, while the weighted mean $^{206}Pb/^{238}U$ age of zircons from the biotite granite is 163.0 ± 1.6 Ma. Muscovite ^{40}Ar-^{39}Ar isochron dating yields mineralization ages of 166.4 ± 1.1 Ma for the greisen-type ore bodies and 168.7 ± 1.2 Ma for the muscovite granite-hosted ore bodies. The Liangyuan Nb-Ta-Rb-W deposit formed during the Middle to Late Jurassic; it is a product of the onset of large-scale Mesozoic granitic magmatism and associated Nb-Ta-Rb polymetallic mineralization in eastern South China, as well as a product of extreme granitic magma fractionation. The timing of rock formation and mineralization is essentially

synchronous. The deposit features quartz vein-type tungsten ore and greisen-type W-Sn-Nb-Ta-Rb mineralization in the shallow zones; greisen-type W-Nb-Ta-Rb ore bodies at the contact zone of the intrusion; and highly fractionated granite-hosted Nb-Ta-Rb ore bodies at depth.

Li et al. (2024) investigated the Xianglushan Rb deposit in Guangxi using techniques such as chemical analysis, optical microscopy, TIMA, and LA-ICP-MS. They identified muscovite, K-feldspar, and plagioclase as the Rb-bearing minerals in the ore, with Rb content decreasing in the order of muscovite > K-feldspar > plagioclase. Although K-feldspar is the primary host mineral for Rb, the distribution of Rb within it is heterogeneous. In both monzogranite and medium-to-fine-grained monzonite, K-feldspar accounts for over 80% of the total Rb, indicating that the Xianglushan Rb deposit is a feldspar-hosted Rb resource.

As one of the world's largest hard-rock rare-metal deposits, the Jiajika rare-polymetallic ore field in western Sichuan is a site of significant importance in mainland China. The Jiajika ore field is composed of (Li-mineralized) fine-grained muscovite granite, coarse-grained/pegmatitic granite, and fine-grained granite pods or lenses, spatially superimposed or intersected by quartz pods or veins (Sha, 2026). Lithium is enriched in spodumene; rubidium is hosted in microcline and muscovite; niobium and tantalum are hosted in columbite-tantalite group minerals and muscovite; beryllium is enriched in beryl; and tin is primarily enriched in cassiterite. Sha (2026) classified the mineralization types in the Jiajika ore field into Li, Rb, Nb-Ta, Be, and Sn mineralization types. Based on correlation and cluster analyses, the elemental assemblages are categorized into three groups: Li, Rb, and Nb-Ta-Be-Sn. Rb-mineralized granites exhibit high total alkali content and are characterized by high Al, K, and Na; Nb-Ta-Be-mineralized granites belong to the calc-alkaline series and are characterized by low K and high Na; while Li-mineralized granites are enriched in Si and depleted in Na and K. Rb-mineralized granites show a positive K anomaly and a distinct negative Nb anomaly. In contrast, Nb-Ta-Be-mineralized granites exhibit a negative K anomaly. Li-mineralized granites share significant similarities with Nb-Ta-Be-mineralized granites, with the primary difference being the relative depletion of K in the Li-mineralized granites. Rubidium-mineralized granites exhibit notably low rare-earth element (REE) contents and lack significant negative Eu anomalies; compared to other rock types, their REE distribution patterns show the shallowest slopes and the lowest degrees of fractionation. The distinction between Nb-Ta-Be-mineralized granites and Li-mineralized granites lies in the fact that the latter possess higher total REE contents; relative to the Jiajika granite body and Rb-mineralized granites, both types exhibit relatively low heavy REE contents and pronounced negative Eu anomalies.

Yuan (2026) classified the igneous rocks in the Jiajika mining area into seven types: (muscovite) microcline pegmatite, muscovite granite pegmatite, muscovite-albite-spodumene pegmatite, fine-grained (inequigranular) muscovite-spodumene granite, fine-grained (inequigranular) muscovite granite with industrial-grade Be mineralization, fine-grained (inequigranular) muscovite granite with industrial-grade Nb-Ta mineralization, and fine-grained (inequigranular) muscovite granite. It was noted that lepidolite is virtually absent from the granitic dikes in the Jiajika area and that rock-type zoning is indistinct. The granitic rocks of the Jiajika area belong to the calc-alkaline series. Li-mineralized granitic dikes are characterized by low Na contents; Be- or Nb-Ta-mineralized dikes by high Na;

and Rb-mineralized dikes by high K and moderate Na. The K/Rb ratio decreases as the degree of mineralization increases. Rare-metal mineralization in the Jiajika area primarily involves Li, Be, Rb, Nb, and Ta. The Jiajika deposit is a granite-dike-hosted rare-metal deposit associated with a Triassic granite dome.

The Shihuiyao Rb-polymetallic deposit in Inner Mongolia, discovered in 2010, is a super-large rare-metal deposit where rubidium is the primary commodity. Muscovite ^{40}Ar-^{39}Ar dating yielded a weighted mean age of 144.7 ± 1.1 Ma and an isochron age of 143.3 ± 1.4 Ma for muscovite from greisenized granite; for flaky muscovite from pegmatite dikes, the weighted mean age was 146.4 ± 1.0 Ma and the isochron age was 143.9 ± 1.5 Ma (Sun et al., 2015). The deposit formed during the Late Yanshanian period. The mining area is characterized by intense folding, well-developed faulting, and frequent, widespread magmatic activity. Large-scale amazonite-bearing granite, greisenized granite, and some granitic pegmatites are distributed within the area, with albite alteration developed in the rocks.

In Nading Village, Cona County, Shannan Prefecture, Tibet, metamorphic and intrusive rocks are well-developed; mineral resources consist primarily of rubidium, beryllium, and lithium, with aquamarine as a secondary commodity. Rare-metal mineralization occurs within muscovite-albite rock and monzogranite (or monzogranitic pegmatite) bodies. Rubidium mineralization is ubiquitous across all granitic rock types in the area; the estimated rubidium metal resource (categories 3341) is 120.4634 million tonnes, classifying it as a super-large deposit (Wang, 2009).

Wang et al. (2025) predicted that potential resources of 780,000 tonnes of lithium and 260,000 tonnes of rubidium could be discovered within the greyish-white, fine-grained monzogranite of the Yangshan area in Gejiu, Yunnan Province.

3.1.5 Pegmatite type

In a broad sense, pegmatite-type rubidium mineralization encompasses granitic pegmatites.

The East Qinling region is a significant area for the distribution of granitic pegmatites and the metallogenesis of rare metals in China; it features a wide variety of granitic pegmatite dikes, forming four distinct zones of concentrated dike swarms. Research by Xu et al. (2016) on the Ziyugou granitic pegmatite-hosted rubidium deposit in Danfeng, Shaanxi, indicates that the Variscan-age, rubidium-bearing granitic pegmatite dikes in the area are large in scale and laterally extensive, exhibiting uniform rubidium mineralization and high Rb_2O content. The Kuanping intrusive body serves as the parent rock for these dikes, with rubidium primarily hosted in microcline and muscovite.

The Tuanbaoshan rubidium deposit is located on the eastern shore of Qinghai Lake in Qinghai Province. Hosted within granitic pegmatite dikes cutting the Paleoproterozoic Huangyuan Group (Pt_1H), it is a large-scale feldspar-hosted rubidium deposit with associated rare metals such as niobium and tantalum (Liu et al., 2010). The deposit formed during the Caledonian period when highly evolved, volatile-rich pegmatitic magmatic-hydrothermal fluids—derived from a deep-seated magma chamber—intruded into ancient strata under the influence of NW-trending transpressional tectonic stress; slow

crystallization subsequently produced bead-like ore bodies. The pegmatite dikes in this deposit occur in large-scale clusters and belts.

The Changzheng-Yalakan granitic pegmatite-hosted rubidium deposit in Daofu County, Sichuan, is controlled by the interplay of magmatism, doming structures, and metamorphism. Late Indosinian to Yanshanian granitic pegmatites constitute the primary ore-bearing bodies, with an average Rb_2O content of 0.13% and a maximum of 0.64% (Qin et al., 2024). The Eastern Tibet region, a key component of the Sanjiang tectonic belt, is a major metallogenic zone for non-ferrous metals (Cu, Pb, Zn) and rare metals (Y, Nb, Ta, Os, Ir, Pt, W, Sn) (Yu et al., 2019). Within this region, the Jianong-Gexiong Nb-Ta-Rb rare-metal enrichment zone is a favorable area for prospecting for pegmatite-type Nb-Ta deposits, high-temperature hydrothermal Rb deposits, and medium-to-low-temperature hydrothermal Pb-Zn deposits.

3.1.6 Alkaline igneous rock type

Alkaline igneous magmas exert a unique control on the mineralization of rare-earth, rare, precious, and non-ferrous metals (including rubidium). Through large-scale tectono-lithofacies mapping of the Dongchuan Fe-Cu-Au ore cluster (a Proterozoic continental rift basin) and the Gejiu Sn-Cu-W-Cs-Rb polymetallic ore cluster (a Triassic back-arc rift basin), Fang et al. (2024) analyzed the volcanic-intrusive sequences, rock assemblages, rift basin evolution, and magmatic-superimposed intrusive structural systems associated with alkaline magmatism. Their study revealed the intrinsic relationships between these features and the superimposed mineralization of Eastern Yunnan-style iron oxide-copper-gold (IOCG) deposits, Cu-Co-rutile-REE deposits, and Sn-Cu-W-Cs-Rb polymetallic deposits. Key findings include: In the Dongchuan Fe-Cu-Au ore cluster, Neoarchean alkaline rocks are dominated by calcitite-albite rocks (2,520 ± 14 Ma) and alkaline ferriferous picrites (2,529 ± 77 Ma). A distinct geological unit (mapped independently as 2.50–1.80 Ga) was formed through the structural overprinting of Mesoproterozoic volcanic-magmatic activity onto the paleokarst weathered crust at the top of the Neoarchean-Paleoproterozoic Xiaoliukou Formation (>2.50 Ga); these units represent new target horizons for Cu-Co-rutile-REE exploration. Rock assemblages—including ferro-sodic alkaline basic rocks, ferro-potassic trachytes, and ferriferous alkaline diabase-gabbros within Member 1 of the Mesoproterozoic Yinmin Formation—formed during the volcanic fault-depression basin-forming stage of the Yinmin period. Members 2 and 3 of the Yinmin Formation serve as the host horizons for Xikuangshan-style Fe-Cu deposits, while the ferro-potassic trachyte in the footwall of the Fe-Cu ore layer acts as the host horizon for monazite-type REE mineralization. During the Grenville orogeny, alkaline mafic intrusive rocks—including alkaline Fe-Ti gabbro (1,097–1,047 Ma), alkaline Fe-Ti diorite, and alkaline monzonite porphyry—gave rise to the Baixila deep-seated IOCG deposit and rutile mineralization. Within the Triassic back-arc rift basin of Gejiu, initial enrichment of Sn, Cu, Zn, Li, Rb, and Cs occurred in Triassic alkaline picrites and tephrites; subsequent Late Cretaceous leucogranite-related superimposed mineralization formed phlogopite-skarn type Sn-Cu-W-Cs-Rb deposits. The superposition of later ore-metal-rich alkaline intrusions onto the initially metal-enriched early alkaline rocks within the rift basin likely constitutes the mechanism behind this extraordinary metal enrichment. In the Dongchuan area, within the structural setting of superimposed magmatic intrusions, magmatic-hydrothermal breccia

pipes played a significant role in controlling the superimposed enrichment and mineralization of Cu, Co, rutile, and rare earth elements. In the Gejiu area, the intrusion of leucogranites into alkaline picrites and tephrites exerted significant control over the superimposed enrichment and mineralization of phlogopite-skarn type Sn-Cu-W-Co-Cs-Rb deposits.

The Shimen rubidium deposit in Songxian County, Henan Province, is hosted within an Indosinian alkaline syenite body, which is composed primarily of K-feldspar (Li et al., 2015). Indosinian magmatism provided an abundant source of material for the formation of rare-metal and rare-earth element deposits—including rubidium—in the region; subsequent tectono-magmatic hydrothermal activity led to the partial mobilization and enrichment of rubidium within the intrusive body, resulting in the formation of the Shimen rubidium deposit.

3.1.7 Volcanic rock type

The Abuda'ertai rubidium and rare metal deposit is a newly discovered volcanic-hosted rare polymetallic deposit in Siziwang Banner, Inner Mongolia. The ore bodies are primarily hosted within the continental acidic volcanic rocks of the Upper Jurassic Baiyingaolao Formation (Liang et al., 2025), and their spatial distribution coincides with that of the rhyolitic porphyry of the same formation. Rubidium content is closely correlated with the intensity of albitization and kaolinization in the host rocks, with rubidium mineralization occurring throughout the rhyolitic porphyry. This area is one of the few rubidium exploration bases in Inner Mongolia with promising prospecting potential. Based on an analysis of the regional and local geological settings, deposit characteristics, ore fabric, and major, trace, and rare-earth element compositions, it is inferred that the formation of the deposit is closely linked to the volcanic rocks.

3.2 Endogenic-exogenic superimposed rubidium deposit

3.2.1 Quaternary hot-spring type

Quaternary hot-spring-type rubidium-cesium mineralization is commonly found along the Yarlung Zangbo Suture Zone on the Tibetan Plateau and in surrounding regions, such as southern Tibet and parts of Sichuan and Yunnan.

Active hot springs in the Tengchong area of Yunnan generally contain rare metals (e.g., Li, Be, Rb, and Cs) and trace elements (e.g., W, Sb, Tl, and Mo), with the enrichment of Li, Rb, Cs, and W being particularly notable. The average concentrations of Li, Rb, Cs, and W in the hot springs are 2,895.1 μg/L, 839.8 μg/L, 417.9 μg/L, and 61.74 μg/L, respectively (Guo, 2019). Rare metal concentrations increase correspondingly with higher spring water temperatures. Helium isotope data indicate a supply of mantle-derived material to the hot springs, and rare metal concentrations rise significantly as the proportion of mantle-derived components increases.

3.2.2 Brine-type

Similar to and often co-occurring with brine-type cesium deposits, brine-type rubidium deposits fall into three categories: surface water subtypes (such as various salt lakes and landlocked seas), underground brine subtypes, and oil/gas field subtypes (Table 1). They are primarily found in the Qinghai-Tibet Plateau and surrounding regions, including Sichuan, Yunnan, and Xinjiang.

Zhao (1987) utilized a natural ion exchanger from a specific location in China to directly adsorb K+, Rb+, and Cs+ from gas field water, while using local natural brine as the desorbent. The process is characterized by the use of natural ion exchangers as adsorbents and high-concentration natural brines as desorbents. It ingeniously combines barium removal from mirabilite with sulfate removal using barium chloride; this approach reduces potassium chloride production costs, prevents barium contamination of the table salt product, enhances the adsorption capacity of the natural ion exchanger, and inhibits calcium sulfate scaling in evaporation tanks. The process employs cold adsorption and hot washing, a single-stage adsorption and washing cycle, and cooling crystallization. Experimental results showed a barium removal rate of 99.81%, a total recovery rate of 77.15%, an 86.48% adsorption rate of K^+ by the natural ion exchanger, and a total potassium recovery rate of 72.10%. The barium sulfate met national Grade II standards, the potassium chloride met national Grade I standards, and the table salt met the Grade I standard for well salt; additionally, a byproduct solution containing 0.95 g/L of Rb and 3.4 g/L of Cs was obtained for the subsequent extraction of rubidium and cesium metals. Production costs were approximately 400 RMB per tonne for potassium chloride, 400 RMB per tonne for barium sulfate, and 80 RMB per tonne for table salt.

3.2.3 Coal type

An increasing number of studies indicate that numerous coal mines in mainland China contain various rare metals, including gallium, germanium, and cesium (Yin, 2026c, 2026d, and 2026e).

Currently, the primary raw materials for the industrial production of rubidium and cesium are solid ores such as pollucite and lepidolite; however, the extraction processes involved are complex and costly. China possesses vast coal reserves, amounting to trillions of tonnes. Because coal seams formed in unique geochemical environments, certain valuable trace elements became enriched within them. The concentrations of rubidium and cesium in some Chinese coal mines are remarkably high—six and twelve times the global average for coal mines, respectively. Clearly, rare metals like rubidium and cesium associated with coal deposits represent a potential resource that could serve as a source for these elements. Consequently, extracting rare metals such as rubidium and cesium from coal mines is of great significance for the comprehensive utilization of coal resources and the sustainable development of the coal industry.

In 2017, Sun et al. filed a patent for a method and process to separate and extract rubidium and cesium from coal. Once this technology is implemented on a large scale, it holds the potential to extract rare metals like rubidium from numerous coal mines, thereby transforming the global supply-demand landscape for rubidium resources.

3.3 Exogenic rubidium deposit

3.3.1 Weathered granite crust type and placer type

Such secondary rubidium deposits occur at the tops of and in the areas surrounding endogenous rubidium deposits, such as the aforementioned granite-hosted types. The near-surface and surrounding areas of the Dayangtian rubidium deposit in Tengchong, Yunnan, host weathered-crust and placer-type rubidium deposits (Du et al., 2025), where the primary rubidium-bearing minerals include K-feldspar, albite, and mica.

4. Ore control

4.1 Hard-rock type

Traditional ore-controlling factors for endogenic metal deposits—such as tectonics and magmatism—remain fundamental to the mineralization of rare metals, including rubidium (Yin et al., 2025). For instance, the northern margin of the Qaidam Basin in Qinghai—situated at the junction of the Paleo-Asian and Tethyan tectonic domains and characterized by a polycyclic arc-basin orogenic system—possesses favorable geological conditions for rare metal and rare earth element (REE) mineralization. Significant progress in critical metal exploration has been made in the region in recent years, leading to the discovery of numerous pegmatite-hosted Li-Be-Rb polymetallic deposits and occurrences; representative examples include the Shinaihai Nb-Ta-Rb deposit, the Amunege Rb-Nb-Ta deposit, and the Xiaridawu Nb-Ta-Rb deposit. The northern margin of the Qaidam Basin has emerged as a new, important metallogenic belt for rare metals and REEs in the northern Tibetan Plateau, demonstrating promising exploration potential for deposits associated with pegmatites and alkali-feldspar granites—specifically those containing Li, Be, Nb, Ta, Rb, La, and Ce (Kong et al., 2021). Given that the role of tectono-magmatic activity in controlling metal mineralization has been extensively discussed in existing literature (Yin et al., 2025), this paper will not reiterate those points. Instead, the discussion regarding the ore-controlling factors for rare metal mineralization (including rubidium) will focus on the specific conditions outlined below.

4.1.1 Magmatic fractional crystallization and hydrothermal metasomatism

Magmatic fractional crystallization and hydrothermal metasomatism are key factors controlling rubidium mineralization in granite, pegmatite, and skarn deposits.

Through major and trace element analyses of muscovite, K-feldspar, and plagioclase from Rb-bearing monzogranite, leucogranite, and greisen in the Xianglushan Rb mining area (northeastern Guangxi), Li et al. (2025) found that Rb concentrations in muscovite (3,826–9,100 ppm) were significantly higher than those in K-feldspar (2,423–2,770 ppm) and plagioclase (0.61–57.80 ppm); furthermore, Rb contents in all three minerals showed a positive correlation with the concentrations of volatile elements such as Li, B, and F. Rubidium primarily enters the crystal lattices of minerals like muscovite by substituting for K and Na ions via isomorphous replacement. Among the various types of Rb-bearing rocks,

greisen exhibited the highest Rb_2O content (averaging 0.1932%). Comprehensive research indicates that magmatic-hydrothermal metasomatism involving volatiles such as F is the dominant mechanism governing the partitioning and enrichment of rubidium in highly fractionated granitic rocks. The Xianglushan Rb deposit is the product of the combined effects of magmatic fractional crystallization and hydrothermal metasomatism.

4.1.2 Degree of magmatic differentiation

Hard-rock rubidium deposits in mainland China—particularly endogenic ones—are invariably closely associated with tectono-magmatic activity. Regarding the control of magmatism over endogenic rubidium mineralization, numerous scholars studying such deposits across various regions of mainland China have consistently identified highly fractionated granite bodies as a common characteristic associated with rubidium and related metal mineralization.

Wu et al. posit that the rare-metal mineralization associated with Yanshanian granites in the Nanling region is linked to the extensive fractional crystallization of granitic magmas (Wen et al., 2024). This crystallization differentiation manifests as the continuous, long-term segregation of crystal mushes and residual melts within the magma chamber. Coarse-grained porphyritic granites represent the cumulates (main body) formed during the early stages of crystallization, whereas fine-grained granites represent the residual, high-silica melts (complementary bodies). Whole-rock Zr/Hf and Nb/Ta ratios serve as indicators of the degree of granitic fractional crystallization. As the degree of magmatic fractionation increases, both whole-rock Zr/Hf and Nb/Ta ratios decrease significantly; notably, when the Nb/Ta ratio drops below 5, intense interaction occurs between the magma and fluids, marking a critical indicator of the granite's mineralization potential (Wen et al., 2024).

A study by Ban et al. (2025) on the Changchengling super-large Rb-Nb-Ta rare-polymetallic deposit in the central Nanling metallogenic belt reveals that the granite porphyry bodies in the area are characterized by high fractionation and whole-rock rubidium mineralization. Among them, the NW-trending Fengchui-Luodai concealed intrusion exhibits the highest Rb content (1,090–1,900 μg/g; average 1,410 μg/g), with mica serving as the primary Rb-enriched mineral. The distribution of the granite porphyry-type rubidium mineralization is controlled by the intersections of fault structures and zones where secondary structures are well-developed. The altered granite porphyry at the top of the concealed intrusive body is a favorable site for the occurrence of rubidium-rich ore bodies. The granite porphyry associated with rubidium-bearing rare-metal polymetallic mineralization formed during the Late Indosinian period. Sericitization at the top of the intrusion and secondary muscovitization at the contact zone between the intrusion and the country rock play a significant role in the enrichment of rubidium and other rare metals. The Changchengling deposit is hosted by granite porphyry, which serves as the parent rock for mineralization. To date, seven rubidium ore bodies have been delineated, trending northeast (NE), northwest (NW), and nearly north-south (SN).

Based on petrographic, whole-rock geochemical, and Nd-isotopic studies of the amazonite granite at Jiangjunshan in the Altay region of Xinjiang, Chen et al. (2024) determined that the amazonite granite is characterized by high SiO_2 (74.55%–77.93%), high K_2O (3.68%–4.37%), and high Al_2O_3 (A/CNK = 1.06–1.41), classifying it as a high-K calc-alkaline

peraluminous granite. The granite is enriched in Rb, Th, Ta, and Hf but strongly depleted in Ba and Sr; it exhibits a "seagull-shaped" rare earth element (REE) pattern, a strong negative Eu anomaly ($\delta Eu < 0.01$), and a tetrad effect ($TE_{1,3} = 0.92–1.21$). The amazonite granite displays extremely low whole-rock K/Rb (63–87), Nb/Ta (2.04–3.45), and Zr/Hf (8.43–9.96) ratios and contains fluorite and magmatic schorl. Geochemical and mineralogical characteristics indicate that the Jiangjunshan pluton underwent intense fractional crystallization and associated magmatic-hydrothermal processes. The amazonite granite formed during the Middle Permian and is cogenetic with the dominant two-mica alkali-feldspar granite. The high Rb content and A2-type granite affinity of the two-mica alkali-feldspar granite suggest it originated from the partial melting of biotite-rich igneous rocks. The petrogenesis and evolution of the Jiangjunshan amazonite granite indicate a high degree of evolution and significant fluid interaction, which played a crucial role in the enrichment of Rb within the granite. As a former accretionary wedge, the Altai region underwent continuous modification that effectively promoted the differentiation of newly formed crust and the creation of localized Rb-enriched source rocks, thereby providing the material basis for the formation of amazonite granite.

In summarizing the exploration models and targets for granite-hosted rare metal deposits (such as rubidium) in Hunan Province, Wen et al. (2024) concluded that the variations in Li, Rb, Nb, and Ta mineralization within the region are linked to the degree of high-level magmatic differentiation. Distinct stages of this differentiation process sequentially gave rise to Rb mineralization associated primarily with muscovite granite, Nb-Ta mineralization associated with muscovite (lepidolite) granite, and Li mineralization associated primarily with greisen (Jianfengling type). During the late stages of magmatic differentiation, Li-rich granites intruded into earlier granite bodies to form greisen-hosted Li-Rb deposits (Zhengchong type) or metasomatized the earlier granites to form altered granite-hosted Li deposits (Huishan type); meanwhile, post-magmatic hydrothermal fluids formed greisen-fluorite vein-type Li deposits (Jiepailing type) within structural fractures at the tops of the granite bodies. Five distinct types of rare metal deposits have been identified in Hunan Province: greisen (porphyry)-type Li-Rb-Cs deposits, muscovite (lepidolite) granite-hosted Li-Nb-Ta deposits, muscovite (two-mica) granite-hosted Rb deposits, altered greisen-type Li deposits, and greisen-fluorite vein-type Li deposits. The mineralization ages for these deposits cluster in two periods—the Jurassic (148–160 Ma) and the Late Cretaceous (86–89 Ma)—with the ore-forming materials derived primarily from magmas. The Zr/Hf and Nb/Ta ratios of the rocks serve as indicators of the rare metal mineralization potential of composite granite bodies.

4.1.3 Intensity of magma melt-fluid interaction and crustal contamination

Wu et al. propose that highly fractionated granites have generally undergone significant crustal contamination. Intense contamination by Al-rich crustal material can render the granite increasingly peraluminous; furthermore, such crustal material supplies abundant hydrous minerals, facilitating extensive magmatic evolution and enriching the magma in rare-metal ore-forming components. These characteristics likely serve as critical controls on the mineralization potential of highly fractionated granites. Taking Hunan Province as an example, highly fractionated granites exhibiting weak melt-fluid interaction show only moderate mineralization potential (Wen et al., 2024), whereas those with strong melt-fluid

interaction demonstrate high potential. Variations in Li, Rb, Nb, and Ta mineralization across Hunan are linked to the degree of magmatic fractionation; distinct stages of this evolution sequentially give rise to Rb mineralization (dominated by two-mica granite), Nb-Ta mineralization (dominated by muscovite granite), and Li mineralization (dominated by lepidolite granite and greisen), exemplified by the Jianfengling-type Li-Rb-Nb-Ta deposit (Wen et al., 2024). During the late stages of magmatic fractionation, Li-rich granites intruding into earlier granite bodies form greisen-type Li-Rb deposits (e.g., the Zhengchong-type Li-Rb-Cs deposit) or metasomatize the early granites to form altered-granite-type Li deposits (e.g., the Huishan-type Li deposit). Hydrothermal fluids from the final stages of magmatic evolution form greisen-fluorite vein-type Li deposits within structural fractures at the tops of granite bodies (e.g., the Jiepailing-type fluorite-Li deposit) or greisen-quartz vein-type W-Sn-Li deposits. Greisen (or greisen-porphyry) serves as a prospecting indicator for Li-Rb deposits, while granite Zr/Hf and Nb/Ta ratios act as petro-chemical markers for identifying rare-metal mineralization.

4.1.4 Oxygen fugacity and remelting of crust-derived materials

Highly fractionated granites are widely distributed across the Tibetan Plateau. A study by Xie et al. (2025) on the newly discovered super-large Gari'atong rubidium deposit in the central Lhasa terrane reveals that Rb mineralization primarily occurs within monzogranite and its host rocks; zircon U-Pb dating yields a weighted mean age of 20.0 ± 0.5 Ma (n=14, MSWD=1.8) for the ore-bearing monzogranite, indicating it is a product of Miocene magmatic emplacement. Rubidium occurs mainly via isomorphous substitution within muscovite and biotite. Geochemical characteristics of these micas indicate that the ore-forming magma originated from the remelting of crustal materials under low oxygen fugacity conditions; subsequent intense fractional crystallization generated a fluorine-rich magmatic-hydrothermal fluid, ultimately forming the large-scale rubidium deposit.

4.1.5 Alteration intensity

A study by Liang et al. (2025) on the Abudaertai Rb-bearing rare polymetallic volcanic-hosted deposit in Inner Mongolia revealed that the distribution of ore bodies coincides with that of the rhyolite porphyry of the Baiyingaolao Formation, and that rubidium content is closely correlated with the intensity of albitization and kaolinization in the host rocks.

The Chaharihada Rb rare-metal deposit in Inner Mongolia is hosted within a Late Triassic syenogranite body located at the northern end of a Hercynian-Indosinian composite batholith. Wang et al. (2020) proposed that mineralization is associated with hydrothermal alteration driven by highly evolved late-stage magmatic activity. The deposit exhibits intense metasomatic alteration and distinct zonation, progressing from a microclinization zone to an albitization zone and finally to a greisenization zone. The albitization zone and its transition zone with the greisenization zone constitute the primary zones of enrichment and mineralization for rubidium and other rare elements. Comparative analysis indicates that the Chaharihada Rb deposit bears strong similarities to the Duobaoshan Rb, Liujiahe Rb, and Qiyishan Rb-W-Sn deposits in terms of geotectonic setting, magmatic characteristics, host rocks, and ore assemblages; all belong to the category of magmatic-hydrothermal metasomatic alkaline to sub-alkaline granite-hosted deposits, characterized

by a favorable geological setting for mineralization and immense potential for rare-metal mineralization.

4.1.6 Fluxing elements and incompatible elements

According to Liu (2023), highly fractionated granites facilitate the formation of rare-metal deposits because they are enriched in incompatible elements (such as Li, Rb, Cs, Nb, and Ta) and fluxing elements (such as F, B, Cl, Li, P, and Na). Consequently, highly fractionated granites and pegmatites possess unique petrogenesis and significant economic potential.

The Beishan region, situated on the southern margin of the Central Asian Orogenic Belt, has undergone complex processes—including arc-continent accretion/collision and continental growth—along with multiple episodes of magmatism that resulted in the formation of Cu, Ni, and rare-metal deposits. Research by Zhang (2019) indicates a weighted mean LA-ICP-MS zircon U-Pb age of 427 ± 8 Ma for the amazonite-bearing granite. The evolutionary sequence of the granitic rocks in the study area progresses from biotite monzogranite to amazonite-bearing granite and finally to amazonite-bearing granitic pegmatite. Overall, SiO_2 content decreases along this sequence, while Al_2O_3 and (Na_2O + K_2O) contents increase; CaO content initially decreases and then increases; and MgO, TiO_2, Fe_2O_3, and P_2O_5 contents remain generally low. The rocks are Na-rich and K-poor, classifying them as peraluminous, high-K calc-alkaline granites. Overall, Sr and Ba contents are low but show wide variation, whereas Rb, Cs, and Pb contents are high; Rb, Nb, and Ta contents increase along the evolutionary trend; and the Nb/U, Y/Nb, and Rb/Sr ratios exhibit significant variation. Primitive mantle-normalized trace element spider diagrams reveal depletion in Ba, Sr, Nb, La, Ce, and Eu, and slight depletion in Y; strong enrichment in Cs, Rb, and Pb; moderate enrichment in Zr, Hf, U, and Th; and slight enrichment in Ta. The granites exhibit relatively low ΣLREE contents and high ΣHREE contents. On chondrite-normalized rare earth element (REE) patterns, the rocks exhibit a transition from LREE depletion to enrichment and from HREE enrichment to depletion, with (La/Yb)N ratios ranging from 0.13 to 4.21; the rock mass displays a strong negative Eu anomaly. The granite is classified as highly fractionated A2-type (PA-type) granite derived from a muscovite-rich source rock. Partial melting of the source rock generated a magma rich in fluorine, rubidium, and fluids. Magmatic evolution involved the fractionation of LREE-rich minerals (such as allanite and monazite) as well as plagioclase and K-feldspar. The Rb-bearing granite-pegmatite complex formed in a tectonic setting characterized by a transition from compression to extension following the closure of the South Tianshan Ocean basin. Muscovite served as the primary source of both the ore-forming element (Rb) and the ore-forming fluids. Melting of the muscovite-rich source rock produced a magma enriched in fluorine, rubidium, and fluids. Rb migrated as F-complexes until the late stages of magmatic evolution, when the complexes hydrolyzed; F^- then reacted with Ca^{2+} to form fluorite or was incorporated into minerals such as mica, while Rb entered feldspar to form mineralized amazonite-bearing granite.

The rare-metal metallogenic belt in western Yunnan, located in the southeastern Tibetan Plateau, is primarily distributed along the Nujiang and Lancangjiang fault zones. Its genetic types include granitic (including greisen), pegmatitic, skarn, tourmaline (sulfide)-quartz vein, phlogopite hydrothermal vein, weathered granite crust, coal-measure, and hot-spring

types. Notably, the granite- and pegmatite-hosted rare-metal deposits contain gemstone resources such as tourmaline and aquamarine. These deposits formed during six distinct periods: the Triassic (240–220 Ma), Early Cretaceous (124–120 Ma), Late Cretaceous (80–70 Ma), Paleocene–Eocene (65–50 Ma), Oligocene (33–30 Ma), and Miocene (25–12 Ma). These periods are associated, respectively, with the post-collisional setting following the closure of the Triassic Paleo-Tethys Ocean, the subduction of the Neo-Tethys Ocean, and the India-Eurasia collision followed by large-scale strike-slip shearing (Li et al., 2025). The Li-Be-Rb-Cs deposits in the region formed mainly during the Late Cretaceous, Paleocene–Eocene, and Miocene, with the Oligocene and Miocene mineralization events being closely linked to shear-related deformation and metamorphism. The deposits are characterized by F-enrichment, B-enrichment, or both, and are closely related to highly evolved granites from various periods. Indicator minerals such as cassiterite, tourmaline, and mica serve to trace the rare-metal mineralization processes and reveal variations in metallogenic element assemblages. Currently, exploration for Li-Rb-Cs is concentrated primarily in the Nujiang metallogenic belt. The Tengchong-Lianghe region is characterized primarily by granite-type and weathered granite-crust-type deposits (in the broad sense), whereas the Gaoligong region is dominated by pegmatite-type and phlogopite-hydrothermal-vein-type deposits (in the broad sense). Beryllium exploration is concentrated in the Gaoligong and Tengchong-Lianghe regions.

4.2 Hot spring and brine types

Studies indicate that rubidium mineralization associated with hot springs and brines in mainland China is controlled by several factors.

Zhu et al. (2025) analyzed stable isotopes (δD and $\delta^{18}O$) and elemental compositions of hot spring waters at Bukadaban Peak—a source area for salt lakes in the Qaidam Basin—and found that the hydrochemical types are primarily Na-Cl, Ca-HCO_3, and mixed Ca-Na-HCO_3. Concentrations of Li, Rb, and Cs in the hot springs vary by two to three orders of magnitude between high and low values, with levels increasing from the mountain slopes to the foothills. Fumaroles (steam vents) located on the slopes exhibit low Li, Rb, and Cs concentrations (averaging 10.6 μg/L, 19.9 μg/L, and 11.0 μg/L, respectively)—levels comparable to those in local shallow groundwater and river water, with Rb/Cs ratios >1. In contrast, hot springs at the foothills—characterized by lateral-to-vertical discharge and subsequent pooling—show high concentrations of Li, Rb, and Cs (averaging 69.1 mg/L, 11.5 mg/L, and 18.8 mg/L, respectively). The Rb and Cs distribution patterns in these waters resemble those of Tibetan hot springs (Rb/Cs <1), although the absolute concentrations of Li and Rb are higher. Hydrogen and oxygen isotope compositions indicate that the hot springs originate from a mixture of magmatic water, meteoric precipitation, and shallow circulating groundwater, with mixing occurring during the ascent of the thermal fluids. The concentrations of Li, Rb, and Cs are governed by multiple processes, including water-rock interactions involving deep-seated magmatic fluids, weathering and leaching by high-temperature shallow groundwater, and evaporative concentration at the surface. Their enrichment reflects a prolonged evolution involving the upwelling of magmatic fluids (and associated water-rock interactions), silicate weathering and leaching by shallow thermal waters, and subsequent surface accumulation, evaporation, and concentration.

4.2.1 Hot spring temperature

The content of rare metals in spring water increases correspondingly with higher temperatures, a phenomenon likely linked to the high rate of concentration via high-temperature evaporation. It should be noted that the ore-controlling factors mentioned here require further scientific statistical data for validation.

4.2.2 Involvement of mantle-derived material and its quantity

Helium isotope studies indicate (Guo, 2019) that hot springs and brines supplied by mantle-derived material exhibit higher concentrations of rare metals such as rubidium, and that the content of these rare metals rises significantly as the proportion of mantle-derived components increases.

5. Discussion

A comparison of cesium and rubidium deposits in mainland China reveals a striking fact: the two share remarkable similarities across numerous aspects, including industrial and genetic types, geological settings, and mineralization mechanisms. Furthermore, these two distinct mineral resources frequently occur in association or coexistence—such as in coal deposits and Quaternary hot springs—and both exhibit endogenic, exogenic, and superimposed (combined endogenic-exogenic) mineralization types.

Much like cesium mineralization, rubidium deposits in mainland China are predominantly associated/paragenetic minerals; no purely independent rubidium deposits have yet been discovered. Although the genetic types of rubidium deposits in mainland China are diverse—indeed, virtually comprehensive—the ore quality is generally low. Moreover, potential liquid rubidium deposits are located in remote highland areas with poor infrastructure, such as transportation networks, posing significant challenges for large-scale extraction and utilization at present.

Regarding the mechanisms of ore formation and the sources of ore-forming materials, the genesis of rubidium deposits is inextricably linked to tectono-magmatic activity, with the active participation of mantle-derived materials playing a crucial role. Even deposits that appear superficially to be entirely exogenous in origin—such as coal-hosted rubidium deposits and liquid rubidium occurrences—actually rely heavily on the involvement of mantle-derived materials and the influence of tectono-magmatic processes.

Whether concerning the rubidium mineralization discussed here or other rare metal deposits (such as those of cesium), their ultimate formation is governed by specific controlling factors. These include magmatic crystallization differentiation and hydrothermal metasomatism, the degree of magmatic differentiation, the intensity of magma melt-fluid interaction, the extent of crustal material contamination, magmatic oxygen fugacity and the remelting of crustal materials, the intensity of alteration, the participation of fluxing and incompatible elements, and the influx and quantity of mantle-derived materials; in the specific case of liquid rubidium mineralization, hot spring temperatures are also a factor.

6. Conclusions

Rubidium mineralization in mainland China is diverse and varied, encompassing nearly all known genetic deposit types found in geological textbooks—such as pegmatite, various granite-hosted, magmatic-hydrothermal, quartz and mica-hydrothermal vein, skarn, volcanic, porphyry, alkaline igneous, and crypto-explosive breccia types. There are also coal-hosted, secondary weathered granite crust, and placer deposits, as well as non-hard-rock types like Quaternary hot springs and surface or subsurface brines.

It must be noted, however, that while these rubidium deposits are diverse, their grades are generally low. Furthermore, the vast majority are located on the Tibetan Plateau and its periphery—regions characterized by poor transportation and inadequate infrastructure—meaning their development faces significant challenges, including high investment costs, harsh natural conditions, and the inevitable disruption of pristine ecosystems.

As with many other rare metal mineralization systems, the formation of rubidium deposits in mainland China is inextricably linked to active tectono-magmatic processes and the input of mantle-derived ore-forming materials. In other words, orogenesis is a crucial prerequisite for the formation of numerous rare metal deposits, including those of rubidium; even liquid-phase deposits—such as brines and/or hot springs—rely on the underlying influence of concealed tectono-magmatic activity.

7. References

01. Ban MJ, Wang L and Mao JW et al. 2025. Geological characteristics, metallogenic regularity, and prospecting significance of the Changchengling rubidium polymetallic deposit in southern Hunan. *Geotectonics and Metallogeny*, (3).

02. Chen D, Luo P and Liu GY et al. 2010. Extraordinary enrichment of rare metals (Sn, Li, Rb, Cs) and magmatic evolution at Jinjiling, southern Hunan. *Geological Review (S1)*: 4. DOI: 10.16509/j.georeview.2025.s1.042.

03. Chen ZW, Yuan C and Lin ZF et al. 2024. Genesis and rubidium enrichment mechanism of amazonite granite at Jiangjunshan, Altay, Xinjiang. *Geotectonica et Metallogenia*, 48 (6): 1394-1415.

04. Chen XF, Fan Y and Zhou TF et al. 2022. A Study on the occurrence state and metallogenic mechanism of rubidium in the Xiwukou deposit, Ningguo, Anhui Province, in the Jiangnan uplift belt. *Earth Science Frontiers*, 29 (1):16. DOI: 10.13745/j.esf.sf.2021.8.4.

05. Cheng JL, Cui ZL and Li FG et al. 2026. Characteristics and prospecting significance of phlogopite-type rubidium deposit in the Diantan skarn belt, Tengchong. *The Chinese Journal of Nonferrous Metals*, 36 (2): 626-641.

06. Du B, Li FG and Bi XL et al. 2025. A brief analysis of the geological characteristics and genesis of the rubidium deposit at Dayangtian, Tengchong, Yunnan. *Yunnan Geology*, 44 (1): 92-95.

07. Du LT.1983. Geochemical characteristics and classification of alkali-metasomatic mineralization. *Geology of Ore Deposits*, (02): 35-43. DOI: CNKI:SUN:KCDZ.0.1983-02-004.

08. Duan XZ, Tan KX and Xie YS et al. 2016. Geological characteristics and genesis of the Shihuyao granite-type niobium-tantalum-rubidium deposit in Inner Mongolia. *Geology and Resources*, 25 (1): 9. DOI：10.3969/j.issn.1671-1947.2016.01.006.

09. Fan FP, Xiao HL and Chen LZ et al. 2022. Geology, petrogenetic and metallogenic ages, and metallogenic model of the Liangyuan Nb-Ta-Rb-W deposit, northern Guangdong. *Acta Petrologica Sinica*, (02): 038.

10. Fang WX, Guo YQ and Li TC. 2024. Volcanic-intrusive rock sequences and metal mineralization in rift basins of the eastern Yunnan region. *Acta Geologica Sinica*, 98 (6): 1776-1802.

11. Guo W. 2019. Characteristics and significance of rare-metal mineralization in the hot springs of Tengchong, Yunnan. *Acta Geologica Sinica*, 93 (6): 1321-1330.

12. Hou YL. 2023. Overview of geological research on rubidium deposits in my country and implications for prospecting. *Western Exploration Engineering*, 35 (2): 117-119. DOI: 10.3969/j.issn.1004-5716.2023.02.034.

13. Kong HL, Zhang JW and Jin MS et al. 2021. Progress in the exploration of pegmatite-type critical metal deposits (lithium, beryllium, etc.) in the Northern Margin of the Qaidam Basin, Qinghai. *Proceedings of the First National Mineral Exploration Conference*.

14. Li HY, Lei L and Chai MC et al. 2025. Hydrothermal metasomatism leads to the enrichment of the rare metal rubidium in highly fractionated granitic rocks. *Journal of Guilin University of Technology*, (6).

15. Li JB. 2020. Analysis of geological characteristics and application prospects of rubidium deposits in Dongkeng mining area, Jianning County, Fujian Province. *Nonferrous Metals Abstracts*, 35 (05): 34-38.

16. Li JL, Liu Q and Xu LB et al. 2015. A brief analysis of the geological characteristics and genesis of the Shimen rubidium deposit in Songxian County, Henan Province. *Mineral Resources and Geology*, 29 (2): 5. DOI: CNKI:SUN:KCYD.0.2015-02-012.

17. Li L, Xia Y and Zhou QM et al. 2024. Study on ore characteristics and rubidium occurrence modes of the Xianglushan rubidium deposit in the Yuechengling area, Guangxi. *Mineral Resources and Geology*, 38 (1): 98-105.

18. Li XF, Xu H and Zhu YT et al. 2025. Metallogenic regularities and prospecting directions for rare metal deposits in Western Yunnan. *Acta Petrologica Sinica*, (7).

19. Liang CF, Han B and Wu LW et al. 2025. Geological characteristics and genesis of rare polymetallic deposits such as rubidium in Abudartai, Siziwang Banner, Inner Mongolia. *Geology and Resources*, 34 (4): 410.

20. Liu HW, Lei AQ and Liu CC. 2010. Geological characteristics and genesis of the Tuanbaoshan feldspar-rubidium deposit in Qinghai Province. *Western Exploration Engineering*. DOI: CNKI: SUN:XBTK.0.2010-07-045.

21. Liu XH. 2023. *Mineralogy, Geochemistry, and Metallogenesis of the Zhengchong Rubidium-Polymetallic Deposit, Dao County, Hunan Province*. Doctoral dissertation, Central South University.

22. Qin YL, Xu YF and Zhan HY et al. 2024. Geological characteristics and prospecting direction of the Changzheng Yalakan granite-pegmatite type rubidium deposit in Daofu County, Sichuan. *Acta Geologica Sichuanica*, 44 (3): 422-427.

23. Sha XB. 2026. *Study on Mineralization Types and Element Association Characteristics of the Jiajika Rare-Metal Ore Field in Western Sichuan*. Doctoral dissertation, Chengdu University of Technology.

24. Shen ZJ, Xie LL and Lin ZY. 2003. Characteristics of major rare earth metal deposits in Hunan Province. *Hunan Geology*. DOI: CNKI:SUN:HNDZ.0.2003-01-006.

25. Sun Y. 2013. *Study on Typical Rubidium Deposits and Their Metallogenic Tectonic Settings in my country*. Doctoral dissertation, China University of Geosciences, Beijing.

26. Sun Y, Wang DH and Wang CH et al. 2019. Metallogenic regularities, new progress, and prospecting directions for rubidium deposits in my country. *Acta Geologica Sinica*. DOI: CNKI:SUN:DZXE.0.2019-06-005.

27. Sun Y, Wang RJ and Li JK et al. 2015. ^{40}Ar-^{39}Ar dating of muscovite and analysis of prospecting potential for the Shihuiyao Rb-polymetallic deposit, Xilinhot. *Geological Review*, 61 (2): 463-468.

28. Sun Y, Wang RJ and Qi F et al., 2013. Current status of global rubidium resources and suggestions for rubidium development and utilization in my country. *China Mining Magazine*, 22 (9): 4. DOI: 10.3969/j.issn.1004-4051.2013.09.003.

29. SunYZ, Zhao CL and Wang JX et al. 2017. A method and process for separating and extracting rubidium and cesium from coal. Document ID: 12940873 (in Chinese). https://www.xjishu.com/zhuanli/24/201710615317.html. Retrieved June 8, 2026.

30. Tang GQ and Wu CZ. 2024. Main genetic types and metallogenic potential of hard-rock rubidium deposits in Xinjiang. *Bulletin of Mineralogy, Petrology and Geochemistry*, 43 (1): 102-126. DOI: 10.3724/j.issn.1007-2802.20240007.

31. Wang J. 2009. Report on the General Survey (Interim) of Rare Metal Deposits in the Nading Mining Area, Cona County, Tibet Autonomous Region. The Sixth Geological Brigade, Bureau of Geology and Mineral Exploration and Development of Tibet Autonomous Region.

32. Wang YG, Li J and Tian Y et al.2020. Geological characteristics and genesis of the Chaharihada rubidium-rare metal deposit in the Yuanbaoshan Area, Beishan Region. *China Mining Magazine*, 29 (S01): 5. DOI: 10.12075/j.issn.1004-4051.2020.S1.085.

33. Wang YS，Guo J and Liu XF et al. 2024. Research on rubidium and cesium resources, extraction technologies, and development and utilization in China. *Acta Geoscientica Sinica*, 45 (5): 823-829. DOI: 10.3975/cagsb.2024.072401.

34. Wang YT, Du JG and Lei RX et al. 2024. Characteristics of ore-forming fluids and mineralization processes of cryptovolcanic breccia-type lithium-rubidium ore bodies in the Weilasto deposit, Inner Mongolia. *Earth Science-Journal of China University of Geosciences*, 49 (12): 4318-4318 DOI: 10.3799/dqkx.2024.054.

35. Wang ZY, Xiao SG and Sun CW et al. 2025. Geological characteristics and prospecting potential of a newly discovered granite-hosted lithium-rubidium deposit in Gejiu, Yunnan. *Advances in Geosciences*, 15 (1): 94-103. DOI: 10.12677/ag.2025.151011.

36. Wen CH, Chen JF and Sun J et al. 2024. Prospecting model and prospecting directions for granite-type lithium-rubidium-niobium-tantalum deposits in Hunan Province. *Land and Resources Guide*, (4): 1-16.

37. Wu CZ, Jia L and Lei RX et al. 2021. Main characteristics and research progress of amazonite granites and associated rubidium deposits in the Central Asian orogenic belt. DOI: 10.18654/1000-0569/2021.09.02.

38. Xiao SG, Chang GH and Wang ZY et al. 2024. The first granite-type lithium-rubidium deposit has been discovered in Gejiu, Yunnan. *Mineral Resources and Geology*, 38 (1): 205-206.

39. Xie JL, Lin B and Qi J et al. 2023. Research progress on granite-type rubidium deposits and prospecting directions for rubidium deposits in the Qinghai-Tibet Plateau. *Gold Science and Technology*, 31 (1): 26-36.

40. Xie JL, Tango JX and Lin B et al.2025. Zircon U-Pb age and occurrence of rubidium in the Gari'atong super-large granite-hosted rubidium deposit, Tibet. *Acta Geologica Sinica*, 99 (8): 2724-2738.

41. Xing P. 2020. *Fundamental Research on the Comprehensive Utilization of Granite-Type Rubidium Ore Resources*. Doctoral dissertation, University of Science and Technology Beijing.

42. Xu F, Song GS and Wang MZ et al. 2016. Geological characteristics and prospecting potential of the Ziyugou pegmatite-type rubidium deposit in Danfeng, Shaanxi Province. *Geology and Mineral Resources of South China*, 32 (1): 9. DOI: 10.3969/j.issn.1007-3701.2016.1.008.

43. Xue Z, Zhang WS and Gao F et al. 2020. Geological characteristics of mineralization and prospecting targets for greisenized granite (used for ceramics) and rubidium deposits in Maishi, Tongcheng County, Hubei Province. *Resources, Environment & Engineering*. DOI: 10.16536/j.cnki.issn.1671-1211.2020.S1.002.

44. Yang F. 2017. Geological characteristics and genesis of the Dongkeng rubidium deposit in Jianning, Fujian. 36 (8). DOI: CNKI:SUN:FJDZ.0.2017-03-007.

45. Yi M. 2025. Uranium, rubidium, gold: major breakthroughs achieved in strategic metal exploration. Hebei Geology, (3): 38.

46. Yin JZ. 2026c. Type and origin of the gallium deposits in Mainland China. *Naturalis Scientias*, 3: 662-675. DOI: https://doi.org/10.62252/NSS.2026.1037.

47. Yin JZ. 2026d. Geology and geochemistry of the germanium deposits in Mainland China. *Naturalis Scientias*, 3: 686-709. DOI: DOI: https://doi.org/10.62252/NSS.2026.1039.

48. Yin JZ. 2026e. Genetic types and geology of cesium deposits in Mainland China. *Naturalis Scientias*, 3: 739-762. DOI: https://doi.org/10.62252/NSS.2026.1041.

49. Yin JZ, Li KN and Shi HY et al. 2025. Mathematical, physical, and chemical interpretations of structural control and contributions to gold mineralization. Preprints ID: 202501.1183. DOI: 10.20944/preprints202501.1183.v1.

50. Yu JS, Li Q and Zhou X et al. 2019. Geological characteristics and prospecting potential of the Jianong niobium-tantalum-rubidium deposit in Basu County, Eastern Tibet. *World Nonferrous Metals.*

51. Yuan TJ. 2026. *Study on the Geological and Geochemical Characteristics and Ore-Bearing Potential of Granites in the Jiajika Mining Area, Sichuan*. Doctoral dissertation, Chengdu University of Technology.

52. Zhang D. 2019. *A Preliminary Study on the Geochemical Characteristics and Mineralization of Rubidium-bearing Granites and Pegmatites in the Xingxingxia Area, Beishan*. Doctoral dissertation, Lanzhou University.

53. Zhao W. 1987. Pilot-scale study on the extraction of potassium, barium, rubidium, and cesium from gas field water in a certain area. *Collected Papers of the Chinese Academy of Geological Sciences (15)*.

54. Zhu ZY, Kong FC and Wang JP et al. 2025. Distribution patterns and enrichment mechanisms of lithium, rubidium, and cesium in the hot springs of Bukadaban Peak, Hoh Xil. *Acta Petrologica Sinica*, (3).

Data availability

The data that support the findings of this study are available from the author upon reasonable request.

Declaration of competing interest

The author declares that he has no competing financial interests or personal relationships that could have appeared to influence the work reported in this paper.

Use of AI tools declaration

The author declares that he has not used Artificial Intelligence (AI) tools in the creation of this article.